Quantum information measures: Properties and analysis of structure and dynamics of multielectronic systems

TESIS DOCTORAL

por

Adrián López Martín

Universidad de Granada

23 noviembre 2017

Editor: Universidad de Granada. Tesis Doctorales
Autor: Adrián López Martín
ISBN: 978-84-9163-800-1
URI: http://hdl.handle.net/10481/49967

El doctorando Adrián López Martín y los directores de la tesis Juan Carlos Angulo Ibáñez y Sheila López Rosa. Garantizamos, al firmar esta tesis doctoral, que el trabajo ha sido realizado por el doctorando bajo la dirección de los directores de la tesis y hasta donde nuestro conocimiento alcanza, en la realización del trabajo, se han respetado los derechos de otros autores a ser citados, cuando se han utilizado sus resultados o publicaciones.

Granada, 23 de Noviembre de 2017

Director/es de la Tesis:

Fdo.: Juan Carlos Angulo Ibáñez

Fdo.: Sheila López Rosa.

Doctorando:

Fdo.: Adrián López Martín

Tesis doctoral dirigida por:

Dr. Juan Carlos Angulo Ibáñez

Dra. Sheila López Rosa

D. Juan Carlos Angulo Ibáñez, Doctor en Física y Catedrático del Departamento de Física Atómica, Molecular y Nuclear de la Facultad de Ciencias de la Universidad de Granada.

D. Sheila López Rosa, Doctora en Física, Profesora Contratada Doctora de la E. T. S. de Ingeniería de Edificación de la Universidad de Sevilla.

MANIFIESTAN:

Que la presente Memoria titulada "Quantum information measures: Properties and analysis of structure and dynamics of multielectronic systems", presentada por Adrián López Martín para optar al Grado de Doctor en Física, ha sido realizada bajo nuestra dirección.

Granada, 23 de Noviembre de 2017

Fdo.: Juan Carlos Angulo Ibáñez

Fdo.: Sheila López Rosa.

Memoria presentada por Adrián López Martín para optar al Grado de Doctor en Física por la Universidad de Granada.

Fdo.: Adrián López Martín

Título de Doctor con Mención Internacional

Con el fin de obtener la Mención Internacional en el Título de Doctor, se han cumplido, en lo que atañe a esta Tesis Doctoral y a su Defensa, los siguientes requisitos:

1. La tesis está redactada en inglés con una introducción en español.
2. Al menos uno de los miembros del tribunal proviene de una universidad no española.
3. Una parte de la defensa se ha realizado en inglés.
4. Durante la realización de esta Tesis Doctoral se ha realizado una estancia en México, en la Universidad Autónoma Metropolitana de México.

Contents

Foreword **1**

Introduction **3**

1 Theoretical foundations: Information-theoretic measures **11**
1.1 Fundamental information measures 12
1.1.1 Shannon entropy 12
1.1.2 Entropic moments 17
1.1.3 Fisher Information 18
1.2 Complexity measures 19
1.2.1 LMC shape complexity 21
1.2.2 Fisher-Shannon complexity 21
1.3 Divergence measures 22
1.3.1 Kullback-Leibler divergence 23
1.3.2 Jensen-Shannon divergence 23
1.3.3 Fisher divergence 24
1.3.4 Jensen-Fisher divergence 25
1.3.5 Quantum similarity measure and quantum similarity index 26
1.3.6 Generalized quantum similarity index 27

2 Fisher-like atomic divergences: Mathematical grounds and physical applications **29**
2.1 Numerical analysis with atomic one-particle densities 31
2.1.1 Neutral atoms 31
2.1.2 Ionization processes 42
2.2 Conclusions 44

3 Jensen-Shannon and Kullback-Leibler divergences as quantifiers of relativistic effects in neutral atoms **47**
3.1 Quantifying relativistic effects: numerical analysis of atomic divergences . 49
3.2 Conclusions 55

4 Generalized quantum similarity in atomic systems: A quantifier of relativistic effects **57**
4.1 Quantifying relativistic effects: numerical analysis of quantum similarity . 62
4.2 Conclusions 71

5 Electron pair densities: An information-theoretical approach **73**

5.1 Electron pair densities and related measures 74
5.2 Results 79
5.2.1 Shannon entropy and disequilibrium 79
5.2.2 LMC shape complexity 86
5.2.3 Jensen-Shannon divergence and quantum similarity index 87
5.3 Conclusions 97

6 A molecular analysis using an information-theoretical approach 101
6.1 The basis of the informational approach to molecular systems 103
6.2 Results 105
6.3 Conclusions 112

7 The relativistic harmonic oscillator 117
7.1 Dirac equation and Dirac oscillator 118
7.2 Information-theoretical analysis of the Dirac oscillator 122
7.2.1 Shannon, entropy, Fisher information and disequilibrium 123
7.2.2 Complexity measures 130
7.3 Conclusions 134

Conclusions 135

Conclusiones 139

Bibliography 144

List of Figures 163

List of Tables 169

Foreword

This Thesis is a contribution to the research on the Information Theory of multielectronic quantum systems. It focuses on numerous and diverse applications of a range of information-theoretic measures to specific atomic and molecular structures. Relativistic and non relativistic multielectronic atomic systems, the relativistic quantum oscillator, and molecular systems are the principal systems under study in this Thesis. A variety of information-theoretical measures, including complexity and divergence measures, are employed in order to establish how these quantities can be related to different physicochemical properties of the systems under consideration. This connections will allow us to reach a better understanding of those systems and propose an alternative methodology of their analysis, which could be applied to other systems in the future.

This Thesis is composed by seven Chapters. The first one is devoted to the description and enumeration of the informational measures used throughout this Thesis. The following six Chapters are focused on the analysis of these mentioned information-theoretic measures applied to atomic systems (Chapters two, three, four and five), molecular systems (Chapter six) and the relativistic quantum oscillator or Dirac oscillator (Chapter seven). Each of these Chapters has a specific introduction, which provides the scientific context and motivation of the work. Let us now summarize the contents of this Thesis.

Chapter 1, namely "Theoretical foundations: Information-theoretic measures", details the definition, properties, scientific context and recent applications of the different information-theoretical measures employed in the development of this thesis. The measures are classified in three different sections: Fundamental information measures (which comprise the Shannon entropy, the entropic moments and the Fisher information), complexity measures (which comprise the Fisher-Shannon complexity and the LMC complexity) and divergence measures (enclosing the Kullback-Leibler divergence, the Jensen-Shannon divergence, the Fisher divergence, the Jensen-Fisher divergence, the quantum similarity measure, the quantum similarity index and the generalized quantum similarity index).

Chapter 2, which is called "Fisher-like atomic divergences: Mathematical grounds and physical applications" is devoted to the study and comparison of the Fisher divergence and the Jensen-Fisher divergence, which is applied to neutral and ionic multielectronic

atomic densities in position and momentum space. We focus in the different descriptions provided by both divergence measures and the connections found with the physical properties of the atomic systems studied, such as the atomic shell structure, ionization potential and nuclear charge, arising due to the local character of both measures.

Chapter 3, which is referred to as "Jensen-Shannon and Kullback-Leibler divergences as quantifiers of relativistic effects in neutral atoms" is dedicated to the study of relativistic effects in multielectronic atomic systems in position space. In order to do that, the Kullback-Leibler and the Jensen-Shannon divergences were employed to compare relativistic and non-relativistic atomic densities, analyzing their value and comparing it with the atomic shell structure and atomic charge.

Chapter 4, entitled "Generalized quantum similarity in atomic systems: A quantifier of relativistic effects", is devoted to the analysis of the contribution that different regions of the atomic density have in relativistic effects. The generalized quantum similarity index is the information-theoretic measure employed to compare relativistic and non-relativistic multielectronic atomic densities. Its main property of regulating which different region of the density domain is considered on the comparison, made it perfect to this precise purpose.

Chapter 5, named "Electron pair densities: An information-theoretical approach", is dedicated to the analysis of electron pair atomic densities. Many and diverse information-theoretic measures are employed to achieve such objective, namely, Shannon entropy, disequilibrium, LMC complexity, Jensen-Shannon divergence and the quantum similarity index. Those quantities are employed to compare both monoelectronic and electron pair atomic densities in position and momentum spaces, for both neutral and ionic systems, which allow us to establish the similarities and differences between both approaches to the atomic density.

Chapter 6, which is titled "A molecular analysis using an information-theoretical approach", is devoted to the analysis of molecular systems using different divergence measures. The main purpose of this chapter is determine a connection between differences in information-theoretic measures and chemical and physical properties of molecules under consideration. The complexity of this study is discussed and a more restricted approach is considered in order to achieve realistic results. We employ the well-studied Jensen-Shannon and Jensen-Fisher divergence measures, which allow us to establish a direct comparison between a reference molecule and the rest of the group considered. Then we match these quantities to physical and chemical properties of the molecules, namely hardness and number of electrons.

Chapter 7, which is called "The relativistic harmonic oscillator", is dedicated to the discussion of the relativistic harmonic oscillator and the study of the properties of the radial part of its density by means of information-theoretic measures. Shannon entropy, disequilibrium, Fisher information, LMC complexity and Fisher-Shannon complexity

are calculated for different values of the quantum numbers, showing a connection between both quantities and the radial density structure of the system.

Introduction to information theory: From Morse coding to quantum information

Every journey has a beginning, and this one started at 1948, with Claude D. Shannon. At this time, Shannon was studying the properties of Morse communications at Bell's laboratories. At that time, human communication had been an essential research theme for decades. Since the early birth of communication technologies, its efficiency, methods and treatments have been studied.

Language has probably been one of the most important skills developed by humankind. Since its first manifestations in form of cave paintings, to the birth of the alphabet and written and spoken words, language has allowed us to transmit and communicate ideas and emotions. Science has been developed mainly thanks to the ability of communicate different theories and discoveries, allowing scientist to achieve greater milestones, something an isolated person or community could never do. From post mail carried by horse, to telegrams carried on electromagnetic pulses by wires, the evolution of communications has been deeply related to the scientific progress.

At first, contemporaneous engineers were mostly interested in economic and utilitarian matters. How could we carry a message further and in the most economic way? This actual question was the origin of Morse code, commonly regarded as one of the cheapest ways of transmitting a message. Everyone knows what Morse is even though it has been almost a century since it reached its prime time. Morse code and Morse communication came into being due to the development of both technical and theoretic communications. A device capable of controlling an electronic current were it would be transmitted kilometers away on a speed not ever witnessed, were another person could interpret a series of those signals as letters, words and finally a message. From dashes and points to complete sentences, using only a battery, a wire and a key paddle, that was Morse's simplicity. While studying Morse code, the first question that arises is how to assign dot and dashes to each letter. That question uncovers one of the main issues on Information Theory: how a message is transmitted, how information can be encoded and what is

the efficiency of the communication channel. In Morse code, the fastest symbols (one dash or one dot) are assigned to the most common letters (being E or T), and the slower symbols (four dashes or four dots) are assigned to the rarest letters (Y and Q).

Now the famous word has finally appeared: information. All languages and communication methods are a mere way of transmitting that elusive concept. What does information mean? When talking about communications, information is just a measure of what one gains from receiving a message. Information is measured in bits, which is just an abbreviation of "Binary digits", and that is precisely what it is: the basic measure of the knowledge gain for a mere "yes" or "no" question. Knowing the result in a coin toss would be exactly a bit, but in a more complicated channel of communication the difficulty increases. In a communication channel there are mainly two magnitudes that characterize the channel:

- Symbol's Number: number of different signals a channel can transmit. In the Morse code example is just two: dashes and dots (although silence should be included to).
- Symbol's quantity: number of symbols needed in order to codify a given message. This magnitude in Morse code is six, as it is the maximum number of dots, dashes, plus a silence, that is needed to characterize a letter, number or punctuation sign.

There is another relevant magnitude, called message space, being the number of different messages that can be transmitted. In Morse code, this message space is composed of alphabet letters, number and basic punctuation signs. How does all of this come together?

In 1928, Ralph Hartley published a paper focused on the study of communication channels called "Transmission of Information", in which he defined information as $H = \log(s^n)$, where s represents the symbol number and n the symbol quantity [1]. Looking in more detail, one would realize that Hartley information is just the message space, i.e. information is a measure of many binary signals, how many "yes" and "no" are needed to codify a message, or in other words, how many "yes" and "no" a person is receiving.

However, years later, Shannon realized that Hartley definition was only taking into account random communication channels, which proves detrimental. A direct example of the reason can be encountered in Morse code, as we have seen, the assignment of the symbols took into account the use of the letters. So Harley's information did not get to measure that kind of "hidden information". The Shannon's research was finally compiled in an article. Firstly, that work was called "A Mathematical Theory of Communication" [2]. However, realizing how influential that work would be, he extended that article, turning it into a book, and changed the name to "The Mathematical Theory of Communication" [3].

The basis of that investigation was the manner information propagated and traveled through different channels, how could it be quantified, how errors affected it, and mainly, how some parts of a message were correlated to others. The way he established that correlation was general enough that most scientific disciplines could take advantage of that research, as it could be applied to almost any field. And so it was. Since his birth, Information Theory has been applied to countless studies in almost every possible subject. Physics, Chemistry, Economics, Medicine, Sociology, etc. Information is everywhere and Shannon's theory helps us to understand the way it behaves and what we should expect from it. It was such an influential work that the number of investigations that has been using the Shannon Entropy or any other measure born with the Information Theory, is truly overwhelming. And it keeps growing. Information Theory has been successfully applied in many different disciplines, such as the study of economic patterns [4], neural networks and analysis in computer science [5–7], characterization and segmentation of DNA chains [8, 9], research on disease behaviors and patterns in medicine [10], evaluation of symbolic patterns and keywords in literary texts [9, 11], and analysis in neurobiology [12], natural language processing [13], cryptography [14], statistical inference [15, 16], atomic and molecular physics [6, 17–22, 22, 22–24, 24–28], among others. In fact, until now, scientists have created a bulk of information theories: Shannon's statistical [3, 29], information theory, Fisher's [30], philosophy [31], semantic [32], dynamic [33] and economical [34] information theories, among others.

Taking a step closer to the theme of this thesis, Shannon's Theory of Information was the main leader to what nowadays is called "Quantum Computation", one of the most promising and influential research themes. Common computers were an incredible advance in technology, changing the way we work, live and research, but quantum computers are expected to be an even more drastic development. It is known that common computers use bits to store and manipulate information by means of transistors, which are only capable of recording two states. Quantum computer use qubits, which are quantum systems itself (molecules, photons or electrons are the main candidates). Due to their quantum properties, it is known quantum systems can achieve superposition states, so they are not limited, as classical system are, to just two states. Theoretically they could store a highly dense amount of information, but this potential is limited. Even though that potential is much higher than a classical one, and it could be improved. Shannon's theory has made possible all of this. It describes how information can be controlled, how a quantum system can store it [35]. The most promising scientific theory today is possible due to Shannon's work more than fifty years ago. But, how has this point been reached? How has Information Theory, a communication-focused discipline, ended being used in Quantum mechanics?

Quantum systems are statistical and probabilistic by nature. In a quantum experiment, one can not in general predict exactly what will happen, one can only know the probability of possible outcomes. With each experiment we may associate a characteristic

degree of predictability, or an amount of uncertainty. Since its beginning, Quantum Mechanics regarded the wave function as its main object of study, because it represents each state of the system under consideration. A quantum system could be studied and explained if its wave function was obtainable. However, dealing with the wave function is hard and not easy to visualize. In fact, there are a few cases where the wave function can be analytically obtained. Besides, usually, a quantum system came in a superposition of states. In those cases, the result of an experiment could not be known precisely beforehand.

This is the perfect context to employ the concept of information as a tool to remove the uncertainty. Information Theory provide us with different measures to quantify this uncertainty [36]. In this framework, there have been many studies regarding the information that can be extracted from those apparent situations in which the ignorance from the outcome is problematic. The most relevant ones are known as extremization techniques, and allow us to estimate the possible outcome distributions when there is a lack of information, from the initial states or even from the system. Two examples of the power of these techniques are (i) the Maximum Shannon Entropy method, which can be used to construct the whole of the conventional or extensive statistical thermodynamics [15, 16, 37], and (ii) the Minimum Fisher Information method, which is able to provide the fundamental wave equations and the conservation laws of natural systems at small and large scales [38].

When dealing with discrete states, the use of the wave function is easy enough. However, with more complex systems, the use of the wave function often becomes a burden. On those cases the probability density is much more approachable. It has a straightforward meaning and a much more intuitive structure. This is the cornerstone of the Density Functional Theory (DFT), which establishes that probability density contains all the relevant information to understand and study quantum systems [39]. Due to this fact, quantum density studies became much more common and atomic and molecular densities started to get more attention.

This situation resulted in the perfect match. On the one hand, there was Density Functional Theory, allowing the study of densities of quantum systems previously unapproachable. On the other hand, there was Information Theory, capable of characterizing probability distributions in regard of its structure qualities. It was the origin of Information Physics. As informational studies and analysis became more common and widely used [6, 15–22, 22, 22–24, 24–28], the information arise as a new paradigm. Until then, the energy was the essential property of physical systems. Energy conservation always had a central role in Physics in general and Quantum Physics in particular. However, as the information got more attention, many physicist started to wonder if information could fulfill that central role instead of the energy and describe the physical/chemical properties of the systems. This is one of the main objectives in this work: to show how physical and chemical properties of atoms and molecules are, indeed, intricately

entwined with informational properties of the electronic densities of the systems they represent.

Chapter 1

Theoretical foundations: Information-theoretic measures

Since the development of Density Functional Theory (DFT), it has been common knowledge quantum densities contain all the information of the quantum system they represent. Information-theoretic measures are used to take advance from this, as they can certainly be used to grasp the specific distribution and structure of the density they are applied to, and transform those magnitudes to a numeric value, that more often than not is strongly linked to physical and chemical properties of the species considered. Thus, these properties of atoms and molecules strongly depend on the spread of the probability density which characterizes their allowed quantum-mechanical states. This spread can be differently grasped and complementary quantified by various information-theoretic measures beyond the celebrated standard deviation or its square, the variance

Furthermore, the information theory of quantum systems provides an entropy-based characterization of atomic and molecular systems, which complements the energy-based representation obtained through the wave function and density functional methods. Measures of uncertainty, randomness, disorder and localization are basic ingredients encountered to play a relevant role for the identification and description of numerous quantum phenomena in physical systems and chemical processes. These features of delocalization, uniformity and order can be quantified by the information-theoretic measures of Shannon entropy, disequilibrium and Fisher information of the corresponding electron densities of the system, respectively.

In this chapter we are going to cover the most common and widely used information measures. Their definitions will be provided and its main properties will be discussed.

1.1 Fundamental information measures

The simplest way of analyzing an atomic or molecular system is on its own, i.e. studying all its properties and characteristics, independently of other systems. By these means, a profile of the system can be isolated and developed, analyzing it properly without taking into account other species.

Regarding this matter, information-theoretic measures arise as the perfect tool to do this. There is a long and curated list of measures which has been employed since the beginning of the theory to review different systems (sometimes not even physical or chemical), which properties are perfectly established and cataloged.

A great number of these measures are what is known as 'individual measures'. As it was said previously, sometimes the most convenient way of interpreting a system is by itself, and information-theoretic measures give this exact possibility, as they are defined with this specific goal: to estimate a precise characteristic of a system's density and to give a numeric value based on it. The exact characteristic these measures take into account is different from one another and derived from its mathematical definition. Let us now discuss some of them.

1.1.1 Shannon entropy

The most commonly used and more famous measure in information theory is *Shannon entropy* S [3, 15]. It was proposed in 1944 by Claude E. Shannon in the context of theory of communications. At the moment he was studying how a channel of communication behaves and how its main properties could be measured. One of the properties he was most interested in was the amount of information gained when a message was successfully transmitted. It was directly related to the uncertainty previous to the sending of the message. Let us consider a communication channel being capable of transmitting N possible message, $\{X_i\}_{i=1}^{N}$, each X_i has a weight or probability associated of p_i. Shannon realized that any function able to measure the degree of uncertainty or information gained, named $H(p_1, p_2, \cdots, p_N)$, must fulfilled some conditions. These conditions were:

- The information gained, H, must be a continuous and symmetric function of $\{p_i\}_{i=1}^{N}$ as small variations of the probability should only cause small changes of the uncertainty.
- If the probability of obtaining a message are all the same, equal to $\frac{1}{N}$, then the uncertainty H should reach its maximum value, as the information gained from such situation would be minimal. So, in the equiprobability situation, the higher number of possibilities (N) for the random variable, the higher the uncertainty is.

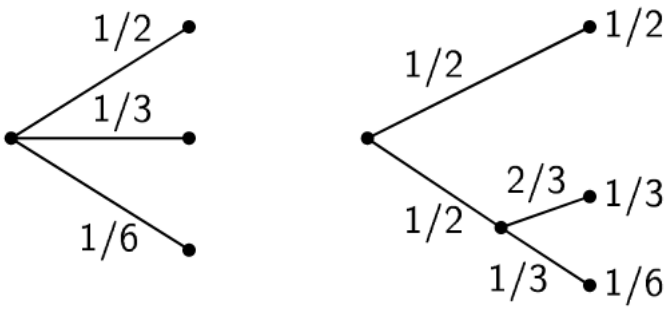

FIGURE 1.1: How to decompose a choice from three different possibilities

- In the case of a composed message, where the second one depends on the first, the uncertainty of the whole message should be the weighted sum of the individual values of uncertainty.

  For example, given the situation in Figure 1.1, where we have three possibilities at the left with $p_1 = \frac{1}{2}$, $p_2 = \frac{1}{3}$ and $p_3 = \frac{1}{6}$; while, at the right, we have first a posibility with $p_1 = \frac{1}{2}$ and $p_2 = \frac{1}{2}$ too, but, if the second possibility occurs we have another message is sent with $p'_1 = \frac{2}{3}$ and $p'_2 = \frac{1}{3}$. In this case we require the uncertainty to satisfy:

$$H\left(\frac{1}{2}, \frac{1}{3}, \frac{1}{6}\right) = H\left(\frac{1}{2}, \frac{1}{2}\right) + \frac{1}{2}H\left(\frac{2}{3}, \frac{1}{3}\right) \tag{1.1}$$

- The uncertainty associated to $\{p_i\}_{i=1}^{N}$ should be equal than the uncertainty associated to $\{p_i\}_{i=1}^{M}$ if $p_{N+1} = p_{N+2} = \cdots = p_M = 0$, i.e., adding an arbitrary set of possible values with null probability to the variable keeps the value of the uncertainty.

The only function H satisfying those conditions must be in the form:

$$H(p_1, p_2, \cdots, p_N) = -K \sum_{i=1}^{N} p_i \log p_i \tag{1.2}$$

where K is any constant, that allows us to choose the base of the logarithm and the unit of measure. Shannon chose the bit as his preferred unit as it was directly related to the concept of uncertainty or information gained with.

Shannon entropy has a series of interesting properties which are worth discussing:

- H is always positive unless all the p_i are equal 0 but one, this one having the unity value.

- For a given number, N, of possible message or events, H is a maximum and equal to $\log N$ when all p_i are equal, i.e., $\frac{1}{N}$.

- The uncertainty of a joint event is less than equal or equal to the sum of the individual uncertainties, being equal only if the events are independent:

  Suppose there are two events, x and y, with M possibilities for the first and N for the second. Let $p(i,j)$ be the probability of the joint occurrence of i for the first and j for the second. The entropy of the joint event is

$$H(x,y) = -\sum_{i=1}^{M}\sum_{j=1}^{N} p(i,j)\log p(i,j) \tag{1.3}$$

  while

$$H(x) = -\sum_{i=1}^{M}\sum_{j=1}^{N} p(i,j)\log\sum_{j=1}^{N} p(i,j) \tag{1.4}$$

$$H(y) = -\sum_{i=1}^{M}\sum_{j=1}^{N} p(i,j)\log\sum_{i=1}^{M} p(i,j), \tag{1.5}$$

  which easily shows

$$H(x,y) \leq H(x) + H(y) \tag{1.6}$$

  with equality holding only if the events are independent (i.e. $p(i,j) = p(i)p(j)$)

- Any change towards equalization of the probabilities $\{p_i\}_{i=1}^{N}$ increases the value of H. Thus, if $p_1 < p_2$ and we increase p_1, decreasing p_2 in the same proportion so p_1 and p_2 values are closer, then H increases.

- The entropy of a joint event (x,y) is equal to the entropy of x plus the entropy of y when x is known:

  Given two events x and y, not necessarily independent, for any value of x we can assume that there is a conditional probability $p_i(j)$ for y having the value j, this is given by

$$p_i(j) = \frac{p(i,j)}{\sum_{j=1}^{N} p(i,j)}. \tag{1.7}$$

  Then we can define the *conditional entropy* of y, $H_x(y)$

$$H_x(y) = -\sum_{i=1}^{M}\sum_{j=1}^{N} p(i,j)\log p_i(j), \tag{1.8}$$

which measures how uncertain we are of y on the average given that we know x. Substituting the value of $p_i(j)$ given in Eq. (1.7), we obtain

$$\begin{aligned} H_x(y) &= -\sum_{i,j} p(i,j) \log p(i,j) + \sum_{i,j} p(i,j) \log \sum_j p(i,j) \\ &= H(x,y) - H(x) \end{aligned} \tag{1.9}$$

which give us

$$H(x,y) = H(x) + H_x(y) \tag{1.10}$$

- Given two related events (x, y) the uncertainty of y is never increased by the knowledge of x. It will always be decreased unless x and y be independent, in which case it is unchanged. It can be easily proved from Eqs. (1.6) and (1.10).

Shannon entropy had, as it has been shown, an origin in discrete probabilities. However, it can be easily generalized to continuous probability densities, $p(x)$:

$$H(p) = -\int_\Delta p(x) \ln p(x) dx \tag{1.11}$$

where $x \in \Delta \subseteq \Re$ and it is assumed that $p(x) \ln p(x) = 0$ when $p(x) = 0$, and the ln is preferred to log as is a custom. Eq. (1.11) is often known as *differential entropy*. Extensive studies of the value of this magnitude applied to many different kinds of continuous probability can be found at [40]. An extension to a multidimensional probability density $\rho(\vec{r})$ can be introduced in a straightforward way:

$$S(\rho) \equiv -\int_\Delta \rho(\vec{r}) \ln \rho(\vec{r}) d\vec{r} \tag{1.12}$$

with $\vec{r} \in \Delta \subseteq \Re^d$.

The differential entropy has a number of properties quite different from its discrete counterpart, being the most worth mentioning that it may take negative values, nevertheless this quantity is actually very useful. This potential negativity does not pose any trouble because it is always true that the lesser uncertainty (let us remember that can be interpreted as an information gain), the lesser the entropy is; the only point now is that the more concentrated is the probability density (the lesser uncertainty), the entropy more approaches towards minus infinity. In order to avoid this trouble and to guarantee that the uncertainty is non negative it is more convenient to define the *exponential Shannon entropy*:

$$L(\rho) = e^{S(\rho)} \tag{1.13}$$

Let us remark that Shannon entropy provides a lower bound for the standard deviation σ of all probability densities, given by

$$S(\rho) \leq \ln \sigma \sqrt{2\pi e}, \tag{1.14}$$

with equality holding for Gaussian distributions. This result is quite useful for the study of quantum-mechanical uncertainty relations [41].

Information-theoretical properties based on Shannon entropy have been extensively employed in recent years within a quantum-mechanical framework, in particular for multielectronic systems. Their use in atomic and molecular systems has provided a wide variety of results [17–22]. Most recently, Shannon entropy has being employed in semantic analysis for event studies in computer science [5], signal analysis on Alzheimer detection [42], tissue analysis on biophysics [43], genetic data research on biochemistry [44], multicriteria decision-making for renewable energy systems [45] or flow analysis on differential geometry [46].

Although they will not use along this Thesis, it is worth noting that there are two other information measures that represent an extension or generalization of the Shannon entropy:

- The Rényi entropy, which for a continuos probability distribution is given by:

$$R^{(\alpha)}(\rho) \equiv \frac{1}{1-\alpha} \ln \int_{\Delta} \rho^{\alpha}(\vec{r}) d\vec{r}, \tag{1.15}$$

  where $\vec{r} \in \Delta \subseteq \Re^d$ and $\alpha > 0$. See Ref. [47] for a survey of it basic properties. The particular value $\alpha = 1$ appears as a limiting case for wich $R^{(1)}(\rho) = S(\rho)$.

- The Tsallis entropy, which for a continuos probability distribution is given by [48]:

$$T^{(\alpha)}(\rho) \equiv \frac{1}{\alpha - 1} \left(1 - \int_{\Delta} \rho(\vec{r})^{\alpha} d\vec{r} \right). \tag{1.16}$$

  where $\vec{r} \in \Delta \subseteq \Re^d$ and $\alpha > 0$. As in the case of the Rényi entropy, the limit $\alpha \to 1$ provides the Shannon entropy, $T^{(1)}(\rho) = S(\rho)$. Remark that the Tsallis expression may be seen as a linearization of the Rényi expression. For an exhaustive review of the basic properties and physical applications of this quantity, see the monograph of Tsallis [49].

1.1.2 Entropic moments

Entropic moments, also known as *frequency moments*, were introduced by Uffink [50], and they are given by:

$$\omega^{(\alpha)}[\rho] \equiv \int_{\Delta} \rho^{\alpha}(\vec{r}) d\vec{r} \tag{1.17}$$

with $\vec{r} \in \Delta \subseteq \Re^d$ and $\alpha \in \Re$. It is straightforward to see that the Shannon entropy, as well as its generalization, the Rényi and Tsallis entropies, can be easily derived from these quantities.

These quantities were studied much earlier by mathematicians [51, 52] and statisticians [53, 54], but their applications to quantum systems and information theory were provided later, particularly with the arising of Density Functional Theory [55, 56].

Entropic moments are measures of uncertainty, which main property is Schur concavity, for details see [35, 57, 58]. The greatest strength of frequency moments is their ability to enhance or diminish the contribution of the integrand over different regions on the whole domain, by increasing or decreasing the value of the power α. When α reaches a high value, ρ^{α} tends to concentrate around its local maxima. On the other hand, when α receives a low value, the whole function is smoothed along its domain. By doing so, a powerful way of analyzing a distribution is achieved, as it allows to focus on different features of the density structure at will.

One of the most widely used frequency moments is the second order one, also known as *disequilibrium*, which corresponds to the case $\alpha = 2$:

$$D[\rho] \equiv \omega^{(2)}[\rho] = \int_{\Delta} \rho^{2}(\vec{r}) d\vec{r} \tag{1.18}$$

with $\vec{r} \in \Delta \subseteq \Re^d$.

This measure is mainly used to describe the level of departure from uniformity of the distribution $\rho(\vec{r})$ [58, 59].

Entropic moments, and disequilibrium as well, are still considered a very useful tool for different kind of projects. In recent years they have been employed to discuss properties on d-dimentional Rydberg systems [60], to quantify electronic distribution in multidimensional harmonic oscillators [61] or magnetoencephalographic rhythms analysis [10].

1.1.3 Fisher Information

All quantities defined before have a *global* charater. They quantify the probability density as a whole; this is because of their analytical structure in terms of the density which has a powerlike (entropic moments) and logarithmic (Shannon entropy) form.

It is of great interest to have also information measures displaying a deeper *local* character, namely their values being more sensitive to strong local changes. The main quantity studied and employed in the literature with such a characteristic in what concerns measures on a single distribution is the so-called *Fisher information*, introduced by Ronald A. Fisher in 1925 [30] in the context of statistical estimation theory. Let us suppose we have an experiment involving some parameter θ and we want to estimate the value of such parameter by making N measurements in the system. These data, $\vec{y} \equiv \{y_i\}_{i=1}^N$, obey $y_i = \theta + x_i$ where $\vec{x} \equiv \{x_i\}_{i=1}^N$ represent the noise in the system that contaminates the real value θ.

This system is determined by a conditional probability given by the family of probability densities $p_\theta(\vec{y}|\theta) = p(y_1, \cdots, y_N, \theta)$. The Fisher information of the measurement can be defined as:

$$I(\theta) = \int \left[\frac{\partial \ln p_\theta(\vec{y}|\theta)}{\partial \theta}\right]^2 p_\theta(\vec{y}|\theta) d\vec{y} \tag{1.19}$$

If we consider the mean-square error of the estimate $\hat{\theta}(\vec{y})$

$$\epsilon^2 = \int \left[\hat{\theta}(\vec{y}) - \theta\right]^2 p_\theta(\vec{y}) d\vec{y} \tag{1.20}$$

we realize the Fisher information fulfills the consequence of the Cauchy-Schwartz inequality known as the Cramér-Rao inequality [40], i.e.,

$$\epsilon^2 \times I \geq 1. \tag{1.21}$$

Then, we can conclude that the parametric Fisher information measures the ability to estimate a parameter or, in other way, the minimum error in estimating θ from the given probability $p(\vec{y}|\theta)$.

In the case with only one measure, then $p_\theta(\vec{y}|\theta) = p_\theta(y|\theta)$ and if the fluctuations x are independent of the value of θ (which is called shift invariance) then $p_\theta(y) = p(y - \theta) = p(x)$. The Fisher information then becomes

$$I(p) = \int_\Delta p(x) \left|\frac{\partial \ln p(x)}{\partial x}\right|^2 dx. \tag{1.22}$$

where $x \in \Delta \subseteq \Re$. This measure can be easily generalized to a multidimensional density of probability $\rho(\vec{r})$:

$$I(\rho) = \int_{\Delta} \rho(\vec{r}) \left| \vec{\nabla}_d \ln \rho(\vec{r}) \right|^2 d\vec{r}, \tag{1.23}$$

where $\vec{r} \in \Delta \subseteq \Re^d$ and $\vec{\nabla}_d$ is the d-dimensional gradient operator.

Fisher information can be interpreted as the expectation value of the quadratic logarithmic derivative of the density. This quantity measures the gradient content in the probability distribution which describes the system, so it reflects the irregularities in the density, being then a measure of a system's disorder. The presence of the squared density derivative makes this information quantity to be much more sensitive to changes in its gradient content even at a local level, notably increasing in the presence of numerous and/or strongly peaked local extrema. The higher this quantity is, the more localized is the density, the smaller is the uncertainty and the higher is the accuracy in estimating the localization of the particle.

It is also worth mentioning that Shannon entropy and Fisher information are employed in two widely used extremization procedures: the Maximum Entropy Method [53] and the Principle of Extreme Physical Information [62], respectively. These extremization methods allow us to estimate the probability distribution from partial knowledge of its variables and are extensively employed, being the maximum entropy method the most popular one. Let us remark that both quantities are closely related to fundamental and/or experimentally measurable quantities of finite electronic and nucleonic systems [63–68], and they are the cornerstones of two alternative formulations of the classical thermodynamics [69, 70].

The Fisher information has also been applied to emphasize (i) relativistic effects in Dirac-Fock atoms [23], and (ii) the aforementioned local character of other relevant information measures, such as the so-called complexity of a given system, initially defined in Ref. [59] and later generalized [71] in a 'global sense'. Further generalizations involving the Fisher information gave rise to complexity measures of local character [72, 73], successfully applied to the study of structural properties of atomic systems [22, 24]. Fisher information is still being used for different kinds of studies, such as time estimation of quantum processes for quantum computing [74], quantifying useful entanglement in quantum systems [6], evaluating variations in surface integrals [75] or identifying entangled phase transitions [76].

1.2 Complexity measures

The term 'complexity' is widely used among different disciplines to talk about how "easy" or "hard" is a concept to grasp or understand. But what's does complexity refer

to in a Physics framework?

Complexity and simplicity are commonly used as antonymous words. If a system is simple, it can't be complex, and vice versa. One could be tempted to consider a system simple when it is easily comprehended, but it goes beyond that. Formally, a system is considered simple when one needs few variables and/or equations to describe it. On the other hand, a system is considered complex if you need a high number of variables/equation to accurately characterize it. For example a completely uniform medium is thought as a simple system, because you just need to know its density at an arbitrary point to completely describe it. It is the same case with a completely random system. There is no real structure in it, so it can be described easily as well. However, when a system has a mix of both characteristics, the task gets harder. More complex, if you like.

The first complexity measure ever conceived was defined by Kolmogorov in the nineteen sixties [77]. It received different names: Kolmogorov complexity, descriptive complexity, algorithmic complexity, even algorithmic entropy. The concept behind it was fairly straightforward: given a binary string of characters, the measure provided the value of the shortest computer program that could be able of generating such string. Despite its usefulness, Kolmogorov complexity has a critical inaccuracy: even though a completely random string should be fairly easy to generate, this measure gave it the highest value of complexity.

But, how can this be related to quantum systems? The concept of complexity is closely related to that of "understanding", in the sense that the latter is based upon the accuracy of model descriptions of the system obtained by using a condensed information about it. Hence, the complexity measures how easily modelling a system may be. In this sense, fundamental concepts such as uncertainty or randomness are frequently employed in the definitions of complexity although some other concepts such as clustering, order, localization or organization might be also important for characterizing the complexity of systems and processes. More specifically, our interest is focused on the density structure of atomic and molecular system. However, as we have mentioned, there is no agreement over an specific definition of complexity, nevertheless we know it has to fulfill some requirements:

- It has to reach its minimal value for those considered as the simplest probability densities, i.e the Dirac-delta distribution (corresponding to perfect order) and the highly flat distribution (corresponding to a maximum disorder).
- It must be invariant under replication, translation and rescaling of the probability density.

Despite these concrete requirements, there are a number of complexity measures that have arise trying to fulfill this purpose. Let us have a look at them. In this Thesis we

focus our attention in those defined in terms of two individual information measures in order to quantify simultaneously the order/disorder, localization/delocalization and randomness or uncertainty of the system under study.

1.2.1 LMC shape complexity

This measure was first introduced by López-Ruiz, Mancini and Calbet [59], although, later on, it has been criticized [78], modified [79] and generalized [80].

The *LMC shape complexity*, C_{LMC}, is defined as a product of two of the more widely used individual information-theoretic quantities: the Shannon entropy and the disequilibrium (see subsections 1.1.1 and 1.1.2, respectively).

$$C_{LMC}(\rho) = D(\rho) \times e^{S(\rho)} \tag{1.24}$$

where S is the Shannon entropy given by Eq. (1.12) and D is the disequilibrium given by Eq. (1.18).

This is a widespread way of defining complexities: as the product of two complementary measures. This quantity measures the complexity of the system by means of a combined balance of the average height of the probability density and its total bulk extent. This the early mentioned conditions are met, as a minimal is reached for values at both extremely ordered and disordered limits, while also satisfying the desirable properties of invariance under scaling transformation, translation and replication [71, 81]. It is also worth mentioning that, as the disequilibrium and exponential Shannon entropy are both always positive, LMC complexity is positive as well. In fact, $C_{LMC} \geq 1$, this lower bound is valid for any d-dimensional distribution [82].

The utility of this complexity has been clearly shown in many different fields [21, 83, 84] allowing reliable detection of periodic, quasiperiodic, linear stochastic and chaotic dynamics [59, 71, 81]. They are currently being employed successfully for many different purposes, such as adjusting the diagnosis on magnetoencephalographic rhythms analysis [10], detecting critical events and patterns at exchange rate in economics [4] or identifying chemically significant regions on chemical reactions [25].

1.2.2 Fisher-Shannon complexity

In contrast with the previous complexity measure, the *Fisher-Shannon complexity*, C_{FS}, is defined as a combination of a global (Shannon entropy) and a local (Fisher Information) measure. Originally, this magnitude was conceived as a mere Fisher-Shannon product, an interesting product due to the fact that it fulfills the inequality $I \times J \geq d$

[40, 85], being d the dimension of the system considered. However it was afterwards redefined as a complexity measure [24, 26] as follows:

$$C(FS)(\rho) \equiv I(\rho) \times J(\rho) \tag{1.25}$$

where I is the Fisher information and J is the so-called "power Shannon entropy":

$$J(\rho) = \frac{1}{2\pi e} e^{\frac{2}{d}S(\rho)}. \tag{1.26}$$

Shannon has been introduced by means of J in order to preserve the scaling invariance of complexity measures and to simplify the expression of its universal lower bound. In contrast with the LMC complexity, FS complexity employs the Fisher information instead of the disequilibrium, which concedes this quantity a local character that the LMC complexity lacks.

The Fisher-Shannon complexity measure has been widely used in several fields, being one of the most relevant in atomic distribution analyses where it has shown to provide essential information about atomic shell structure and ionization processes or structural studies on many-fermion systems [22, 24, 26, 27]. More recently, the Fisher-Shannon complexity has been employed as a convenient tool in the study of confined multidimensional atoms properties [28] or exotic potential distributions [86].

1.3 Divergence measures

Until now, we have defined information and complexity measures which are able to quantify different features of a given distribution such as organization, pattern, uncertainty or order, among others. This framework allows us to analyze physical and chemical properties of the systems from an information-theoretical point of view. It is also interesting to have at our disposal other density functionals which enable us to measure the "distance" and/or similarity among various densities.

Divergence measures arise from this exact purpose. They are able to quantify how similar or different two systems are, regarding a specific trait of their probability densities [40, 87–94]. Once more, the precise attribute depends on the definition of the measure itself; nevertheless, as the usual way of defining a divergence measure arises from a generalization of an individual measure, the divergence tends to focus on the same specific feature as the individual measure did.

There are some requirements on the mathematical formulation of divergence measures that must be fulfilled in order to consider them as a distance between distribution:

- The divergence between two distributions, ρ_1 and ρ_2, has to be non-negative.
- This quantity vanishes only when the two distributions are identical ($\rho_1 = \rho_2$).
- It has to be symmetric, i.e. the divergence between ρ_1 and ρ_2 must the same as the divergence between ρ_2 and ρ_1

However, it is worthy mention that they do not necessarily verify the triangular inequality. This kind of measures are known as semi-metrics [95] instead of metrics, as it would be the case of an usual and proper mathematical distance.

1.3.1 Kullback-Leibler divergence

The *relative entropy*, *cross entropy* or *Kullback and Leibler divergence*, KL, is given by [88]

$$KL(\rho_1, \rho_2) \equiv \int_\Delta \rho_1(\vec{r}) \ln \frac{\rho_1(\vec{r})}{\rho_2(\vec{r})} d\vec{r}, \tag{1.27}$$

is the pioneering global measure of differences between probability distributions introduced within the information theory. It quantifies the information supplied by the data for discriminating between the distributions, being a 'directed divergence' (therefore not symmetric). Specially remarkable is its property of non-negativity, and the fact that the minimum null value is reached only for identical distributions $\rho_1 = \rho_2$.

It is also worth noticing that Shannon entropy, $S(\rho_1)$, can be obtained by taking $\rho_2 = 1$ in the KL expression in Eq. (1.27), so it can also be interpreted as the relative entropy of ρ_1 with respect to the uniform distribution.

The KL divergence constitutes an essential tool within the information theory, as shown by its applications for obtaining minimum cross entropy estimations and for determining atomic [96] and molecular [97] properties, or indexing and image retrieval [95], the introduction of an informational quantum dissimilarity measure to study the relativistic effects on the electron density [98] or the employment of KL measures to analyze molecular reaction paths [99]. Most recently this measure has been applied in visual analysis in neurocomputing [7], distance estimation in artificial vision [100], improving neural network vocabulary speech recognition [101], emotion analysis on neurological processes [102] or change detection on satellite images [103].

1.3.2 Jensen-Shannon divergence

The *Jensen-Shannon divergence*, JSD, is also an information measure between two or more distributions [104, 105], closely related to the Kullbac-Leibler divergence and the Shannon entropy. Attending to its definition,

$$JSD(\rho_1, \rho_2) \equiv \frac{1}{2}\left[KL\left(\rho_1, \frac{\rho_1+\rho_2}{2}\right) + KL\left(\rho_2, \frac{\rho_1+\rho_2}{2}\right)\right], \tag{1.28}$$

JSD represents the mean dissimilarity (understood in terms of the KL measure) of each density with respect to the mean one. Notice the symmetry of JSD (i.e. invariance under the exchange of ρ_1 and ρ_2), and also that the main properties of KL are transferred into JSD: the Jensen-Shannon divergence is always non-negative, vanishing only if $\rho_1 = \rho_2$. In fact, JSD is the square of a true metric [106] or, in other words, its square root constitutes a distance in a rigorous mathematical sense.

Using the above definition together with Eqs. (1.12) and (1.27), the Jensen-Shannon divergence can be also expressed in terms of the Shannon entropy as

$$JSD(\rho_1, \rho_2) = S\left(\frac{\rho_1+\rho_2}{2}\right) - \frac{1}{2}[S(\rho_1) + S(\rho_2)], \tag{1.29}$$

allowing to interpret also the JSD divergence as the 'entropy excess' of the mean density with respect to the mean entropy of the individual densities. So, we observe that the aforementioned non-negativity of JSD arises from the convexity of the Shannon entropy functional S. It is worthy to point out that there are a Jensen-like divergences based on the Rényi and Tsallis entropies, i.e. Jensen-Rényi and Jensen-Tsallis divergences [95, 107]. Their definitions are analogous to Eq. (1.29) using Rényi and Tsallis entropies, respectively.

Different properties and generalizations of JSD have been discussed and employed in past years [92, 108, 109]. Nowadays this measure is still being used for many different purposes: establishing computer vision patterns [110], analyzing twitter streams to quantify collective attention [111], examining distribution of coherence in multipartite quantum systems [112], semantic analysis to measure conceptual relations on neural networks [113], visual analysis in neurocomputing [7] or key frame extraction for video analysis [114].

1.3.3 Fisher divergence

A first attempt to define a comparative measure of local character among distributions was inspired on a global character one, namely the relative entropy KL defined in subsection 1.3.1, which in fact constitutes a 'relative version' of the Shannon entropy S. In doing so, the Fisher information was considered in order to build up a local-character relative measure [115]:

$$FD(f, g) \equiv \int_\Delta f(\vec{r}) \left|\vec{\nabla} \ln \frac{f(\vec{r})}{g(\vec{r})}\right|^2 d\vec{r} + \int_\Delta g(\vec{r}) \left|\vec{\nabla} \ln \frac{g(\vec{r})}{f(\vec{r})}\right|^2 d\vec{r}, \tag{1.30}$$

which is referred as *Fisher divergence* (FD), according to the concept of divergence among distributions previously introduced in the information-theoretical context by other authors[116]. From the FD definition, it is immediately observed that it preserves the desirable properties for establishing the quantitative comparison, namely symmetry, non-negativity, and vanishing for identical distributions. It is worthy to point out that each individual term of the FD definition is known as *relative Fisher information*, RF, [117], which scarce applications have been carried out with similar aims to those of the Kullback-Leibler relative entropy, that is, to perform a comparison of a distribution with respect to an a priori one [118]. There are not many applications of FD [115], but one of the mos recent and interesting ones is this one on signal analysis on beam splitters [119], which had this measure as the main tool to characterize the main properties of the different channels employed.

1.3.4 Jensen-Fisher divergence

More recently, the concave character of the Fisher functional has been considered to define a new Fisher-based divergence, namely the *Jensen-Fisher divergence* [120]

$$JFD(f,g) \equiv \frac{1}{2}[I(f) + I(g)] - I\left(\frac{f+g}{2}\right), \tag{1.31}$$

where I is the Fisher information given by Eq. (1.23). The concavity (convexity) of Fisher information (Shannon entropy) guarantees a non-negative Jensen-like measure. The just mentioned non-negativity, together with the property of reaching the minimal null value only when comparing identical distributions, are essential properties which must verify any functional in order to be considered as an appropriate divergence measure. The applications of JFD in Ref. [120] are limited to some specific functions of mathematical interest, by comparing the results arising from the use of the local and global measures, namely JFD and JSD.

No one of the aforementioned comparisons of the local divergence measures FD and JFD with respect to the global one JSD (Refs. [115] and [120] respectively) concluded that the local ones are better or worse than the global ones. Instead, it was emphasized that they grasp different facets of the distributions in order to quantify the divergence among them, taking into account their behavior at a global or local scale. This fact was clearly highlighted in Ref. [121] regarding the comparison between FD and JSD, not only by considering atomic densities but also by means of simple examples, so avoiding the request of a quantum-mechanical knowledge in order to get a better understanding of the 'local' and 'global' concepts.

1.3.5 Quantum similarity measure and quantum similarity index

The recent explosion in the knowledge based on chemical research has given rise to a surge of interest in chemical similarity. Molecular modeling, quantitative structure activity relationships ($QSAR$) and quantum information are relevant examples of such interest. Chemical similarity is often described as the inverse of a measure of distance in an appropriate space. In particular, the Quantum Similarity Theory (QST) [122] was originally developed in order to establish quantitative comparisons between molecular systems by means of their fundamental structural magnitudes (i.e. electron density functions).

The *Quantum Similarity Measure*, QSM, between two systems [123] was be defined as:

$$QSM(\rho_1, \rho_2) \equiv \int_\Delta \rho_1(\vec{r_1}) \Omega(\vec{r_1}, \vec{r_2}) \rho_2(\vec{r_2}) dr_1 dr_2, \tag{1.32}$$

being $\rho_1(\vec{r_1})$ and $\rho_2(\vec{r_2})$, the electron density functions of both systems under consideration, and $\Omega(\vec{r_1}, \vec{r_2})$ is a separation operator. Most often Ω is chosen as the Dirac delta function $\delta(\vec{r_1} - \vec{r_2})$ reducing Eq. (1.32) to an overlap integral. The other most frequently used operator is r_{12}^{-1}, as it transform Eq. (1.32) to a Coulomb-type integral.

Quantum Similarity Index, QSI, is then defined by normalizing QSM:

$$QSI(\rho_1, \rho_2) \equiv \frac{\int_\Delta \rho_1(\vec{r}) \rho_2(\vec{r}) d\vec{r}}{\sqrt{\int_\Delta \rho_1^2(\vec{r}) d\vec{r} \int_\Delta \rho_2^2(\vec{r}) d\vec{r}}} \tag{1.33}$$

Considering QSM, an alternative way to define QSI is just:

$$QSI \equiv \frac{QSM_{12}}{\sqrt{QSM_{11} QSM_{22}}} \tag{1.34}$$

The main properties of QSI, apart from symmetry under exchange of distributions, are: (i) it ranges over the bounded interval $[0, 1]$ and (ii) the maximum value 1 is only reached for identical distributions.

When the selected operator is the overlap one, self-similarities can be considered as the square of the norm of the density function in the chosen metric. Self-similarity is a very important measure of localization, called also linear entropy [58], in contrast with the (nonlinear) Shannon entropy (both the linear and the Shannon entropies being closely related to Rényi entropies $R_q[\rho(\vec{r})]$ of order 2 and 1 [77], respectively, as $QSM_{11} = e^{-R_2}$ and $S = R_1$), or in other contexts, information energy and inverse participation number [124].

QSM_{11} and QSM_{22} are known as quantum self-similarity or quantum autosimilarity index (QAI) and are obtained, independently of the operator Ω, when comparing a system with itself. It is related to the electronic charge density occupation in the space, that is, it provides information on the charge concentration of the considered quantum object.

In recent works on neutral atoms [125] and ionization processes [82**?**] it has been shown the relevant role played by the linear momentum $\vec{p}$ as the basic variable of the one-particle momentum density $\Pi(\vec{p})$, not only in order to quantify the degree of similarity between two atomic systems but also to provide information on structural characteristics and shell-filling features. It is also shown, as previously known, that QSI associated to the position-space density $\rho(\vec{r})$ only provides information on how close the atoms are located at the periodic table. In order to get additional knowledge on the groups the system belongs to, shell structure and periodicity, it is necessary to take into account the momentum variable. It has been employed for the definition and description of quantum polyhedra [126], the discussion of their properties [127] and in reactivity studies in chemical processes [128].

1.3.6 Generalized quantum similarity index

A *Generalized Quantum Similarity Index* can be defined from QSI itself [129]. This index, as compared to the pioneering QSI, constitutes a one-parameter generalization modifying the number of functions to be compared and the weights associated to each of them:

$$QSI_q(\{\rho_i, \lambda_i\}_{i=1}^n) \equiv \frac{\int_\Delta (\rho_1^{\lambda_1}(\vec{r}) \dots \rho_n^{\lambda_n}(\vec{r}))^q d\vec{r}}{(\int_\Delta \rho_1^q(\vec{r}) d\vec{r})^{\lambda_1} \dots (\int_\Delta \rho_n^q(\vec{r}) d\vec{r})^{\lambda_n}} \tag{1.35}$$

with $\sum_{i=1}^{n} \lambda_i = 1$ and $0 < \lambda_i < 1$ for all $i = 1, \dots, n$. This measure does not depend on the normalization of any of the chosen densities $\rho_i(\vec{r})$ and belongs to the interval $[0, 1]$ for any $q > 0$. QSI_q constitutes a generalization of QSI measure in three different ways: (i) The number of probability densities considered is not necessarily two. QSI_q quantifies the total overlap among an arbitrary number of probability densities. (ii) The order q allows for the enhancement or diminishment of the contributions of different regions within the densities domain. (iii) The weights λ_i control the relative importance of each function in the comparison.

Being a so recent measure, QSI_q has not yet being employed in many different studies, but it will be discussed throughly in Chapter 4, where it would be used to analyze relativistic effects in neutral and ionized atoms.

Chapter 2

Fisher-like atomic divergences: Mathematical grounds and physical applications

In order to quantify the dissimilarity among two probability distributions, the concept of 'divergence' plays a fundamental role [92, 104, 105]. There exists a variety of definitions, within the frameworks of statistics and information theory, each one with its own characteristics which make them more or less appropriate according to the aims for performing a comparative study, as well as the reasons for considering those distributions relevant enough for the specific problems afforded.

The interest of this concept for physicists and mathematicians has grown progressively in the last few decades, giving rise to a diversity of successful applications within different fields. For illustration, let us mention the analyses of DNA sequences [8, 116, 130], or the management of digital images regarding their detection and registration [131], among many others.

There exists a strong resemblance between the meaning of the concepts 'divergence' and 'dissimilarity', the latter being the opposite to that of 'similarity'. Since the early eighties, the concept and measures of 'similarity' have played a relevant role within the same scientific fields where the divergence among distributions have been considered as an appropriate functional, being conceptually interpreted as a quantifier of 'how distant' the distributions considered are. In this sense, it is worthy to point out the use of molecular similarities in order to find a correlation, whenever possible, among the topological features of the electron cloud and the most relevant or experimentally accessible physical and chemical properties of the molecular systems [122, 132]. Additional fields where the concept of similarity appears relevant includes graph theory (where similarities in taxonomy or protein sequence homology are sought [20, 133]), and fuzzy set theory (where similarity is applied in e.g management, medicine or meteorology [134]). More recently,

the increasingly applied 'quantum information theory' (QIT) has given rise to a new field where some divergence measures appear relevant [109, 135]. Specially remarkable are the applications of the so-called 'Jensen-Shannon divergence' as measure of entanglement in a QIT framework [136], and also together with other measures of similarity [123, 137–142] in the analysis of many-electron systems [115, 125].

As we have seen in Chapter 1, a variety of divergence measures have been applied successfully to the study of many-electron systems. Most usually, measures of global character have been considered, because of their variety and the aims of their use. More scarce and recent are the studies by means of local-character divergence measures, with a higher sensitivity to differences at smaller scales than those of the global ones.

The focus of the present work resides in studying the differences, regarding their local behavior, among the electron charge densities of neutral atoms and/or singly-charged ions so as to link them with their physical and chemical properties in accordance with the Hohenberg and Kohn theorem [143]. In doing so, two different divergence measures of local character are employed, emphasizing their strengths and weaknesses for the aims here afforded. The results obtained from each measure, as well as the discrepancies among them, are justified on a physical basis.

Computations will be performed in both conjugated spaces, namely position (r) and momentum (p), by means of the accurate Near-Hartree-Fock wave functions of Koga et al [144–146], which will be employed in all the calculations of non-relativistic atomic densities in the following chapters. The reason underlying this interest is due to the Fourier transform connection between the conjugated r and p spaces, the momentum density containing relevant information on the valence region at small momentum p values, reaching its global maximum. In this manner we will explore in this case the valence region in contrast with the position space, where we mainly explore the core region.

For our present purposes, i.e. the analysis and comparison of neutral atoms and ionized species throughout the Periodic Table in terms of their one-particle densities in both conjugated position and momentum spaces, the domain of definition is the whole three-dimensional space. In this sense, it should be pointed out that (i) all analytical expressions given in the present work for an specific space (position or momentum) will be also valid in the conjugated one by replacing the corresponding variables and distributions, and (ii) for atomic systems in the absence of external fields, it is sufficient to deal with the spherically averaged densities $\rho(r)$ and $\gamma(p)$ defined over the non-negative real line $[0, \infty)$. The results presented in this chapter have been compiled into an article and published [147].

2.1 Numerical analysis with atomic one-particle densities

Both Fisher-like FD and JFD local measures, defined in Chapter 1 in Eqs. (1.30) and (1.31), respectively, are employed in this work, in order to analyze the divergence among different position- and momentum-space one-particle densities in atomic systems, interpreting the obtained results according to the main physical characteristics of the atoms considered, such as nuclear charge, valence subshells and their occupation numbers, or groups of the Periodic Table they belong to, among others. Additionally, FD and JFD are employed for the study of atomic ionization processes, by analyzing the divergence between the neutral and singly-charged cationic species. The results are interpreted, from a physical point of view, according to the ionization potential of the initial neutral system, as well as the quantum numbers of the electrons ejected and/or promoted.

2.1.1 Neutral atoms

Having in mind previous remarks, our first motivation is to look for an answer to the following question: how similar/different the Fisher-like divergences FD and JFD are? The term 'similar/different' regards both their range of values as well as their capability to provide structural patterns on the systems under comparison.

Accurate near-Hartree-Fock wave functions are employed [144–146], in order to compute the one-particle densities in position and momentum spaces, $\rho(\vec{r})$ and $\gamma(\vec{p})$ respectively. Atomic units (a.u.) are used throughout.

In Figure 2.1(a), the FD and JFD divergences between the one-particle densities of Boron (nuclear charge $Z = 5$) and all those of the neutral atoms with nuclear charges $Z = 1 - 103$ are displayed in position space, i.e. they are computed for the densities $\rho(\vec{r})$ of the corresponding systems at their ground state. Some comments are in order:

- Both curves reach the minimum value 0 at $Z = 5$, as should be expected.
- For systems from $Z = 5$ on, $FD_r(5, Z)$ and $JFD_r(5, Z)$ behave (roughly) linearly; however, their slopes are extremely different, being much higher for FD_r (around 6.8) than for JFD_r (around 0.12). Such a difference is quantified by a factor of (almost) 60 among them. This means that the values of FD_r are extremely sensitive to the differences between the nuclear charges of the systems involved, as compared to such a sensitivity for JFD_r.
- For the just discussed region $Z \geq 5$, a very slight structure (i.e. departure from linearity) can be observed at a very small scale.

A similar analysis can be done in momentum space, as displayed in Figure 2.1(b):

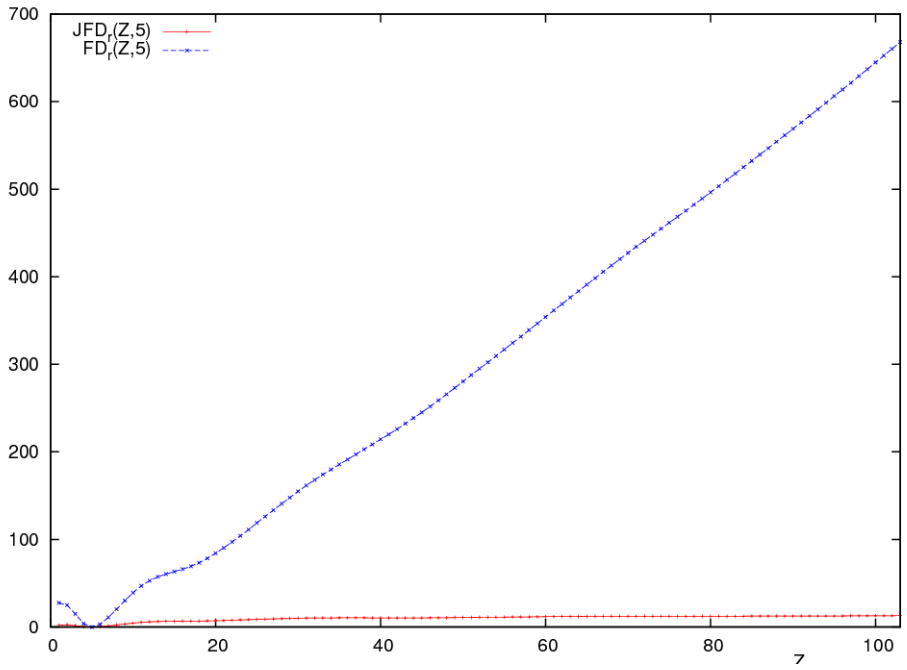

(a) Position space

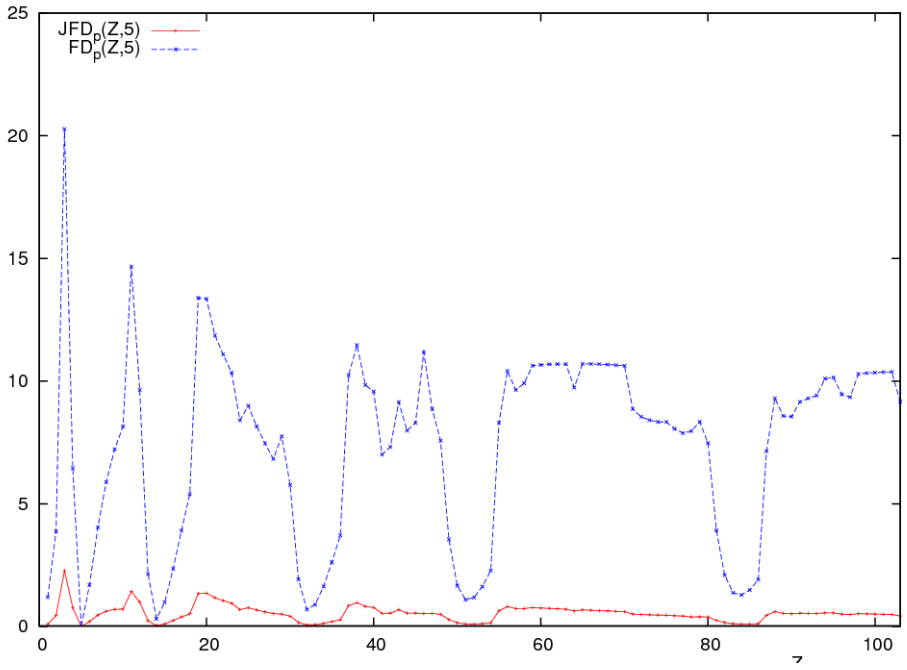

(b) Momentum space

FIGURE 2.1: Fisher-like divergences JFD and FD between Boron ($Z = 5$) and all neutral atoms with nuclear charges $Z = 1 - 103$, in (a) position and (b) momentum spaces. Atomic units are used.

- Now there is no linearity at all, neither for FD_p nor for JFD_p. The presence of numerous local extrema (apart from the absolute minimum 0 at $Z = 5$) is very apparent, much clearly in the FD_p curve than in the JFD_p one.

- At a first glance, there exists a structural similarity in what concerns location of extrema, but not systematically. The main minima correspond to Z values of systems around the atoms belonging to the same group of Boron (this fact occurs in both curves). As one should expect, and according to the interpretation of the Fisher-like divergences as measures of 'structural distance' among systems, lower divergence appears when comparing systems sharing relevant physical properties, such as shell-filling and location at the Periodic Table.

  This fact can be explained by taking into account that densities of both spaces reach their maximum values in/around their respective origins. And due to the connection existing between them, via the Fourier transforms of the wave functions the densities are computed from, the behavior of the momentum density in the surrounding of its origin is clearly conditioned by the behavior of the position-space density in the outermost region or, equivalently, that of the highest occupied orbitals in position space [22, 115, 125, 148, 149].

- On the other hand, let us distinguish the just discussed main/major extrema (with this subjective terminology we refer to those more apparent) from minor ones. Minor extrema are more numerous in FD_p than in JFD_p. Their appearance is associated to comparisons involving a system suffering from the so-called 'anomalous shell-filling' (i.e. having non-filled subshells apart from the valence one). In this sense, it is clear that the Fisher divergence FD_p is more sensitive to the presence of those anomalies as compared to JFD_p.

- Let us notice again the difference between the range of values displayed by FD_p and JFD_p, as also occurred in position space. The difference can be quantified by a 'mean scaling factor' (not so clearly as in position space), that is, the ratio FD_p/JFD_p provides a (roughly constant) value around 10 for all the systems here considered, and enhancing again the Fisher divergence FD_p with respect to the Jensen-Fisher one JFD_p.

Boron has been chosen as reference only for illustration. Similar conclusions are obtained from the analyses with any reference system within the whole set $Z = 1 - 103$ of ground state neutral atoms.

The strong differences among the shapes of the position- and momentum-space curves were analyzed in detail for the Fisher-Shannon divergence FD in Ref. [115], with similar aims to those of the present work. However, the same study remained, to the best of our knowledge, to be performed by using the recently introduced Jensen-Fisher divergence JFD, as done in the present work. The main conclusions in the aforementioned work on

FD [115] were obtained from a numerical analysis choosing a variety of reference systems, namely the whole group of noble gases. Nevertheless, in that work it was asserted that the conclusions arising having as reference system any one of the Periodic Table were exactly the same. In this sense, we have just discussed the differences among the FD and JFD divergences on the analysis of a unique system, namely Boron ($Z = 5$). As will be discussed later, choosing a different reference system with nuclear charge Z will make the behavior of the Jensen- Fisher divergence, mainly in position space (JFD_r), to strongly differ in the structural patterns within the regions $Z < Z'$ and $Z > Z'$, contrary to the case of FD_r.

To conclude the comparative discussion for the FD and JFD measures in both conjugated spaces, it is worthy to remark that the absolute scale of values in position space is much higher than in the momentum one. This comment applies to both measures. To justify this feature, we must remember that the results are provided through a measure of 'content of gradient', namely the Fisher information. In what concerns atomic systems, the exponential decrease of the position space density $\rho(\vec{r})$ makes its gradient to be much higher (in absolute value) than that for momentum space densities $\gamma(\vec{p})$, which are known to decrease much more slowly (with a p^{-8} long-range behavior [150]), having null derivative at the origin. So, changes in the values of the position space density are quite relevant, even for small shifts from a given location, as compared to those of the momentum space density.

Let us now focus on Figure 2.2, devoted to the comparison of the Jensen-Fisher divergence curves $JFD(Z, Z')$ as functions of Z for two different reference systems, namely Argon (nuclear charge $Z' = 18$) and Calcium ($Z' = 20$). The comparison is performed in position (a) and momentum (b) spaces.

Before analyzing the figures, let us recall that the systems chosen as reference ones (Ar and Ca) display extremely different physical properties, in spite of the closeness of their nuclear charges (18 and 20). This is due to their shell structure which, in fact, determines the group of the Periodic Table the atoms belong to: Argon is a noble gas (group VIIIA, of closed-shell systems), while Calcium is an alkaline-earth (group IIA, whose elements are characterized for having as valence subshell a completely filled 's' one). We could consider these two elements very similar, if similarity is understood in terms of closeness of their nuclear charges. However, they could be considered very different, if the comparison is focused on their physical properties and shell-filling.

In position space, Figure 2.2(a), it is evident that lower divergence values (or, equivalently, higher similarities) are attained when comparing systems with close values of their nuclear charges, independently of their shell structure. It is in this sense that the divergence in position space appears related to the closeness of the systems' nuclear charges, rather than to the similarity of their shell structures. The fact of dealing with a pair of systems with similar values of their nuclear charges makes the corresponding

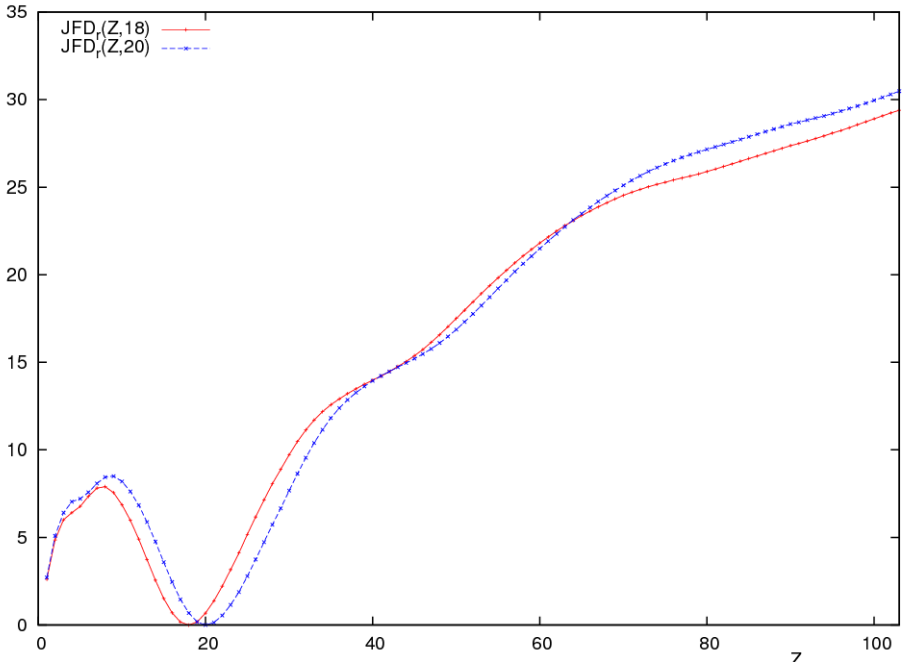

(a) Position space

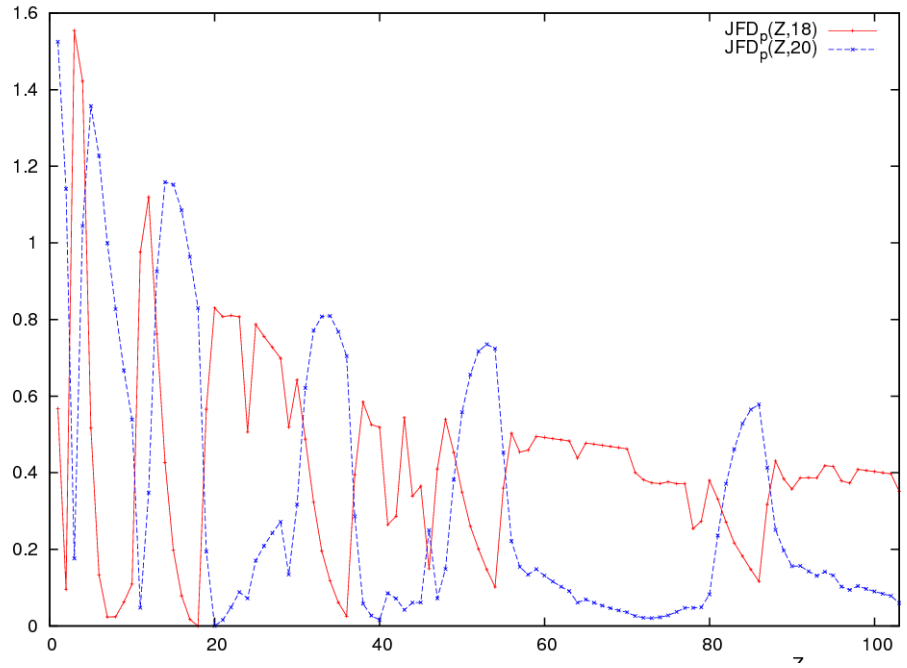

(b) Momentum space

FIGURE 2.2: Jensen-Fisher divergences JFD of Argon and Calcium (nuclear charges $Z = 18, 20$ respectively) with respect to all neutral atoms with nuclear charges $Z = 1 - 103$, in (a) position and (b) momentum spaces. Atomic units are used.

curves to be similar also. On the opposite, the momentum space analysis, Figure 2.2(b), reveals the very different structure of both curves. Such an structure has its grounds in the shell-filling patterns, exactly as described for Boron when discussing the previous Figure 2.1(b). Main local minima for both Argon and Calcium appear around the location of systems belonging to their respective groups, namely noble gases an alkaline-earths. Minor extrema are determined, in both cases, when performing a comparison with a system of anomalous shell-filling.

To illustrate the just mentioned relevance of the shell structure in the display of local extrema, let us consider the local minima or Argon ($Z' = 18$). Most of them can be classified as follows:

- Systems belonging to the same group of Argon at the Periodic Table: $Z = 2, 18, 36, 54, 86$ (most of the noble gases, with the only exception $Z = 10$).
- Systems displayed also as minima of the curve for Calcium: $Z = 29, 90, 93, 97$. All belong to the set of the so-called 'anomalous shell-filling' systems. For $Z = 29$ an electron is promoted from the inner $4s$ subshell to the valence one $3d$. Something similar happens with the other systems, now with the promotion from $5f$ to $6d$ subshells.
- Local maxima of the curve for Calcium: $Z = 41, 44, 46$. We deal again with anomalous shell-filling systems, characterized by the promotion of electrons from the subshell $5s$ to the $4d$ one.
- A few additional minima for Argon include the anomalous systems $Z = 24, 57, 78$, with the following respective inner-subshell to valence-subshell promotions: $4s$ to $3d$, $4f$ to $5d$ and $6s$ to $5d$.

As compared to the results arising from the study in terms of the Fisher divergence FD, provided in Ref. [115] for the same reference systems, comments and conclusions are roughly those of the previous paragraphs. The main differences between the studies based on FD and JFD are given below:

- The most important difference regards the position-space analysis. While $FD_r(Z, Z')$ as function of Z for any fixed Z' displays an unimodal shape [115] (i.e. it is an increasing function for $Z \geq Z'$, while a decreasing one for $Z \leq Z'$), the shape of the $JFD_r(Z, Z')$ curves is bimodal (with a pair of local extrema, always ordered as maximum-minimum). The increasing character of $FD_r(Z, Z')$ for higher Z values remains, while the monotonicity for lower ones is lost.

  The reason for finding those so different behaviors arises from the definition of FD in terms of quotients of densities, and JFD in terms of the arithmetic mean. Let

us keep in mind the exponential short-range behavior of the densities, governed by the nuclear charge as $\rho(r) \sim \exp(-2Zr)$. All integrals defining both FD and JFD get their values mainly from the contribution of the surround of the origin $r = 0$. The quotient of exponentials provides an integrand with, near the origin, behaves as

$$\left| \vec{\nabla} \ln \frac{e^{-2Zr}}{e^{-2Z'r}} \right|^2 = 4(Z - Z')^2, \tag{2.1}$$

that is, a parabola centered at $Z = Z'$ where it reaches its minimum value zero.

On the other hand, dealing with a sum of densities when one of them has values near the origin much higher/lower than the other, makes their arithmetic mean to contain a term almost negligible as compared to the other, namely

$$\frac{\rho_1 + \rho_2}{2} \approx \frac{\rho_1}{2} \quad \text{if} \quad \rho_1 \gg \rho_2. \tag{2.2}$$

For a normalized-to-unity exponential $\rho(r) \sim \exp(-2Zr)$, the Fisher information is $I(\rho) = 4Z^2$. So,

$$JFD(\rho_1, \rho_2) = \frac{1}{2}\left[I(\rho_1) + I(\rho_2)\right] - I\left(\frac{\rho_1 + \rho_2}{2}\right) \tag{2.3}$$

$$= \frac{1}{2}[4Z_1^2 + 4Z_2^2] - I\left(\frac{\rho_1 + \rho_2}{2}\right). \tag{2.4}$$

Let us consider integer parameters, ordered as $Z_1 > Z_2 \geq 1$ without loss of generality. For fixed Z_2, the limit $I\left(\frac{\rho_1 + \rho_2}{2}\right) \to 2Z_1^2$ as $Z_1 \to \infty$ is obtained and, consequently with Eq. (2.3), $JFD(\rho_1, \rho_2)$ approaches zero as far as Z_1 becomes larger for fixed Z_2.

It is observed in Figure 2.2(a) that for (roughly) Z a half of $Z' = 18, 20$ the curves invert their monotonic behavior, reaching progressively lower values (i.e. approaching 0) as the quotient Z_2/Z_1 becomes smaller.

This means that the difference of nuclear charges is not enough to justify the bimodality of JFD_r, contrary to the FD_r case (see comments on Figure 2.2(a)). Let us take into account that the arithmetic mean of two quantities, with one of them much higher than the other, is roughly a half of the highest one. Consequently the other is almost negligible in computing the arithmetic mean appearing in the definition of JFD_r, a quantity which, in this context, becomes extremely small. Such is not the case of FD_r, defined in terms of quotients instead of means. In fact, differences in the order of magnitude of two quantities are emphasized in the value of their quotient, i.e. just the opposite situation as discussed for their arithmetic mean.

- In spite of the aforementioned comment on the 'structural similarities' of FD_p and JFD_p in momentum space, based on the presence of a number of local extrema, it is remarkable that (i) while most relevant minima corresponding to systems in the same group of the Periodic Table are displayed by both measures, (ii) some of the minor extrema in FD_p are lost in JFD_p, such as e.g. the curve for Argon at $Z = 64$, a system with an electron promoted from $4f$ to $5d$. Something similar happens for systems $Z = 78, 91, 98$, displayed as local maxima in the FD_p curve for Calcium, but not in the JFD_p one.

- The scale employed in both Figures 2.2(a) and 2.2(b) (of JFD_r and JFD_p respectively) is lower than the corresponding ones (i.e. with identical reference systems to those of JFD) for FD_r and FD_p (see Figs. 2a and 2b, respectively, of Ref. [115]) by a factor around 15. So, for a given system (in any space), FD is more than one order of magnitude higher than JFD.

Let us now pay attention to Figure 2.3. We choose the set of noble gases ($Z' = 2, 10, 18, 36, 54, 86$) as reference systems. Each curve corresponds to the divergence of one of those systems with respect to all neutral atoms, with nuclear charges ranging from $Z = 1$ to 103. The comparative analysis is based on the divergence of the corresponding position space one-particle densities. The divergence measures employed are the Fisher (FD) and the Jensen-Fisher (JFD) ones, in Figs. 3a and 3b respectively.

Most comments on these figures have a strong resemblance with those of Figure 1a, where the same comparison was carried out for Boron. The most apparent feature observed in Figure 2.3(a) can be summarized with a unique term: unimodality. For any of the atoms considered (specified by its nuclear charge Z'), the function $FD_r(Z, Z')$ vanishes at $Z = Z'$ (absolute minimum and unique extremum), and its value progressively increases as does the distance between Z and Z'. In spite of the absence of local extrema (apart from the null one), some changes of curvature are appreciated in all curves. As previously mentioned, the unimodality is justified by the so strong relevance of the core region as compared to the valence one. Effects arising from shell-filling patterns are not strong enough to produce the presence of local extrema, but only the aforementioned regions of curvature.

As also observed in Figure 2.2(a) for Argon and Calcium, bimodality is a systematic feature in all JFD_r curves of noble gases apart from Helium (Figure 2.3), as also happens with the rest of atoms in the Periodic Table for any $Z' \geq 3$. A reasoning for the display of a low Z region with an unexpected behavior, as compared to that of the Fisher divergence FD_r, was provided above on the basis of a 'masking effect' when dealing with pairs of systems with nuclear charges distant enough. The bimodality implies the appearance of a maximum as the first local extremum, whose location moves forward if the reference system's nuclear charge Z' increases. For illustration, while the maximum for Neon ($Z' = 10$) appears at $Z = 4$, the maximum for Radon ($Z' = 86$) shifts up to $Z = 27$.

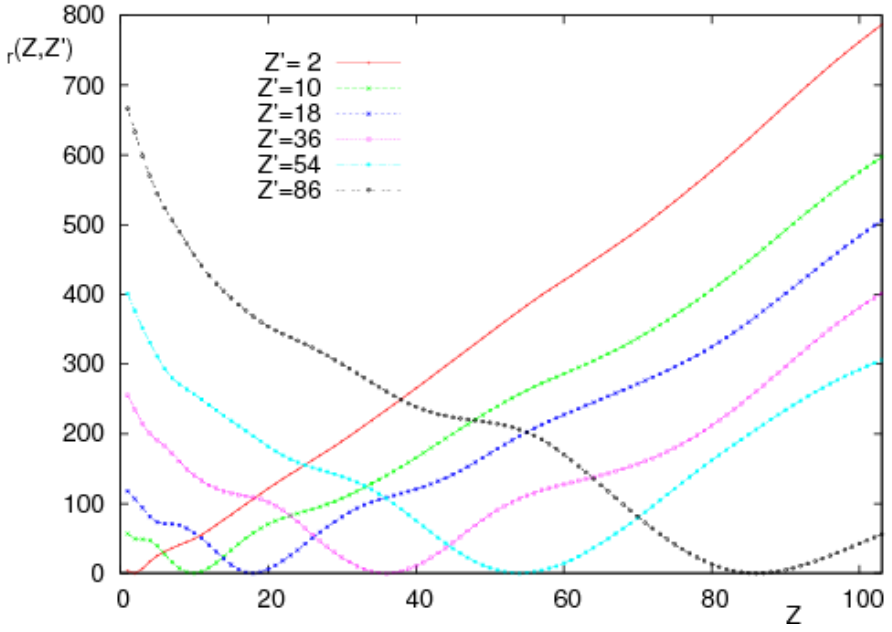

(a) Fisher divergence FD_r

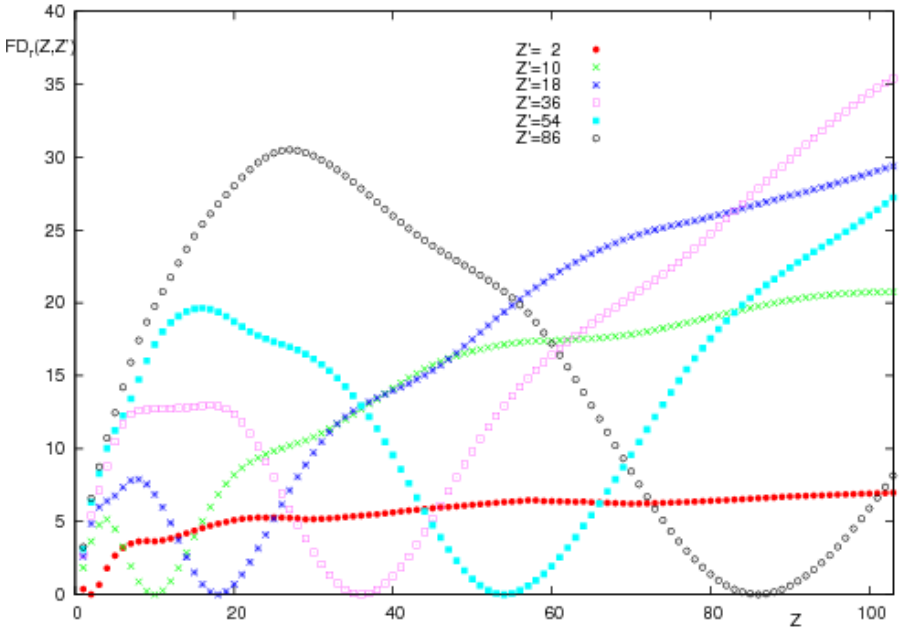

(b) Jensen-Fisher divergence JFD_r

FIGURE 2.3: Position-space divergence of each noble gas with respect to all neutral atoms with nuclear charges $Z = 1 - 103$, by using (a) the Fisher divergence FD_r, and (b) the Jensen-Fisher divergence JFD_r. Atomic units are used.

This fact supports the above reasoning: for heavier reference systems, it is necessary to perform the comparison, by means of JFD_r, with heavy enough elements in order to deal with a couple of systems with values of their charge densities of similar order of magnitude, so avoiding a negligible contribution of the smallest one to their arithmetic mean, with the consequences on the interpretation of JFD_r previously discussed.

The request of dealing with systems having close enough nuclear charges, in order to get an appropriate physical interpretation of JFD_r, does not apply to FD_r. If we think on the Fisher-like divergences as local measures of 'dissimilarity' regarding the structure of atomic systems, it is much better to consider divergences defined in terms of quotients instead of sums, as explained previously.

To conclude the discussion of the results for noble gases in position space, as displayed in Figure 2.3, let us remark again the extremely different ranges of values the divergences FD_r and JFD_r belong to, up to a factor around 23 among them.

A similar analysis to that just performed for the Fisher-like divergences of noble gases in position space can be carried out in the momentum one. In doing so, let us observe Figure 2.4, where the results are displayed for the Fisher (a) and Jensen-Fisher (b) divergences, FD_p and JFD_p respectively. The family of noble gases has been chosen again, for illustration, as reference systems in the comparative processes. Before going into the detailed analysis, let us notice the existence here again of a proportionality factor among the divergence ranges of Figure 2.4(a) and 2.4(b), with a value around 11 now in momentum space.

Focusing on the structure of the different curves, according to their local extrema, some comments are in order:

- There exists a set of 11 elements displayed as local minima in all curves, independently of using FD_p (as in Figure 2.4(a)) or JFD_p (as in Figure 2.4(b)). These atoms are $Z = 2, 24, 41, 44, 46, 54, 57, 78, 86, 90, 97$. Apart from the noble gases $Z = 2, 54, 86$, the other atoms belong to the anomalous shell-filling class. Their anomalies were described when discussing Figure 2.2(b).

- Other noble gases are displayed as minima in some of the six curves, but not systematically. Such is the case of $Z = 18, 36$, appearing (for both divergences) as minima in four curves, those of the lighter ones $Z' = 2, 10, 18, 36$, their appearance failing for $Z' = 54, 86$.

- The anomalous systems $Z = 29, 64$ are detected by the Fisher divergence FD_p within all the six curves, but the detection is successful only in (i) four of the JFD_p curves of noble gases for $Z = 64$, (ii) five curves for $Z = 29$. Let us point out: (i) the absence of $Z = 64$ as an extremum for $Z' = 18, 86$ and that of $Z = 29$ for the curve $Z' = 86$ in the Jensen-Fisher case, and (ii) the anomaly of system $Z = 64$ is exactly the same as that of $Z = 57$, namely the promotion of an electron from the $4f$ subshell to the $5d$ one. In this sense, the system 'gets' to keep the $4f$ subshell half-filled. On the other hand, the anomaly of $Z = 29$ makes the system to have a completely filled valence subshell $3d$.

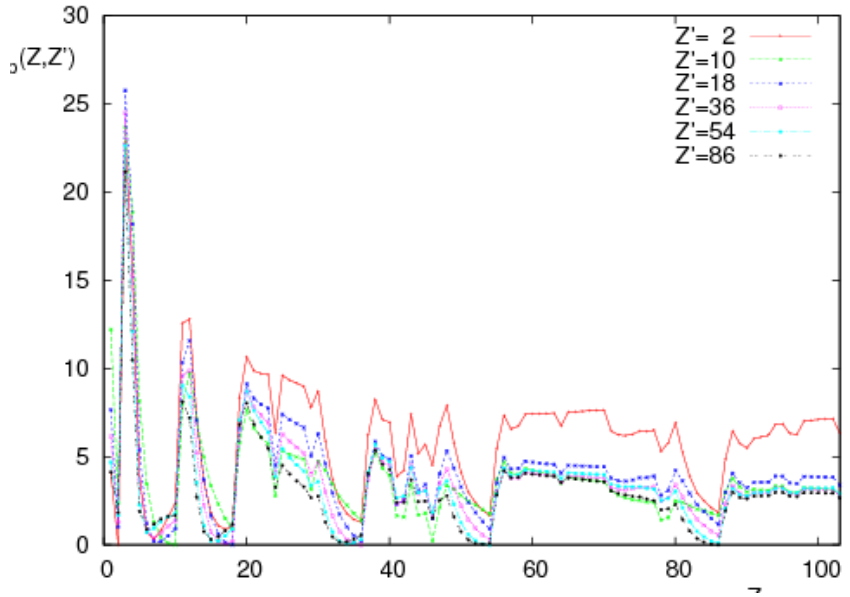

(a) Fisher divergence FD_p

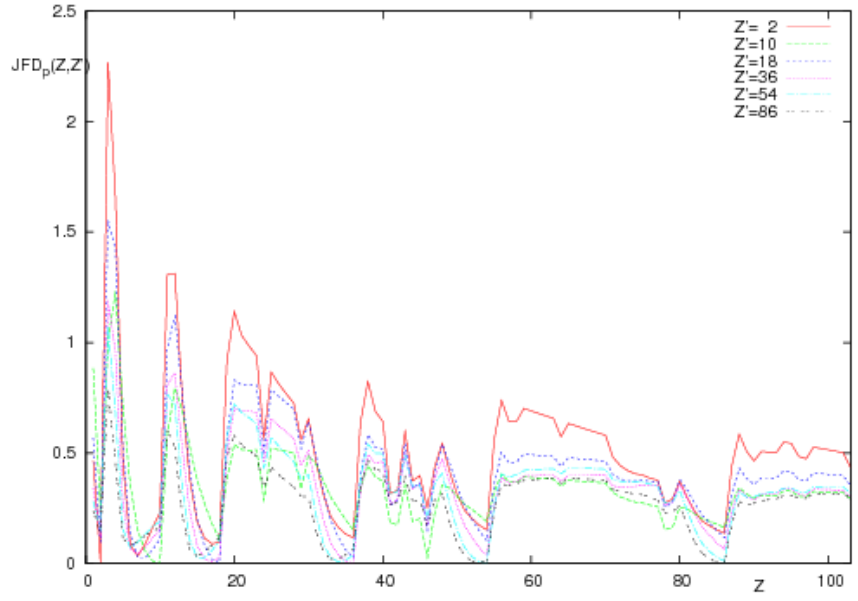

(b) Jensen-Fisher divergence JFD_p

FIGURE 2.4: Momentum-space divergence of each noble gas with respect to all neutral atoms with nuclear charges $Z = 1 - 103$, by using (a) the Fisher divergence FD_p, and (b) the Jensen-Fisher divergence JFD_p. Atomic units are used.

- Within the first set (without including noble gases), there are other systems which anomaly makes them to have a half-filled ($Z = 24$) or a completely filled ($Z = 46$) valence subshell.

It is concluded, from the above numerical analyses and discussions, that the Fisher divergence FD is more appropriate than the Jensen-Fisher one JFD, at least within

the context considered in this work: to get as much as possible information regarding atomic shell structure, by means of divergence functionals of local character.

2.1.2 Ionization processes

The ionization of a neutral atom (N), giving rise to a singly-charged cation (C), is a process which modifies the one-particle densities of the initial system, in both position and momentum spaces, namely the functions $\rho(\vec{r})$ and $\gamma(\vec{p})$. In order to quantify the extent of those modifications in what concerns the local character, the Fisher and Jensen-Fisher divergences appear as appropriate candidates. Let us denote as $FD(NC)$ and $JFD(NC)$ the Fisher like divergences for a pair neutral-cation (NC), with a subscript r or p to specify the conjugate space we are dealing with.

From a physical point of view, the most relevant quantity in the description of the aforementioned ionization processes is the experimentally accessible 'atomic ionization potential' (AIP), which accounts for the 'effort' required to provoke the ejection of an electron from the neutral atom.

A question afforded in Ref. [151] was the following: to which extent the NC divergence and the AIP values are related one with each other? In that work, the Jensen-Shannon (JSD) and the Fisher (FD) divergences were employed, in both conjugate spaces also.

The main conclusion regarding the connection between $FD(NC)$ and AIP required to distinguish two different kinds of ionization processes: (i) those where the electron is ejected from a 's' subshell, namely with angular momentum quantum number $l = 0$, and (ii) electrons ejected from non 's' subshells, namely 'p' or 'd' ones (with $l = 1, 2$ respectively). In the analysis of the resemblance between the appearance of local minima of the AIP and local maxima of FD, the results can be summarized as follows:

- There exists a one-to-one correspondence among all minima (eight) of AIP and all maxima of $FD(NC)$ when dealing with 's' ejections, independently of the space considered for the divergence.
- The same applies to 'p' or 'd' ejections (seven minima of AIP) when considering the position space divergence $FD_r(NC)$.
- However, for 'p' or 'd' ejections none of the momentum space $FD_p(NC)$ maxima belong to the set of AIP minima.
- Final conclusion: there exists a perfect correlation among the structure of AIP and $FD(NC)$ for the 's' processes. The same is true for 'p' and 'd' ejections if restricting FD to the position space, but there is no correlation at all in the momentum one.

ht

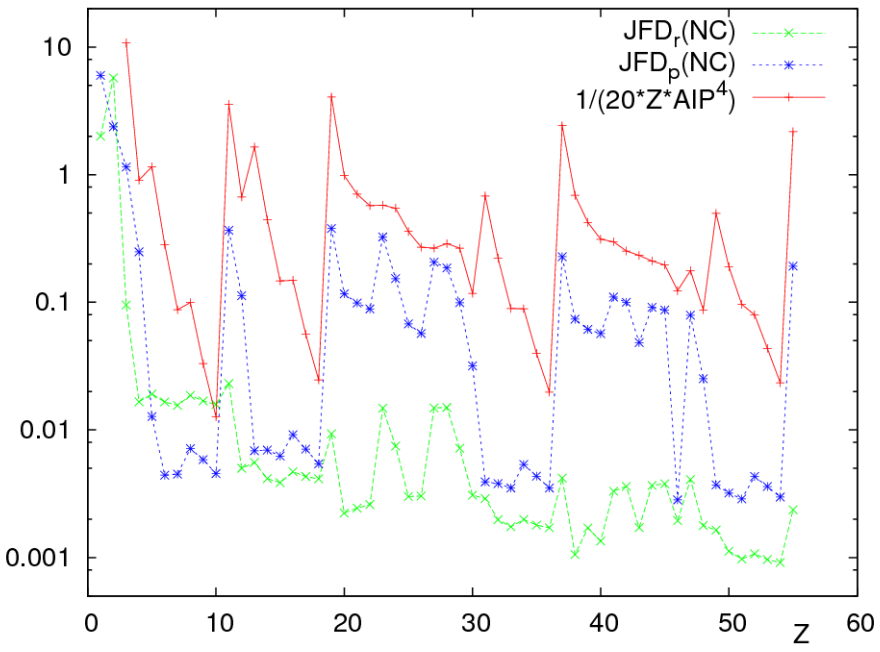

FIGURE 2.5: Position- and momentum-space Jensen-Fisher divergences $JFD(NC)$ between each neutral atom (N) and its singly-charged cation (C) with nuclear charges $Z = 3 - 55$, and a qualitative fit in terms of the atomic ionization potential (AIP) of the neutral atom. Atomic units are used.

Taking into account the main aim of the present work, we look for a possible connection of the Jensen-Fisher divergence $JFD(NC)$ with the atomic ionization potential AIP. If such a correlation exists, the analysis of how strong/slight is, as compared to the just discussed one for $FD(NC)$, should be carried out. In order to have a first feeling, let us have a look at Figure 2.5, where $JFD(NC)$ curves are displayed for both conjugate spaces, together with a simple function of AIP. This function has been considered in order to better compare all functions. This functional dependence allows to perform easily an inversion of maxima and minima, a scaling and a shift. In this way, it is observed, at a first glance, a similar structure for the three curves.

Let us now analyze in detail the location of extrema. Following the procedure of distinguishing two different kinds of ionization processes, the differences and similarities between $FD(NC)$ and $JFD(NC)$, as well as the interdependence with AIP, are described below:

- The aforementioned one-to-one correspondence between AIP and $FD(NC)$ for 's' ejections remains when dealing with $JFD(NC)$ instead. This comment applies for both conjugate spaces.

- For 'p' and 'd' ionizations, the position space $JFD_r(NC)$ displays the five maxima $Z = 5, 8, 13, 16, 34$, but not $Z = 31, 49$ to complete the list of AIP minima for these processes. Let us remember that $FD_r(NC)$ displayed all of them.

- However, in momentum space the situation is the opposite: while $FD_p(NC)$ displayed none of the AIP minima, $JFD_p(NC)$ is able to detect the systems $Z = 8, 16, 34$ enclosed in the list of AIP minima. Also $Z = 14$ appears together with the three previous systems, but $Z = 13$ is the closest one in AIP.

The above observations can be understood by taking into account the atomic shell structure. For illustration: let us consider alkalines, which have a unique electron in the outermost subshell. They have low AIP values. Ionizing a neutral alkaline (initial system, N) provides the system to transform into a singly-charged cation (final system, C). The outermost subshell of the initial system becomes empty, and the outermost subshell of the final system is very different (regarding both its characteristic quantum numbers as well as its occupation). These differences are revealed by the NC divergence: a so relevant difference between systems N and C, regarding their respective shell structures, make the divergence to reach higher values, as compared to those ionization processes provoking not so relevant changes in the atomic shell structure.

Similar comments apply to systems for which the ionization provokes the disappearance of a subshell, in spite of not being the outermost one. Such is the case of many systems with anomalous shell-filling [151].

Contrary to the study in previous sections, the Jensen-Fisher divergence $JFD_p(NC)$ in momentum space displays values much higher (around 100 times) than those of the position one. This is due to the effect of the ionization in the outermost region, being almost negligible in the surround of the nucleus (both systems have identical nuclear charge Z). The sensitivity in position space is mainly due to the core, while in momentum space to the valence region.

To conclude the divergence analysis of ionization processes, let us mention the existence of few additional minor maxima of $JFD(NC)$ which are not displayed as minima of AIP. Among them, the anomalous shell-filling systems $Z = 41, 42, 44, 45$ are included, all characterized for the promotion of an electron of the 5s subshell to the 4d one.

2.2 Conclusions

The Fisher and the Jensen-Fisher divergences, built up from the Fisher information densities, are well-defined functionals, from a mathematical point of view, in particular regarding characteristic properties of a 'distance among distributions', namely non-negativity, symmetry and minimum null value only for identical distributions.

However, their level of usefulness for one-particle densities in position and momentum spaces, their behavior in terms of the nuclear charge throughout the atomic Periodic Table as well as their applications in the study of ionization processes appear to be

very different, most usually in favour of the Fisher divergence FD as compared to the Jensen-Fisher JFD one.

The definition of FD and JFD in terms of quotients and sums of densities, respectively, is an essential point to justify the results here obtained. In position space, the quotients enhance differences on the decreasing exponential rate, while the sums or means mask the contribution of one density with respect to the other when dealing with systems of different enough nuclear charges. This fact provokes the well-known unimodality of FD_r to be replaced by the bimodality of JFD_r.

The above mentioned masking makes the highly structured curves in momentum space to lose some of the local extrema of FD_p in passing to JFD_p. Such a loss affects the minor peaks, mostly corresponding to anomalous shell-filling systems, while the main peaks (corresponding to systems belonging to the same group of the Periodic Table) remain in both measures. Specially relevant is that reference systems with similar nuclear charges display also similar curves in position space, but not necessarily in the momentum one, where the essential property for getting a higher or lower similarity is the shell-structure of the systems under comparison.

The main peaks of both divergences are also found in the study of ionization processes, in which a neutral atom loses an electron, giving rise to a singly-charged cation. The well-known correspondence among FD local maxima and the local minima of the ionization potential is also found for JFD as far as the electron be ejected from a 's' subshell'. For other kind of subshells ('p' or 'd') the results depend on the space considered. While JFD_r loses some of the FD_r maxima, the opposite occurs in momentum space. This fact is justified on the basis of the relevance of core and valence regions, the latter being extremely sensitive to the change of electrons, while in the former being dominant the (unaltered) nuclear charge.

Chapter 3

Jensen-Shannon and Kullback-Leibler divergences as quantifiers of relativistic effects in neutral atoms

The study of the relativistic effects on the atomic densities and related functionals has been focus of attention of many researchers, not only for hydrogen-like atoms but also for many-electron systems. In particular, as the number of electrons in the atom increases, and its nuclear charge Z as well, relativistic effects become more important and have to be taken into account to understand atomic or molecular properties, e.g. the asymptotic behaviour of atomic ionization potentials for large Z or bond lengths and molecular geometries [152, 153]. Some other important atomic and molecular properties, such as dipole polarizabilities, electron affinities, excitation energies, dipole moments or correlation and structure effects are the object of recent studies and modern computations in the relativistic framework [154, 155]. In order to take into account the relativistic effects, the Dirac-Fock equation must be solved, enclosing the Schrödinger one as the nonrelativistic limit. Solving the Dirac equation is a much more difficult task compared to that for the Schrödinger case, requiring the use of sophisticated models and/or numerical routines. Its solution allows us to determine the wave functions in the conjugate space, as well as the position and momentum one-particle densities, $\rho(\vec{r})$ and $\gamma(\vec{p})$ respectively. These densities play a relevant role within the so-called 'information-theory', allowing an interpretation of many density functionals in terms of physical and chemical properties in many-electron systems. In doing so, a variety of tools and magnitudes have been considered in the literature. Some density functionals deserve special attention, such as the Shannon entropy [3] and the Fisher information [30] among others. Composite functionals defined, most usually, in terms of (at least) one of the aforementioned

Shannon and Fisher quantities have been studied, both theoreticly and numerically, in recent years. They belong to the class of 'complexity measures', enclosing different definitions in order to quantify a so subjective concept as complexity is (see Ref. [156] and references therein). Furthermore, exploring quantitatively the level of similarity/dissimilarity between two different systems in terms of meaningful divergence measures appears actually as a very interesting field. Different information-theoretic divergence measures [157] have been recently applied in many areas including statistical pattern recognition, quantum information theory, or analysis of multielectronic systems. Last case includes the particularly important aim of analyzing the similarity and discrepancy among quantum-mechanical or multielectronic models and systems, such as atoms, ions, or relevant parts of them, throughout the Periodic Table [151, 158].

A pioneering attempt to analyze the relativistic effects on the atomic densities was carried out by studying the charge density $\rho(\vec{r})$ of hydrogen-like systems at their ground and excited states, in e.g. Ref. [159], with successful results. In that work no density-functionals were considered, but the density itself, in position space. Much more recent are the studies of relativistic effects on density functionals. Among them, the Fisher information for the charge density of ground-state neutral atoms [23] and the position- and momentum-space densities of hydrogen-like systems for arbitrary states [160], provide also interesting conclusions. Within Ref. [160] many other quantities are considered in both conjugated spaces: Shannon and Rényi entropies, variance, relative entropy, and shape complexity, all of them only for ground-state hydrogen.

Regarding other comparative measures of recent interest, works on the quantum similarity index (QSI) deserve to be mentioned. Let us remark the study of atomic QSI in both position and momentum spaces provided in Ref. [161], where that functional is applied to different systems and/or states separately for the Schrödinger and the Dirac cases. Using the same functional, a direct comparison between the relativistic and nonrelativistic densities for a variety of atoms was provided in a pioneering work [98], by considering a functional dependence on the respective charge densities (i.e. only in position space).

The main aim of this work is to study the relativistic effects in atomic systems along the Periodic Table, by means of their one-particle densities in position space. For this purpose we compute the Kullback-Leibler divergence [88] KL, (also referred as 'directed divergence' or 'information gain'), and the so-called Jensen-Shannon divergence JSD [92].

The KL measure is perhaps the most important nonsymmetric divergence measure of information theory and has been extensively studied and applied in a great variety of fields [8, 130, 162]. The JSD measures in fact the statistical dependence between an arbitrary number of probability distributions and there are some important reasons why researchers choose JSD as a measure of divergence, among them: (i) it is

a symmetrized and smoothed version of the KL and hence it shares its mathematical properties and intuitive interpretability, (ii) it has significance in the framework of statistical physics, information theory, and mathematical statistics [11], (iii) JSD is related to other information-theoretical functionals (being a special case of the Jensen difference [95] and the Csiszár divergence [91]) and it is the square of a metric [163]. Due to the aforementioned properties, the JSD can be applied within a wide variety of fields. Its use in the framework of quantum information theory [135, 163] or in the study of multielectronic systems [115, 151, 158] is very recent. In addition, the JSD divergence has been employed as measure of distinguishability between mixed quantum states. Distances between quantum states play a central role in quantum information theory. An appropriate measure of distance is the quantum JSD ($QJSD$) between quantum states. Majtey et al. [135, 163] studied this distance as a geometrical measure of entanglement and applied it to different families of states. The results presented in this chapter have been compiled into an article and published [164].

The relativistic calculus used on this chapter were obtained from the MCDHF2005 software package [165]. This numeric tool allowed us to compute different density function of relativistic atomic systems in position space, for both ground and excited states. A more detailed discussion of the methods used by the program can be found in [166, 167]. We will be using this software package in all the following chapters in order to calculate all the relativistic densities needed.

3.1 Quantifying relativistic effects: numerical analysis of atomic divergences

It is well-known that the relativistic effects are more apparent when dealing with heavier quantum systems. Such is the case, for instance, of neutral atoms with large nuclear charge Z. Most studies on relativistic effects have dealt with the energy spectra, various expectation values and the structural properties of the charge density. Among the last ones, it is worthy to remark the contraction of the radial density profile $D(r) = r^2\rho(r)$ towards the origin.

The just mentioned well-known contraction of $D(r)$ belongs to the class of 'qualitative effects', analyzed in detail by comparing the respective plots of the Hartree-Fock and Dirac-Fock radial densities. However, it is desirable to have at our disposal appropriate quantifiers of differences between these densities.

This problem has been considered in the past within the especialized literature, by looking for appropriate comparative functionals $F(\rho_S, \rho_D)$, so providing a quantitative measure of similarity or disimilarity among the Schrödinger and Dirac distributions, ρ_S and ρ_D respectively. To the best of our knowledge, the main functionals considered

with such an aim are (i) the so-called 'quantum similarity measure' (QSM), an overlap integral of both densities, and (ii) the 'quantum similarity index' (QSI), defined in terms of QSM together with a normalization factor. The main properties which makes QSI an appropriate measure of similarity are: (i) the values of $QSI(\rho_1, \rho_2)$ are constrained to the bounded interval $[0, 1]$ for arbitrary denity functions ρ_1 and ρ_2, and (ii) the maximum value $QSI(\rho_1, \rho_2) = 1$ is reached only in the case $\rho_1 = \rho_2$.

In order to compute the above functionals, say $F(\rho_S, \rho_D)$, first we need appropriate packages to build up both ρ_S and ρ_D. In the Schrödiger case, the well-known near-Hartree-Fock wave functions of Refs. [144, 145] are employed, with a recognized accuracy as discussed in detail within the above references. The expansions on Slater-type basis sets, extremely accurate as compared to numerical Hartree-Fock wave functions, provide us with analytical expressions of ρ_S for any system. On the other hand, the output of the multiconfigurational Dirac-Fock package MCDFGME V 2005.10 [165] consists of a tabulation of the respective radial densities, arising from ρ_D, onto a log-like mesh grid of points, with controllable fineness.

Once the densities are computed, it is necessary to perform a variety of numerical integrations to determine any of the functionals $F(\rho_S, \rho_D)$. First, we should worry about the accuracy of those integrations, in order to get realistic conclusions from the results obtained. To check the above accuracy, let us consider e.g. the divergence $KL(f_0, f_\epsilon)$ between hydrogen-like functions $f_\epsilon(r) = e^{-2(1+\epsilon)r}$, where ϵ plays the role of a 'perturbative' parameter. It is worthy to remark, from the analytical expression of this KL, that (i) it is proportional to ϵ^2, (ii) it vanishes for $\epsilon = 0$, and (iii) extremely low KL values are obtained for ϵ small enough. The numerical computation of KL, over the same grid as that employed for atomic systems, provides values whose relative deviations from the analytical ones are below 5×10^{-6}, for ϵ within the range $[0, 1]$. This probe provides us with a high confidence, in what follows, on the accuracy of the numerical results.

For the distributions considered in the present work, the functional $QSI(\rho_S, \rho_D)$ has been studied in the literature, mostly attending to its dependence on the nuclear charge Z for all ground-state neutral atoms throughout the Periodic Table. It is found a monotonically decreasing behavior of QSI with Z (see Figure 3.1), so providing as main conclusion that 'similarity decreases as far as considering heavier atomic systems'. Let us remark that higher similarities between ρ_S and ρ_D are interpreted as 'less relevant relativistic effects', and conversely. Nevertheless, notice the extremely narrow interval $[0.985, 1]$ of QSI values displayed in Figure 3.1, even for a system as heavy as $Z = 103$.

So, $QSI(\rho_S, \rho_D)$ does not provide any evidence of other atomic properties apart from the just mentioned nuclear charge Z, such as e.g. shell structure or location of the systems at the Periodic Table. Subsequent studies, based on QSI also, allowed an interpretation of the displayed results attending to shell-filling patterns. In doing so, main applications

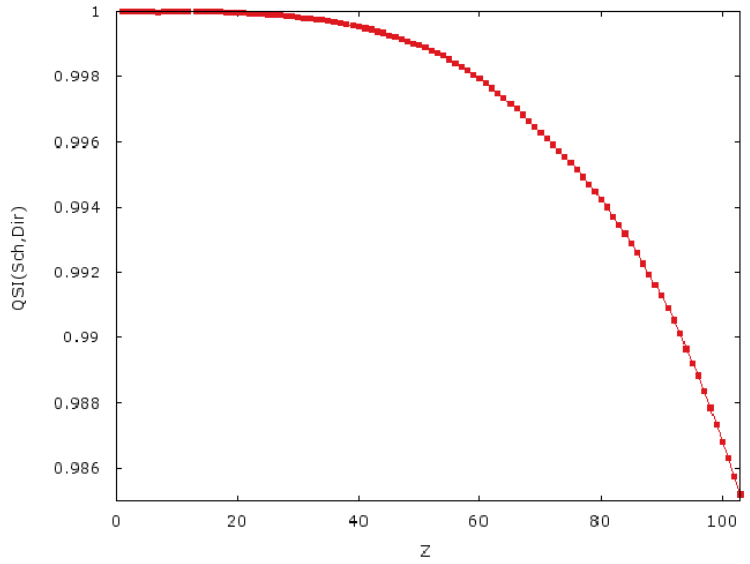

FIGURE 3.1: Quantum similarity index $QSI(Sch, Dir)$ between the Schrödinger (nonrelativistic) and Dirac (relativistic) one-particle densities for ground-state neutral atoms with nuclear charge $Z = 1 - 103$. Atomic units (a.u.) are used.

which deserve to be mentioned are those in the conjugate space, namely QSI between the momentum-space one-particle densities.

Turning out to the main aims of the present work, and considering Schrödinger-Dirac divergences as measures of dissimilarity between the relativistic and nonrelativistic distributions, one should expect a monotonically increasing behavior of the divergence as long as the nuclear charge Z increases. This fact has been recently studied in detail for variety of hydrogenic quantum states [168], by using divergence functionals, as a subsequent analysis of a previous work based on complexity measures [169]. For the many-electron systems here considered (i.e. ground-state neutral atoms), other features such as e.g. the shell-filling patterns, are also relevant in JSD and KL as functions of Z, as will be shown in this section.

Let us denote as JSD(Sch,Dir) and KL(Sch,Dir) the Jensen-Shannon and Kullback-Leibler divergences, respectively, between the Schrödinger (i.e. nonrelativistic) and Dirac (i.e. relativistic) charge densities (ρ_S and ρ_D, respectively) for a given system with nuclear charge Z.

In this section we determine numerically the aforementioned JSD and KL values for a variety of nuclear charges. The numerical results are analyzed, in order to get a basis on the dependence of JSD and/or KL on the nuclear charge Z, as well as on the occupation and quantum numbers of the outermost subshells. Systems with nuclear charges within the range $Z = 1 - 103$ will be considered throughout. All numerical results are provided in atomic units (a.u.).

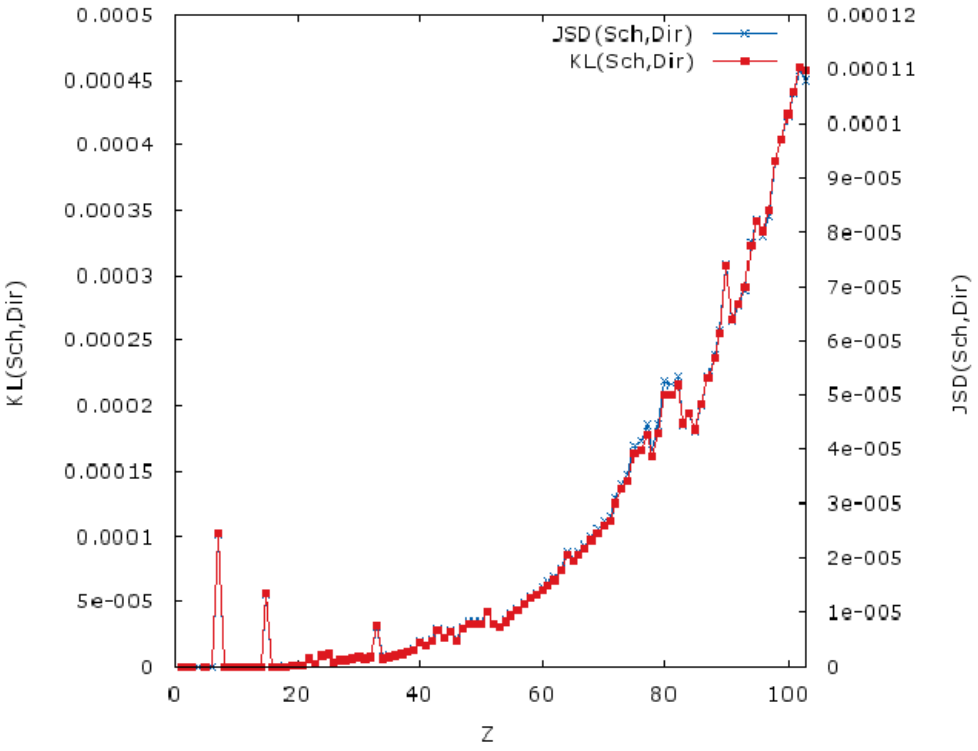

FIGURE 3.2: Jensen-Shannon $JSD(Sch, Dir)$ and Kullback-Leibler $KL(Sch, Dir)$ divergences between the Schrödinger (non-relativistic) and Dirac (relativistic) one-particle densities for ground-state neutral atoms with nuclear charge $Z = 1 - 103$. Atomic units (a.u.) are used.

Let us first analyze the dependence of both JSD and KL on the nuclear charge Z, on the basis of the curves in Figure 3.2. Notice that, in spite of the small values displayed in the figure, they are above the numerical accuracy of the integration method, previously discussed. Similar global behaviors are observed for both quantities, displaying increasing trends with Z, as expected. In fact, the aforementioned behaviors appear almost identical, excepting a global factor of (roughly) 10 (notice the different scales employed in the left- and right-hand sides). We could say that the information provided by JSD and KL is roughly the same (at a global level, at least), so simplifying the numerical discussion in what follows.

However, the increasing trend is not monotonic at all, neither for JSD nor for KL. This appears evident through the presence of a number of local extrema, so displaying curves with apparent irregularities. These behaviors are in contrast with those observed for one-electron systems in previous works. The reason for obtaining so structured curves underlies on the shell structure of the multielectronic systems here considered, as previously mentioned.

Considering the long-range decrease $\rho(r) \sim e^{-\alpha r}$, the asymptotic $\sim re^{-\alpha r}$ is induced for the integrands of JSD and KL. However, integrands defining QSI behave as $\sim e^{-2\alpha r}$.

	JSD **maxima**	JSD **minima**
Closed shell	30(3d) 48(4d) 80(5d) 102(5f)	– – – – – – – –
Half-filled	7(2p) 15(3p) 25(3d) 33(4p) 43(4d) 51(5p) 64(4f) 95(5f)	83(6p)
Anomalous	45(5s)	41(5s) 44(5s) 46(5s) 78(6s) 91(5f) 96(5f)

	KL **maxima**	KL **minima**
Closed shell	30(3d) 80(5d) 102(5f)	– – – – – – – –
Half-filled	7(2p) 15(3p) 25(3d) 33(4p) 43(4d) 51(5p) 64(4f) 95(5f)	83(6p)
Anomalous	45(5s)	44(5s) 46(5s) 78(6s) 91(5f) 96(5f)

TABLE 3.1: Classification scheme of most local extrema of JSD (up) and KL (down) between Schrödinger-Dirac densities for atoms with nuclear charges within the range $Z = 1 - 103$. 'Anomalous' or outermost orbitals are given within parentheses.

The latter decreases much faster than the former, so does not capture 'almost nothing' from valence region.

A more detailed discussion on JSD and KL extrema is in order. In doing so, let us pay attention to Table 3.1, where most systems associated to local maxima and minima are classified, attending to relevant patterns of their shell structure. Such is the case of systems with (i) closed subshells, (ii) half-filled valence subshell, and (iii) those suffering from the so-called 'anomalous shell filling'. Focussing on the table for JSD, it is observed a strong connection between these three types of systems and the displayment of local extrema for JSD as function of Z:

- Most JSD maxima correspond to systems with valence subshell either closed or half-filled. There appear clear differences attending to the value of the orbital momentum quantum number: for the p-subshell case, half-filled systems are displayed as maxima ($Z = 7, 15, 33, 51$, with the unique exception $Z = 83$), not the closed-shell ones. However, a variety of systems with d or f valence subshell appear in the JSD maxima column, divided in the closed-shell ($Z = 30, 48, 80, 102$) and hall-filled ($Z = 25, 43, 64, 95$) boxes.

- The criterium governing the displayment of minima in JSD appears to be the anomalous shell-filling, affecting subshells 5s, 6s and 5f. This happens for a total of 6 systems, the unique exception being $Z = 45$ in the 5s case.

- KL extrema are roughly the same as those for JSD. The only differences are systems $Z = 41$ (Nb) and $Z = 48$ (Cd), two transition metals appearing as very slight extrema in the JSD case but not in the KL one. So, the set of 18 extrema

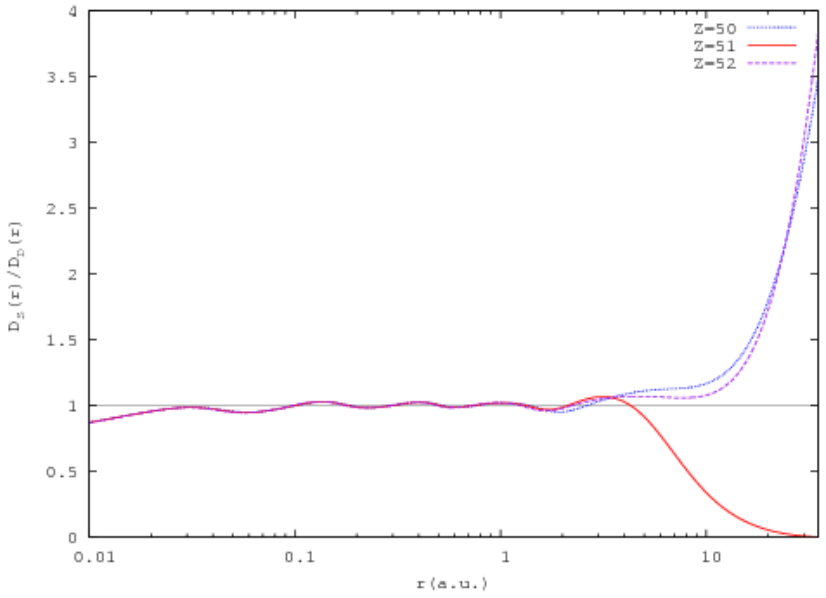

FIGURE 3.3: Schrödinger-Dirac quotients $D_S(r)/D_D(r)$ of radial densities $D(r) = r^2\rho(r)$ for contiguous atomic systems $Z = 50, 51, 52$. Atomic units (a.u.) are used.

in KL (12 maxima, 6 minima) is enclosed in the corresponding set for JSD (20 extrema, 13 maxima, 7 minima).

The above classification of extrema, for both JSD and KL, provides us with an evidence that the relevance of relativistic effects on atomic charge densities do depend on physical properties of the system considered, other than its heavieness as determined by the nuclear charge Z. It appears particularly important their shell structure, a well-known pattern determining the main physical and chemical properties, and governing the classification scheme of periods and groups in the Periodic Table.

For illustration, let us notice that all elements belonging to the nitrogen family (group VA) and the whole group IIB appear, in Table 3.1, as extrema for both JSD and KL, almost systematically as maxima. The rest of JSD extrema consists of transition metals in the middle region of the Periodic Table, one lantanide and four actinides.

To better interpret these results, attending to the structural features of the radial density $D(r)$, let us pay attention to the illustrative Figure 3.3. The Schrödinger-Dirac quotient $D_S(r)/D_D(r)$ is plotted for system $Z = 51$ (a local maximum for both JSD and KL), and also for its neighbors $Z = 50, 52$. All quotients remain close to unity in the core region, but strong deviations appear beyond $r \sim 4$ a.u. (valence region), in opposite ways for $Z = 51$ and for its neighbors.

3.2 Conclusions

Relevance of relativistic effects onto atomic systems has been quantified, in terms of differences between Hartee-Fock (HF, non-relativistic) and Dirac-Fock (DF, relativistic) one-particle densities. The analysis of the numerical results extends previous studies with similar aims, mostly of qualitative nature attending to the structural properties of the distributions. The exceptions to the above are the studies on the quantum similarity index (QSI) between the HF and DF densities.

The present work emphasizes the dependence on the nuclear charge Z of Shannon-like comparative functionals for all ground-state neutral atoms throughout the Periodic Table. The functionals here considered are the Jensen-Shannon (JSD) and Kullback-Leibler (KL) divergences, intimately related on their theoretic definition and properties, but also on their respective dependences on Z.

Far beyond the expected increasing trend with Z, both JSD and KL display a number of minima and maxima, for a variety of atomic systems as determined by strict patterns on their shell structure, in particular the occupation and the quantum numbers of the outermost subshells. Recent applications of Jensen-like divergence measures in hydrogenic HF and DF systems emphasized the relevance of the electron quantum numbers in quantifying relativistic effects.

These results for neutral atoms are clearly in contrast with those provided by QSI in previous works, as far as applied to one-particle densities in position space. Certainly the capability of QSI to display shell structure has been proved, whenever be applied in the conjugate momentum space.

Here the novelty is the capability of both JSD and KL to display the aforementioned shell-structure on the basis of relativistic effects in position-space atomic one-particle densities.

Justifying the patterns governing the appearance of local extrema (mostly for systems with filled and half-filled valence susbshell, or those suffering from anomalous shell-filling) remains as an open problem. Most probably the underlying reason will be the respective long-range behaviors of the HF and DF densities, and this is what we are studying at present.

Chapter 4

Generalized quantum similarity in atomic systems: A quantifier of relativistic effects

Much effort is devoted to analyzing the role of relativity in a huge variety of quantum mechanical systems. Considering the above term, performing a rigorous and precise analysis, from both analytical and numerical points of view, constitutes an enormous task as compared to the non-relativistic one. In particular, relativistic effects in atomic densities and related functionals for many-electron systems were widely analyzed over the last few years (see an exhaustive review in Ref. [170]). As both the number of electrons (N) in the atom and its nuclear charge (Z) increase, relativistic effects become more important and have to be taken into account to understand atomic or molecular properties [154, 155, 171–173].

Recent developments in relativistic quantum theory have made it possible to obtain accurate electronic properties for heavy elements with the aim of predicting their chemical and physical behaviors [153–155, 164, 172, 174]. In particular, the study of actinide and transactinide elements is an important multidisciplinary area of research involving nuclear physics, atomic physics and chemistry. Changes in periodic trends due to relativistic effects are outlined for the superheavy elements [175] and atomic calculations help to understand the role of relativistic and many-body effects [170, 172, 176–178], and also provide important information for planning and interpreting experimental measurements [173]. The high level of accuracy required for the analysis of relativistic and correlation effects makes these calculations very challenging [179]. However, valence region plays a relevant role for many other properties (e.g., ionization potential [173], state configuration [180]), so relativistic effects warrant a deeper analysis in that region.

For illustration, let us consider the behavior of these three coinage elements: Cu, Ag and Au. Their properties are quite different, in spite of having the same valence electron

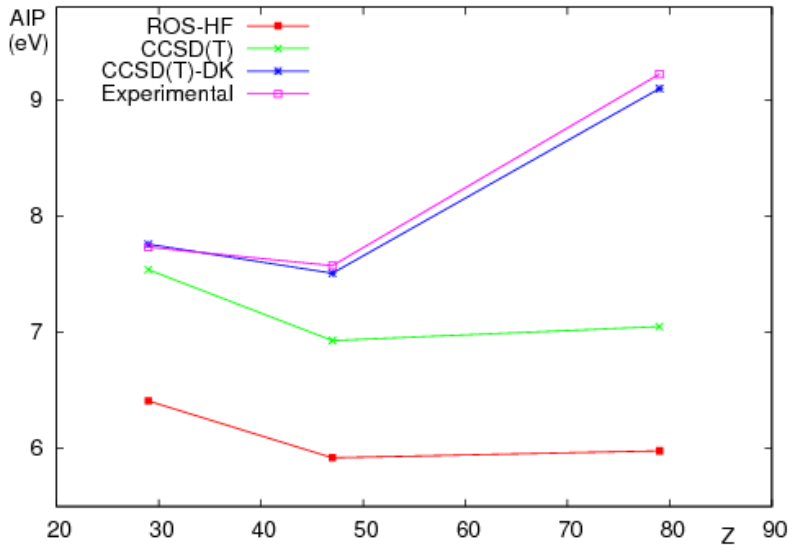

FIGURE 4.1: Atomic ionization potential (AIP, in eV) of ground-state neutral atoms in Group 12: copper (Cu, nuclear charge $Z = 29$), silver (Ag, $Z = 47$) and gold (Au, $Z = 79$). Curves correspond to AIP values obtained from: non-relativistic ROS-HF (red filled squares), non-relativistic CCSD(T) (green crosses), relativistic CCSD(T)-DK (blue stars), and experiments (magenta empty squares).

structure and without a reasonable explanation for this behavior within a nonrelativistic framework. Different chemical and physical properties of Au and Ag result mainly from large relativistic effects in Au, such that neglecting them would cause Ag and Au to be quite similar. Deviations from the expected pattern of non-relativistic atomic ionization potentials (AIP) in the series Cu, Ag, and Au, are clearly displayed in Figure 7.1. They are due to large relativistic effects in gold [174]. For this group of atoms the valence subshell is ns^1 (with $n = 4, 5, 6$ respectively). So, one should expect a decreasing sequence of AIP's for increasing n. Experimental data show that the AIP of Ag is lower than the AIP of Cu, as expected. However, contrary to our expectations, the AIP of gold is the largest within the family of coinage metals. This experimental finding can be understood by employing three approximations with gradually improved theoretical levels for calculating ionization potentials,[174, 181] as demonstrated in Figure 7.1. The lowest theoretical level is the nonrelativistic Restricted Open Shell Hartree-Fock one-electron calculation (ROS-HF), which treats interelectronic interactions only approximately. This model is completely insufficient in describing AIP's of any of the three coinage metals. Clearly, electron correlation effects are inevitable.

Sophisticated description of the electron correlation provides the Coupled Cluster CCSD(T) method. Normally, this is an excellent many-electron model, capable of interpreting and predicting atomic and molecular properties very accurately. Nevertheless electron correlation effects, as represented by the difference between ROS-HF and CCSD(T) calculations, are similar for all three valence isoelectronic coinage metals. The AIP of Cu calculated using the nonrelativistic CCSD(T) method agrees with experimental values

reasonably well. When relativistic effects are neglected for Ag, the CCSD(T) result deviates from experimental values considerably, while for Au the nonrelativistic result is completely misleading. The relativistic approximation, used in calculations presented in Figure 7.1, is reasonably satisfactory for reproducing and predicting ionization potentials of Cu, Ag, Au, and many other atoms and molecules. The relativistic AIP values (blue stars) in [**?**] display very small deviations from the experimental ones (magenta squares), with slight underestimation for Ag and Au systems and an extremely small overestimation (almost an overlap) in the case of Cu.

Relativistic versus non-relativistic calculations on the first 100 atoms, $Z = 1 - 100$, were published in 1973 by J.P. Desclaux [176]. The relativistic/non-relativistic ratios for many expectation values were are provided there. Not only the nuclear charge Z but also the group (1-18) has a strong effect on the size of the relativistic effects, especially for valence electrons. For more information see Sections 2.3. and 3.2. of Ref. [170], which provides a much more recent overview on relativistic effects. Some other works emphasize that relativistic effects on the higher n-levels come from the innermost half-wave, nearest to the nucleus [170, 177, 178].

In this work, an information-theoretical tool enables one to scan and analyze specific regions of the electron density and to quantify their respective relative contributions to relativistic effects. For this purpose, the Dirac-Fock equation must be solved, enclosing the Schrödinger equation as the non-relativistic limit. Solving this equation requires the use of sophisticated models and/or numerical routines. Its solution allows us to determine the wavefunctions in conjugate spaces, as well as the position and momentum one-particle densities, $\rho(\vec{r})$ and $\gamma(\vec{p})$, respectively. A direct consequence of last comment is the shortage of relativistic analyses on one-particle densities of many-electron systems (e.g. atoms, molecules), beyond those dealing with energy spectra.

The availability of analytical solutions for the Schrödinger (i.e., non-relativistic) and Dirac (i.e., relativistic) equations, describing one-electron systems, has allowed a deeper insight into the relevance of relativistic effects onto, for example, one-particle densities (in position and momentum spaces), or some of their functionals and expectation values, for hydrogenic atoms [159, 160, 169, 182]. Similar studies for many-electron systems have also been carried out. Focusing on ground-state neutral atoms, a new ingredient emerges in the interpretation of results, namely the atomic shell structure. Let us emphasize that the main conclusion arising from the comparison between the Schrödinger and Dirac hydrogenic densities (ρ_S and ρ_D respectively, in what follows) is that their dissimilarity increases with the nuclear charge Z, as one should expect. The question posed by some authors is if the same applies for many-electron systems.

One-particle densities, which describe the state of quantum systems, play a relevant role within the so-called "information-theory", allowing for the interpretation of many density functionals in terms of physical and chemical properties in many-electron systems.

In doing so, a variety of tools and magnitudes have been considered in the literature. Some density functionals deserve special attention, such as the Shannon [3] and Tsallis [48] entropies and the Fisher information [30], among others. Composite functionals, namely "complexity measures", defined in terms of the aforementioned Shannon and/or Fisher quantities have also been used to describe atomic and molecular properties (see Ref. [156] and references therein). Let us remark that functionals based on complexity measures have been used to analyze the relativistic effects not only in hydrogenic systems [169], but also in atoms throughout the Periodic Table [183, 184].

Quantitatively exploring the level of similarity/dissimilarity between two different systems in terms of their densities actually appears to be a very interesting field. Quantifying the dissimilarity between two, or more, many-electron systems by means of their one-particle densities is also a hot topic within the physical applications of information theory. Among those divergence measures suitable to study atomic or molecular systems, those that are especially relevant are the Kullback-Leibler or relative entropy [88, 185, 186], the Fisher divergence [120, 187] and the Jensen-Shannon divergence [104].

On the other hand, Quantum Similarity Theory [122] attempts to give a quantitative measure of the degree of similarity between two quantum objects, based on the comparison of their one-particle densities with later applications to other quantities. To quantify the degree of similarity between the compared systems, a general QSI [137] can be defined via the computation of an integrated measure between the density functions attached to the quantum systems.

Reports of recent studies analyzing relativistic effects using these kinds of functionals (measuring similarity/dissimilarity between non-relativistic and relativistic densities) are provided in Refs. [98, 161], by considering the QSI. In these works, $QSI(\rho_S, \rho_D)$ was obtained for all ground-state neutral atoms with nuclear charge $Z = 1 - 103$. As expected, QSI monotonically decreases with increasing Z and the results are interpreted as follows: relativistic effects are more relevant for heavy systems, where the 'relevance' of those effects is understood as a higher dissimilarity (i.e., lower similarity QSI) between ρ_S and ρ_D. In these studies, there is no trace of shell-filling patterns, that is, QSI appears to depend exclusively on Z but not on the location of the considered system in the Periodic Table. The core region was deeply analyzed in Ref. [98], with QSI revealing the similarity based exclusively on this region of the densities. However, this measure is not able to capture any features of valence regions, which is essential from both the physical and chemical points of view. As the authors propose, it would be necessary to investigate whether the valence region can be highly weighted in a similarity study. This last aim was achieved in Ref. [161] by considering QSI between the respective momentum-space densities. This procedure, in contrast with previous position-space analyses, revealed the importance of the valence region (as compared to the core) in order to obtain significant differences between the relativistic and non-relativistic electron distributions.

A qualitative leap was achieved in Ref. [164] by considering two alternative functionals whose definitions arise from the Shannon entropy, as measure of 'content of information' in a distribution. These functionals are the Jensen-Shannon and the Kullback-Leibler divergences: JSD and KL, respectively. In the aforementioned study [164], both divergence measures are analyzed for one-particle densities in position space, considering their dependence on the nuclear charge Z. Contrary to the monotone behavior of QSI, both JSD and KL display a variety of local extrema, with their appearance being governed by clear shell-filling patterns. Focusing on JSD (because its set of extrema encloses that of KL), particularly relevant systems are those with (i) closed subshells, (ii) half-filled valence subshell and (iii) anomalous shell-filling. Most of them correspond to JSD maxima, that is, with significant relativistic corrections (let us remark that $JSD = 0$ is the minimum value for identical distributions). It was argued that the reason behind these results was the difference between the long-range behaviors of the relativistic and non-relativistic distributions. There is a 'dramatic' change in passing from the monotone QSI to the highly structured JSD (and KL), the latter displaying a diversity of extrema, classified according to specific physical criteria, discussed in detail within the next section.

The main aim of this work is to analyze relativistic effects on neutral atoms throughout the Periodic Table $Z = 1-103$, by means of their one-particle densities. For this purpose we compute the so-called 'Generalized Quantum Similarity Index' (QSI_q) [129] between the Dirac and Schrödinger densities for a given system. This measure is a generalization of the QSI. The analysis is carried out for different values of the parameter q. We will deal with uniformly weighted couples of functions. We will use the functional defined in Eq. (1.35) of Chapter 1:

$$QSI_q(\rho_1, \rho_2) = \frac{\int [\rho_1(\vec{r})\rho_2(\vec{r})]^{q/2}\, d\vec{r}}{\sqrt{\int \rho_1^q(\vec{r})d\vec{r} \int \rho_2^q(\vec{r})d\vec{r}}} \tag{4.1}$$

in order to go far beyond the well-known results provided by QSI, which correspond to the particular case of $q = 2$, as we have seen in Chapter 1. The particular choice $\lambda_1 = \lambda_2 = 1/2$, necessary to get QSI for the above particular case, also corresponds to the least-biased comparative between two distributions on the basis of similarity. The results presented in this chapter have been compiled into an article and published [188].

Let us emphasize the role played by the parameter q in the definition of QSI_q, as given by Eq. (4.1), for the sake of simplicity (similar arguments also apply to the definition in Eq.(1.35)). In doing so, consider any of the integrals in the denominator for $q = 2$. This choice provides $\langle\rho\rangle = \int \rho^2(\vec{r})d\vec{r}$. The quantity $\langle\rho\rangle$ is the *mean density* (i.e., an average of the density values over its domain). We could say, roughly speaking, that the density values are classified into two categories: 'low' and 'high', according to the threshold $\langle\rho\rangle$. Focusing on the low values (enclosing those at the outermost region), let us notice that they become even lower if raised to a high power q and, consequently,

diminish in their contribution to the value of the integral as far as q increases. On the contrary, let us consider a local maximum of $\rho(\vec{r})$: the density values at that point and its vicinity become higher as q increases, so that their contribution to the whole integral appears much more relevant, in relative terms.

The above comments apply to each integral in the denominator of QSI_q and similarly also in the numerator. Again with $q = 2$, the numerator in Eq. (4.1) becomes $\int \rho_1(\vec{r})\rho_2(\vec{r})d\vec{r} = \langle\rho_1\rangle_2 = \langle\rho_2\rangle_1$. The last two terms in this expression are interpreted as follows: $\langle\rho_i\rangle_j$ is the expectation value of ρ_i on ρ_j. Any of these terms provide a threshold to establish 'lower and higher' density values.

It is in this sense that the parameter q is employed throughout in order to modify the enhancement of different regions, within the density domain, for comparative purposes.

4.1 Quantifying relativistic effects: numerical analysis of quantum similarity

Considering the definition of QSI_q, in terms of three integrals to be computed numerically, first we are concerned with the accuracy of the present calculations. We check the accuracy by comparing the numerical and analytical values of $QSI_q(f, g)$ for a pair of simple functions (to get the analytical expression) imitating the atomic ones and integrating over the same grid of points as that employed for atomic systems. Choosing $f(\vec{r}) = e^{-r}$ and $g(\vec{r}) = e^{-\alpha r}$, with $\alpha > 0$ and $r = |\vec{r}|$, the relative error between the analytical and numerical values of $QSI_q(f, g)$ are systematically below 10^{-9}, for any $\alpha \in [0, 50]$ and $q \in [0.2, 2.5]$. Consequently, we are confident to nine significant figures (at least) for all values shown throughout.

Let us proceed with the application of QSI_q to atomic systems, particularly by comparing the Schrödinger (ρ_S) and Dirac (ρ_D) one-particle densities. In order to compute this functional, first we need appropriate packages to build up both ρ_S and ρ_D. In the Schrödinger case, the well-known near-Hartree-Fock wavefunctions of Refs. [144, 145] are employed, with a recognized accuracy discussed in detail within the above references. The expansions on Slater-type basis sets, which are extremely accurate compared to numerical Hartree-Fock wavefunctions, provide us with analytical expressions of ρ_S for any system. On the other hand, the output of the multiconfigurational Dirac-Fock package MCDFGME V 2005.10 [165] consists of a tabulation of the respective radial densities, arising from ρ_D, onto a log-like mesh grid of points, with controllable fineness.

On the basis of the above realistic densities ρ_S and ρ_D, a second test of numerical accuracy is performed by testing their normalization. Notice that the value of QSI_q does not depend on the normalization of any of its density arguments (contrary to JSD and KL), so one should not worry about normalization to interpret results regarding QSI_q.

However, normalization could be relevant in pointwise comparisons among distributions, such as those discussed in this Section. We checked, up to the level of accuracy descibed above, that we handle normalized-to-unity densities ρ_S and ρ_D for all systems considered here.

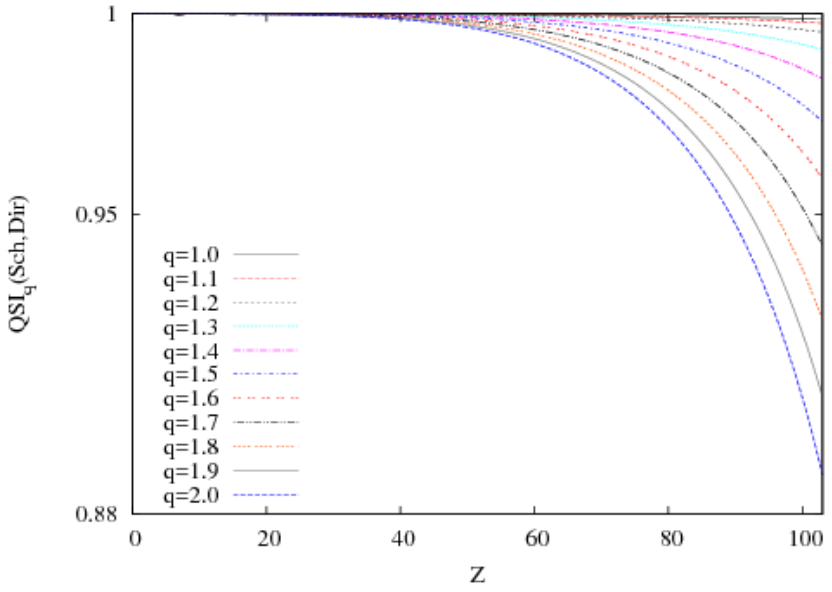

(a) High-order ($1.0 \leq q \leq 2.0$)

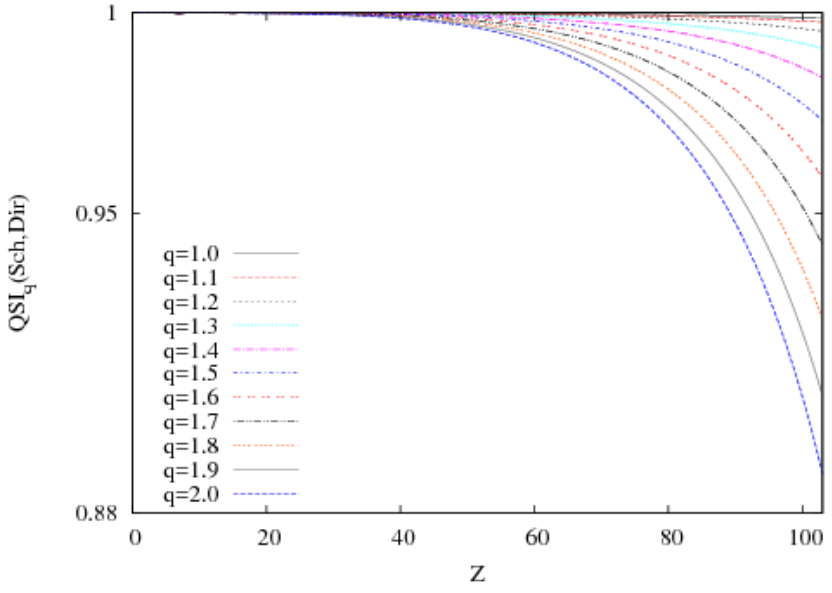

(b) Low-order ($0.4 \leq q \leq 1.0$)

FIGURE 4.2: (a) High-order ($1.0 \leq q \leq 2.0$) and (b) low-order ($0.4 \leq q \leq 1.0$) generalized quantum similarity index $QSI_q(Sch, Dir)$, between Schrödinger and Dirac densities for neutral atoms with nuclear charge $Z = 1 - 103$. Atomic units (a.u.) are used.

We will frequently employ the equivalent notation $QSI_q(Sch, Dir) = QSI_q(\rho_S, \rho_D)$. Curves of the above functional, as a function of the nuclear charge Z, are displayed

in Figure 4.2 for a variety of values for the parameter q. Attending to the structural patterns of these curves, the figure is split into two subfigures, namely Figures 4.2(a) and 4.2(b), respectively: the former for the range $1 \leq q \leq 2$ and the latter for $q \leq 1$.

Figure 4.2(a), for 'upper' values of q, consists of a variety of (roughly) monotone curves, with a higher decreasing rate as q increases. Curves appear perfectly ordered, from above to below from $q = 1$ to $q = 2$. With the scale employed here, they are almost indistinguishable from the upper axis (i.e. from $QSI_q = 1$) for systems as 'light' as $Z \lesssim 25$.

The discussion changes considerably when referring to Figure 4.2(b), which encloses curves for 'lower' values of q, within the range $0.2 \leq q \leq 1.0$. The scale in the vertical axis is much narrower than in Figure 4.2(a), thus revealing (i) a number of irregularities for $q = 1$, which were not appreciable in the adjoining figure and (ii) that overall, QSI_q is much closer to unity for values of parameter q in the range $0.2 \leq q \leq 1$ than for values represented in Figure 4.2(a). Nevertheless, the most evident feature in Figure 4.2(b) is the collection of highly structured curves, in contrast with Figure 4.2(a). The structure is revealed through a number of local extrema within the whole abscissa range $Z = 1-103$. Notice the illustrative example of the coinage elements (Cu, Ag, Au), referred to in the Introduction, on the basis of 'irregularities' in the respective ionization potentials. The peculiarity of Au ionization potential, as compared to its coinage companions (see Figure 7.1), is also clearly revealed through the similarity functional QSI_q in Figure 4.2.

It appears pertinent to analyze in detail the set of atomic systems corresponding to the aforementioned extrema, bearing in mind that a lower similarity (equivalently, a higher dissimilarity) between ρ_S and ρ_D should be interpreted in terms of the relevancy of relativistic effects. The opposite applies to the 'divergence' among densities, as discussed in Ref. [164], regarding the Jensen-Shannon and Kullback-Leibler divergences, $JSD(\rho_S, \rho_D)$ and $KL(\rho_S, \rho_D)$, respectively.

In doing so, let us pay attention to Table 4.1. As also observed roughly in Figure 4.2(b), diminishing q progressively causes QSI_q to display a (progressively increasing) number of extrema (see first two columns of Table 4.1), enclosing the whole set of JSD extrema when q is low enough (see Table 4.1). These results support the well-known relativistic/non-relativistic long-range behaviors as their underlying justification.

Let us proceed with the interpretation of the results provided in Table 4.1. A detailed numerical analysis provides us with a variety of minima for each q; many of them are hard to distinguish in the Figure 4.2(b). The exact number of minima found for each q is exhaustively displayed in Table 4.1, regardless of the magnitude of their depth. Some comments are in order:

- The number of $QSI_q(Sch, Dir)$ minima systematically increases (from 1 to 25) as q decreases (from 2.0 to 0.2).

q	Number of minima	Closed shell (CS)	Half-filled (HF)	Anomalous (AN)	Exchange between neighbors
1.6 - 2.0	1		**7**		
1.4	2		**7,15**		
1.2	4		**7,15,25,33**		
1.0	15	**30,48,80,102**	**7,15,25,33,43,51,** 77,**95**	**45 ($5s^1 4d^8$)** **64 ($4f^7 5d^1$)** 90 ($5f^0 6d^2$)	
0.8	17	**30,48**,70,**80,102**	**7,15,25,33,43,51,** 77,**95**	**45 ($5s^1 4d^8$)** 58 ($4f^1 5d^1$) **64 ($4f^7 5d^1$)** 89 ($5f^0 6d^1$)	90 (AN) to 89 (AN)
0.7	18	12,70,**80,102**	**7,15,25,33,43,51,** 77,**95**	29 ($4s^1 3d^{10}$) **45 ($5s^1 4d^8$)** 45 ($5s^1 4d^8$) 47 ($5s^1 4d^{10}$) 58 ($4f^1 5d^1$) **64 ($4f^7 5d^1$)** 79 ($6s^1 5d^{10}$) 89 ($5f^0 6d^1$)	30 (CS) to 29 (AN) 48 (CS) to 47 (AN)
0.6	20	12,**102**	**7,15,25,33**,37,**51**, 55,83,87,**95**	29 ($4s^1 3d^{10}$) 41 ($5s^1 4d^4$) **45 ($5s^1 4d^8$)** 47 ($5s^1 4d^{10}$) 58 ($4f^1 5d^1$) **64 ($4f^7 5d^1$)** 79 ($6s^1 5d^{10}$) 89 ($5f^0 6d^1$)	43 (HF) to 41 (AN) 80 (CS) to 79 (AN)
0.4	23	10,12,18,**102**	**7,15,25,33**,37,**51**, 55,75,83,87,**95**	29 ($4s^1 3d^{10}$) 41 ($5s^1 4d^4$) **45 ($5s^1 4d^8$)** 47 ($5s^1 4d^{10}$) 58 ($4f^1 5d^1$) **64 ($4f^7 5d^1$)** 79 ($6s^1 5d^{10}$) 89 ($5f^0 6d^1$)	
0.2	25	2,4,10,12,18,**30**, **48**,70,**102**	**7,15,33,51**,55,75, 83,87,**95**	24 ($4s^1 3d^5$) 41 ($5s^1 4d^4$) **45 ($5s^1 4d^8$)** **64 ($4f^7 5d^1$)** 79 ($6s^1 5d^{10}$) 89 ($5f^0 6d^1$) 92 ($5f^3 6d^1$)	25 (HF) to 24 (AN) 29 (AN) to 30 (CS) 47 (AN) to 48 (CS)

TABLE 4.1: $QSI_q(Sch, Dir)$ local minima ($0.2 \leq q \leq 2.0$), classified into three categories, for ground-state neutral atoms with nuclear charge $Z = 1 - 103$. For systems with anomalous shell filling, the anomaly is specified within parentheses. Systems that are also local maxima of JSD are shown in bold (and in red, online)

- The classification of minima into three categories (systems with closed shells, half-filled or suffering from anomalous shell filling) is exhaustive; that is, all minima of QSI_q belong to one of these categories for the whole interval of q considered here.

- Focusing on bold numbers, it is observed that all JSD maxima (provided in Ref. [164]) are recovered for the threshold value $q = 1.0$. Nevertheless, a few half-filled systems ($Z = 7, 15, 25, 33$) appear before.

- In this sense, especially remarkable is the case $Z = 7$, displayed as a (slight) minimum for the case $q = 2.0$ or, equivalently, for the usual QSI. The existence of any extremum in QSI is not reported in the literature (to the best of our knowledge), so 'breaking' the monotonic nature of QSI.

- Once a system is displayed as a minimum for a given q, most usually it remains as minimum for lower values of q. There are few exceptions to this comment, in most cases due to their replacement by an anomalous (AN) neighbor within a range of q. The aforementioned replacements are the following: the closed-shell systems $Z = 30, 48, 80$ at Group 12 of the Periodic Table (replaced, respectively, by the previously emphasized 'gold trio' Cu-Ag-Au at Group 11, namely $Z = 29, 47$ for $\mathbf{q = 0.4 - 0.7}$, and $Z = 79$ for $\mathbf{q = 0.2 - 0.6}$), the half-filled ones $Z = 25, 43$ (replaced, respectively, by $Z = 24$ for $q = 0.2$, and $Z = 41$ for $\mathbf{q = 0.2 - 0.6}$), and the anomalous $Z = 90$ (replaced by $Z = 89$ for $\mathbf{q = 0.2 - 0.8}$).

  For most systems displayed as minima at one or more q-curves (e.g., system Z), the existence of a 'threshold q-value' is observed, say $q_0(Z)$, characterized as follows: system Z is displayed as local minimum at any curve with $q \leq q_0(Z)$, while it is not for $q > q_0(Z)$. This means that, most usually, once a system is displayed as a minimum for a given q, it remains as a minimum for lower values of q or, equivalently, it is displayed as a minimum for the whole range $0.2 \leq q \leq q_0(Z)$.

  There are few exceptions to this comment, in most cases due to the replacement of a minimum, in decreasing q, by an anomalous neighbor within a range of lower q's. The aforementioned replacements are the following: the closed-shell systems $Z = 30, 48, 80$ in Group 12 of the Periodic Table (replaced, respectively, by the previously emphasized 'gold trio' Cu-Ag-Au in Group 11, namely $Z = 29, 47$ for $q = 0.4 - 0.7$ and $Z = 79$ for $q = 0.2 - 0.6$); the half-filled systems $Z = 25, 43$ (replaced, respectively, by $Z = 24$ for $q = 0.2$, and $Z = 41$ for $q = 0.2 - 0.6$), and the anomalous system $Z = 90$ (replaced by $Z = 89$ for $q = 0.2 - 0.8$).

  Once a system is displayed as a minimum for a given q, most usually it remains as minimum for lower values of q. There are few exceptions to this comment, in most cases due to their replacement by an anomalous (AN) neighbor within a range of q. The aforementioned replacements are the following: the closed-shell systems $Z = 30, 48, 80$ at Group 12 of the Periodic Table (replaced, respectively, by the previously emphasized 'gold trio' Cu-Ag-Au at Group 11, namely $Z = 29, 47$

for $\mathbf{q = 0.4 - 0.7}$, and $Z = 79$ for $\mathbf{q = 0.2 - 0.6}$), the half-filled ones $Z = 25, 43$ (replaced, respectively, by $Z = 24$ for $q = 0.2$, and $Z = 41$ for $\mathbf{q = 0.2 - 0.6}$), and the anomalous $Z = 90$ (replaced by $Z = 89$ for $\mathbf{q = 0.2 - 0.8}$).

- It is worthy to remark that, far beyond the extrema displayed by $JSD(Sch, Dir)$, the functional $QSI_q(Sch, Dir)$ displays a variety of additional extrema when q is low enough, in all the three categories (closed-shell, half-filled and anomalous). A graphical comparative between JSD and QSI_q will be provided in a later figure, for a selected intermediate q value. Regarding the whole q-range, analysis is carried out on the basis of [**?**](b), together with the indispensable help of Table 1. The aforementioned new extrema (i.e., those not appearing in JSD but in QSI_q for sufficiently low q) are shown below:

- Closed-shell: $Z = 2, 4$ ($q = 0.2$), $Z = 10, 18$ ($q = 0.2 - 0.4$), $Z = 12$ ($q = 0.2 - 0.7$) and $Z = 70$ ($q = 0.2,\ 0.7 - 0.8$).
- Half-filled: $Z = 37$ ($q = 0.4 - 0.6$), $Z = 55, 75, 83, 87$ ($q = 0.2 - 0.6$) and $Z = 77$ ($q = 0.7 - 1.0$).
- Anomalous: apart from the above-mentioned anomalous systems replacing closed-shell or half-filled ones, we find the new ones $Z = 58$ ($q = 0.4 - 0.8$), $Z = 92$ ($q = 0.2$) and the system $Z = 90$ ($q = 1.0$) replaced by $Z = 89$ for $q = 0.2 - 0.8$.

Anomalies in shell-filling systematically occur on systems with valence subshell of type d.

Summarizing the above comparative discussion of QSI_q and JSD extrema, we could say that (i) the usual $QSI = QSI_{q=2}$ is roughly monotone, (ii) similar structures are found for both JSD and $QSI_{q=1}$, and (iii) the just mentioned structure is considerably enriched by lowering q, thus improving the results provided by JSD.

Going beyond the above comparison between $JSD(Sch, Dir)$ and $QSI_q(Sch, Dir)$, we visualize the correspondence between their structures in Figure 4.3. For this purpose, the particular case of $q = 0.9$ is considered in order to make a comparison of sufficient quality. Different scales are employed for $JSD(Sch, Dir)$ and $QSI_{0.9}(Sch, Dir)$, so the curves display the deviation of each quantity from its corresponding extreme value (0 and 1, respectively). In spite of the extremely small deviations, they are within the numerical integration accuracy, previously discussed.

At first sight, a number of relevant maxima in the JSD curve coincide with marked minima of $QSI_{0.9}$, considering their location over the Z-axis. This observation is in perfect accordance with the results provided in Table 1, for q close to 0.9, with most of them being extrema for both functionals. To discern not so relevant extrema, Table 4.1 constitutes an indispensable aid.

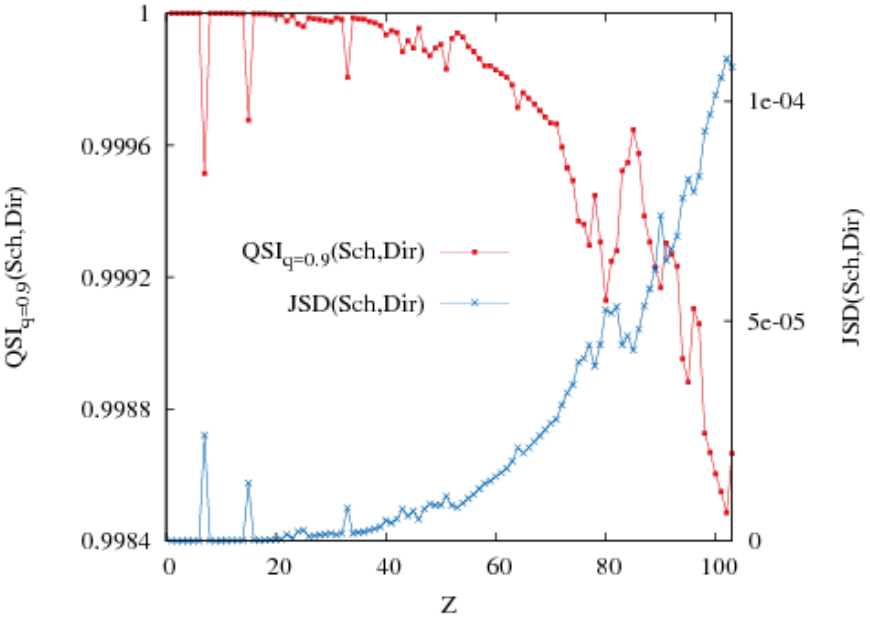

FIGURE 4.3: Generalized quantum similarity index $QSI_q(Sch, Dir)$ of order $q = 0.9$, and Jensen-Shannon divergence $JSD(Sch, Dir)$, between Schrödinger and Dirac densities for neutral atoms with nuclear charge $Z = 1 - 103$. Atomic units (a.u.) are used.

Turning to Figure 4.3, a set of apparent extrema is displayed through both JSD and $QSI_{0.9}$. It is worth remarking the presence of minima for $Z = 7, 15, 33$ within the region of light systems. Notice (in Table 1) that they are within the first few extrema appearing as minima of QSI_q, for a wide range of q (even above unity), and are also maxima of JSD. Similarly, this occurs with $Z = 25$ regarding the range q, with the corresponding maximum/minimum (for each functional) being not so apparent, but clearly displayed. Let us remark that the just mentioned four systems belong to the class of half-filled systems.

The medium region ($Z = 40 - 70$) is more involved, with a higher number of extrema but is not as apparent as for lighter systems. We emphasize the display of peaks in the respective curves for $Z = 43, 45, 48, 51, 64$ (the last two are clearly displayed, the others not so much). The region of heavier systems contains again, as for light ones, relevant peaks. Particularly interesting are those for $Z = 80, 90, 95, 102$ for both functionals, but the half-filled $Z = 77$ also in $QSI_{0.9}$, not in JSD. It is remarkable that peaks within the medium-heavy region correspond to systems belonging to all three categories in Table 1, contrary to the light region, which is only sensitive to half-filled systems.

The above discussion on Figure 4.3 forces us to resume discussion on Figure 4.2(b). To avoid being too exhaustive, let us focus on the curve for $q = 0.4$, which displays a total of 23 minima. Many of them did not appear in JSD: the closed-shell systems $Z = 10, 12, 18$, the half-filled systems $Z = 37, 55, 75, 83, 87$, and the anomalous systems $Z = 29, 41, 47, 58, 79, 89$. Not all of the respective peaks are deep enough to be distinguished

throughout the curve. Notice the slight local extrema at $Z = 41$ and the medium ones at $Z = 47, 55$. Much more relevant are: (i) the absolute minimum $Z = 79$ (Au) and the next local minimum $Z = 83$ and (ii) the next 'pair of contiguous minima' $Z = 87, 89$.

Now, and after discussing in detail the appearance and relevance of QSI_q local extrema and their 'interconnection' with those of the JSD, we feel compelled to justify these results. Several questions arise immediately, for instance: is there any physical reason for, for example, half-filled systems to be displayed as extrema? Or, what is the reason behind the 'exchange between neighbors' shown in Table 4.1 We proceed below to look for answers to these questions, on the basis of the structural patterns governing Schrödinger and Dirac one-particle densities.

Up to now, within this section, we have been concerned with (di)similarity among densities in terms of global functionals $F(\rho_S, \rho_D)$. Let us now consider the respective radial densities $D_S(r)$ and $D_D(r)$, with $D(r) = 4\pi r^2 \rho(r)$ defined in terms of the spherically averaged density $\rho(r)$. Similar comparative analyses among atomic radial densities, in a relativistic framework, were exhibited in the literature (see e.g. Refs. [170, 172, 177, 178]).

One way to quantify Schrödinger-Dirac discrepancies at any point, say r, is to quantify the ratio $D_S(r)/D_D(r)$ or, to be more precise, the deviation (from above or from below) of this ratio from unity.

The above quotient is displayed in Figure 4.4 for two half-filled systems included in Table 4.1, namely $Z = 7$ and $Z = 51$ in Figures 4.4(a) and 4.4(b), respectively. For comparative purposes, ratios of the respective closest neighbors (i.e. those with nuclear charges $Z \pm 1$) are also displayed. The aim is to understand, on the basis of density structural patterns, the main properties of half-filled systems within the set of QSI_q and JSD extrema, interpreted in terms of relativistic effects.

Let us consider Figure 4.4(a), enclosing the Schrödinger-Dirac density ratios for the trio $Z = 6, 7, 8$. All respective ratios remain roughly constant up to $r \sim 2$ a.u. Beyond that threshold, apparent differences appear: the ratio for the half-filled Nitrogen ($Z = 7$) strongly decreases, reaching a value as low as 0.15 at $r \sim 10$ a.u. On the contrary, its neighbors $Z = 6, 8$ display a slowly decreasing behavior up to $r \sim 12$ a.u. and then grow at an explosive rate following roughly parallel paths. The conclusion is that, within the outermost region, the Dirac density profile dominates the Schrödinger one for the half-filled system, while the opposite applies for its neighbors.

Similar conclusions on the long-range behaviors are obtained from the analysis of Figure 4.4(b), which displays the density ratios for the trio $Z = 50, 51, 52$, enclosing the half-filled $Z = 51$. The opposite increasing/decreasing behaviors occur when passing $r \sim 3$ a.u. Below that threshold, the three curves roughly follow the same path, which displays some kind of slightly oscillatory behavior around unity (due to the contraction of inner subshells towards the nucleus, a well-known relativistic effect). Deviations

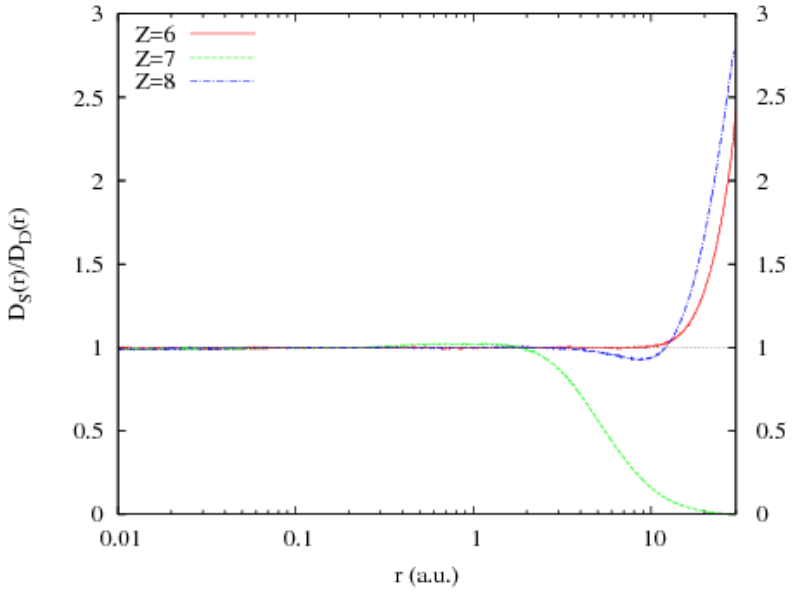

(a) Nuclear charges $Z = 6, 7, 8$

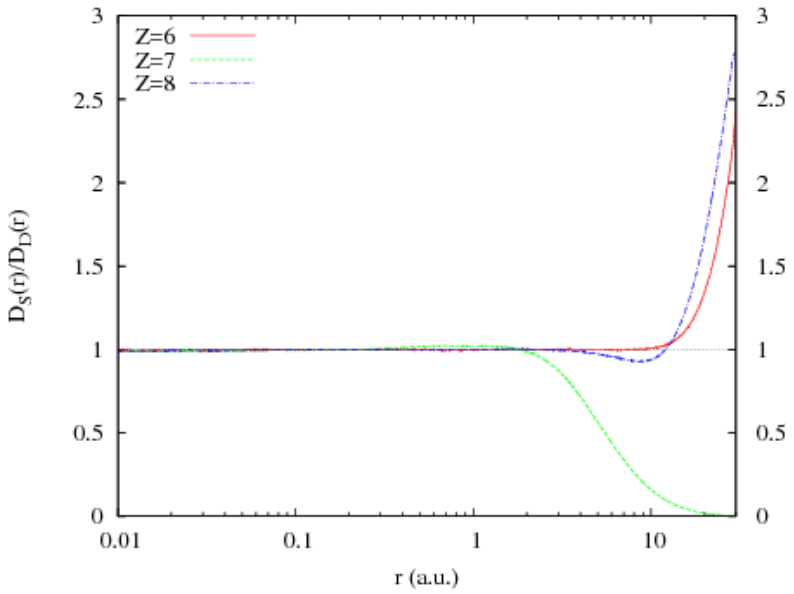

(b) Nuclear charges $Z = 50, 51, 52$

FIGURE 4.4: Quotient of Schrödinger and Dirac radial densities $D(r)$ for the trios of neutral atoms with nuclear charges (a) $Z = 6, 7, 8$, and (b) $Z = 50, 51, 52$. Atomic units (a.u.) are used.

from this value are small, maybe with the exception of the core region where all three curves diminish up to 12% from unity. Thus, dominance of the Dirac profile over the Schrödinger one appears both at short and long ranges: only slightly in the former and significantly in the latter.

Now, we consider a similar study regarding the aforementioned 'exchange between neighbors'. For illustration, the density ratios for the trio $Z = 29, 30, 31$ are displayed

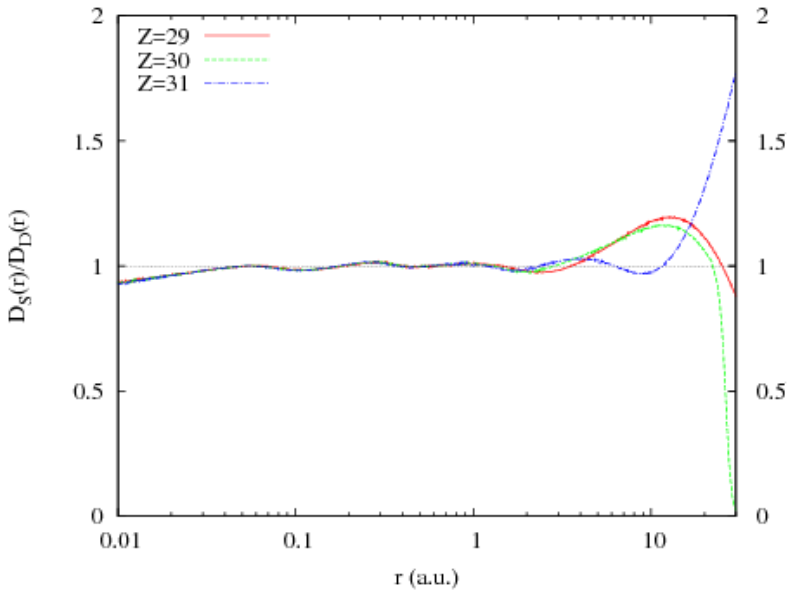

FIGURE 4.5: Quotient of Schrödinger and Dirac radial densities $D(r)$ for the trio of neutral atoms with nuclear charges $Z = 29, 30, 31$. Atomic units (a.u.) are used.

in Figure 4.5. It is important to remember that systems $Z = 29$ (anomalous) and $Z = 30$ (closed-shell) exchange their role as minima through Table 1, within the range $q = 0.2 - 0.7$. This could be justified by considering their respective density ratios (see Figure 4.5), with similar curves through the graph (in fact overlapping up to $r \sim 10$ a.u.) and sharing a decreasing behavior beyond that value. The other member of the above trio (i.e., $Z = 31$) displays significant differences from $r = 5$ a.u. onwards. It first decreases (while its companions increase) and then all three curves invert their monotonic behavior (from $r \sim 10 - 12$ a.u. onwards). For the inner region, the reason behind the observed oscillatory behavior is the same as for Figure 4.4(b).

In summary of the main points of the above numerical discussion, we emphasize the ability of the QSI_q to detect relativistic effects in atomic systems at the one-particle level. These results go beyond those previously reported within this context, based on other comparative functionals (e.g., the usual QSI, the JSD and KL divergences). The reason behind this appears to be clearly determined by the proper weight of the density in the outermost region, as observed in this manuscript and previously suggested in Ref. [98].

4.2 Conclusions

Properly quantifying differences between Schrödinger and Dirac one-particle atomic densities requires the capability to distinguish the relative contribution of inner and outermost regions. Such is not the case of the pioneering quantum similarity index QSI (which almost completely neglects the outermost region) but of its generalization QSI_q.

Deficiencies of QSI to capture sufficient information from the valence region were solved, in part, by means of Shannon-like functionals in a recent work. There, the main conclusion was that main differences among atomic charge densities, due to relativistic effects, could be due to their long-range behaviors.

Conclusions from the present QSI_q-based study are two-fold: First, the characteristic parameter of this functional allows for continuous scanning of the relative contributions due to the inner and outermost regions, progressively revealing the relevance of shell-filling patterns. Second, the structure of the radial density for selected systems, chosen from the set of QSI_q extrema, is explored in detail and compared with that of their neighbors. The results obtained here reaffirm the well known features emphasized in previous works that regard long-range behaviors as those most affected by relativistic effects.

A detailed numerical analysis within the range $0 < q < 2$ enhances the following observations: (i) In going from the monotone case ($q = 2$) up to $q = 1$, appearance of local extrema resembles that of Shannon-like functionals and (ii) diminishing the parameter below the (rough) threshold $q = 1$ progressively increases the number of extrema, preserving the previously known patterns of classification. From the above conclusions, one main open problem immediately arises: a theoretical justification of the numerical results discussed here. It is particularly important to understand the influence, beyond the prominence of relativity, of the charge density in closed-shell, half-filled and anomalous systems, most probably on the basis of the spin-orbit interaction. It is pertinent also to analyze the first AIP in both the Schrödinger and Dirac cases.

Chapter 5

Electron pair densities: An information-theoretical approach

One-eletron densities have a very straightforward meaning in atomic physics. They are directly related to the probability of finding an electron in a determinate region of the atom. One can study different regions of the atomic density and thus one can understand the way electrons populating that region behave. There is a huge amount of information coded inside monoelectronic densities. However, there is some information that this kind of density lacks, mainly information about the electron correlations. These densities don't directly give us any information at all about how the position of an electron conditions the position of the others. It is in this context when electron pair densities arise. Two-electron densities directly tell us the way the position of an electron is conditioned by the position of all the others, and with them one can understand different behaviors that are impossible to study using bare monoelectronic densities.

As we have treated in the previous chapters, the magnitudes of the information theory are very useful when trying to understand different traits and behaviors of atomic systems. In the past years there have been plenty of studies of quantum systems by means of the informational measures. Most of these studies have been focused on the monoelectronic atomic systems, providing analyses on, e.g., the Shannon entropy[189], Fisher information [22–24], similarity indices [125, 190], different divergences measures [115, 151] and complexity measures [22, 24, 27]. However, as previously mentioned, studies focused on two-electron densities require another point of view in order to analyze correlation-like qualities [191–196]. We now would like to employ some of these measures in order to try to establish some relations between the informational measures and properties of the electron pair densities.

In past years there have been some successful attempts to study the electron pair densities, exposing uncertainty relationships [192], calculating information theoretical measures such as Shannon-related measures [189, 193, 195] or similarity measures [192, 193,

197, 198]. This knowledge gained over the electron pair densities has translated in numerous and diverse applications. Two-electron densities have been employed to the analysis and detection of chemical bonds in molecules, finding that regions where electrons presented a higher correlations were directly related to the position of the bonds [199, 200]. Electron pair densities have also been employed as a scale-down method used to study many particle systems [201–205]. Even an alternative density functional theory has been developed, with electron pair density as the functional key [206–208].

Some of the analyses made in the past on the electron pair density could not be as exhaustive as would have been desirable due to technical limitations of the numerical methods used, unable to calculate the two electron densities for all the atomic systems in the Periodic Table. We want to complete these studies with a more extensive list of informational quantities, using these past results as a supporting floor, and extending them to all the neutral atomic systems in the Periodic Table, as well as for cations and anions.

This chapter is structured as follows: in the first section we show the formulation of the pair densities and how their aspect would be when used in the context of the Hartree-Fock method. Then we are adapt the different informational measures we will use in this study, starting from the traditional monoelectronic measures we discussed in Chapter 1. These measures comprise the Shannon entropy, the disequilibrium, the LMC complexity, the Jensen-Shannon divergence and the quantum similarity index. In the second section we will provide and discuss the numerical results regarding the measures showed in the previous section. First we will calculate the Shannon entropy for one-electron and electron pair densities in both position and momentum spaces, in order to better understand the different information that each density allows to grasp. We will then discuss the results. An identical study will be done, using the disequilibrium measure, as an alternative source of information. The LMC complexity will be calculated and discussed likewise, as well as the corresponding information planes in order to establish . We will consider the Jensen-Shannon divergence and will use it for the direct comparison between the one and two electron densities first, and then to compare neutral-ion pair densities, as this would be a brand-new study inside the electron pair density paradigm. After that we will address the results of the QSI calculations, in order to complete past studies that only dealt with a limited set of the atomic systems in the Periodic Table. Finally, some conclusions will be discussed and future works will be proposed

5.1 Electron pair densities and related measures

In terms of the N-electron wave function, the two-electron densities are defined as

$$\Gamma(\vec{r}_1, \vec{r}_2) = \int \Psi(\vec{x}_1, \vec{x}_2, \cdots, \vec{x}_N)\Psi^*(\vec{x}'_1, \vec{x}'_2, \cdots, \vec{x}'_N)d\sigma_1 d\sigma_2 d\vec{x}_3 \cdots d\vec{x}_N \qquad (5.1)$$

in the position space, and

$$\Pi(\vec{p}_1, \vec{p}_2) = \int \Phi(\vec{y}_1, \vec{y}_2, \cdots, \vec{y}_N)\Phi^*(\vec{y}'_1, \vec{y}'_2, \cdots, \vec{y}'_N)d\sigma_1 d\sigma_2 d\vec{y}_3 \cdots d\vec{y}_N \tag{5.2}$$

in the momentum space, respectively. The variables $\vec{x}_i = \vec{r}_i\sigma_i$ and $\vec{y}_i = \vec{p}_i\sigma_i$ are combined coordinates which include the spin, $\Psi(\vec{r_i})$ is the wave function in the position space for the i electron, $\Phi(\vec{p_i})$ is the wave function in the momentum space for the i electron, and N is the total number of electrons.

As previously mentioned, the physical meaning of these densities regards the probability of finding an electron with a compatible state within the region $\vec{r}_1 d\vec{r}_1$ if there is another electron in a compatible state within the region $\vec{r}_2 d\vec{r}_2$. These densities are directly related to the electron correlations, as the compatibility of an electron state is in organically determined by the compatibility of its state with those of the others. They naturally give us a relation of correlation between electrons. Additionally, another difference between one-electron and two-electron densities deserves to be pointed out: the latter is bidimensional while the former is monodimensional. There is a much higher amount of information to extract from these kind of densities, e.g., the possible state of an electron in the atomic space is conditioned by the possible state of another one. However, the computational cost considerably increases, more precisely, amount of the square rate of the one-electron density case. This is exciting, as there is an enormous new information to be analyzed, but we have to be careful in our ways, as it would be much more demanding, so we will have to make compromises in order to do so.

The two-electron densities are going to be calculated by the Hartree-Fock approach, so the wave functions should be seen as:

$$\Psi(\vec{x}_1, \vec{x}_2, \cdots, \vec{x}_N) = \frac{1}{\sqrt{N}} \begin{vmatrix} \phi_1(\vec{r}_1, \sigma_1) & \phi_2(\vec{r}_1, \sigma_1) & \cdots & \phi_N(\vec{r}_1, \sigma_1) \\ \phi_1(\vec{r}_2, \sigma_2) & \phi_2(\vec{r}_2, \sigma_2) & \cdots & \phi_N(\vec{r}_2, \sigma_2) \\ \vdots & \vdots & \vdots & \vdots \\ \phi_1(\vec{r}_N, \sigma_N) & \phi_2(\vec{r}_N, \sigma_N) & \cdots & \phi_N(\vec{r}_N, \sigma_N) \end{vmatrix} \tag{5.3}$$

being N the number of electrons and each $\phi_i(\vec{r_j}, , \sigma_j)$ an eigenfunction of the principal quantum number n, the orbital quantum number l and its projection onto the z-axis m. The functions $\phi_i(\vec{r_j}, , \sigma_j)$ have the following dependency in r and σ:

$$\phi(\vec{r}, \sigma) = \varphi(\vec{r})\chi(\sigma) \tag{5.4}$$

being φ the spatial component and χ the spinorial one. Both functions respectively verify its corresponding orthogonal relation:

$$\int \varphi_i^*(\vec{r})\varphi_j(\vec{r})d\vec{r} = \delta_{ij} \tag{5.5}$$

and

$$\sum_{\sigma} \chi_i^*(\sigma)\chi_j(\sigma) = \delta_{m_{\sigma_i} m_{\sigma_j}} \tag{5.6}$$

where m_σ is the spin projection.

In order to obtain the two-electron density, we can write $|\Psi(\vec{x}_1, \vec{x}_2, \cdots, \vec{x}_N)|^2$ as follows:

$$|\Psi(\vec{x}_1, \vec{x}_2, \cdots, \vec{x}_N)|^2 = \frac{1}{N!}\sum_{\sigma,\sigma'}(-1)^{\sigma+\sigma'}\prod_{j=1}^{N}\phi_i^*(\vec{r_j}, \sigma_j)\phi_i(\vec{r_j}, \sigma_j'), \tag{5.7}$$

integrating $\forall j = 3, \cdots N$, the orthogonality relation from Eq. (5.6) imposes that $\sigma_3 = \sigma_3', \cdots, \sigma_N = \sigma_N'$. In addition, given a value for σ_1, there are only two possibilities for σ_1':

i) $\sigma_1' = \sigma_1$, making then $\sigma_2' = \sigma_2$.

ii) $\sigma_1' = \sigma_2$ making then $\sigma_2' = \sigma_1$.

Taking these consideration into account, the Eq. (5.7) can be expressed as

$$\begin{aligned}|\Psi(\vec{x}_1, \vec{x}_2, \cdots, \vec{x}_N|^2 = \frac{1}{N!}\sum_{\sigma}\left[\prod_{j=3}^{N}|\phi(\vec{r_j}, \sigma_j)|^2\right] \times \\ \times \left[|\phi(\vec{r}_1, \sigma_1)|^2|\phi(\vec{r}_2, \sigma_2)|^2 - \phi_i^*(\vec{r}_1, \sigma_1)\phi_j(\vec{r}_1, \sigma_2)\phi_j^*(\vec{r}_2, \sigma_2)\phi_i(\vec{r}_2, \sigma_1)\right]\end{aligned} \tag{5.8}$$

The pair $\{\sigma_1, \sigma_2\}$ can take $N(N-1)$ different values, and for each of them, any term of the summation in σ contains $(N-2)!$ times this term. We can then write Eq. (5.1) in the form:

$$\Gamma(\vec{r}_1, \vec{r}_2) = \frac{1}{N!}\sum_{i=1}^{N}\sum_{i\neq j=1}^{N}(N-2)!\left[|\phi(\vec{r}_1)|^2|\phi(\vec{r}_2)|^2 - \phi_i^*(\vec{r}_1)\phi_j(\vec{r}_1)\phi_j^*(\vec{r}_2)\phi_i(\vec{r}_2)\right] \tag{5.9}$$

So, the two-electron densities or electron pair densities can be expressed as follows:

$$\Gamma(\vec{r}_1, \vec{r}_2) = \frac{1}{N-1} \left[N\rho(\vec{r}_1)\rho(\vec{r}_2) - \Gamma_x(\vec{r}_1, \vec{r}_2) \right] \tag{5.10}$$

in the position space, and

$$\Pi(\vec{p}_1, \vec{p}_2) = \frac{1}{N-1} \left[N\gamma(\vec{p}_1)\gamma(\vec{p}_2) - \Pi_x(\vec{p}_1, \vec{p}_2) \right] \tag{5.11}$$

in the momentum space, respectively. The functions $\rho(\vec{r_i})$ and $\gamma(\vec{p_i})$ are the one-electron densities and $\Gamma_x(\vec{r}_1, \vec{r}_2)$ and $\Pi_x(\vec{p}_1, \vec{p}_2)$ are the exchange densities in the position and momentum space respectively.

Due to the higher computational requirements the electronic pair densities demands, it is often needed to employ spherically averaged densities, defined as

$$\Gamma(r_1, r_2) = \frac{1}{(4\pi)^2} \int \Gamma(\vec{r}_1, \vec{r}_2) d\Omega_1 d\Omega_2 \tag{5.12}$$

in the position space, and

$$\Pi(p_1, p_2) = \frac{1}{(4\pi)^2} \int \Pi(\vec{p}_1, \vec{p}_2) d\Omega_1' d\Omega_2' \tag{5.13}$$

in the momentum space, where Ω_i and Ω_i' are the solid angles in the respective spaces.

Eqs. (5.12) and (5.13) provide the densities in which we will focus our attention in this chapter, as they still store most of the relevant information we are interested in, while being their manipulation less cumbersome.

Once defined the densities to be analyzed, let us define the information-theoretical measures we are going to use in this electron pair densities paradigm. All these quantities were considered before for one-electron densities, but now we show how they can be translated using the two-electrons densities.

The Shannon entropy (defined in Eq. (1.12) for the one-electron density) of the electron pair densities are given by:

$$S(\Gamma) = -\int \Gamma(\vec{r}_1, \vec{r}_2) \ln \Gamma(\vec{r}_1, \vec{r}_2) d\vec{r}_1 d\vec{r}_2 \tag{5.14}$$

for the position space, and

$$S(\Pi) = -\int \Pi(p_1, p_2) \ln \Pi(p_1, p_2) dp_1 dp_2 \tag{5.15}$$

for the momentum space, respectively.

We have already discussed the properties of the Shannon entropy for one-electron densities. It is, fundamentally, a measure of the dispersion or spreading of the probability density. Considering that the electron pair density is, in its spherically averaged form, bidimensional, while its corresponding monoelectronic ones is monodimensional, a higher value on the Shannon entropy can be expected just due to the more natural spreading of the density. The Shannon entropy has already been employed in the past for studying electron pair densities [189, 192, 193, 198] showing how correlation effects can be successfully detected with this measure, and establishing relation between its values and atomic properties.

Similarly, we can define the disequilibrium for two-electron densities as we did for one electron densities in Eq. (1.18). In position space, it takes the form

$$D(\Gamma) = \int \Gamma(\vec{r}_1, \vec{r}_2)^2 d\vec{r}_1 d\vec{r}_2, \tag{5.16}$$

and in momentum space

$$D(\Pi) = \int \Pi(p_1, p_2)^2 dp_1 dp_2 \tag{5.17}$$

Using these magnitudes, the LMC complexity can be defined in a similar way as it was done for the one-electron density in Eq. (1.24):

$$C_{LMC}(\Gamma) = D(\Gamma) \times e^{S(\Gamma)} \tag{5.18}$$

for the position space, and

$$C_{LMC}(\Pi) = D(\Pi) \times e^{S(\Pi)} \tag{5.19}$$

for the momentum space.

Now we can define a divergence measure such as the Jensen-Shannon divergence employing the definition in terms of the Shannon entropy given by Eq. (1.29):

$$JSD(\Gamma_A, \Gamma_B) = S\left(\frac{\Gamma_A + \Gamma_B}{2}\right) - \frac{1}{2}\left[S(\Gamma_A) + S(\Gamma_B)\right], \tag{5.20}$$

in position space, and

$$JSD(\Pi_A, \Pi_B) = S\left(\frac{\Pi_A + \Pi_B}{2}\right) - \frac{1}{2}\left[S(\Pi_A) + S(\Pi_B)\right], \tag{5.21}$$

in momentum space, respectively.

A similarity measure, QSM, can also be proposed for electron pair densities as follows:

$$QSM(\Gamma_A, \Gamma_B) = \int \Gamma_A(\vec{r}_1, \vec{r}_2)\Gamma_B(\vec{r}_1, \vec{r}_2)d\vec{r}_1 d\vec{r}_2, \tag{5.22}$$

for the position space, and

$$QSM(\Pi_A, \Pi_B) = \int \Pi_A(\vec{p}_1, \vec{p}_2)\Pi_B(\vec{p}_1, \vec{p}_2)d\vec{r}_1 d\vec{r}_2, \tag{5.23}$$

for momentum space.

The quantum similarity index, based on QSM as we previously saw in Eq. (1.34), can be defined base as well using the two-electron densities in the form

$$QSI(\Gamma_A, \Gamma_B) = \frac{\int \Gamma_A \Gamma_B d\vec{r}}{\left(\int \Gamma_A^2 d\vec{r} \int \Gamma_B^2 d\vec{r}\right)^{1/2}}, \tag{5.24}$$

for position space, and

$$QSI(\Pi_A, \Pi_B) = \frac{\int \Pi_A \Pi_B d\vec{r}}{\left(\int \Pi_A^2 d\vec{r} \int \Pi_B^2 d\vec{r}\right)^{1/2}}, \tag{5.25}$$

for momentum space.

Both measures QSM and QSI have already been used in the past for analyzing two electron properties for a brief list of atoms and molecules [197, 209]. In this work we pretend to do a more exhaustive and systematic analysis of atomic systems using QSI.

5.2 Results

5.2.1 Shannon entropy and disequilibrium

Electron pair density has many differences with common monoelectronic density, being one of the most notable ones its higher uncertainty. When considering electron pairs the result is a rise on spreading. As has been discussed previously, Shannon entropy is a perfect uncertainty quantifier, hence it will be used in this section in order to study in which way spreading is presented in electron pair density.

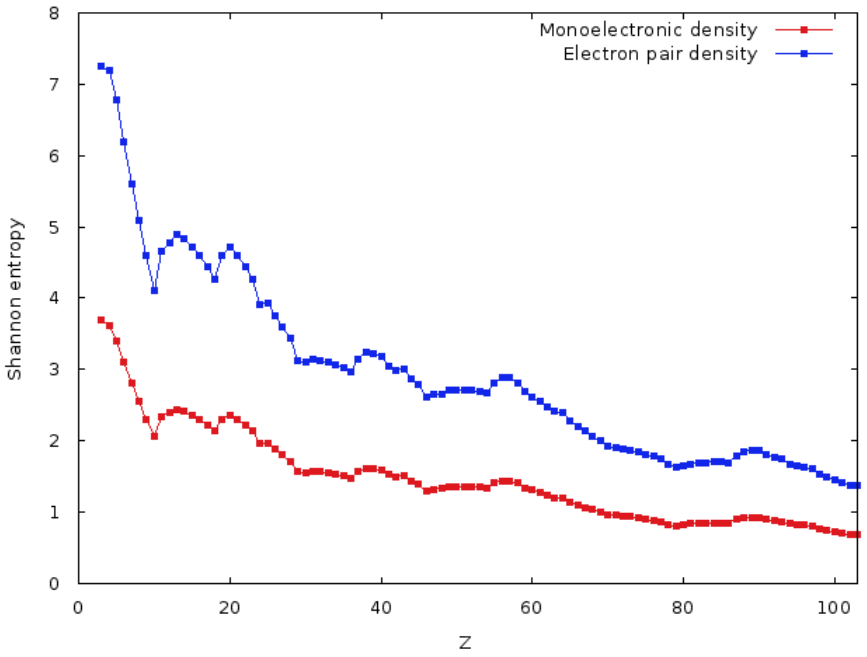

(a) Lineal scale

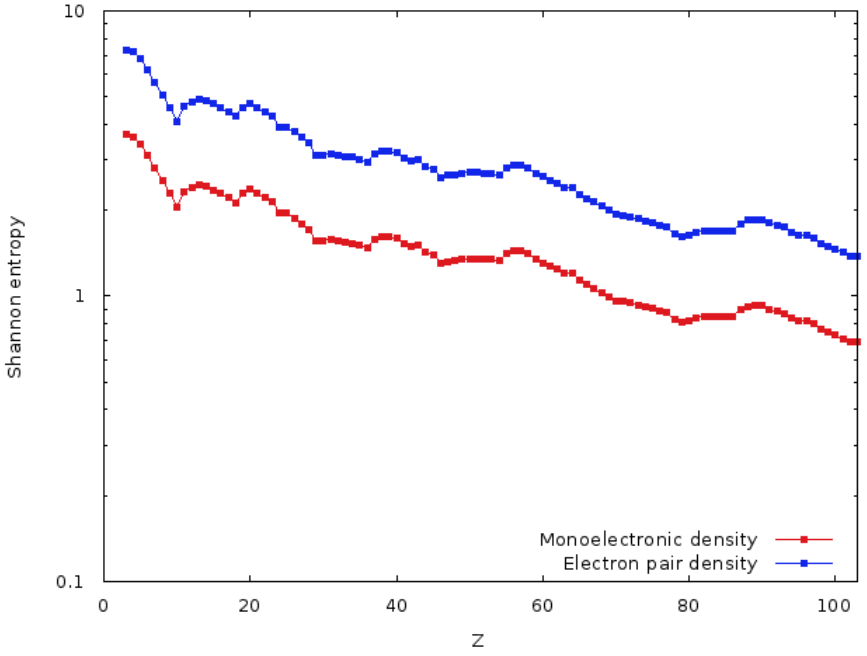

(b) Logarithmic scale

FIGURE 5.1: Shannon entropy in position space of both monoelectronic and electron pair densities respectively, of neutral atoms with nuclear charge $Z = 2 - 103$ (a) in lineal scale, (b) in logarithmic scale. Atomic units are used (a.u.)

In Figure 5.1 Shannon entropy in position space applied to monoelectronic and pair electron density has been represented. This has been calculated for neutral atoms with nuclear charge $Z = 2 - 103$. It can be observed that the curve corresponding to the Shannon entropy of the pair electron density, $S(\Gamma)$, is always above of the one-electron density ones, $S(\rho)$. As we expected, a higher uncertainty corresponding to the two-electron density with respect to the monoelectronic ones is confirmed.

A more detailed analysis of both curves shows a global decreasing tendency, although not general. Despite such global tendency, there are many irregularities in that monotonous behavior, more apparent in the case of $S(\Gamma)$, however there are still many local extrema present in both curves.

Both, the differences of the entropy values between the two curves, as well as the monotonous tendencies already mentioned, and also the appearance of local extrema in both cases, can be more clearly appreciated in Figure 5.1(b), which shows the same magnitudes, now in a logarithmic scale. In a lineal scale, due to the higher values of $S(\Gamma)$, the structural details of $S(\rho)$ are hidden. This is the reason behind using the logarithmic scale. In this way, local extrema of the monolectronic curve are clearly observed, despite being less prominent, in relative terms, compared with the pair curve.

First, is worth mentioning that the general monotonous tendencies for both densities as the charge increases, has an obvious interpretation attending to (i) physical implications of such a charge increment, and (ii) the meaning of Shannon entropy in a information-theoretical context. This information-theoretical meaning was mentioned in chapter (1), where the properties of Shannon entropy were discussed, particularly how this measures is capable of quantifying spreading or delocalization. An increment on the nuclear charge produces a stronger attraction over the electronic cloud towards the nucleus, producing a higher concentration of the electronic density, both pair and monoelectronic densities, around the origin. This provokes a higher localization of those distributions, i.e. a lower delocalization, which traduces on a lower value of the Shannon entropy.

Focusing our attention at the curve's structure in Figure 5.1, the next discussion points should be (i) Z values in which the extrema appears, and (ii) differences at the extrema distribution between both curves. Besides those two points, it would be desirable to know the reasons behind those matters. In order to answer these questions, the Table 5.1 is shown, in which the mentioned extrema are given, distributed in maximum and minimum respectively.

From Table 5.1 we can observe some interesting global tendencies, besides a few concrete exceptions:

- For the entropy at the pair density, $S(\Gamma)$, all the maxima include the IIA group of the Periodic Table (alkaline earth elements). The only exception is the presence of $Z = 13$, instead of $Z = 12$ (Magnesium).

Maxima		**Minima**	
$\mathbf{S}(\rho)$	$\mathbf{S}(\mathbf{\Gamma})$	$\mathbf{S}(\rho)$	$\mathbf{S}(\mathbf{\Gamma})$
3	4		
13	13	10	10
20	20	18	18
25	25	24	24
31	32	30	29
38	38	36	36
	43		42
50	50	46	46
57	56	54	54
84	84	78	79
89	88	86	86

TABLE 5.1: Local extrema of Shanon entropies, $S(\rho)$ and $S(\Gamma)$ in position space for neutral atoms with nuclear charge $Z = 2 - 103$.

- There are another five additional elements in the mentioned collection, being $Z = 25, 43$ with a half-filled valence shell, and $Z = 32, 50, 84$, with a p valence sub-shell.
- The minima are mainly composed by noble gases, without exception.
- Additional minima are: $Z = 24, 29, 42, 46, 79$, all of them with the same anomalous shell filling pattern: a sub-shell d half or completely filled, and an intern half-filled or empty s subshell.
- A comparative analysis between both densities is now required. Despite being both of them very similar, there are still some remarkable differences:
  - Some maximum of $S(\Gamma)$ do not match those in $S(\rho)$, in such cases the maximum fall to a system next to the original one. This happens with the systems with $Z = 4, 32, 56, 88$ in $S(\Gamma)$, which corresponding maximum in S_ρ are $Z = 3, 31, 57, 89$, respectively. Those replacement are emphasized in Table 5.2 and corresponds to systems with one or two electrons in the valence subshell ($Z = 3 - 4, 31 - 32$) or those with an additional electron in the s subshell ($Z = 56 - 57, 88 - 89$).
  - These differences with the maxima appears in some minima as well. Those systems with $Z = 30, 78$ for $S(\Gamma)$ correspond with $Z = 29, 79$ for $S(\rho)$. The light system have a half or complete s subshell (with anomalous filling on the internal subshells), and the heavy systems have an empty or full valence subshell (with anomalous filling on the internal subshells as well).

The resemblance between $S(\rho)$ and $S(\Gamma)$ is evident when looking at Figure 5.2, attending not only its extrema position but the absolute value oh both magnitudes as well. In Figure 5.2(a) we can see, again the respective curves in logarithmic scale, allowing

Maxima		
System		**Valence subshell**
3	Li	$2s^1$
4	Be	$2s^2$
13	Al	$3p^1$
20	Ca	$4s^2$
25	Mn	$3d^5$
31	Ga	$4p^1$
32	Ge	$4p^2$
38	Sr	$5s^2$
43	Tc	$4d^5$
50	Sn	$5p^2$
56	Ba	$6s^2$
57	La	$6s^2 5d^1$
84	Po	$6p^4$
88	Ra	$7s^2$
89	Ac	$7s^2 6d^1$

Minima		
System		**Valence subshell**
10	Ne	$2p^6$
18	Ar	$3p^6$
24	Cr	$4s^1 3d^5$
29	Cu	$4s^1 3d^{10}$
30	Zn	$4s^2 3d^{10}$
36	Kr	$4p^6$
42	Mo	$5s^1 4d^5$
46	Pd	$5s^0 4d^{10}$
54	Xe	$5p^6$
78	Pt	$6s^1 5d^9$
79	Au	$6s^1 5d^{10}$
86	Rn	$6p^6$

TABLE 5.2: Valence subshell of systems corresponding to the local extrema of Shannon entropy in position space.

a more precise scrutiny. It is apparent the extreme similarity between both curves, almost resembling an identical copy, just vertically displaced. Effectively, after looking at Figure 5.2(b) we can conclude that the only discrepancy is a multiplying factor, which is traduced in the logarithmic scale as a vertical displacement with a value of $\log 2$. The resulting curves clearly overlap, which means that we could affirm that $S(\Gamma) \approx 2S(\rho)$ for every system with $Z = 2 - 103$.

As we have mentioned above, the results in the momentum space have been very difficult to obtain, mostly due to the higher computational prowess needed to perform the calculations. Although we work with spherical averaged densities, the integration grid is still bidimensional which greatly increases the number of calculations needed to reach a required precision. Even for the one-electron density, calculations in momentum space require a much more extensive grid than in the position space, which multiplies to the square for the electron pair density, i.e., if a grid with n points is needed for the case of monoelectronic density, the electron pair density will require n^2 points.

In Figure 5.3 we can see the Shannon entropy values for monoelectronic and electron pair densities in momentum space for neutral atoms with nuclear charge $Z = 2 - 103$. As we observed in position space, the values of Shannon entropy of the two-electron density are much higher than the values of the one-electron density. In this case, no complex structure can be observed, just a monotonous increment, that increment is more noticeable at lower Z values, and even more for the pair density. For higher values of Z this stabilizes.

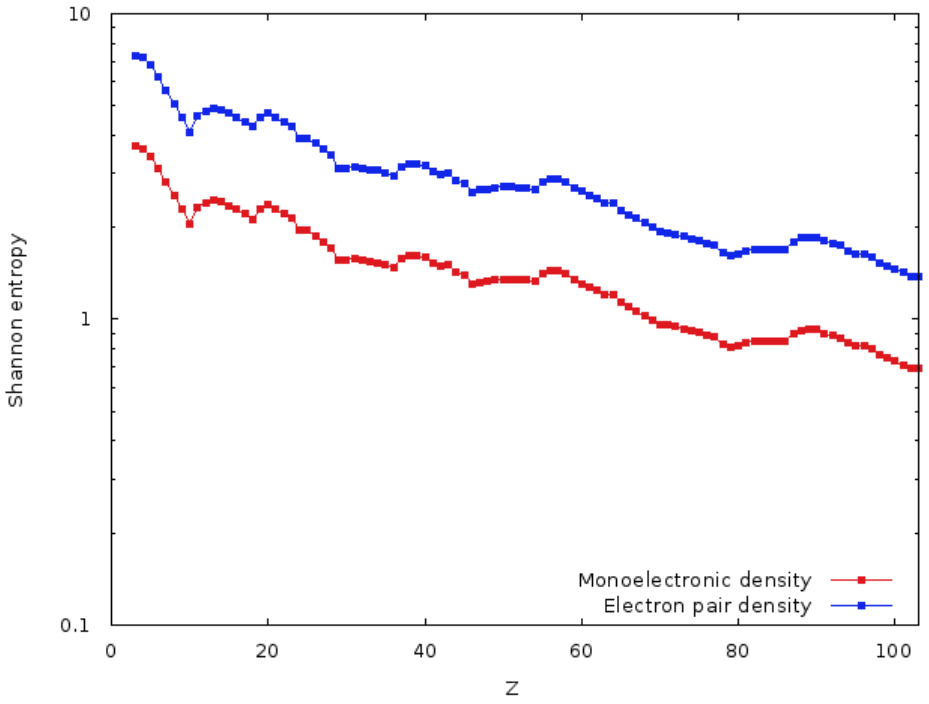

(a) $S(\rho)$ and $S(\Gamma)$

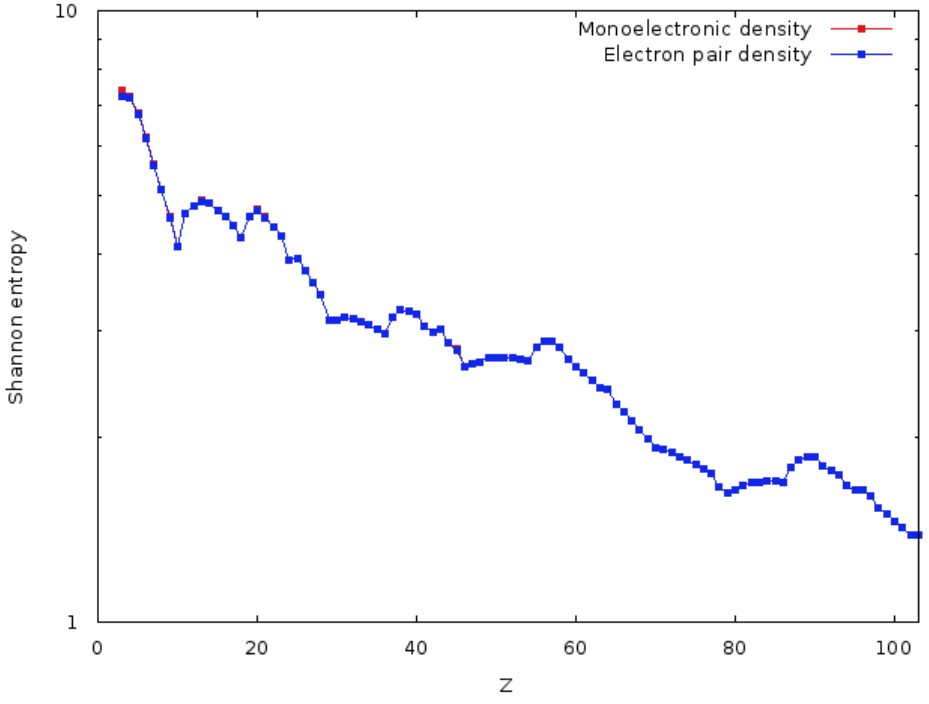

(b) $2S(\rho)$ and $S(\Gamma)$

FIGURE 5.2: Shannon entropy in position space of the monoelectronic and electron pair density $S(\rho)$ and $S(\Gamma)$ respectively, for neutral atoms with $Z = 2 - 103$; (a) $S(\rho)$ and $S(\Gamma)$ vs. Z, (b) $2S(\rho)$ and $S(\Gamma)$ vs. Z. Atomic units (a.u.) are used.

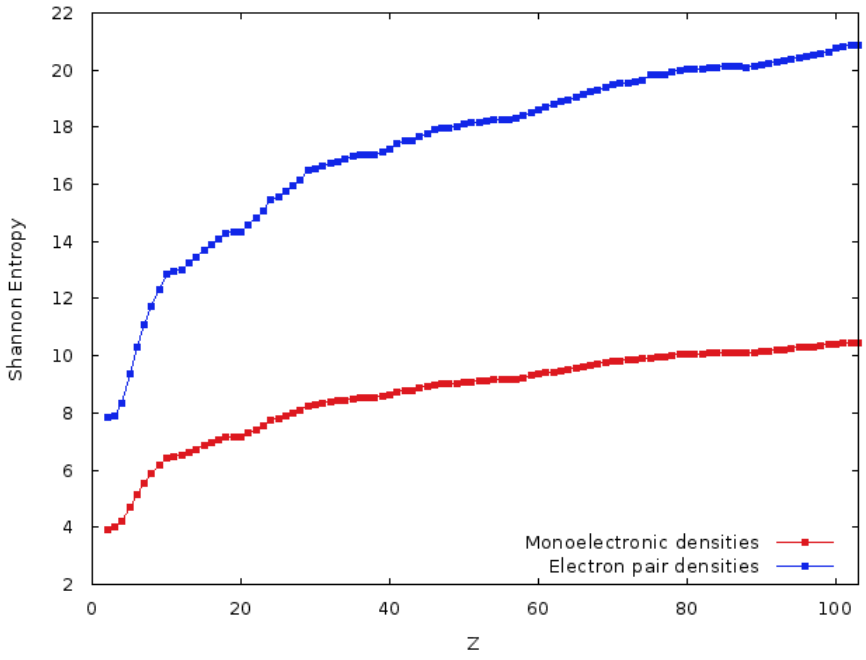

FIGURE 5.3: Shannon entropy of the monoelectronic and electron pair densities for neutral atoms with $Z = 2 - 103$ in momentum space Atomic units (a.u.) are used.

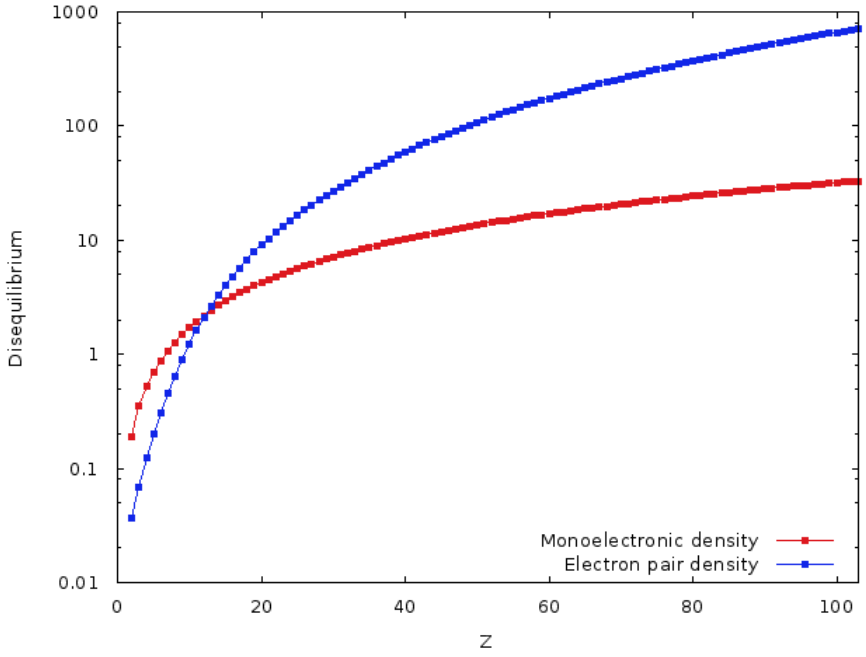

FIGURE 5.4: Disequilibrium for monoelectronic and electron pair densities $D(\rho)$ and $D(\Gamma)$, respectively, in position space for atomic system with $Z = 2 - 103$. Atomic units (a.u.) are used.

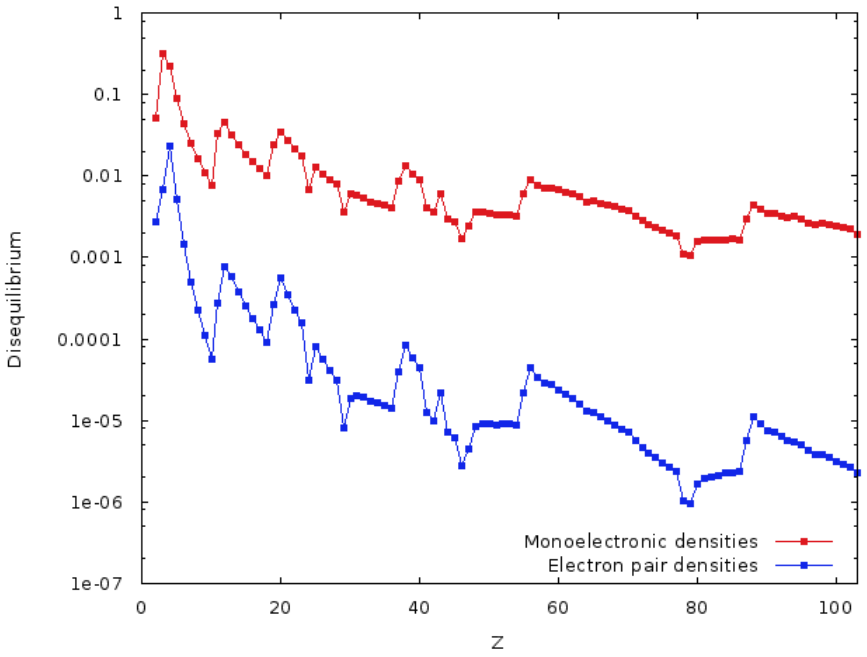

FIGURE 5.5: Disequilibrium for monoelectronic and electron pair densities $D(\rho)$ and $D(\Gamma)$, respectively, in momentum space for atomic system with $Z = 2 - 103$. Atomic units (a.u.) are used.

In Figure 5.4 the disequilibrium for monoelectronic and electron pair densities in position space for atomic systems with nuclear charge $Z = 2 - 103$ have been depicted. We can observe in the figure that, for both densities, the disequilibrium increases, this is due to the higher nuclear attraction over the electronic cloud. A notable growth can be appreciated for the one-electron density, even more than the two-electron density. The most remarkable trait is how the curves intersect around $Z = 10$. For light systems, with a low nuclear charge, the value of the disequilibrium for the electron pair density is lower than the monoelectronic density value. This is due to the low quantity of electron pairs with such a low number of electrons, which reduces the effect of the contraction provoked by the nucleus. At higher values of Z this is the opposite, which results in a higher disequilibrium value. We can see in Figure 5.5 the disequilibrium of those densities in momentum space, and how they present identical extrema structure and almost the same monotony tendencies as the Shannon entropy in position space (see Figure 5.1).

5.2.2 LMC shape complexity

After the analysis of the Shannon entropy and the disequilibrium, we are able to obtain the LMC complexity measures, given by Eqs. (5.18) and (5.19). In Figure 5.6, the LMC complexity measure of the electron pair density is shown for atomic systems with nuclear charge $Z = 2 - 103$ in position and momentum space, as well as the monoelectronic one. A much more detailed discussion of the monoelectronic case can be

found in the Ref [24]. As we can observed for the two-electron case 5.6(a) for the position space, multiple local extrema appears, matching those of the Shannon entropy previously discussed. This is due to the fact that the exponential entropy is the most dominant factor at the LMC complexity, in this case, which defines its extrema structure. However its value is much higher, understandable due to the exponentiation of the Shannon entropy, and also to the fact that the disequilibrium acts as a modulator, increasing even more the value for higher Z. Comparing with the monoelectronic case 5.6(b), the minima exhibited by the electron pair density present the same structure, as both present a local minimum in $Z = 10, 18, 24, 36, 42, 46,$ (i.e. noble gases and anomalous filling systems). The maximum structure, however, is slightly different. In momentum space the situation is the same, but in this case the extrema present in the curve are those appearing in the disequilibrium, as the Shannon entropy in momentum space has barely any structure, which are modulated by the Shannon entropy value, causing a general incremental tendency.

Previously mentioned comments about the LMC complexity measure can be observed at Figure 5.7(a), which shows the information plane $D - L$ in the position space for monoelectronic and electron pair densities. The analogous plane, conformed by the square of those quantities, i.e $D^2 - L^2$, for the monoelectronic density, has been depicted in Figure 5.7(b). It shows a similar structure than the previous one, however, a more notable overlap takes place between the both curves.

5.2.3 Jensen-Shannon divergence and quantum similarity index

All results presented before are for the study of individual information measures, i.e., Shannon entropy, disequilibrium and LMC complexity measure for both monoelectronic and electron pair densities. Now, we are interested in the analysis of the differences between those densities. In order to do that we will employ divergence measures precisely for this objective.

Firstly, let us consider the Jensen-Shannon divergence. In order to quantify the correlation between electrons, we should examine the comparison between the electron pair density and the product of the monoelectronic densities, i.e. the functions $\Gamma(\vec{r}_1, \vec{r}_2)$ and $\rho(\vec{r}_1)\rho(\vec{r}_2)$ in position space, and with $\Pi(\vec{p}_1, \vec{p}_2)$ and $\gamma(\vec{p}_1)\gamma(\vec{p}_2)$ in momentum space. In the hypothetic case of those variables having no correlation, JSD value should be zero. So, this allows us to use JSD as a measure of the disparity between the monoelectronic and electron pair densities in each position and momentum spaces.

In Figure 5.8, the Jensen-Shannon divergence between the electron pair density and the product of the corresponding monoelectronic densities for atomic systems with nuclear charge $Z \in [2, 103]$ in position space is shown. It can be observed the decreasing tendency of JSD when the nuclear charge of the system increases, which means that the

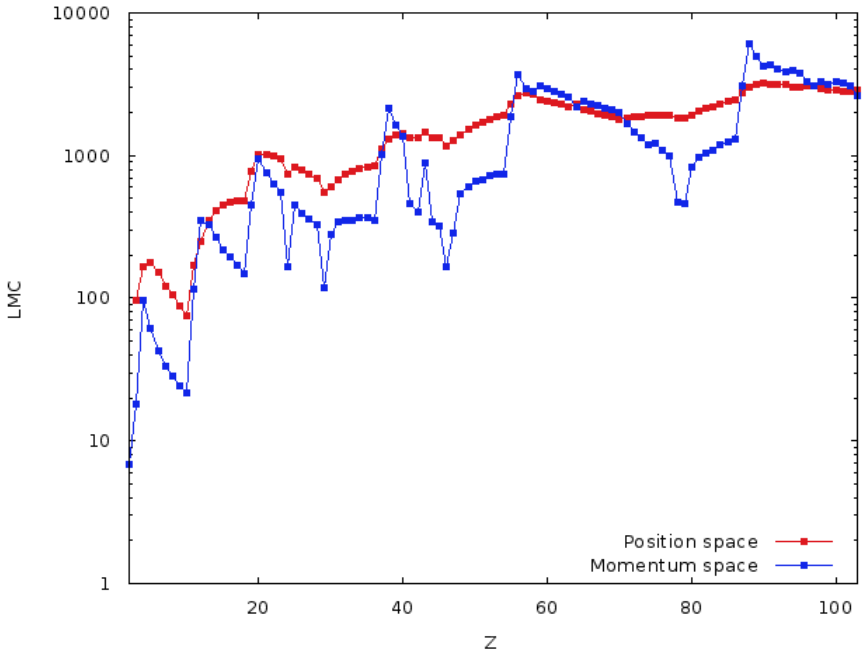

(a) Electron pair density

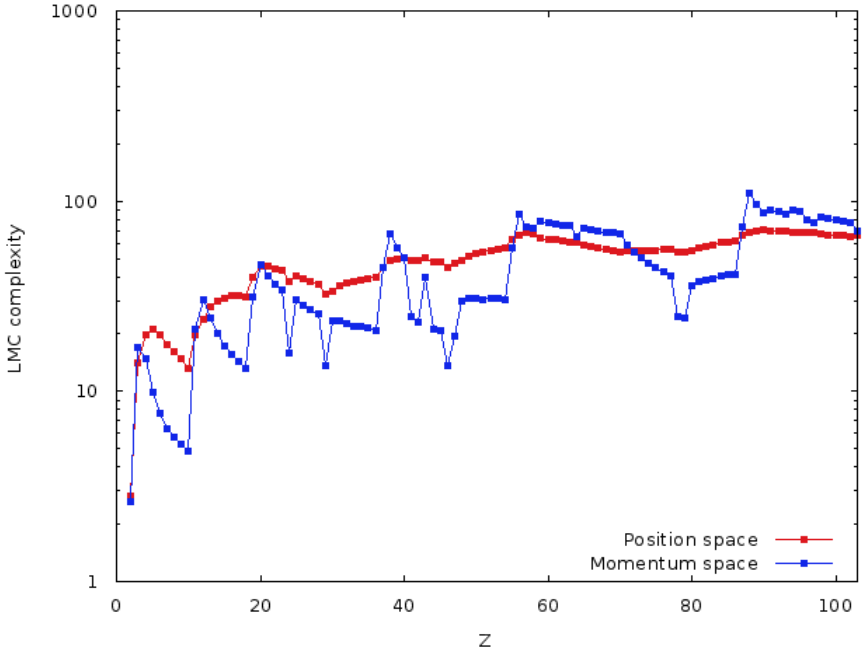

(b) Monoelectronic density

FIGURE 5.6: LMC complexity (C_{LMC}) of the (a) Electron pair and (b) Monoelectronic density, in position and momentum space for system with nuclear charge $Z = 2 - 103$ on a logarithmic scale.

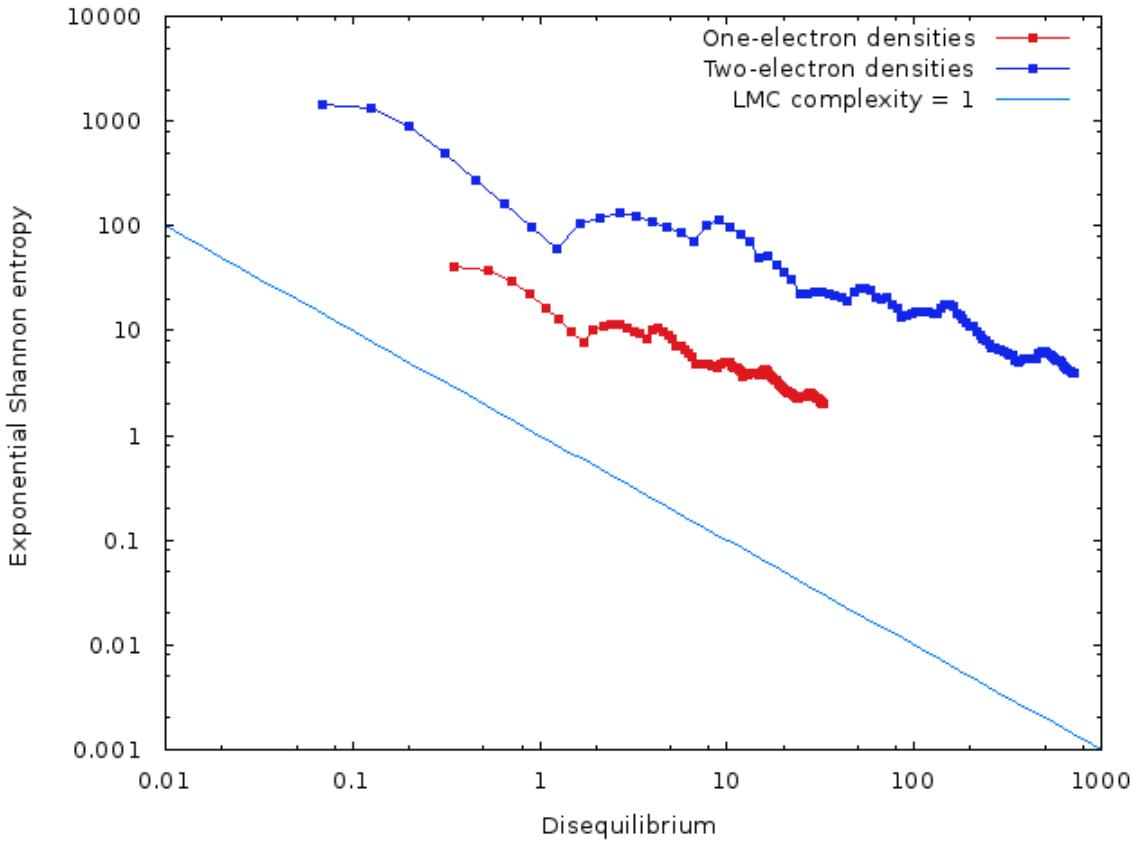

(a) $D - L$ plane for monoelectronic and electron pair densities

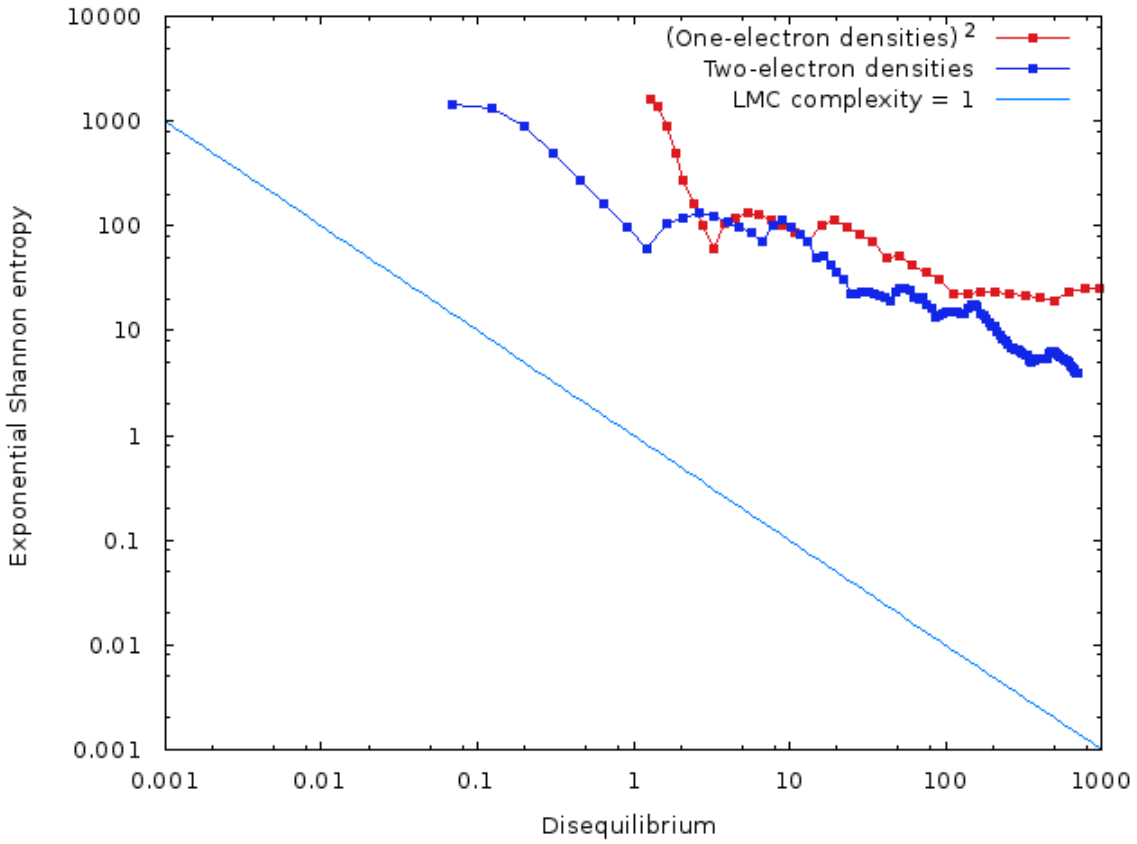

(b) $D^2 - L^2$ plane for monoelectronic densities and $D - L$ for electron pair densities

FIGURE 5.7: Information planes: (a) $D - L$ plane for monoelectronic and electron pair densities, (b) $D^2 - L^2$ plane for monoelectronic densities and $D - L$ for electron pair densities. Atomic units (a.u.) are used.

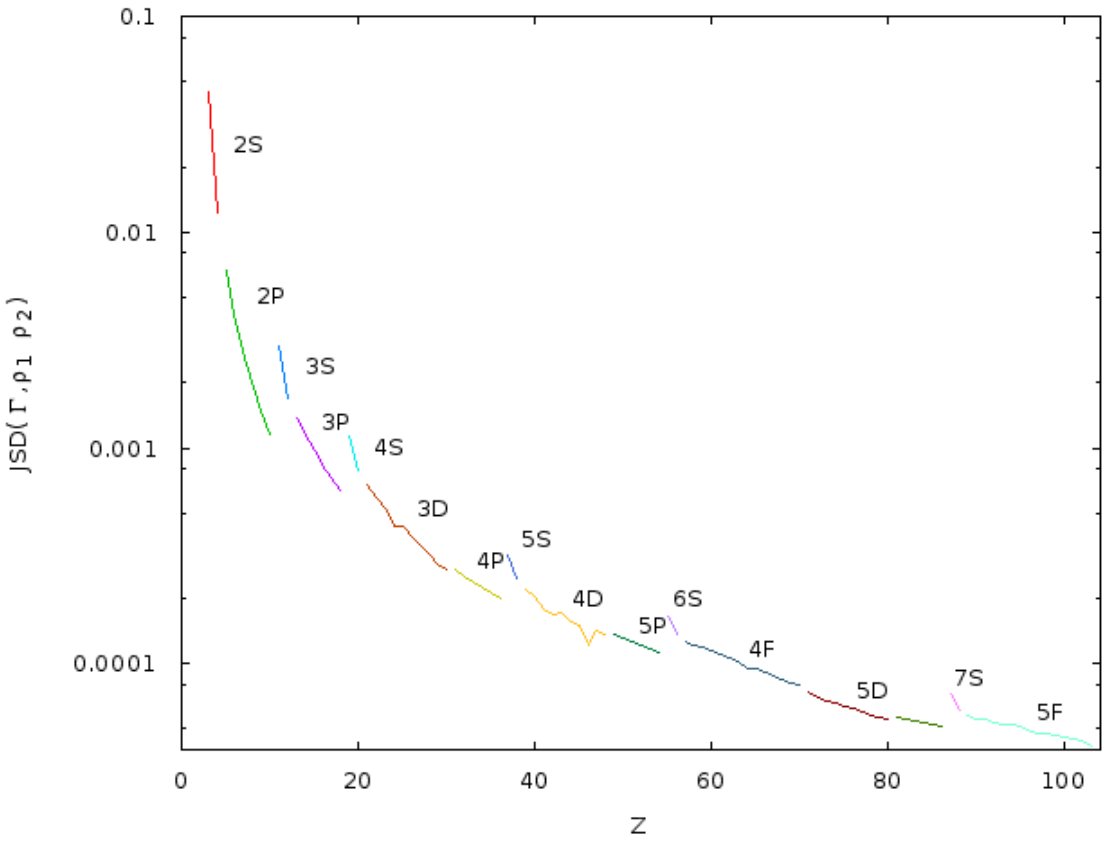

FIGURE 5.8: Jensen-Shannon divergence in position space, JSD_r, between the electron pair density and the product of monoelectronic densities, for atoms with nuclear charge $Z = 2 - 103$. Atomic units (a.u.) are used.

correlation decreases as the number of electrons increases. This was predictable, because the relative number of electrons determines how strong or weak are the relevance of the correlation between the mentioned electrons. For example, if we have information about the position of an electron within a group of three, this knowledge becomes much more relevant than if we have a group of thirty electrons, when the information about just one does not tell us much more about the other twenty nine.

Notwithstanding, some patterns are still noticeable, clearly related to the shell filling structure. The tendency is monotonous, without many exceptions for a long period, however some discontinuities appear when changing from a period to another (i.e. when a new shell starts to fill). Each segment can be assigned to a particular shell, in the way the figure shows. Besides, some less relevant extrema appear, all of them related to anomalous shell filling systems.

The Jensen-Shannon divergence between electron pair density and the product of monoelectronic densities in momentum space does not give us much relevant information. The conclusions we arrive are the same, in fact, the curves in both spaces are almost indistinguishable as it can be seen in Figure 5.9 where JSD in both position and momentum spaces have been depicted.

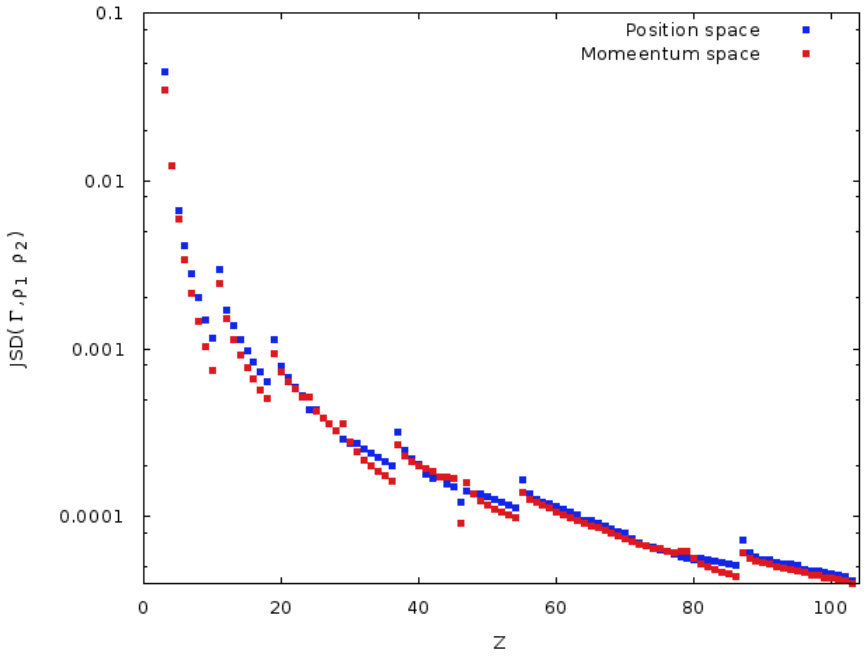

FIGURE 5.9: Jensen-Shannon divergence in momentum and position spaces, JSD_r and JSD_p, respectively, between electron pair densities and a product of monoelectronic densities, for neutral atoms with nuclear charge $Z = 2 - 103$. Atomic units (a.u.) are used.

Until now, we have analyzed neutral atoms and their properties, but it would be interesting to consider their corresponding ions. Applying divergence measures to the analysis of ions will allow us to find which electrons have a higher impact on the whole density. In order to do that we inspect the Jensen-Shannon divergence between an ion atom (cation or anion) electron pair density and their corresponding monoelectronic density in both position and momentum spaces. This is shown in Figure 5.10. Despite the difference in absolute value, having the momentum space a higher divergence values, the extrema structure is the same for both spaces. In the position space, the maxima are located at $Z = 11, 16, 19, 24, 37, 41, 44, 46$, being mainly alkaline elements, showing the most influential electrons are those added after an s subshell is filled. The minima are located at $Z = 9, 15, 17, 23, 35, 40, 43, 45$ most of them have a p subshell filled or almost filled, showing than the least relevant electrons, the electrons providing the least amount of change in the position space density in this case are those who fill a p subshell or are added after a p subshell is half-filled. The momentum space presents the same extrema structure, showing that relevant or irrelevant electrons act the same in both spaces. The same patron is repeated for both, cations (Figure 5.10(a)) and anions (Figure 5.10(b)), however, due to some systems are not present in the comparatives (Koga functions employed in this work are not available for some specific systems such as noble gases) the results are not as definitive as would be desirable.

Let us now use the Jensen-Shannon divergence, JSD, to show which systems present a more relevant differences when a monoelectronic densities or electron pair densities of

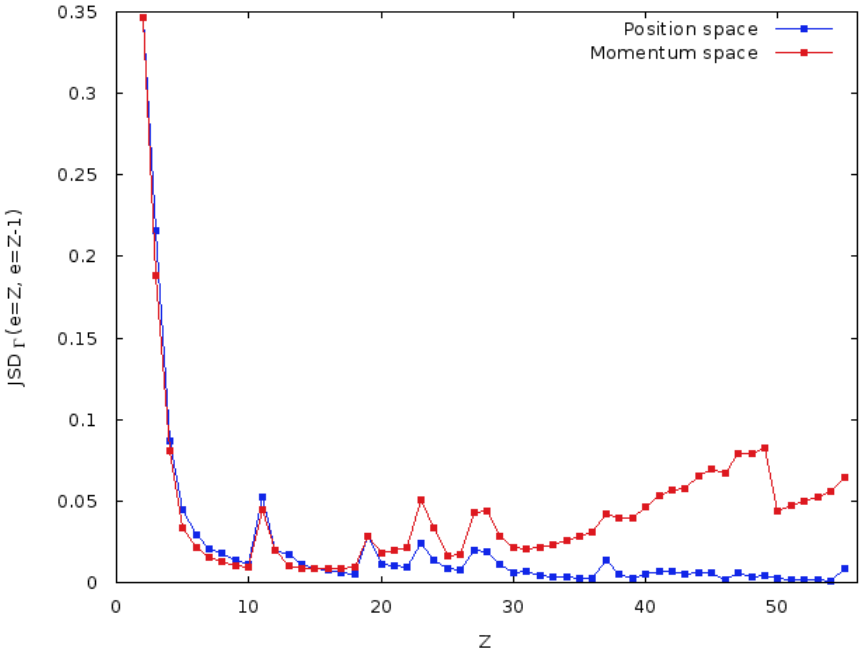

(a) Neutral-cation pair densities

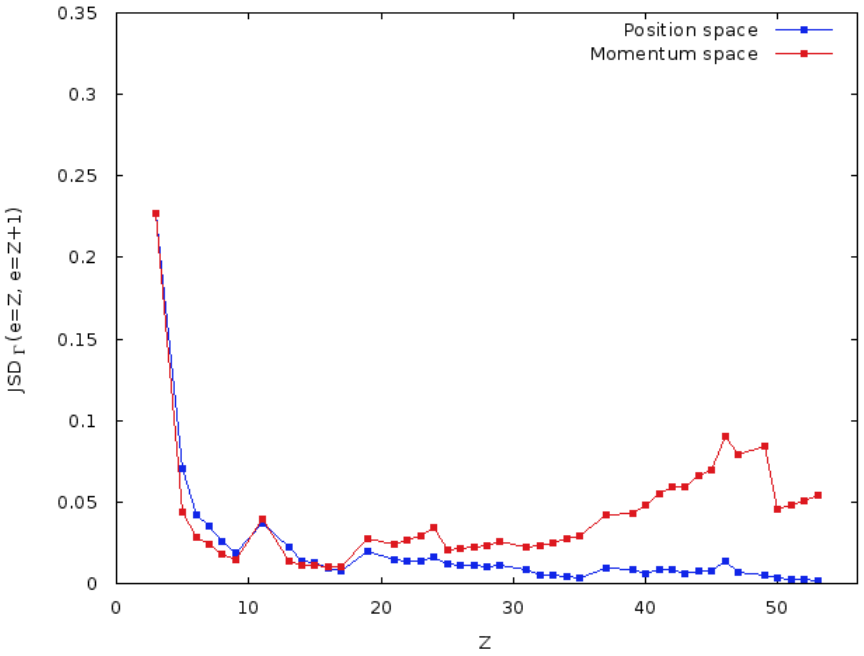

(b) Neutral-anion pair densities

FIGURE 5.10: Jensen-Shannon divergence calculated in momentum and position space between a neutral atom electron pair density and its corresponding simple (a) cation, (b) anion density for systems with an atomic charge $Z \in (2, 54)$. Atomic units (a.u.) are used.

ion atoms are considered. In this sense, Figure 5.11 shows the JSD calculated in momentum and position space, respectively, for monoelectronic and pair electron densities of different ions. First let us discuss Figure 5.10(a) where cations for atomic systems with nuclear charge $Z \in [2, 54]$ as been considered. The curves show us a decreasing behavior when the nuclear charge increases and, in this case, the momentum space present a smaller values of JSD. However, in the figure appears an interesting pattern,

cations corresponding to a full or half-filled shell, i.e., $Z = 4, 12, 20, 25, 30, 38, 43, 48$, have a greater difference, a higher value of JSD. However, alkaline systems or those with an only one valence electron or presenting anomalous filling patters have a smaller discrepancy, smaller values of JSD, which is exactly the opposite behavior that we obtained in Figure 5.9. This fact corroborates the importance of an one electron has in the whole density distribution, causing mayor changes on the density depending on its corresponding orbital. In Figure 5.11(b), where the anions have been considered, shows exactly the same pattern, but with less structure, due to the fewer available system as it was previously discussed.

Let us now discuss the results corresponding to the other comparative measures, the quantum similarity index, QSI. In Figure 5.12 QSI in position space between the electron pair densities for some systems with different chemical structure and the other atoms along the Periodic Table have been represented. The systems under consideration have been the Helium, Lithium, Beryllium and Neon. The curves show a general increasing tendency until the system is compared with itself, and then a decreasing tendency. This is completely understandable because the density structure would be similar for atoms with a similar number of electrons. This is nothing new, QSI showed the same tendency using monoelectronic densities [125]. However, there are some new interesting patterns in this case. In addition to the general global tendency, there is some local structure: a change in the curvature of the curve distributed along different segments. The precise point where the curvature start changing is situated at an atom of the same chemical group as the atom used in the comparison. This behavior is also modulated by the similarity between the general electronic configuration, which is effectively more similar for atoms in the same group.

For the case of the momentum space, the quantum similarity index, QSI, between the electron pair density of the same systems considered in the position space, and another atoms with nuclear charge $Z = 2 - 130$ has been calculated. In this case, due to the great structure of the curves, we have separated them into three graphics in order to preserver legibility. First, we are going to discuss the results for Helium and Lithium showed in Figure 5.13. The extrema correspond to the systems with atomic charge $Z = 2, 3, 10, 11, 18, 19, 36, 46, 54, 86$. Those system are mainly noble gases ($Z = 2, 10, 18, 36, 54, 86$) but there are also some alkaline systems ($Z = 3, 11, 19$) and the Palladium ($Z = 46$). We can also see how there are two kind of regions: in the first kind both curves present the same behavior but, in the second one, they present the opposite.

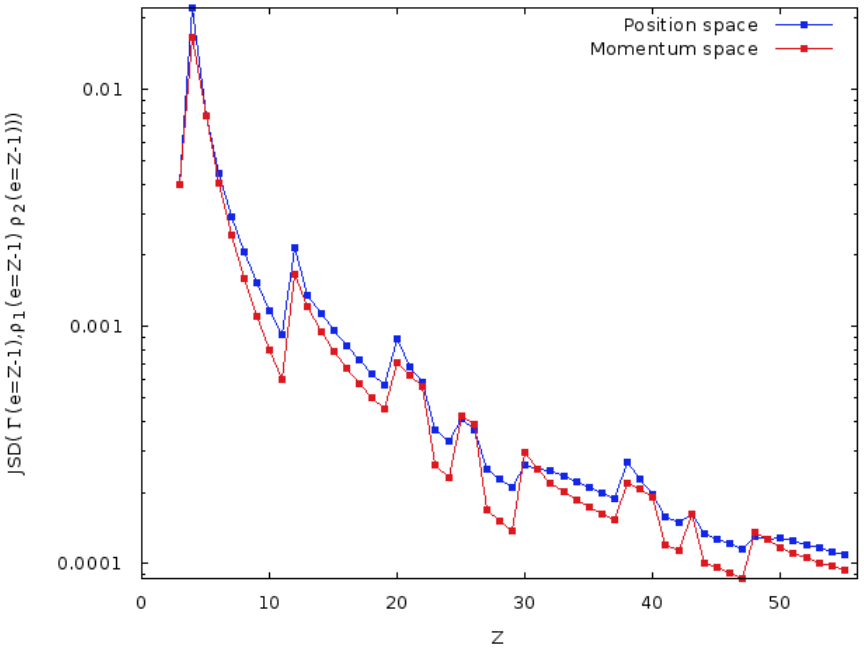

(a) Cation comparison

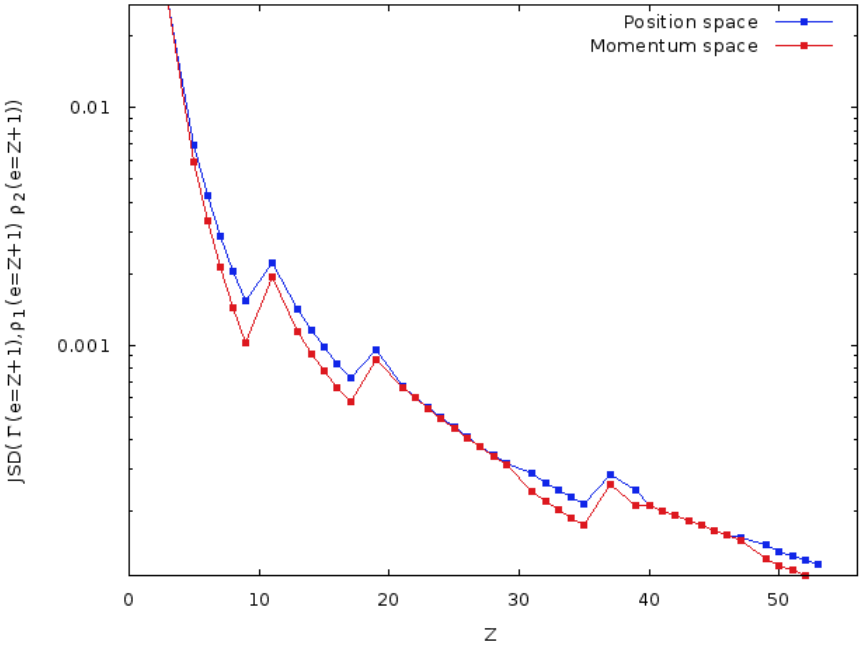

(b) Anion comparison

FIGURE 5.11: Jensen-Shannon divergence calculated in momentum and position space between a (a) cation, (b) anion atom electron pair density and the correspondent monoelectronic density for systems with an atomic charge $Z \in (2, 54)$. Atomic units (a.u.) are used.

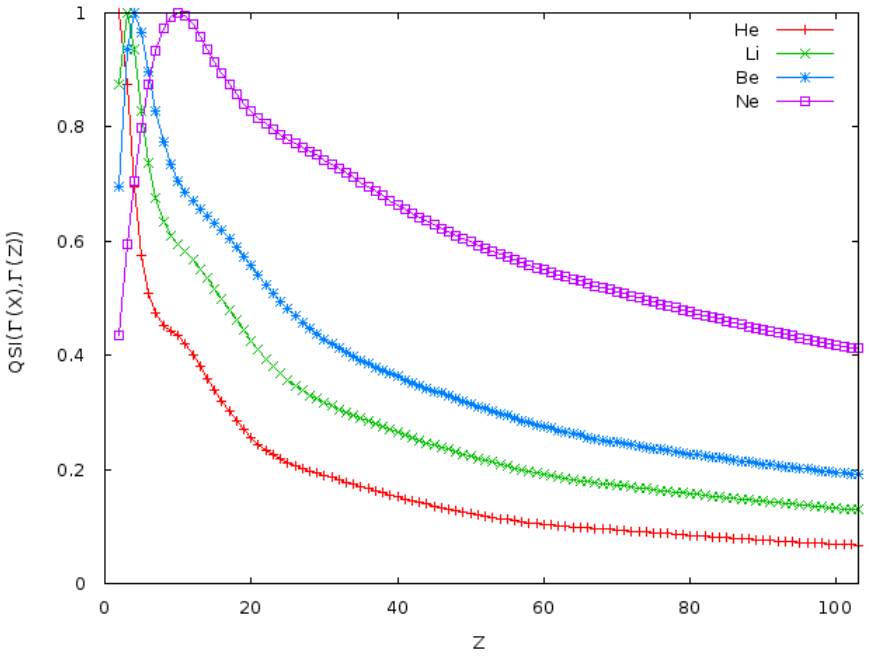

FIGURE 5.12: Quantum similarity index in position space, QSI between the electron pair density correspondent to Helium, Lithium, Beryllium and Neon, and the others atoms with nuclear charge $Z = 2 - 103$. Atomic units (a.u.) are used.

The region with opposite behaviors is located around noble gases and alkaline elements. In that zone maxima for the Helium corresponds with minima in the Lithium and vice versa. The second region comprises all the other systems of the Periodic Table, and Lithium and Helium have the same extrema structure. This suggest that, as Lithium and Helium have such a similar number of electrons but a very different electronic configuration, the first region represent the zone where those electronic configuration become more relevant as their differences enhances, but the second region represent the zone where those differences are neglected and care more about the bare electron number.

Let us focus our attention in the comparison of the curves corresponding to Helium and Neon which haver been depicted in Figure 5.14. It can be seen that both curves present almost the same structure on the whole region, with the most relevant extrema on the systems with $Z = 2, 10, 18, 36, 54, 86$. This is understandable due to both systems present a not very different number of electrons and a very similar electronic configuration. However there are some discrepancies, as the present opposed extrema at the systems with $Z = 29, 46, 59$ being all of them maxima for the Neon but minima for the Helium curve.

Finally, let us take a look at the pair Lithium-Beryllium represented in Figure 5.15. Again the structure is very similar in both cases. Both present minima at the noble

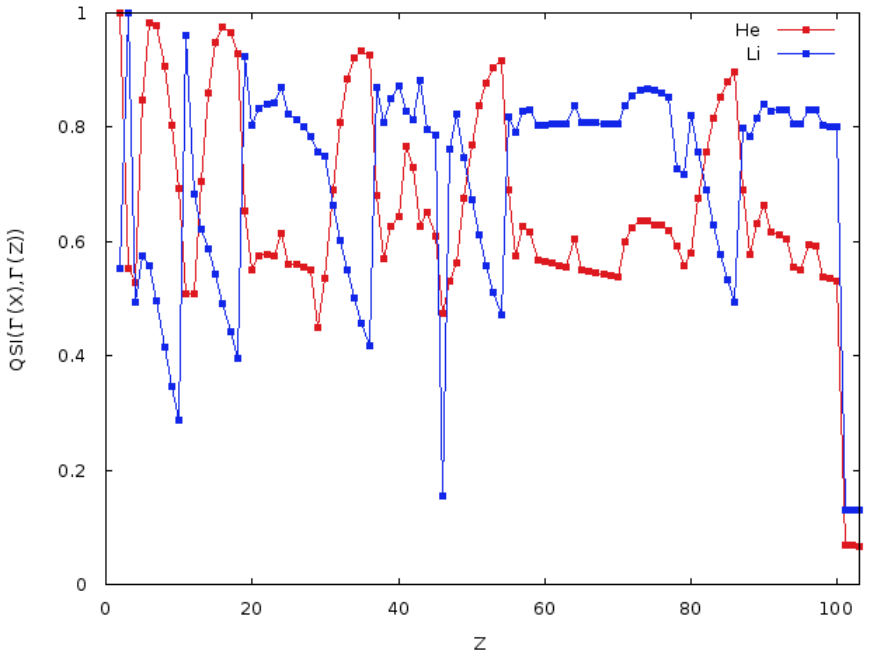

FIGURE 5.13: Quantum similarity index in momentum space, QSI between the electron pair density correspondent to Helium and Lithium, and the others atoms with nuclear charge $Z = 2 - 103$. Atomic units (a.u.) are used.

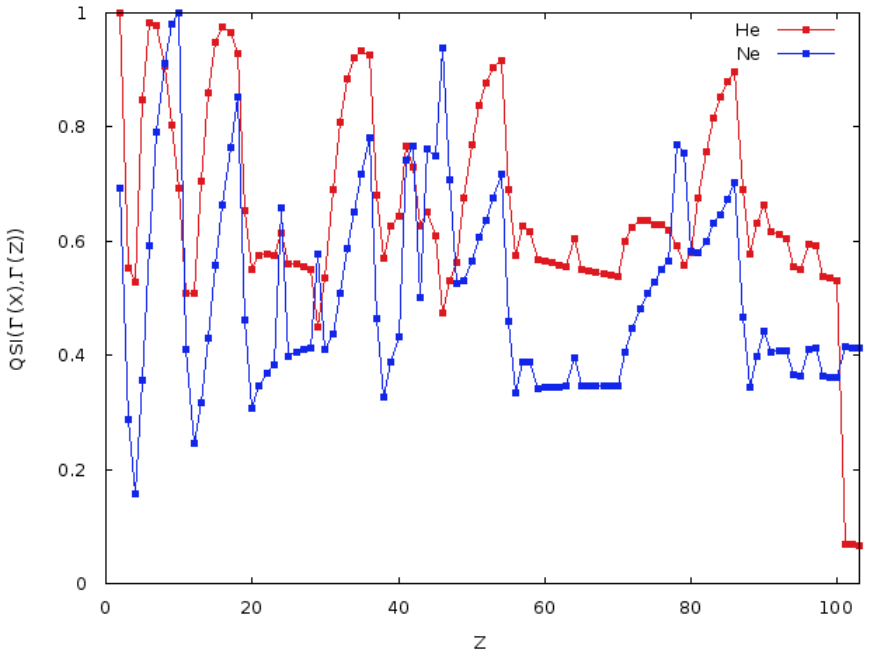

FIGURE 5.14: Quantum similarity index in momentum space, QSI_r between the electron pair density correspondent to Helium and Neon, and the others atoms with nuclear charge $Z = 2 - 103$. Atomic units (a.u.) are used.

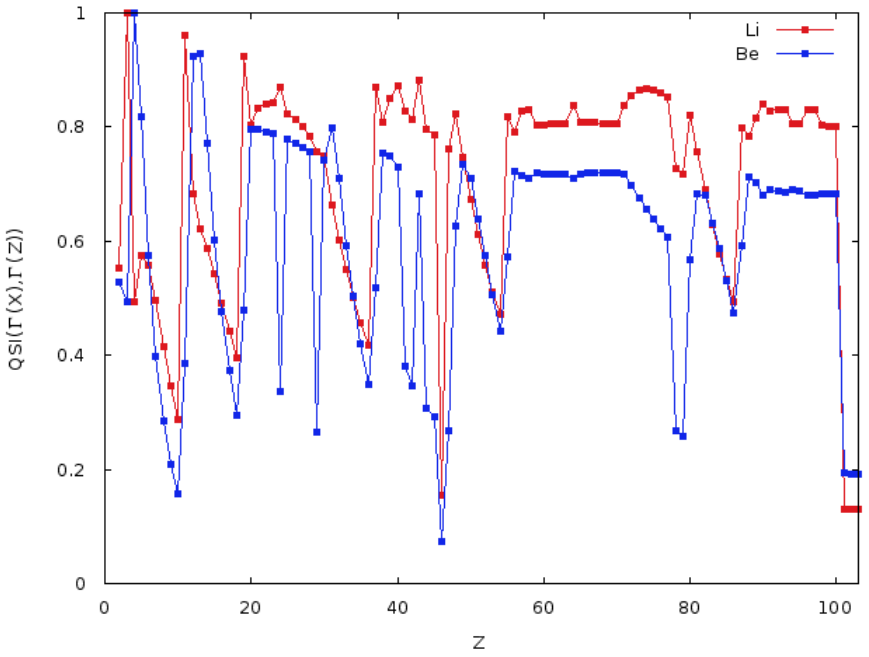

FIGURE 5.15: Quantum similarity index in momentum space, QSI_r between the electron pair density correspondent to Lithium and Beryllium, and the others atoms with nuclear charge $Z = 2 - 103$. Atomic units (a.u.) are used.

gases, while the maxima appear at the alkaline systems for the Lithium and the earth-alkaline systems for the Beryllium.

5.3 Conclusions

A variety of informational measures has been employed in electron pair densities in order to better understanding the differences between those densities and the monoelectronic ones, and also to try to grasp the information, complementarily to the one electron densities. The information measures employed for this purpose comprise Shannon entropy, disequilibrium, the LMC complexity, the Jensen-Shannon divergence and the quantum similarity index.

The Shannon entropy has been calculated for the one electron and two electron densities in both position and momentum space. In position space we found a high resemble between both quantities, with a similar extrema structure but an elevated value for the two electron case. Thus, the Shannon entropy has proved its success when quantifying electronic configuration properties when applied to the pair electron densities, providing an even more sensibility to these qualities due to its higher value when compared with its one electron alternative. Not additional information has been encountered, though, which probably means that Shannon entropy is not able to quantify the information about the electronic correlation. In momentum space the resemblance was considerable

as well, although in both cases there is barely structure, just a monotonous increase. We can say that the Shannon entropy behaves very similarly in position and momentum spaces and that, in terms of spreading and delocalization, both densities behave in an analogous manner in both position an momentum space.

The disequilibrium has been quantified in a comparable way for both kind of densities in position and momentum space. In position space, it showed an structure-free monotonous type of behavior, much akin to Shannon entropy in momentum space. Although, a relevant difference could be observed: the curves for monoelectronic and electron pair densities had an intersection for $Z = 10$. This occurrence, along with the knowledge that disequilibrium quantifies the relative strength of the nuclear attraction towards the electron cloud, is a measure of the exact point where the electron interaction significantly reduces the effect of the nuclear contraction.

The LMC complexity in position space showed the same structure as the Shannon entropy, which means a domination of the Shannon entropy over the disequilibrium. The spreading effect affects the electron pair densities in a more relevant way as the nuclear contraction. Considering how the electronic interaction mentioned above and how it affected the disequilibrium, the Shannon-dominated LMC is another prove of the more predominant effect of the electron interaction in the two-electron density when compared with the one-electron density. This change to the opposite situation in the momentum space, where the disequilibrium is what causes the extrema apparition and Shannon entropy just modulates the structure.

The Jensen-Shannon divergence has been used as a direct comparison between the monoelectronic and the electron pair densities of neutral atomic systems. It was showed that the correlation between these two densities increased with the number of electrons, as JSD value decreased with Z, showing how the correlation between electrons decreases as their number increases. Patterns between the JSD value and the shell filling structure of the systems were found, indicating a clear effect on the relative shape of the density is produced as a shell is completed showing a high disimilarity is provoked when additional electrons are considered after a shell is filled.

Cations and anions electronic densities have also been analyzed using the Jensen-Shannon divergence. When the difference between monoelectronic and electron pair atomic ion densities where calculated for position space, they shown a decreasing difference with the nuclear charge Z as well. However, for momentum space, although a decreasing tendency also appears initially, after the $Z = 17$ the tendency inverses, and start to increases, what suggest that the momentum distribution has a greater contrast at higher Z. Also it was discovered than alkaline systems showed a greater difference, once more implying that the electron that cause the most relevant change in the electron pair structure are the once added after a shell is filled. The same pattern was recorded for cation and anion and for both spaces.

When the electron pair densities of neutral and ion systems were directly compared using JSD, a decreasing tendency was found. Alkaline systems, anomalous shell filling systems and systems with only a valence electron, where the one showing the most divergence when compared, supporting the idea of single electrons being the most perturbing element at a two-electron density level. This was found for both, position and momentum space.

Employing the quantum similarity index showed us that, when comparing systems with different electronic configuration (noble gases, alkaline and earth-alkaline), its differences were based not only on its electronic configuration but on the different number of electrons as well. Thus, systems with an electronic configuration as different as a noble gas and an alkaline had the same behavior when compared with systems with, i.e. $Z \in (60, 80)$, implying that at some regions on the Periodic Table the electronic configuration differences are less important than the number of electrons of the systems when comparing electron pair density structures.

In general, information theoretical measures have been proved successful when employed to quantify electron pair densities characteristics. It has been proved the well-known existing dissimilarities between one-electron and two-electron densities. Some previous studies, performed by other authors [185], have been extended to new systems, confirming known tendencies and finding new ones. New measures such as Jensen-Shannon divergence has been used, which value have been verified, even when comparing unexplored systems as two electron ion densities.

In the future we would like to extend these studies to other systems. A general and structured analysis of ions systems would be promising as well. However, the most interesting matter would be an study using gradient-based measures, as the Fisher information and derivatives. Those measures were out of these study due to the much higher complexity and computational difficulty they supposed.

Chapter 6

A molecular analysis using an information-theoretical approach

The role of atomic densities in Quantum Physics is one of the most fundamental topics and a very interesting and throughly investigated subject due to its implications in Physics and Chemistry. As we have previously mentioned, the Density Functional Theory establishes that probability density contains all the relevant information to understand and study quantum systems [39]. Due to this fact, quantum density studies became much more common and atomic and molecular densities started to get more attention because they constitute the critical base of many other quantum systems such as quantum thermodynamics, quantum computation, many-bodies systems and molecular physics or chemistry [132, 139, 210–212]. In this framework, Information Theory provides an entropy-based characterization of the atomic and molecular systems, which complements the energy-based representation obtained with the wave function and density functional methods. The physical and chemical properties of these systems can be described by means of spreading measures of entropic character of the one-electron density $\rho(\vec{r})$. In addition to the present Thesis, numerous studies have been performed regarding this topic, e.g., Shannon entropy analyses of entangled atoms [213], electronic structure analysis of atomic systems using similarity measures [125], the relevance of quantum similarity measures for ionization processes [190], divergence calculations and their relationship with atomic shell structure [115], investigation about the relationship between quantum-mechanical kinetic energy and Shannon entropy [214], inquires about electronic correlation in a informational-versus-energetic perspective [192], periodicity properties in ionization processes [151] or quantification of relativistic effects in hydrogenic systems [169] among others.

The study of molecular systems is more complicated as compared to the atomic case. Nevertheless, this field is really interesting because when the proper characteristics of a molecular system have been analyzed one can obtain a more approximate knowledge

about fascinating related subjects such as reaction properties, reaction paths or possible material traits. This is the reason because there has been an increasing interest in characterizing and classifying different physical systems, in particular molecular ones, in terms of a few fundamental properties, not only in Physics but also in Chemistry and Biology. This is a formidable task since the variety of descriptors to be employed is enormous. Indeed, the concept of chemical space has been suggested but not yet well defined [215, 216]. This space has a two-fold role. It allows one to gather a great variety of molecules (e.g., all organic molecules present in biological systems). On the other hand, it might be considered as a multi-dimensional descriptor space in the sense of a region defined by a particular choice of descriptors to characterize as many chemical compounds as possible. Notwithstanding, the large number of physicochemical properties to be chosen as descriptors is an important disadvantage, since the risk of employing irrelevant and redundant descriptors is really high.

From an information-theoretical point of view, different analysis of molecular systems have been performed during the last years. Information-theoretical functionals, in particular complexity measures, have been employed for analyzing of physical and chemical properties of molecules and their relation with their atomic constituents [217–221]. Reaction paths and their relation with informational quantities have been studied [151, 222–227]. Many different chemical phenomena have also been correlated with different information-theoretic measures [192, 228–231]. An alternative to the above mentioned chemical space has been recently proposed using different concepts of Information Theory, i.e. the Information-theoretic space [232, 233], which allow us to describe and classify a huge diversity of atomic and molecular systems, from simple atoms and molecules to biological and pharmacological molecules. The interest on this subject leads even to the proposition of a particular informational measure for molecular systems, the Molecular Similarity Measure, MSM [137], similar to the QSM, already defined in Section 1.3.6, but particularly applied to molecular densities. This measure has been characterized [234] and afterwards generalized [235–237]. MSM has been applied to describe molecular structure [238, 239], molecular properties analysis [240] and to classify molecules [241].

The main aim of this Chapter is to establish a variety of relationships among the values of divergence measures between molecular systems and some of their respective physical and chemical properties. In order to do that, we will employ the Jensen-Shannon divergence and the Jensen-Fisher divergence, defined in Chapter 1 in Subsections 1.3.2 and 1.3.4, respectively. They will be calculated between the molecular densities of different pair of molecules extracted from a large and varied collection. Right after, the values of the calculated divergence measures will be compared with a number of physical and chemical quantities of the molecules under comparison, in order to find a clear connection between both of them. The study we wanted to develop was a much more ambitious than we initially thought. At the beginning we managed a much more wide selection of

molecules, but we had to restrict the scope of the project and seek a much more humble objective due to the great difficulty of analyzing the obtained results. However, we have no doubt that this study can establish a starting point of what we think could be a very promising research field.

This chapter will be structured as follows. In the first section the main physicochemical properties under study are defined, as well as the software packages using for the calculations. The following section is devoted to the results obtained for the Jensen-Shannon and Jensen-Fisher divergences calculations. The last section will conclude with the main conclusions we extracted from the results and describe the following steps we want to take in order to do a more complete and relevant analysis.

6.1 The basis of the informational approach to molecular systems

This chapter focuses on the analysis of some molecular properties and their relation with information-theoretic divergence measures. Different divergence measures and some of their applications to the atomic case have been widely discussed in the previous chapters. As it has been mentioned before, molecular systems are much more complex due to the huge variety of kind of systems that we can consider, e.g., different electronic structure, composition, shape, size, among others. This fact makes the information theoretical analysis of the systems an arduous task, because there are a large number of interesting physicochemical properties which deserve to be considered.

We have focused our attention to the analysis of several reactivity properties such as ionization potential (IP), chemical potential and hardness (η). These properties were obtained at the density functional theory (DFT) level, by use of the Janak's theorem [242], analogous to the Koopmans' theorem [243] for relating the first vertical ionization energy and the electron affinity to the HOMO and LUMO energies, which are necessary to calculate the conceptual DFT properties.

The hardness (η) is a good descriptor of chemical reactivity of the molecule in the sense of the resistance to changes in its electron distribution, hence molecules with larger values of η are interpreted as less reactive molecules [244]. This magnitude is defined as:

$$\eta = \frac{1}{2}\left(\frac{\partial \nu}{\partial N}\right)_{v(r)}, \tag{6.1}$$

where

$$\nu = \left(\frac{\partial E}{\partial N}\right)_{v(r)} \tag{6.2}$$

is the electronic chemical potential of the system, N is its number of electrons, $v(r)$ is the external potential which the system is exposed to and E is the total energy. Using finite differences, Eq. (6.1) can be expressed as:

$$\eta \approx \frac{E_{N+1} - 2E_N + E_{N-1}}{2} = \frac{I - A}{2} \tag{6.3}$$

where E_N is the energy of the neutral system, E_{N-1} is the energy of the cationic system, E_{N-1} is the energy of the anionic system, I is the ionization potential and A is the electron affinity. Applying the Koopmans' theorem [245], Eq. (6.3) becomes:

$$\eta \approx \frac{\varepsilon_{LUMO} - \varepsilon_{HOMO}}{2} \tag{6.4}$$

where ε_{HOMO} is the energy of the highest occupied molecular orbital and ε_{LUMO} is the energy of the lowest unoccupied molecular orbital [143]. However, it is common for the electron affinity be negative instead of positive, in which case the corresponding anion is unstable and its energy cannot be described. In those cases an approximated method was introduced by Tozer and De Proft [246]. That method allowed the hardness to be computed using only the neutral and cationic energies as:

$$\eta \approx \frac{\varepsilon_{LUMO} - \varepsilon_{HOMO}}{2} + \varepsilon_{HOMO} + I \tag{6.5}$$

where I is obtained by:

$$I = E_{N-1} - E_N. \tag{6.6}$$

Let us remark that the main aim of this analysis is to quantify the level of similarity/dissimilarity between two different molecular densities. In order to do that, there are some issues that must be previously considered: (i) the space where molecular densities will be calculated, i.e the selected grid in order to guarantee both whole densities will be fully contained in this considered space, and (ii) the relative position of the molecules, i.e., the molecule orientation. The first problem has been solved by using a selected integration space as a direct combination of the space containing each molecule individually, both centered on the center of mass of the molecule (as we will considered neutral molecules, it will be the center of charge as well). It will be named "super-molecule space". This secures that any information-theoretic measure of each molecule calculated in the super-molecule space will have the same value as if it has been obtained in its own molecule space. In previous chapters, spherically averaged densities have been considered, so the relative position between the systems compared supposed no issue. Nevertheless, in molecular calculations of information-theoretic measures the relative position between molecules has to be considered, as the value of divergence measures is highly dependent

on it [247]. The common standard is considering the angle which gives the least value of the measure, as any additional difference would be a result of the varied position. We will adopt this convention in the successive calculations.

The electronic structure calculations performed in the present study for the whole set of molecules were carried out with the Gaussian 03 suite of programs [248] at the CISD/6-311++G(3df,2p) level of theory. For this set of molecules we have calculated the Jensen-Shannon and Jensen-Fisher divergences by employing the necessary software along with 3D numerical integration routines [249, 250] and the DGRID suite of programs [251]. As mentioned above, the values of the conceptual DFT properties have been obtained at the B3LYP/6-311++G(3df,2p) level of theory.

6.2 Results

Initially, we compiled a highly diversified list of molecules given in Table 6.1, with many different types of molecules, different properties and number of atoms. As we wanted to establish a concrete relationship between information-theoretic measures and the chemical and physical properties of the molecules we started this study with divergence calculations between some simple test molecules and the rest of the molecule of the whole list.

Some of the results we obtained are displayed in Figure 6.1, where the Jensen-Fisher divergence between two different test molecules, H_2 and HF, and all others within the list. It appears that nothing conclusive can be affirmed from the data. It happened the same with all other attempts we made with different information-theoretic measures. Maybe that the first approach was somehow optimistic. Most probably, dealing with such an enormous group of different molecules was not an appropriate way. Thus, it seems more feasible and useful to restrict the selected group to restrict our group to a shorter list of more similar molecules in order to be able to establish conclusive relationships.

As our second approximation to the matter, we have selected two groups of similar diatomic molecules. The first one is composed by diatomic molecules with an atom of Hydrogen and another Hydrogen or an halogen, also known as hydrides. Those molecules being: H_2, HF, HCl, HBr and HI. The other group is composed by molecules with an atom of Sodium and an atom of Hydrogen or an halogen atom. Those other molecules are: NaH, NaF, $NaCl$, $NaBr$ and NaI. All of them are Sodium salts, but the NaH which is a different kind of molecule. We have selected those groups of molecules because they have a limited number of electrons, making calculations much more accessible; and they were less difficult and similar to each other, so that establishing a relation between their chemical properties and the information-theoretic measures becomes a not so difficult task.

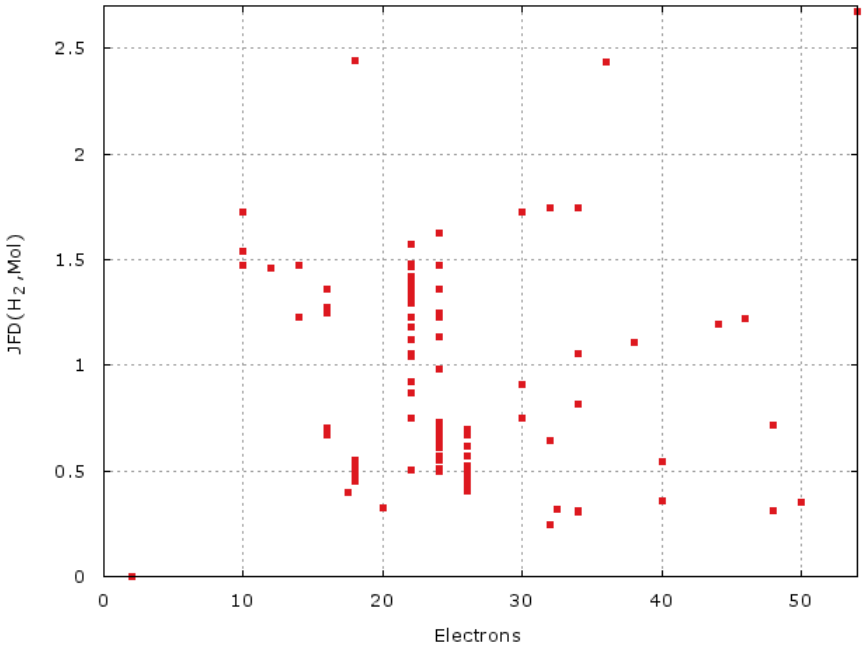

(a) Molecule H_2

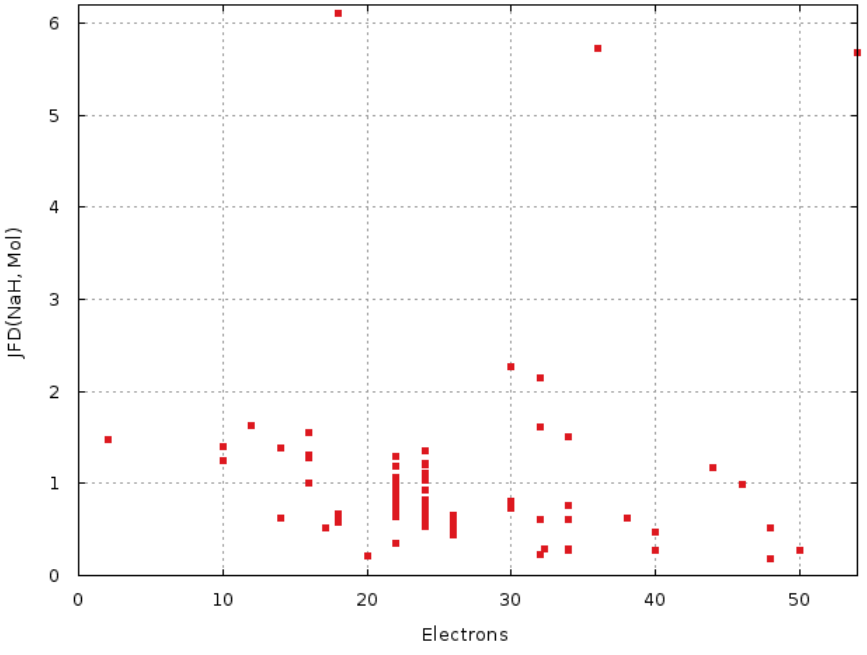

(b) Molecule NaH

FIGURE 6.1: Jensen-Fisher divergence calculated between the molecular densities of (a) H_2 and (b) NaH, and the whole list of complex molecules.

Label	Molecule	Name	e^-
1	H_2	Hydrogen	2
2	CH_4	Methane	10
3	NH_3	Ammonia	22
4	LiOH	Lithium hydroxide	12
5	Li_2O	Dilithium oxide	14
6	CH_3NH_2	Methyl amine	18
7	HF	Hydrogen fluoride	10
8	HBO	Boron hydride oxide	14
9	HCO	Formyl radical	15
10	HCCO	Ketenyl radical	16
11	H_2CO	Formaldehyde	16
12	CH_3O	Methoxy radical	17
13	CH_3OH	Methyl alcohol	18
14	C_3H_3	Radical propargyl	21
15	CH_2CCH_2	Allene	22
16	C_3H_4	Cyclopropene	22
17	CH_3CCH	Propyne	22
18	C_3H_5	Allyl radical	24
19	C_3H_6	Cyclopropane	24
20	CH_3CHCH_3	Isopropyl radical	24
21	$CH_2CH_2CH_3$	N-propyl	24
22	C_3H_8	Propane	26
23	NO	Nitric oxide	15
24	NHO	Nitrosyl hydride	16
25	NH_2OH	Hydroxylamine	18
26	CH_3CN	Acetonitrile	22
27	CH_3NC	Methyl isocyanide	22
28	C_2H_5N	Aziridine	24
29	CH_3NHCH_3	Dimethylamine	26
30	$CH_3CH_2NH_2$	Ethylamine	26
31	CH_3F	Methyl fluoride	18
32	CH_2NN	Diazomethane	22
33	NH_2CN	Cyanamide	22
34	$NHCHNH_2$	Aminomethanimine	24
35	O_2	Oxygen	16
36	H_2O_2	Hydrogen peroxide	18
37	HCCOH	Ethynol	22
38	CH_2CO	Ketene	22
39	CH_3CO	Acetyl radical	24
40	C_2H_4O	Ethylene oxide	24
41	CH_3CHOH	Ethoxy radical	24
42	CH_3CHO	Acetaldehyde	24
43	CH_3OCH_3	Dimethyl ether	26
44	CH_3CH_2OH	Ethanol	26
45	HN_3	Hydrogen azide	22
46	HCNO	Fulminic acid	22
47	HOCN	Cyanic acid	22
48	HNCO	Isocyanic acid	22
49	$CHONH_2$	Formamide	24
50	BO_2	Boron dioxide	21
51	N_2O	Nitrous oxide	22

Label	Molecule	Name	e^-
52	CO_2	Carbon dioxide	22
53	CH_2O_2	Dioxirane	24
54	HCOOH	Formic acid	24
55	CH_3OO	Methylperoxy radical	26
56	CH_3OOH	Methyl peroxide	26
57	FCN	Cyanogen fluoride	22
58	NO_2	Nitrogen dioxide	24
59	HNO_2	Nitrous acid	24
60	O_3	Ozone	24
61	FNO	Nitrosyl fluoride	24
62	CF_2	Difluoromethylene	24
63	NaOH	Sodium hydroxide	20
64	FO_2	Dioxygen monofluoride	26
65	NF_2	Difluoroamino radical	26
66	F_2O	Difluorine monoxide	26
67	MgOH	Magnesium hydroxide	22
68	PO	Phosphorus monoxide	24
69	HBS	Hydrogen boron sulfide	22
70	H_2CS	Thioformaldehyde	24
71	CH_3S	Thiomethoxy	25
72	SiO_2	Silicon dioxide	30
73	NS	Mononitrogen monosulfide	24
74	HCl	Chloride hydride	18
75	SO	Sulfur monoxide	24
76	CH_3SCH_3	Dimethyl sulfide	34
77	CH_3CH_2SH	Ethanethiol	34
78	PO_2	Phosphorus dioxide	32
79	CH_3Cl	Methyl chloride	26
80	OCS	Carbonyl sulfide	30
81	SO_2	Sulfur dioxide	32
82	ClCN	Chlorocyanogen	30
83	ClNO	Nitrosyl chloride	32
84	SF_2	Sulfur difluoride	34
85	OClO	Chlorine dioxide	34
86	ClO_2	Chlorine dioxide	34
87	PS	Phosphorus sulfide	31
88	S_2	Disulphur	32
89	H_2S_2	Disulphur hydride	34
90	CS_2	Carbon disulfide	38
91	SSO	Disulfur monoxide	40
92	CCl_2	Dichloromethylene	40
93	$MgCl_2$	Magnesium dichloride	46
94	S_3	Sulfur trimer	48
95	$SiCl_2$	Dichlorosilylene	48
96	ClS_2	Sulfur chloride	49
97	HBr	Bromide hydride	36
98	CH_3Br	Methyl bromide	44
99	HI	Iodide hydride	54
100	CH_3I	Methyl iodide	62
101	SiCl	Silicon chloride	31

TABLE 6.1: List of molecules considered in the first approach to the information-theoretical molecular analysis. Labeled from 1 to 101.

In Figure 6.2 it is displayed the Jensen-Fisher divergence between a molecule of the H-group of molecules previously discussed, and the rest of molecules in the group. We can see how there is a similar tendency for all of them: JFD increases until it reaches a value where it stabilizes, that point is higher the more electrons the molecule has. This kind of behavior is mostly due to the capacity of JFD of grasping the structure of the more external electronic shells, as all those molecules share a great resemblance in their electronic structure.

We observe in Fig. 6.3 different representations of the Jensen-Shannon divergence calculated between a reference molecule (in this case a molecule of the hydride group) and the rest of the selected molecules. It can be appreciated a general trend: obviating NaH, all the sodium salt molecules have a very similar distribution when compared to hydrides, independently of the particular hydride considered, so that they separate in two groups, where the molecules of the same kind have a lower JSD value and the molecules of the opposite group have a higher value. When compared to another hydride, the JSD is just dependent on the difference of the number of electrons, being lower when compared

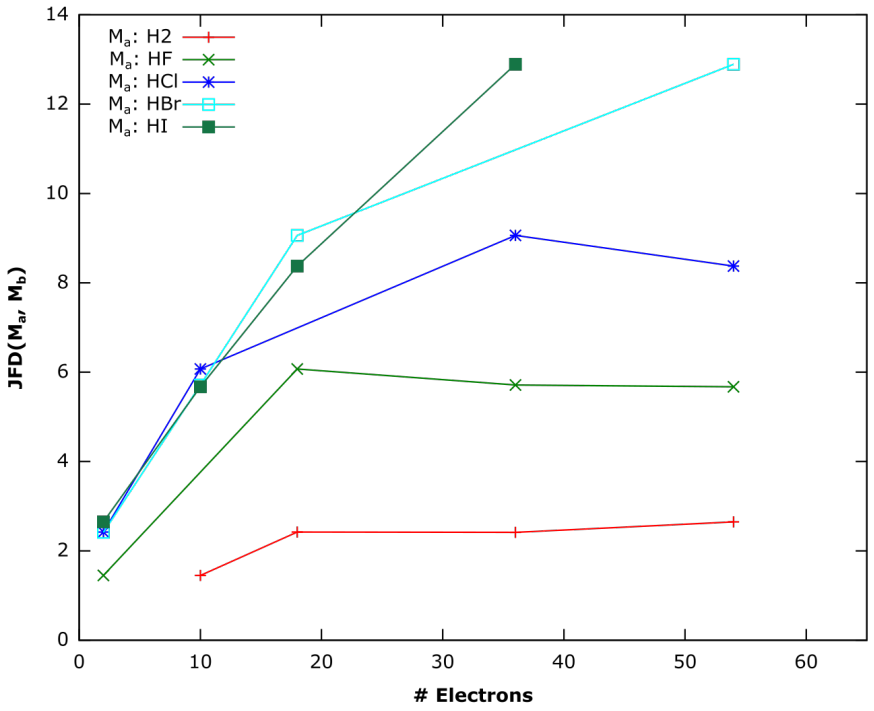

FIGURE 6.2: Jensen-Fisher divergence between the densities of a molecule and the rest of molecules of the hydrides group

to a molecule with a similar number and higher otherwise. This tell us that JSD takes into account the general electronic structure, being radically dissimilar for a different kind of molecule which is independent of the possible similarity on the electron number. However, when considering molecules of the same kind, JSD only quantifies the difference of the number of electrons.

In Figure 6.4 the pattern discussed above repeats. In this case it has been represented the Jensen-Shannon divergence between a reference molecule chosen from the Sodium salts group and the rest of the molecules of the restricted group. Again, when calculating JSD between different kinds of molecules, the structure of the results displays a similar pattern, disregarding of the reference molecule considered. However, when considering molecules of the same group, the determinant factor is again the difference between the number of electrons. The molecules are still separated in two distinguishable groups, nevertheless. Notwithstanding, when considering the NaI reference molecule, JSD shows a different structure when compared with the molecules in the hydride group, this is due to the higher electron number difference, which has a more crucial relevance, in this case due to such a difference. The molecule NaH has different behavior in this case as well.

In Figure 6.5 the values of the Jensen-Fisher divergence have been represented for reference molecules of the hydride group when compared with all the molecules of the restricted group. In this case, there is no apparent separation in two groups of higher

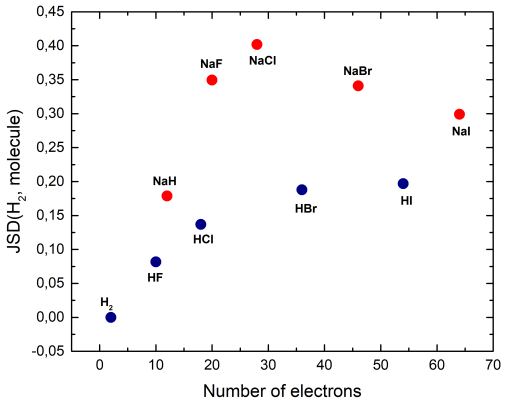

(a) H_2

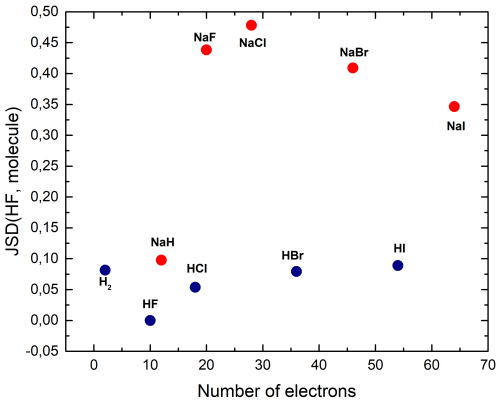

(b) HF

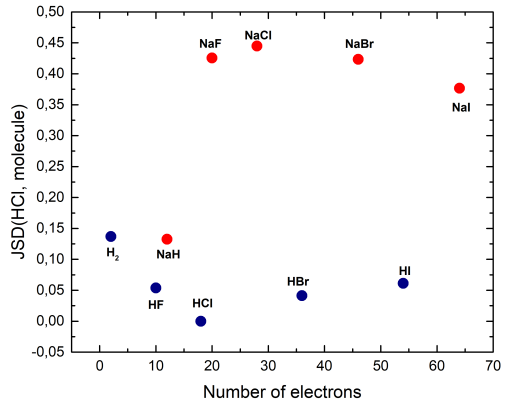

(c) HCl

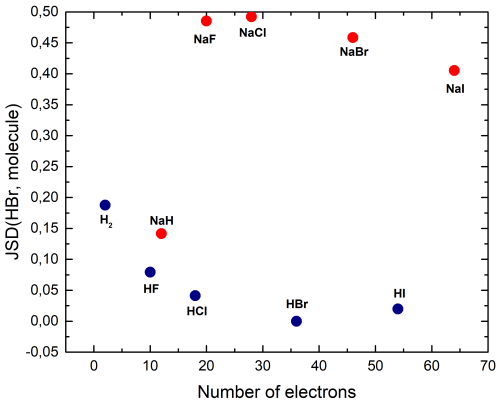

(d) HBr

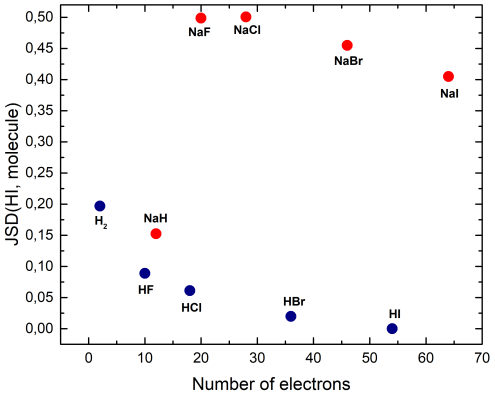

(e) HI

FIGURE 6.3: Jensen-Shannon divergence calculated between molecules in the H-group (H_2,HF, HCl, HBr, HI) molecules and the rest of the molecules.

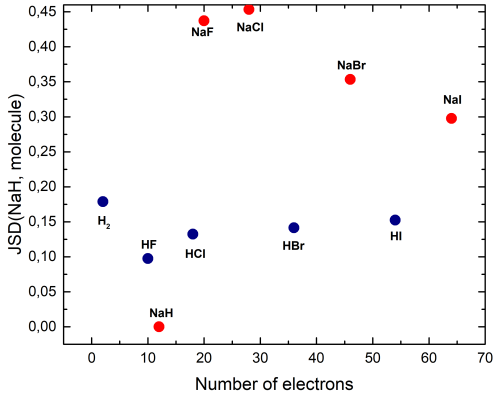

(a) NaH

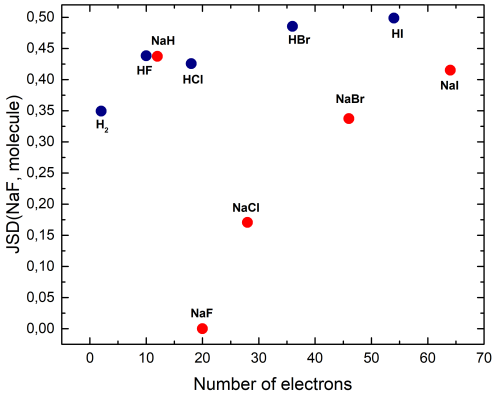

(b) NaF

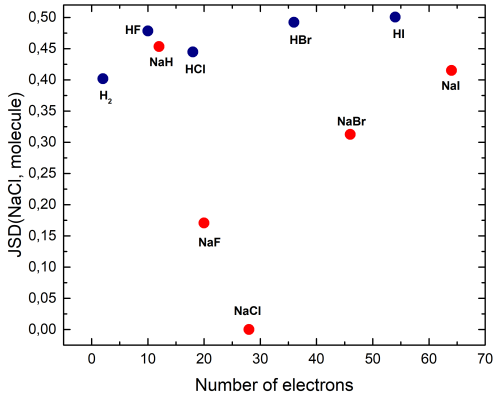

(c) $NaCl$

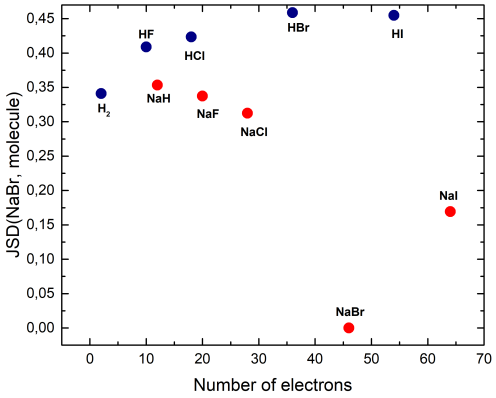

(d) $NaBr$

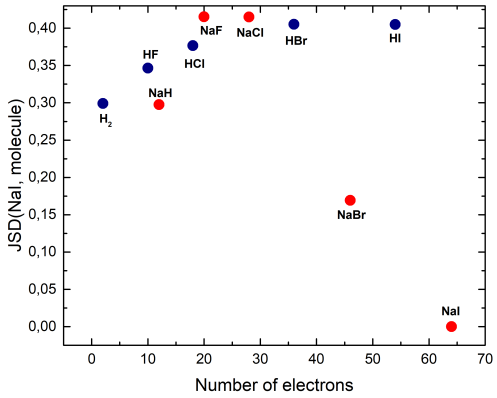

(e) NaI

FIGURE 6.4: Jensen-Shannon divergence calculated between molecules in the Na-group (NaH,NaF, $NaCl$, $NaBr$, NaI) and the rest of molecules.

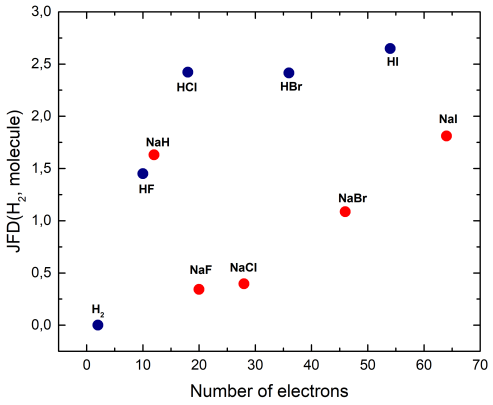

(a) H_2

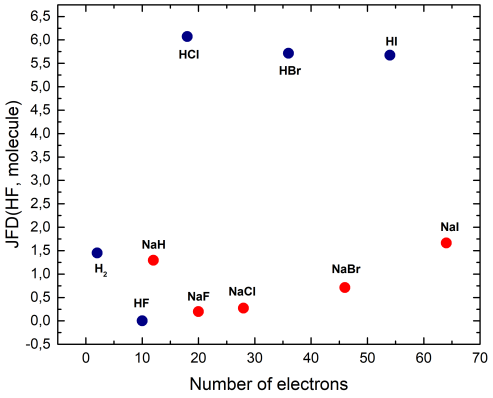

(b) HF

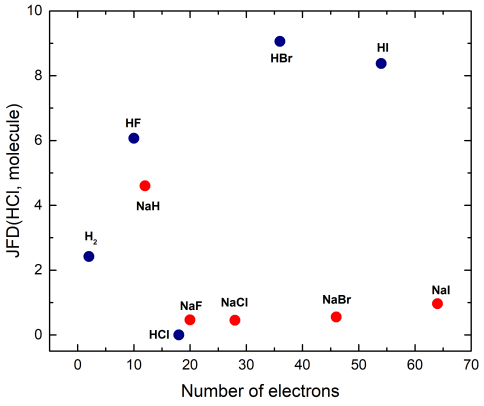

(c) HCl

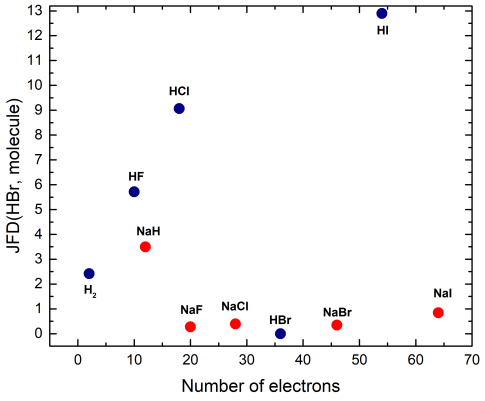

(d) HBr

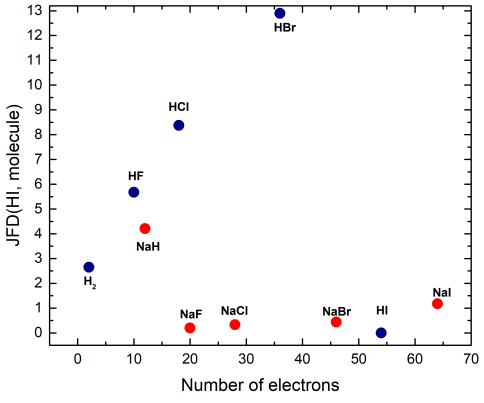

(e) HI

FIGURE 6.5: Jensen-Fisher divergence calculated between molecules in the H-group (H_2,HF, HCl, HBr, HI) and the rest of molecules.

and lower value, as it happened with JSD. However, there is still an interesting pattern: the JFD values structure has a distinguishable form for the opposite group, which remains the same for every reference molecule considered, despite not differencing both groups in terms of relative value.

A similar result can be appreciated in Figure 6.6, where the values of Jensen-Fisher divergence have been calculated for the Sodium salts group. When compared with the molecules of the hydride group, a characteristic pattern is recognizable.

Now we present the results of the Jensen-Shanon divergence calculated for all the molecules and the reference molecule H_2 as well as the difference of the hardness of the compared molecules, both in Figure 6.7. We can see an interesting pattern: every maximum of JSD corresponds to a minimum of the difference of hardness, and vice versa. The monotonicity of the curves are opposed as well.

The same pattern was found for the same calculations, but using HI instead of H_2. In Figure 6.8 is evident the mentioned pattern. Once more every maximum of JSD correspond with a minimum of the difference of the hardness and vice versa, as well as the monotony of the curves is opposed too.

6.3 Conclusions

Information-theoretic measures have been applied to a restricted group of molecular systems. There have been established some clear relationships between the informational quantities such as the Jensen-Shannon divergence and the Jensen-Fisher divergence, and chemical and physical properties such as the hardness and the number of electrons.

First a direct correlation between informational measures and a diverse number of chemical properties was tried to be determined by employing a much wider and complex group of molecules. We could not find a clear match, as the results were of much higher complexity that could be managed with easiness. We decided to restrict group of molecules to a more limited and simpler one: diatomic molecules with both a Hydrogen or Sodium atom, and another hydrogen or halogen atom.

The Jensen-Shannon divergence was calculated between a reference molecule of the two groups of hydrides and sodium salts and the rest of the molecules of the restricted group. It was found how the JSD value was independent of the reference molecule when compared with another molecule of the opposite group. However, when compared with a molecule of the same group a lower difference between the number of electrons translated into a lower JSD value. The NaH molecule, not belonging to neither of those groups had a different behavior. The NaI molecule, with the highest number of electrons, had a different behavior as well: when compared with the molecules of the opposite group, the resultant structure was dependent on the difference of electrons,

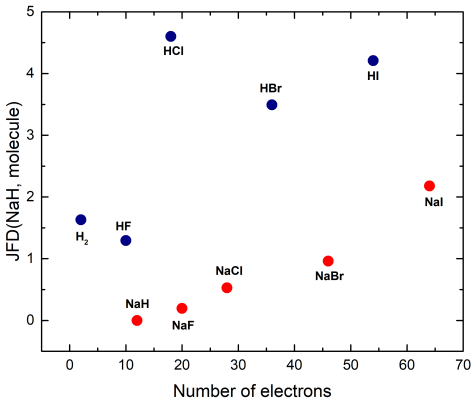

(a) NaH

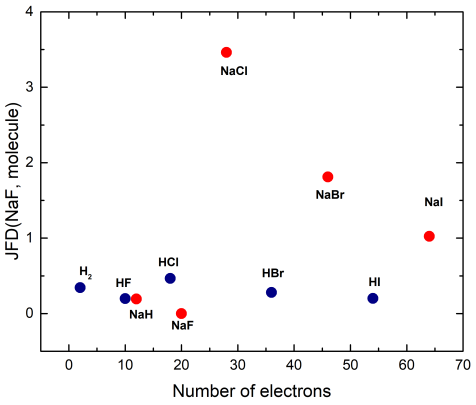

(b) NaF

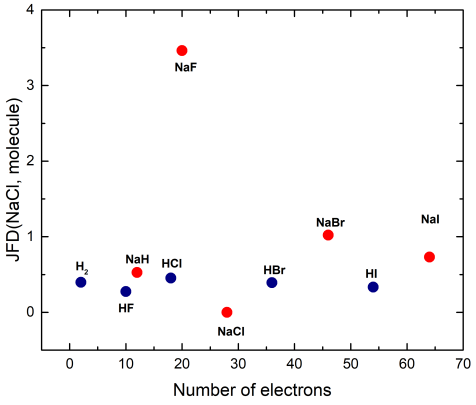

(c) $NaCl$

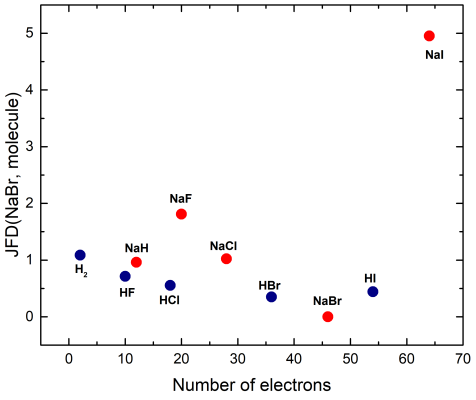

(d) $NaBr$

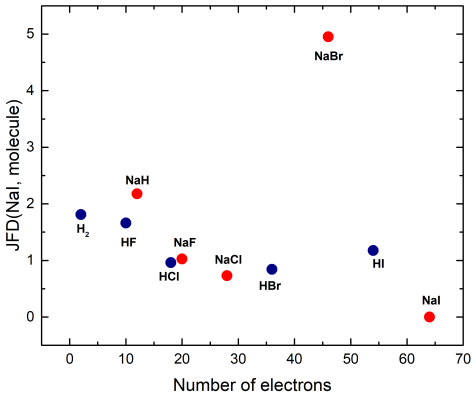

(e) NaI

FIGURE 6.6: Jensen-Fisher divergence calculated between molecules in Na-group (NaH,NaF, $NaCl$, $NaBr$, NaI) and the rest of molecules.

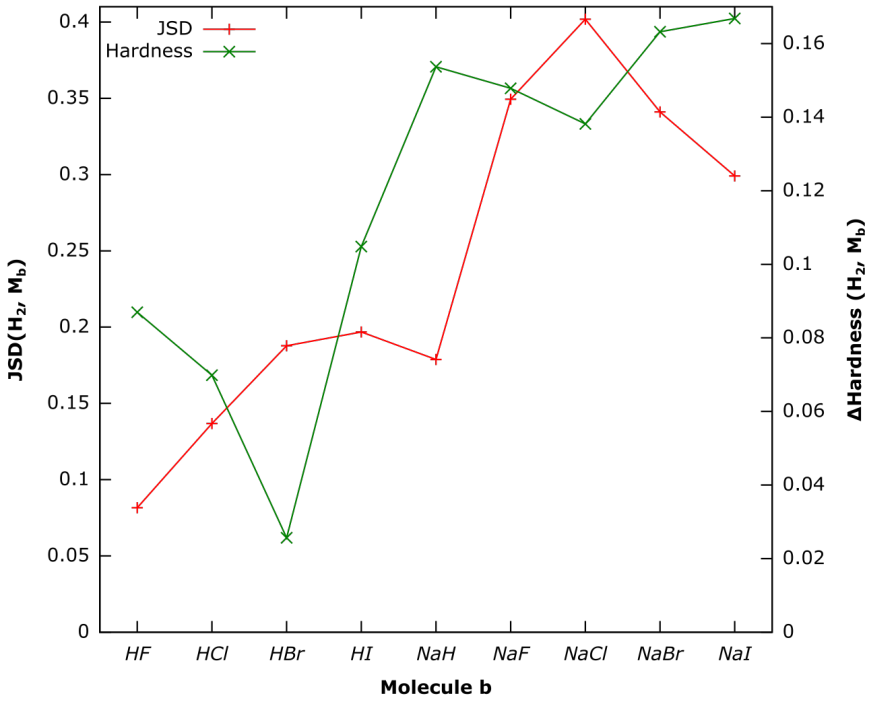

FIGURE 6.7: Jensen-Shannon divergence (red) calculated between the molecular densities of H_2 and the rest of molecules of both groups and the difference of the hardness of the compared molecules (green)

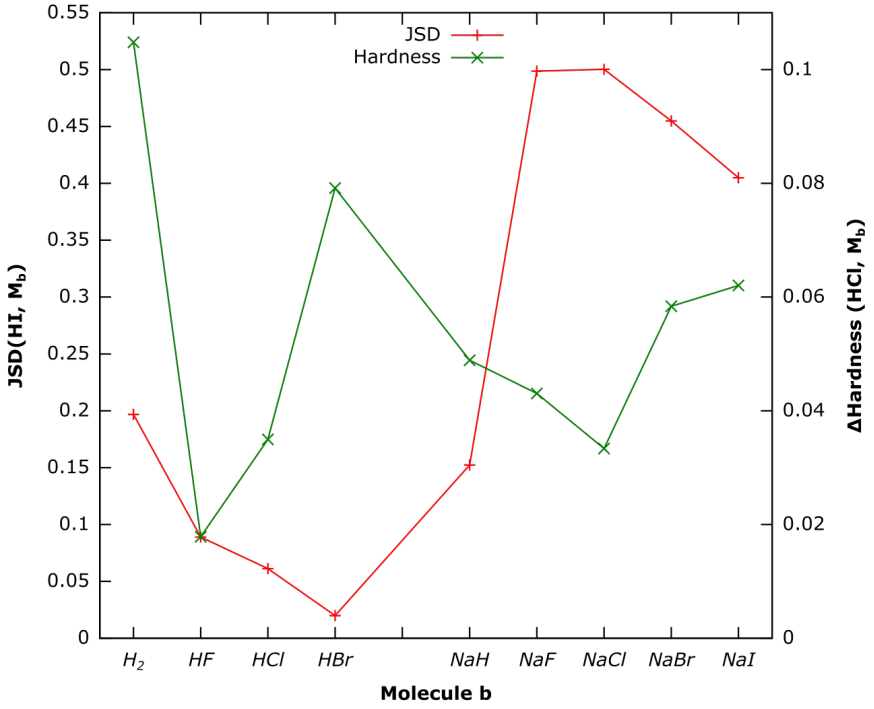

FIGURE 6.8: Jensen-Shannon divergence (red) calculated between the molecular densities of HI and the rest of molecules of both groups and the difference of the hardness of the compared molecules (green)

We have calculated the Jensen-Fisher divergence between each molecule in the hydride group and the other molecules in the group and compared with their electron number, which showed how JFD is related to the difference of the electron number between the molecules under comparison, increasing its value as the difference decreases and reaching a maximum value dependent on the number of electrons the test molecule has. The results also show how this tendency shared between systems with similar atomic shell structure, which also tell us that JFD can grasp the electronic properties of the molecules which is applied to.

The Jensen-Shannon divergence was calculated between a reference molecule, H_2 and NaH and the rest of the hydride group and Sodium salt molecules, and compared with the values of hardness of each molecule it was compared with, discovering a inverse relation between the JSD value and the hardness value.

Although the relationships observed have been quite humble, this field is very promising and rich, and we are certain that in the future there will be more strong links established between divergence measures and chemical properties of molecules. In the near future we want to slowly diversify the molecules to be considered in order to broad the scope of our studies, but at the same time, staying in a approachable and realistic territory. Then we will search for connections with other chemical properties, first directly related to the ones studied in this work, namely hardness and number of electrons, such as electrophilicity, chemical potential or softness. At the end, in more ambitious future studies we plan to apply all the knowledge gain with the previous work to more complex and exotic molecules, such as proteins, to determine how informational divergences calculated between the many kinds of proteins translate into differences between their properties.

Chapter 7

The relativistic harmonic oscillator

In the previous chapters, how information-theoretic measures can be applied to the analysis of atomic systems, both relativistic and non- relativistic, has been shown. A clear relation between atomic properties (such as nuclear charge, electronic configuration, groups at the Periodic Table or ionization potential) and different divergence measures has been established. In doing so, the Schrödinger/Dirac equation for atomic systems had to be solved for both neutral and ionized states. All those cases were numerically approached, as the many-electron atomic problem has not an analytical solution, either relativistic or non-relativistic. This is not surprising, particularly in the relativistic case, because there are not many problems in relativistic quantum mechanics being both analytically soluble and interesting. The Dirac equation, the main tool used on this matter, although elegant and very well studied, it contains very few particular cases in which can be analytically solved, namely the hydrogen atom, a particle in a homogeneous magnetic field, a particle in the field of an electromagnetic plane wave, the Morse oscillator and the harmonic oscillator, which will be the cornerstone of this chapter [252].

The relativistic harmonic oscillator, frequently called Dirac oscillator, has been analyzed in some contexts in the past [253], However, interest in this topic has recently grown due to its importance in many-body theories [254]. Since then, this system has been studied in many different frames of reference such as hadronic spectra modeling, usefulness in quantum chromodynamics and supersymmetry models [255, 256].

From an information-theoretical point of view, the non-relativistic harmonic oscillator has been thoroughly studied, showing the power of information-theoretic measures on this analysis. Some recent studies deal with log-periodic oscillator using Shannon entropy and Fisher information, and LMC and FS complexities [257] as well, and the application

of joint entropy [258] and Fisher information [259] to quantum damped oscillators, among others.

The purpose of this chapter is to apply some of these information measures to the Dirac oscillator. Particularly, we will analyze its Shannon entropy, Fisher information, disequilibrium as individual measures, besides LMC and Fisher-Shannon complexities. We seek establishing a similar relationship between these information-theoretic functionals and relevant attributes of the Dirac oscillator as we have previously done in the atomic case.

This chapter is structured as follows. First we introduce and discuss in detail the Dirac equation, particularly when applied to the relativistic quantum oscillator, then providing the known Dirac wave functions of the relativistic harmonic oscillator and their associated probability densities. A much more in-depth discussion of the equations and their physical origin can be found in Ref. [260]. Then, diverse individual measures will be computed for the corresponding density: Shannon entropy, Fisher information and disequilibrium, and a direct relation between these measures and the quantum numbers will be provided. Next, complexity measures will be considered , paying attention to their behavior in terms of the state quantum numbers. Finally the main conclusions will be discussed, as well as their implications.

7.1 Dirac equation and Dirac oscillator

In the relativistic framework, the free particle Dirac equation (in natural units: $\hbar = c = 1$) is given by:

$$H_{free}\psi = (\alpha \cdot \boldsymbol{p} + m\beta)\psi = i\frac{\partial \psi}{\partial t}, \tag{7.1}$$

where H_{free} is the free-particle Dirac Hamiltonian, $\boldsymbol{p} = -i\nabla$ is the momentum, m is the mass of the particle considered, and α and β are the 4×4 Dirac matrices:

$$\alpha = \begin{pmatrix} 0 & \sigma \\ \sigma & 0 \end{pmatrix}, \quad \text{and} \quad \beta = \begin{pmatrix} 1 & 0 \\ 0 & 1 \end{pmatrix} \tag{7.2}$$

being σ the 2×2 Pauli Matrices, and the 1's and 0's stand for 2×2 unit and zero matrices, respectively.

The Dirac equation can be expressed in the Lorentz covariant form by using the gamma matrices, i.e., $\gamma^0 = \beta$ and $\gamma = \beta\alpha$, then multiplying by β:

$$\left(i\gamma^\mu \partial_\mu - m\right)\psi = 0 \tag{7.3}$$

Let us remark that an electromagnetic interaction can be considered beyond the free particle Dirac equation (7.1) by means of the standard minimal-coupling prescription $\boldsymbol{p} \to \boldsymbol{p} - e\boldsymbol{A}$ or, in covariant form $p^\mu \to p^\mu - A^\mu$, with $A^\mu = (\phi, \boldsymbol{A})$, where $\boldsymbol{A}$ is the vector potential and ϕ is the scalar electromagnetic potential.

The oscillator potential, which gives rise to a non-relativistic quadratic Hamiltonian in both the momenta and the spatial coordinates, should give a linear equation in the relativistic case. In order to obtain that, we have to perform the following substitution in the free particle Hamiltonian in the Eq. (7.1):

$$\boldsymbol{p} \to \boldsymbol{P} - im\omega\beta\boldsymbol{r}, \tag{7.4}$$

where ω is the oscillator frequency. It is noteworthy that this term is not hermitian. However, the complete hamiltonian remains hermitian due to the presence of the α matrix. The Dirac oscillator equation results then:

$$i\frac{\partial\psi}{\partial t} = H\psi = (\alpha \cdot (\boldsymbol{p} - im\omega\boldsymbol{r}\beta) + m\beta)\psi \tag{7.5}$$

It is worth noting that the interaction is introduced on this way in order to obtain a Lorentz covariant interaction (due to the inclusion of the β matrix), and also to avoid that a pure linear term could be gauged away. The choice of Eq. (7.5) also guarantees the C,P, T invariance properties of the Dirac oscillator [261].

It is straightforward to check that the Dirac oscillator can be seen as a the square root of the linear harmonic oscillator. If we take the square of the hamiltonian in Eq. (7.1):

$$H^2 = (\boldsymbol{\alpha}\dot{(}\boldsymbol{p} - i\omega\beta\boldsymbol{r}) + m\beta)^2 = p^2 + m^2\omega r^2 + (4 * \boldsymbol{S} \cdot \boldsymbol{L} - 3)m\omega\beta, \tag{7.6}$$

where $\boldsymbol{S} = \boldsymbol{\sigma}/2$ is the spin and $\boldsymbol{L} = \boldsymbol{r} \times \boldsymbol{p}$ is the orbital angular momentum of the oscillating particle, so that it can be seen as a Klein-Gordon equation with a harmonic oscillator interaction plus a spin-orbit coupling term. This is an interesting and useful fact because Eq. (7.6) could be employed to obtain the energy eigenvalues of the Dirac oscillator, as will be shown later.

Defining the total angular momentum of the Dirac oscillator in the typical way, namely $\boldsymbol{J} = \boldsymbol{L} + \boldsymbol{S}$ it is easy to verify that the system retains the total angular momentum, but neither $\boldsymbol{L}$ nor $\boldsymbol{S}$ are separately conserved:

$$[\boldsymbol{L}, H] = i\left(\boldsymbol{\alpha} \times \boldsymbol{p}\right) - m\omega\beta\left(\boldsymbol{r} \times \boldsymbol{\alpha}\right), \tag{7.7}$$

$$[\boldsymbol{S}, H] = -i\left(\boldsymbol{\alpha} \times \boldsymbol{p}\right) + m\omega\beta\left(\boldsymbol{r} \times \boldsymbol{\alpha}\right). \tag{7.8}$$

The sum rules of angular momentum imply that $j = l \pm \frac{1}{2}$, where j is the total angular momentum quantum number and l is the orbital quantum number. We also use the parity of our system (that is $(-1)^l$ for the eigenfunctions of radially symmetric problems in the Dirac framework) to classify the eigenfunctions. In order to do that, let us define:

$$\epsilon = \begin{cases} +1 & \text{if parity is} \quad (-1)^{j+1/2} \\ -1 & \text{if parity is} \quad (-1)^{j-1/2} \end{cases} \tag{7.9}$$

being in both cases $l = j + \frac{\epsilon}{2}$. With this consideration, we can define the solution of the Dirac oscillator as:

$$\Psi(\boldsymbol{r}, t) = \frac{1}{r}\left\{ \begin{array}{l} F_{n,l}(r)\mathcal{Y}^{\pm}_{jml}(\theta, \phi) \\ iG_{n,l'}(r)\mathcal{Y}^{\pm}_{jml'}(\theta, \phi) \end{array} \right\} e^{-iEt} \tag{7.10}$$

where $\mathcal{Y}^{\pm}_{jml}$ and $\mathcal{Y}^{\pm}_{jml'}$ are spinor spherical harmonics of order l and l', respectively [262]:

$$\mathcal{Y}^{\pm}_{jml}(\theta, \phi) = \left(\begin{array}{c} \sqrt{\frac{l \pm m + \frac{1}{2}}{2l+1}} Y_{l,m-\frac{1}{2}}(\theta, \phi) \\ \pm\sqrt{\frac{l \mp m + \frac{1}{2}}{2l+1}} Y_{l,m+\frac{1}{2}}(\theta, \phi) \end{array} \right) \tag{7.11}$$

where $Y_{l,n}$ are the standard spherical harmonics. Notice that $\mathcal{Y}_{jml}$ and $\mathcal{Y}_{jml'}$ have opposite parity, so $l' = j - \epsilon/2$.

It is easily to verify that the eigenfunctions of the Dirac oscillator equation must have the same form as those of the non-relativistic one [256], so we can define the so-called "large" and "small" radial components as:

$$F_{n,l}(r) = A\left(\sqrt{m\omega}r\right)^{l+1} \exp\left(-m\omega r^2\right) {}_1F_1\left(-n, l + 3/2, m\omega r^2\right), \tag{7.12}$$

and

$$G_{n,l'}(r) = A\left(\sqrt{m\omega}r\right)^{l'+1} \exp\left(-m\omega r^2\right) {}_1F_1\left(-n, l' + 3/2, m\omega r^2\right) \tag{7.13}$$

respectively. ${}_1F_1\left(a, b, c\right)$ are the confluent hypergeometrical functions, $n = 0, 1, 2, ...$ and A is the normalization constant:

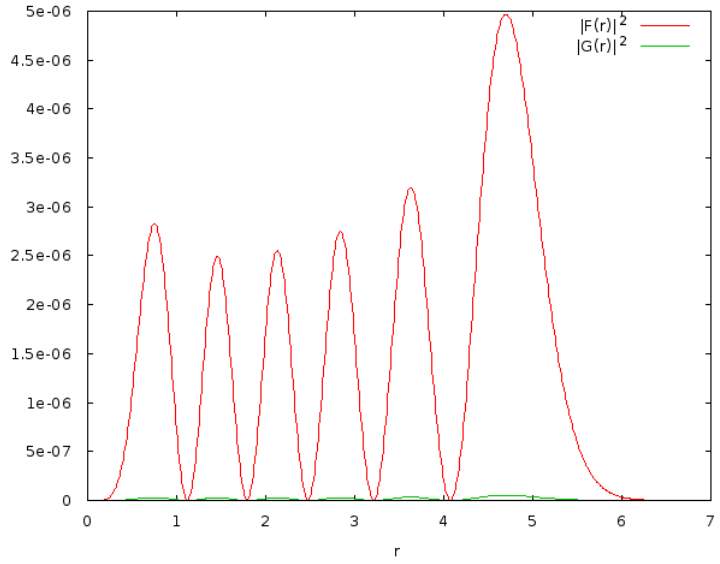

FIGURE 7.1: Comparison of the large ($F_{n,l}(r)$) and small ($G_{n,l}(r)$) components of the harmonic oscillator Dirac density. Atomic units (a.u.) are used.

$$A = \left(\frac{m\omega}{\pi}\right)^{\frac{1}{4}} \left[\frac{n!2^{n+l+\epsilon/2+3/2}}{(2n+2l+1-2\epsilon)!!}\right]^{\frac{1}{2}} \left[\left(n+l+1-\frac{\epsilon}{2}\right)^3 + \left(n+l-\frac{\epsilon}{2}\right)\right]. \tag{7.14}$$

Let us remark that for the $F_{n,l}(r)$ function, the energy is positive, being defined as:

$$E^+ = \left\{m\omega\left[2(2n+l+1)+\epsilon(2j+1)+m^2\right]\right\}^{1/2} \tag{7.15}$$

and the orbital momentum is $l = l' = j + \epsilon/2$. On the other hand, for the $G_{n,l}(r)$ function the energy is negative and is given by

$$E^- = -\left\{m\omega\left[2(2n+l+2)+\epsilon(2j+1)+m^2\right]\right\}^{1/2} \tag{7.16}$$

and the angular momentum is $l' = j - \epsilon/2$ [256].

In Figure 7.1 the reasons behind the name of each component are manifest. Their respective contribution to the total density have a very different magnitude. The large component's contributions, $F_{n,l}(r)$, is much larger than that of the small one, $G_{n,l}(r)$, although the latter is still significant to the system and can't be completely neglected.

After some mathematical manipulations, the probability density can be written down in the following separable form:

$$\rho_{njm}(\vec{r}) = \rho_{radial}(r)\rho_{angular}(\Omega) \tag{7.17}$$

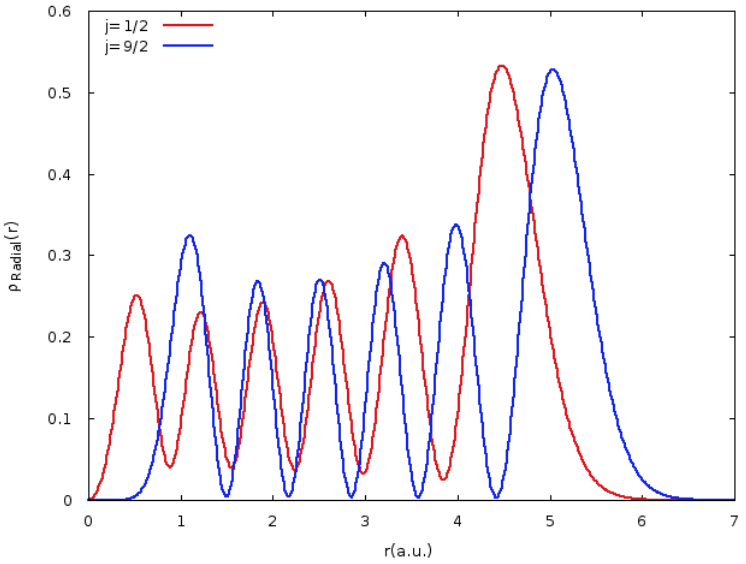

FIGURE 7.2: Radial density of the relativistic harmonic oscillator for fixed values $n = 5$, $w = 1$ and two different values of j, $j = 1/2$ (red) and $j = 9/2$ (blue). Atomic units (a.u.) are used.

where $\rho_{radial}(r)$ and $\rho_{angular}(\Omega)$ are the radial and the angular part, respectively. For the sake of simplicity we are going to restrict the analysis to the radial part of the density, which can be expressed as:

$$\begin{aligned}\rho_{radial}(r) &= |F_{n,l}(r)|^2 + |G_{n,l'}(r)|^2 \\ &= 0.564192^{\mathrm{l}+n+1} e^{-r^2 w} \frac{n!}{(2\mathrm{l}+2n-1)!!} \left| \frac{(r\sqrt{w})^{\mathrm{l}+1} \sqrt[4]{w}\, {}_1F_1(-n;\mathrm{l}+\frac{3}{2};1.r^2 w)}{\sqrt{(\mathrm{l}+n+\frac{1}{2})^3 + (\mathrm{l}+n-\frac{1}{2})^2}} \right|^2 \\ &+ 0.564192^{\mathrm{l'}+n+2} e^{-r^2 w} \frac{n!}{(2\mathrm{l'}+2n+3)!!} \left| \frac{(r\sqrt{w})^{\mathrm{l'}+1} \sqrt[4]{w}\, {}_1F_1(-n;\mathrm{l'}+\frac{3}{2};1.r^2 w)}{\sqrt{(\mathrm{l'}+n+\frac{3}{2})^3 + (\mathrm{l'}+n+\frac{1}{2})^2}} \right|^2 \end{aligned} \tag{7.18}$$

7.2 Information-theoretical analysis of the Dirac oscillator

Before analyzing the information measures, it is convenient to take a look at the shape of the radial probability density corresponding to the possible states of the system. In Figure 7.2 the probability density for different values of the total momentum number j is depicted. It can be observed that, for a fixed principal quantum number, n, and frequency, w, the radial probability density suffers a global translation to a higher values of r when the total angular momentum j increases. The relative height of the extrema homogenizes and they slightly but appreciably get sharper.

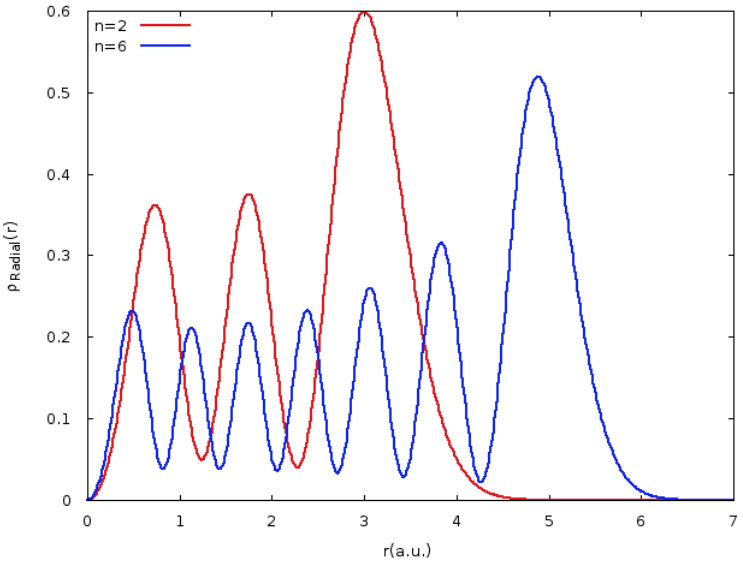

FIGURE 7.3: Radial density of the relativistic harmonic oscillator for a fixed value of $j = 1/2$, $w = 1$ and two different values of n, $n = 2$ (red) and $n = 5$ (blue). Atomic units (a.u.) are used.

The behavior with respect to the principal quantum number n is shown in Figure 7.3. We can perceive how the radial density of the relativistic oscillator changes when the principal quantum number n varies. It can be appreciated how the oscillations of the density increase, and at the same time the maximum value decreases and also it extends to a higher values of r.

Finally, in Figure 7.4, the radial probability density for different values of the frequency w is shown. It can be observed that, for fixed values of the quantum numbers n and j, the radial density suffers a contraction towards the origin when the frequency w increases. Its maxima reach higher values and its oscillations become sharper .

7.2.1 Shannon, entropy, Fisher information and disequilibrium

Let us now discuss how the different information-theoretic measures quantify these changes previously observed in the radial probability density. We start with the analysis of the most widely used information functionals, i.e. Shannon entropy, Fisher information and disequilibrium.

In Figure 7.5 the disequilibrium of the Dirac oscillator for different states with a fixed principal quantum number $n = 5$ and a varying total angular momentum number j from 1/2 to 9/2 is represented. It can be observed an increasing behavior of the disequilibrium as the total angular momentum j increases. This tendency has a high slope for low values of j, and stabilizes for high ones. Taking into account that the disequilibrium quantifies the degree of departure from uniformity of a given probability density, we can establish a relationship between j values of the states and the spreading of their radial probability

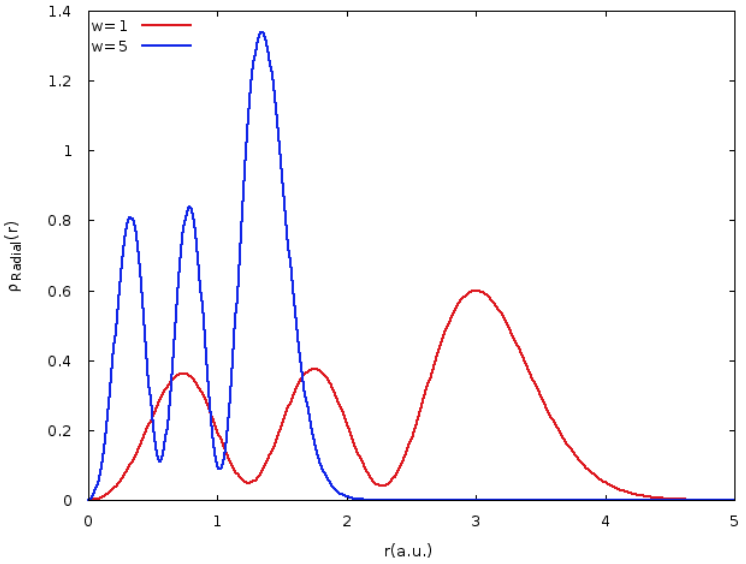

FIGURE 7.4: Radial density of the relativistic harmonic oscillator for a fixed value of $n = 3$, $j = 1/2$ and two different values of w, $w = 1$ (red) and $w = 5$ (blue). Atomic units (a.u.) are used.

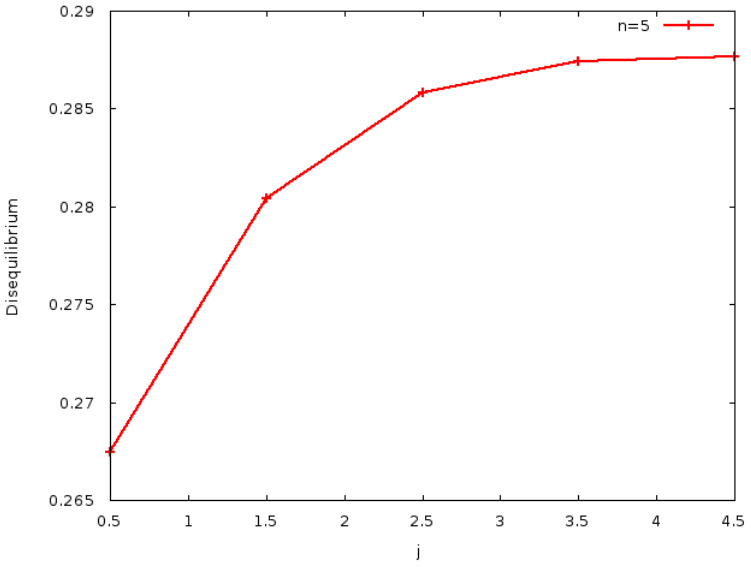

FIGURE 7.5: Disequilibrium of the radial density of the relativistic harmonic oscillator, for fixed values of $n = 5$ and $w = 1$, and $j \in \left[\frac{1}{2}, \frac{9}{2}\right]$. Atomic units (a.u.) are used.

densities, i.e., for a fixed quantum number n, the radial density of the Dirac oscillator concentrates around density maxima as the total angular momentum j increases.

In Figure 7.6 the disequilibrium for a fixed value of frequency, $w = 1$, and different values of j and n has been represented. We can see how the tendency observed in the previous figure is manifested again, i.e. lower (higher) values of j correspond to lower (higher) values of disequilibrium. We can observe now that for a given value of j, higher values of the principal quantum number n also correspond to lower value of disequilibrium, which means that the density becomes more uniform as n increases for a fixed value of

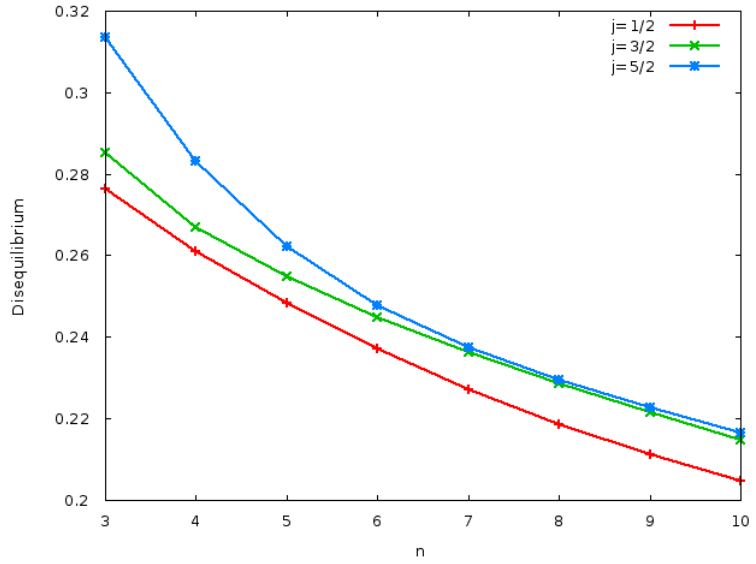

FIGURE 7.6: Disequilibrium of the radial density of the relativistic harmonic oscillator, for each of the values of $j = \frac{1}{2}, \frac{3}{2}$ and $\frac{5}{2}$, with $w = 1$ and $n \in [3, 10]$. Atomic units (a.u.) are used.

j. This behavior has been observed in Figure 7.3. Let us also remark that the difference between states with $j = \frac{3}{2}$ and $j = \frac{5}{2}$ reduces when the principal quantum number increases, while the difference between those with $j = \frac{3}{2}$ and $j = \frac{1}{2}$ increases.

The disequilibrium of the radial density for fixed values of j and n and different values of the frequency w is shown in Figure 7.7. It can be observed how a higher value of the frequency translates into a higher value of the disequilibrium in a monotonous way, increasing faster for low values of w but stabilizing for a greater values of w. This behavior is understandable when looking at Figure 7.4, as the different cycles tend to get sharper and closer one to each other as the frequency rises, so, it was expected that the disequilibrium reached higher values.

If we focus our attention on the Shannon entropy, we can observe that it has an opposite behavior to that of the disequilibrium. In Figure 7.8, the dependence of this measure on the value of total angular momentum j for fixed values $n = 5$ and $w = 1$ can be observed. Shannon entropy exhibits a decreasing behavior as the quantum number j increases. The decrement is faster for low values of j and becomes slower as j increases. It is well known that the Shannon entropy measures the spreading of the probability density, so we can conclude that the probability density which describes the Dirac oscillator becomes more concentrated within its domain as the total angular momentum j of the system increases. Let us remark that the minimal change $j \to j + 1$ in the total quantum number implies a great reduction of the Shannon entropy value, but this implication quickly gets less significant.

In Figure 7.9, the Shannon entropy is depicted as a function of the principal quantum number n of the state. This has been done for different values of the total angular

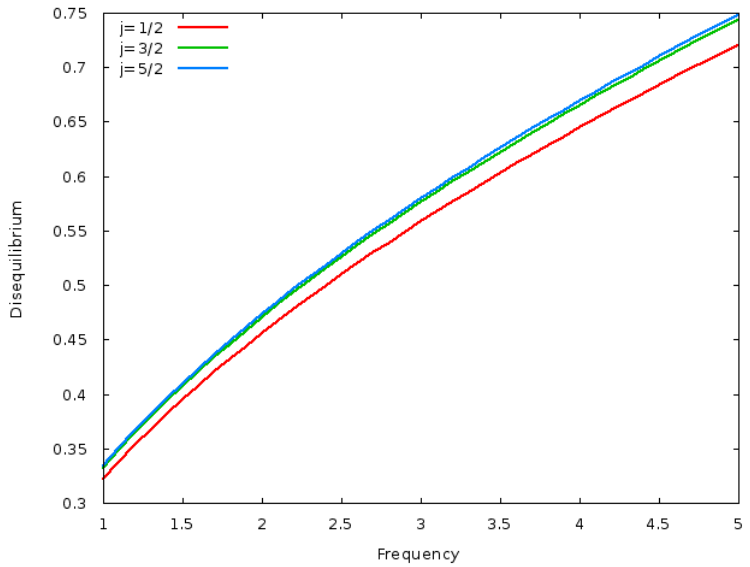

FIGURE 7.7: Disequilibrium of the radial density of the relativistic harmonic oscillator, for a fixed value of $j = \frac{1}{2}, \frac{3}{2}$ and $\frac{5}{2}$, and $n = 3$, with frequency $w \in [1, 5]$. Atomic units (a.u.) are used.

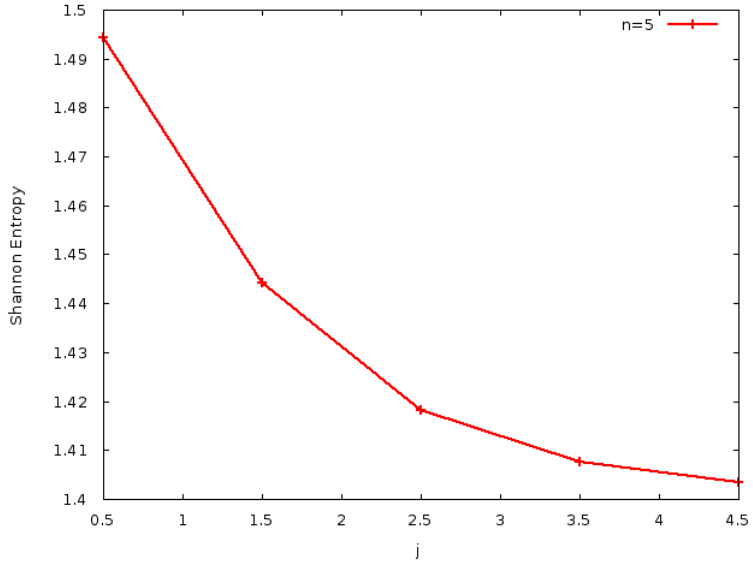

FIGURE 7.8: Shannon entropy for the radial density of the relativistic harmonic oscillator, for a fixed value of $n = 5$, $w = 1$ and $j \in \left[\frac{1}{2}, \frac{9}{2}\right]$. Atomic units (a.u.) are used.

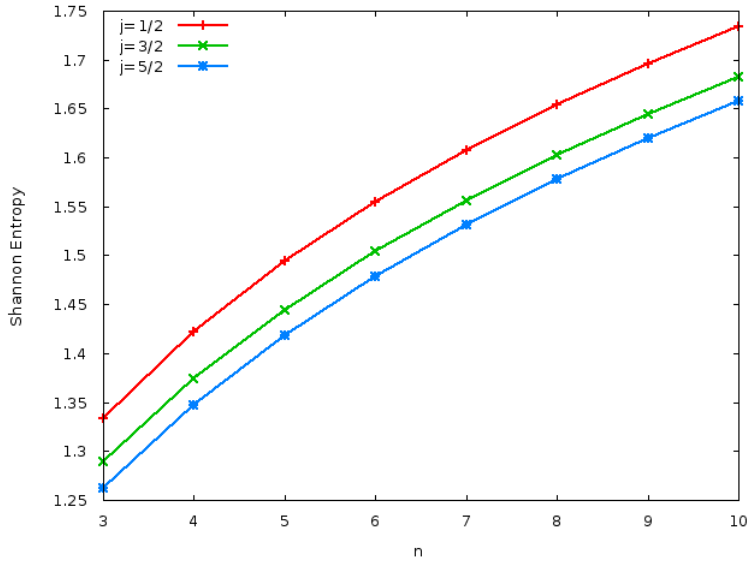

FIGURE 7.9: Shannon entropy of the radial density of the relativistic harmonic oscillator, for each of the values $j = \frac{1}{2}$, $\frac{3}{2}$ and $\frac{5}{2}$, with $w = 1$ and $n \in [3, 10]$. Atomic units (a.u.) are used.

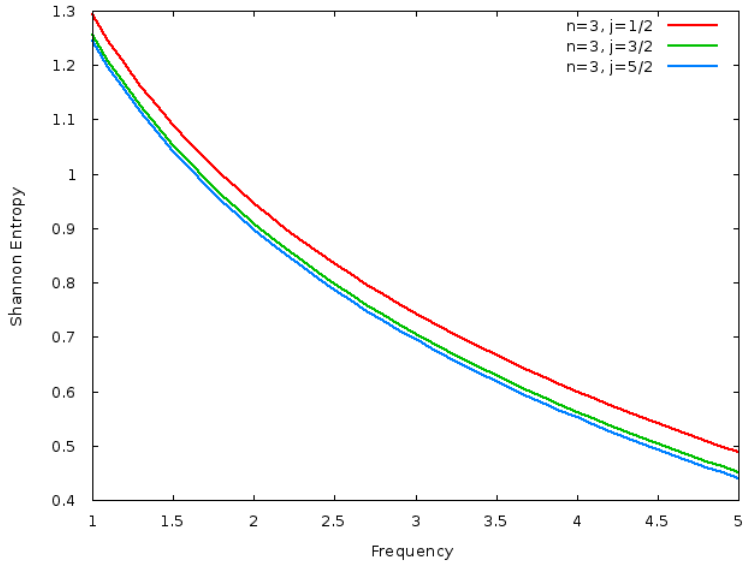

FIGURE 7.10: Shannon entropy of the radial density of the relativistic harmonic oscillator, for each of the values of $j = \frac{1}{2}, \frac{3}{2}$ and $\frac{5}{2}$, and $n = 3$, with $w \in [1, 5]$. Atomic units (a.u.) are used.

momentum, specifically for $j = 1/2, 3/2$ and $5/2$, and for a frequency value $w = 1$. It can be observed from the figure that the Shannon entropy increases when the principal quantum number n does. Observing Figure 7.3 it is obvious how the density becomes more delocalized for higher values of n. In this case, unlike the disequilibrium measure, the differences between $j = \frac{1}{2}$, $j = \frac{3}{2}$ and $j = \frac{5}{2}$ remain constant along all the range of n.

Finally, we analyze the dependence of the Shannon entropy on the frequency of the

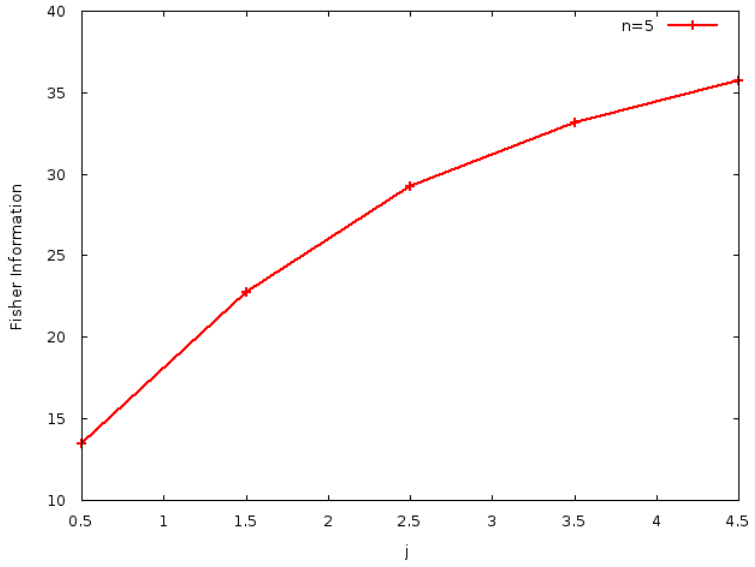

FIGURE 7.11: Fisher information of the radial density of the relativistic harmonic oscillator, for a fixed value of $n = 5$, $w = 1$ and $j \in \left[\frac{1}{2}, \frac{9}{2}\right]$. Atomic units (a.u.) are used.

system. In Figure 7.10, it is displayed the Shannon entropy of the radial density for fixed values of j and n in terms of the frequency w. We realize how its value monotonically decreases, this being due to the shrinking of the density for higher values of the frequency, which translates into a lower value of the Shannon entropy.

For the Fisher information, we can observe in Figure 7.11 its dependence on the total angular momentum j for fixed values of $n = 5$ and $w = 1$. It can be noted that Fisher information increases as j reaches higher values, being the increase more abrupt for lower values of j. This quantity measures the spatial local-wise concentration of the density cloud and quantifies its gradient content, thus revealing the irregularities of the density and providing a quantitative estimation of its fluctuations. It is a measure of the system's disorder. For the Dirac oscillator, Fisher information describes how the density becomes smoother at higher values of j for a fixed value of the principal quantum number n. This is in complete agreement with the disequilibrium values previously discussed.

With regard to the Fisher information dependence on the principal quantum number n, we can observe that it also has an increasing behavior. In Figure 7.12 Fisher information of the radial density for a fixed values of j and w is represented in terms of the value of the principal quantum number n. It can be seen that, for a fixed value of the total angular momentum j, Fisher information increases when the principal quantum number n also does. It was expected, because of the number of extrema of the probability density becomes larger as the number n increases (see Figure 7.3), which causes Fisher information to become higher too.

In Figure 7.13 the Fisher information of the radial density of the Dirac oscillator is displayed for fixed values of n and j, and different values of frequency w. It can be

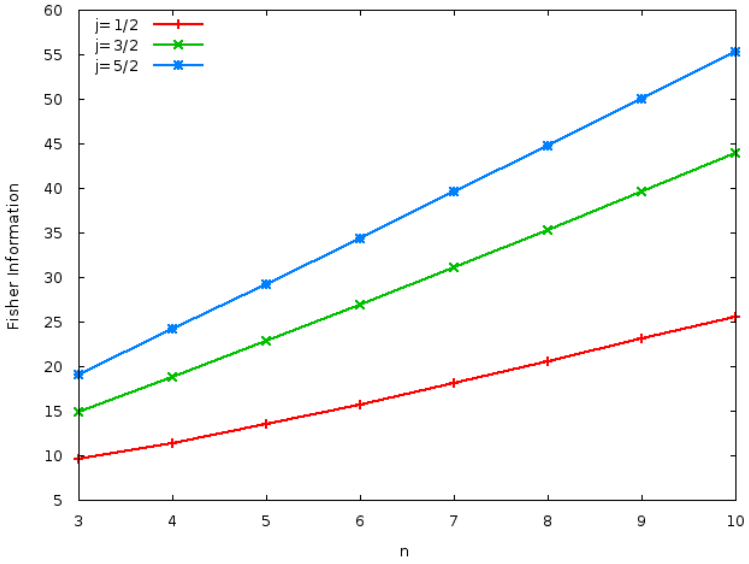

FIGURE 7.12: Fisher information of the radial density of the relativistic harmonic oscillator, for a fixed value of $j = \frac{1}{2}, \frac{3}{2}$ and $\frac{5}{2}$, $w = 1$ and $n \in [3, 10]$. Atomic units (a.u.) are used.

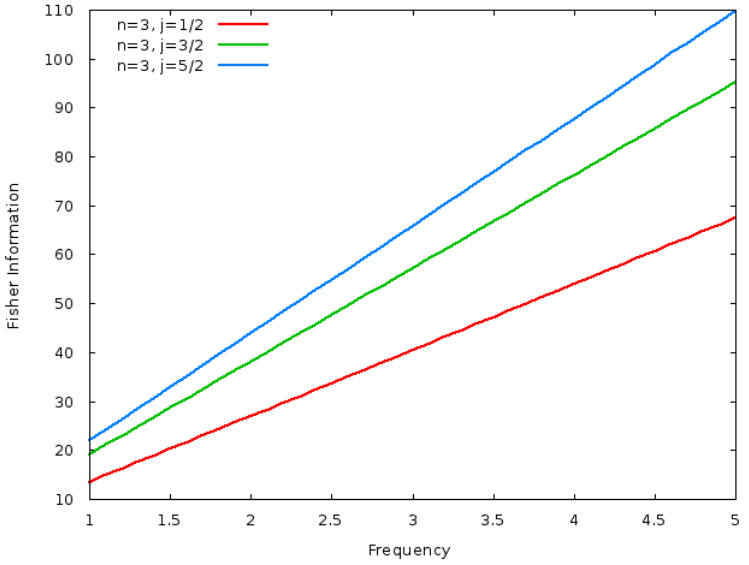

FIGURE 7.13: Fisher information of the radial density of the relativistic harmonic oscillator, for each of the values $j = \frac{1}{2}, \frac{3}{2}$ and $\frac{5}{2}$, with $n = 3$, and frequency $w \in [1, 5]$. Atomic units (a.u.) are used.

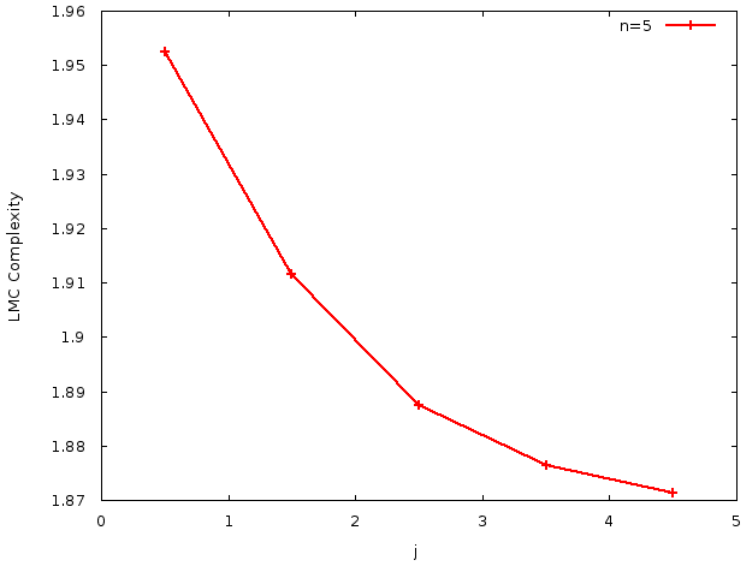

FIGURE 7.14: LMC complexity of the radial density of the relativistic harmonic oscillator, for $n = 5$, $w = 1$ and $j \in \left[\frac{1}{2}, \frac{9}{2}\right]$. Atomic units (a.u.) are used.

appreciated from the figure how Fisher information increases with the value of the frequency w. This is mostly due to the fact that increasing the frequency translates into a compression of the radial density towards the origin, increasing the overall slope of the oscillations, what then translates into a higher value of the Fisher information. This behavior is again independent of j. However, it is shown how for lower values of j the growth is slower than for higher ones. This is due to the already high values that a higher j induces in the Fisher information.

7.2.2 Complexity measures

An extension of the information-theoretical analysis of the Dirac oscillator, is naturally performed by considering the complexity concept through the Fisher-Shannon, FS, and the LMC complexity measures. These measures allow to grasp composite information-theoretic aspects of the systems, i.e., delocalization/uniformity and disorder/uniformity of the probability density which describes the system.

In Figure 7.14 the LMC complexity measure dependence on the total angular momentum j is revealed (for a fixed value of both n and w). It can be observed that higher LMC values are reached for lower values of the total angular momentum j, while higher values of j entail a decrease of the LMC ones. This is mostly due to the fact that, as j increases, the extrema get sharper, so the similarity of the density to a delta distribution increases, and therefore its complexity decreases. As previously discussed, as the total angular momentum increases, the radial probability density of the systems becomes more localized (smaller Shannon entropy values) and is more away from uniformity (larger disequilibrium values).

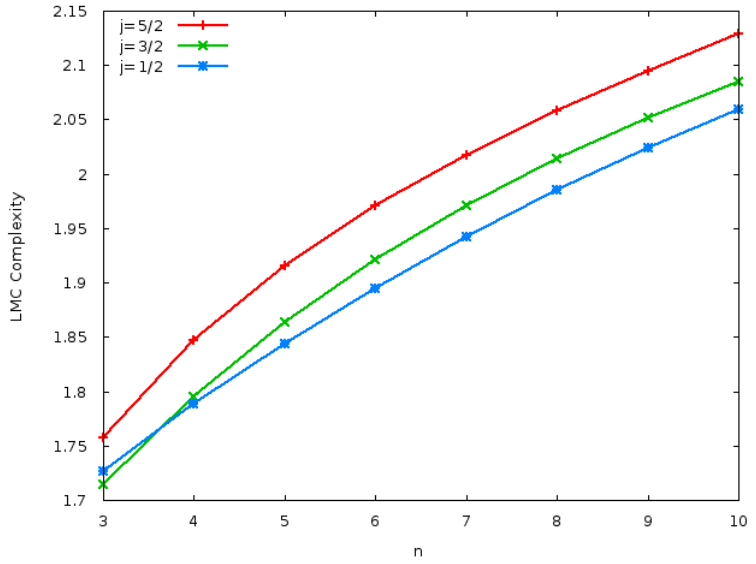

FIGURE 7.15: LMC complexity of the radial density of the relativistic harmonic oscillator, for each of the values $j = \frac{1}{2}, \frac{3}{2}$ and $\frac{5}{2}$, with $w = 1$ and $n \in [3, 10]$. Atomic units (a.u.) are used.

However, the situation is completely different if we consider the dependence of this magnitude on the principal quantum number n. In Figure 7.15 the LMC complexity measure for different values of n is depicted. This figure shows that, for fixed values of j and w, the LMC complexity increases when the principal quantum number n also does. Such an observation is closely related to the fact that increasing the quantum number n makes new extrema to appear, which consequently increases the complexity value of the density. It is worth mentioning that there is a swap in going from $n = 3$ to $n = 4$ for both $j = \frac{3}{2}$ and $j = \frac{1}{2}$. Until now we had seen how the ordering of the respective curves for different j stayed the same for all the range of n, being this case the first one breaking such a tendency.

In Figure 7.16(a) the values of the LMC complexity of the radial density of the relativistic harmonic oscillator are displayed for fixed j and n and a range of values for the frequency w. A very interesting feature can be observed, i.e. the LMC complexity measure remains constant for all values of w here considered. This becomes more apparent when taking into account the information plane L-D depicted in Figure 7.16(b). The curve corresponding to fixed values of both n and j is a straight line. This means that different values of the frequency, when the principal quantum number and the total momentum number remain the same, conform an isocomplexity curve.

For the Fisher-Shannon complexity (FS) we can perform a similar analysis. This measure is a combination of Shannon entropy and Fisher information that classify a distribution in terms of its global and local similarity to an uniform distribution, although due to the fact that Fisher information also quantifies the gradient content of the distribution, its analysis is certainly different from that of the LMC complexity (which is

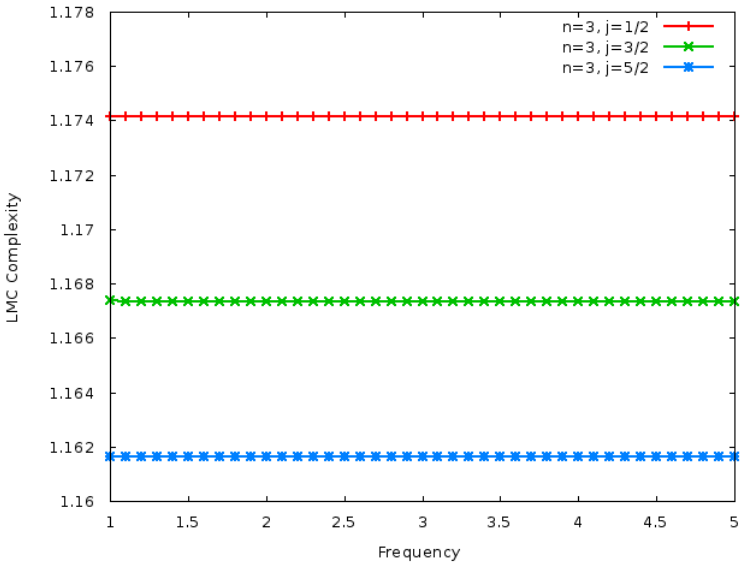

(a) LMC complexity measure

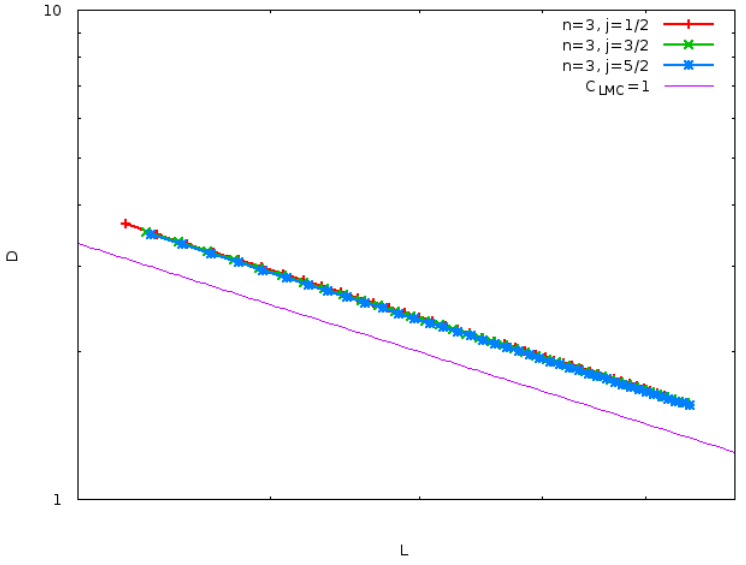

(b) Information plane

FIGURE 7.16: (a) LMC complexity measure, and (b) information plane subtended by the exponential entropy (L) and the disequilibrium (D) of the radial density of the relativistic harmonic oscillator, for each of the values $j = 1/2{,}3/2$ and $5/2$, $n = 3$, and frequency $w \in (1, 5)$. Atomic units (a.u.) are used.

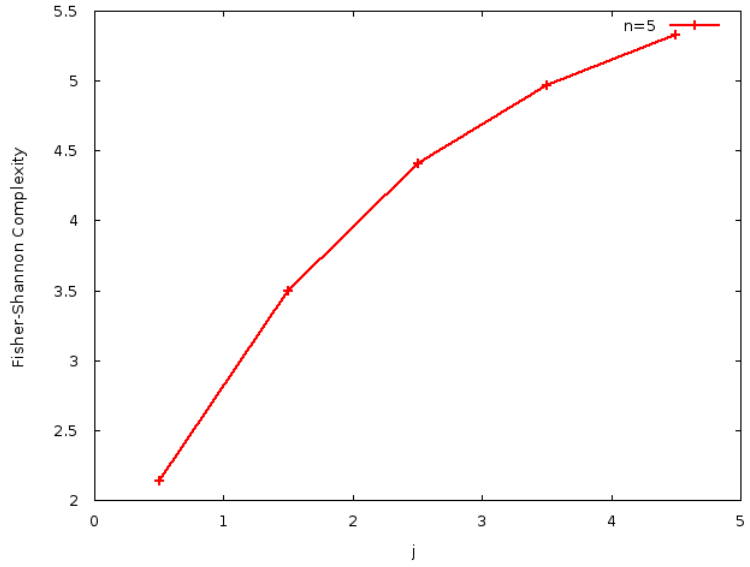

FIGURE 7.17: Fisher-Shannon complexity of the radial density of the relativistic harmonic oscillator, for a fixed value of $n = 5$ and $w = 1$, and $j \in \left[\frac{1}{2}, \frac{9}{2}\right]$. Atomic units (a.u.) are used.

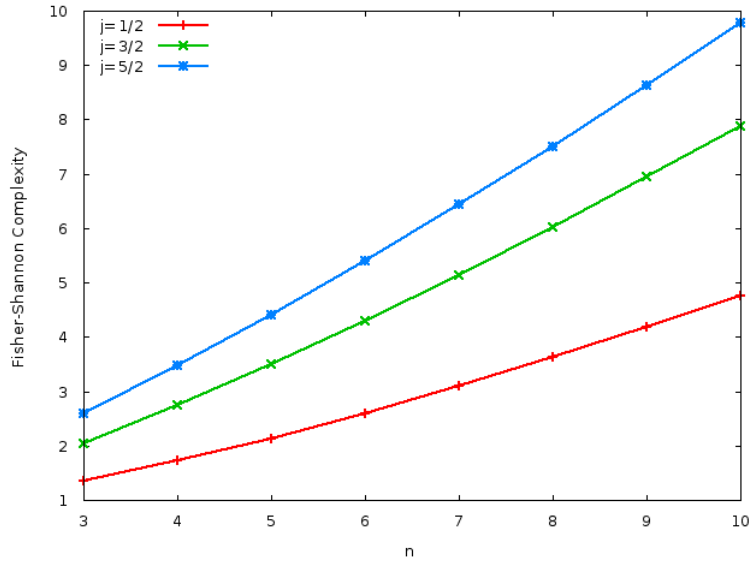

FIGURE 7.18: Fisher-Shannon complexity of the radial density of the relativistic harmonic oscillator, for each of the values $j=\frac{1}{2},\frac{3}{2}$ and $\frac{5}{2}$, with $n \in [3, 10]$. Atomic units (a.u.) are used.

composed by the product of two measures with a global character). In Figure 7.17, the FS dependence on the total angular momentum j is depicted. We can observe that the behavior is completely opposite to that observed in Figure 7.15 for the LMC complexity. For fixed values of $n = 5$ and $w = 1$, the Fisher-Shannon complexity increases as the j value does, which is caused by the increasing slope of the density produced by the growth of j, which increases Fisher information without decreasing Shannon entropy, which globally makes the complexity to augment.

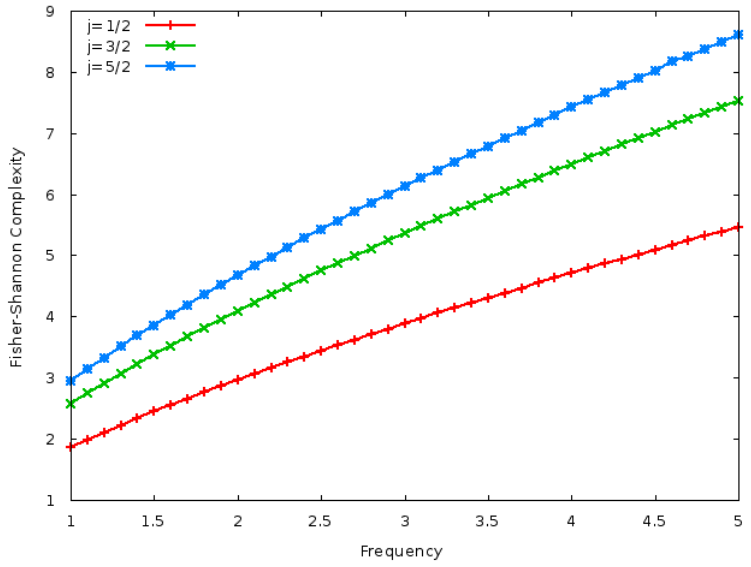

FIGURE 7.19: Fisher-Shannon complexity calculated for the radial density of the relativistic harmonic oscillator, for each of values $j = \frac{1}{2}, \frac{3}{2}$ and $\frac{5}{2}$, $n = 3$, with $w \in [1, 5]$. Atomic units (a.u.) are used.

Contrary to the LMC case, the Fisher-Shannon complexity depends on the principal quantum number n, as it is shown in Figure 7.18. We can observe how the general tendency is a steady grow with the value of the principal quantum number n. This behavior is mostly due to the high increase of Fisher information with each new extrema appearing with a high n, while the Shannon entropy decreases, but not it in a sufficient amount to be significant.

Finally, in Figure 7.19, the Fisher-Shannon complexity of the relativistic harmonic oscillator for particular values of j and n and a range of values of the frequency is represented. The general tendency of the FS complexity is to increase as the frequency does, with a higher rate for higher values of the total angular momentum j. This is due to the considerable increase of the Fisher information, which increases notably as the density compress towards the origin, and at a higher rate than the decrease of Shannon entropy.

7.3 Conclusions

We have studied how different information-theoretic measures can be related to the different states of the relativistic harmonic oscillator. Understanding how changes on quantum numbers affect the radial density that describes those states, we have established a connection between these changes and the radial density structure. In doing so, we have applied disequilibrium, Shannon entropy, Fisher information and both LMC and Fisher-Shannon complexities of different states of the Dirac oscillator, for several values of the principal quantum number n and the total angular momentum j.

First, when studying the disequilibrium of the radial density, we have concluded that it increases with j due to the sharpening of its extrema, decreasing with n as the number of extrema augments, and decreasing also with w as a consequence of the compression of the radial density towards the origin. When Shannon entropy is applied, its value increases with n but decreases with j and w, caused by the spreading of the radial density when new extrema appears but a point-wise localization, instead, when the extrema stretch or the radial density concentrates around the origin. Finally, Fisher information revealed how the gradient content increases with all n, j and w as all of them enhance the oscillatory behavior of the radial density; n by increasing the number of extrema, w and j by making them sharper.

After all those individual quantities, the complexity magnitudes were used. LMC shape complexity, and the corresponding information plane, showed that Shannon's factor was more predominant than the disequilibrium one, but the general trends are very similar. However, the exchange for $j = \frac{1}{2}$ and $j = \frac{3}{2}$ expose how relevant the disequilibrium value was in those cases, as it gets to mask the enhancement Shannon's entropy receives from the LMC complexity. On the other hand, LMC remains constant for different values of w, imposing that n and j stayed the same, so revealing itself as a frequency-independent descriptor. Finally, Fisher-Shannon complexity was considered, revealing how predominant the increment of gradient with all n, j and w is, as it gets to overshadow the relevance of Shannon entropy, as the general trend matches that of Fisher Information.

In conclusion, we have confirmed information-theoretic measures as powerful tools to analyze the radial density structure of the relativistic harmonic oscillator. They completely detect its complex behavior and effectively quantify it, allowing for a straightforward scrutiny. We have observed how the oscillator radial density gets modified with the principal quantum number, the total momentum number and the frequency, and how each one affects differently some characteristic of the radial density, which are detected by each of the measures employed. The increase of extrema and general oscillation with the principal quantum number is quantified by an increment on Fisher information and Shannon entropy, and as a decrease on disequilibrium. In contrast, the sharpening with the total momentum number entails an increment on disequilibrium and Shannon entropy, and a decrement of Fisher information. On the other hand, the shrinking of the radial density due to the increment of frequency is detected as an increment of the disequilibrium, a reduction of the Shannon entropy and a increment of the Fisher information.

Conclusions

The main aim of this work is intend to establish direct relationships between different information-theoretic measures in a variety of quantum systems and representative physical and chemical features of such systems. In particular we have studied neutral and ionized atomic systems (in a relativistic and non-relativistic regimen), molecular systems, and the relativistic harmonic oscillator. Fundamental measures from the information theory have been used, as well as complexity and divergence measures. All of them have been defined in Chapter 1.

Chapter 2 has been devoted to the comparison between the Fisher divergence (FD) and the Jensen-Fisher divergence (JFD), both applied to the atomic density of neutral and ionized atoms in position and momentum spaces. Regarding position space FD as a function of the atomic nuclear charge, its definition in terms of a quotient makes FD_r to display an unimodal behavior as it enhances the differences between densities. In contrast, the definition of JFD as a sum of terms results in a masking of those differences providing it with a bimodal structure. That structure is mainly linked to differences with the atomic charge. On the other hand, the appearance of numerous local extrema in the momentum space divergences are governed by the similarities and differences on atomic shells of the systems under comparison. Once again, replacing the quotient in FD by a sum in JFD induces a masking effect, so provoking a loss of extrema in JFD as compared to those of FD. Although the global structure is preserved, only extrema corresponding to systems with anomalous shell-filling remain. In what concerns Fisher-like comparisons between a neutral system and its singly charged ions, both measures FD and JFD display the expected pattern accordingly with the ionization potential of the neutral involved. All extrema are conserved for both measures for s shells.

In Chapter 3 we provide the analysis comparison of the Jensen-Shannon and the Kullback-Leibler divergences when applied to the study of the quantification of relativistic effects in atomic systems, for both position and momentum densities of relativistic atoms. In position space both measures showed the relation between the nuclear charge of the atom considered and the higher relevance of relativistic effects, which are manifested as a higher contrast between the relativistic and non-relativistic atomic densities. In momentum space the concluding results reveal that those systems with filled and half-filled shells are the most affected by relativistic effects. Evidences were found suggesting

that the different long-range behaviors of the Dirac-Fock and Hartree-Fock densities are responsible for those extrema.

In Chapter 4, the contribution that different regions of the atomic density have onto the relevance of relativistic effects employing the generalized quantum similarity index was analyzed. It was found that relativistic effects are highly dependent on the shell-filling pattern of the atomic systems considered, being the closed-shell, the half-filled and the anomalous systems those which more relevant relativistic effects. It was also confirmed that the outermost regions are the most affected ones by relativistic effects. The quantum similarity index has proved itself an useful and highly convenient tool for the study of region-dependent atomic effects, due to the weighting control that its parameter provides.

Chapter 5 focuses on the study of the electron pair densities and their difference as compared to the monoelectronic densities, by means of a number of varied information-theoretical measures. Shannon entropy was successfully applied to electron pair densities, showing a dependence on atomic shell structure much akin to the monoelectronic ones. Despite showing in overall a higher value for the electron pair density, the Shannon entropy is not able to grasp critical differences between both paradigms, as that measure shows a very similar behavior in both, momentum and position spaces, for one-electron and two-electron densities. The disequilibrium displays an analogous behavior to Shannon entropy, but in the opposed spaces. The LMC shape complexity exhibits a dominance of the Shannon factor over the disequilibrium one in position space, whereas the disequilibrium is the responsible for the extrema in momentum space, where Shannon entropy is just a modulator. Both Shannon entropy and disequilibrium act as quantifiers of the electronic interaction and of its importance over the nucleus repulsion, providing an accurate depiction of the relative relevance on different atomic species. Divergence measures were successfully used as tools of direct comparison between the two kinds of densities. Jensen-Shannon divergence proved the connection between the number of electrons and the electron correlation. It also presenting the atomic systems with an electron added to a complete shell structure as those which the highest difference between the two kind of densities, whereas those atomic systems with a complete shell are the most similar ones. When the Jensen-Shannon divergence was employed for the study of cations and anions, it was found that, in position space, differences between densities diminished for increasing number of electrons of the systems. In momentum space, however, the monotonic tendency inverses after reaching a certain number of electrons (namely, 17). Alkaline systems displayed the greatest difference between densities for both cations and anions and momentum and position space. On the basis of the quantum similarity calculations, it was founds found that the difference between densities was not only dependent on the electronic configuration, but on the different number of electrons as well, showing that, at some regions of the Periodic Table the difference between electronic configurations are irrelevant, being the number of electron

the deciding factor. Overall, the general usefulness of the information measures has been proved, confirming that there is none of them capable of substituting any of the others, but showing each one a different relevant aspect of the one-electron/two-electron relationship.

Chapter 6 was dedicated to the analysis of molecular systems using divergence measures in order to establish an initial approach to this barely explored framework. The intrinsic complexity of this matter has been proved, showing how difficult is to establish a direct relationship between differences of chemical properties and informational quantities, due to the much more varied nature of the molecular systems. However, some preliminary results were reached. For a restricted group of molecules it was found how the value of the Jensen-Shannon divergence is independent of the reference molecule considered when compared to a molecule of a different group (molecules with a much higher number of electrons being the exception). However, when comparing with a molecule of the same group the JSD value was dependent on the number of electrons. This is understood as a prove that the general electronic structure due to the type of a molecule has a more critical impact in the density of the molecule than just the bare electron number. A similar conclusion arises when calculating the Jensen-Fisher divergence, showing a dependency on the number of electrons when comparing molecules with a similar classification. On the contrary a general behavior, mostly independent of the number of electrons of the molecule, was found when comparing different kinds of molecules.

In Chapter 7, the radial density of the relativistic harmonic oscillator it was studied by employing different informational measures in order to analyze the higher or lower resemblance between the different states of such a system. The disequilibrium, the Shannon entropy and the Fisher information quantify the sharpening of the extrema and the increased homogeneity produced by a higher total angular momentum, the homogenization and the new oscillations appearing as the principal quantum number increases, and the concentration towards the origin as well as the stretching of the oscillations with a higher frequency value. The LMC shape complexity showed isocomplexity lines for equal values of the principal quantum number and the total angular momentum, despite the variation of the frequency, and a predominance of the disequilibrium over the Shannon entropy in the other cases as well. The Fisher-Shannon complexity reveals how the gradient increase is more relevant than the compression of the radial density.

Globally, this Thesis has shown how different information-theoretic measures are able to quantify diverse physical, chemical and structural properties of the quantum systems they were applied to. Such measures have proven to be very useful tools for the analysis and understanding of how those properties vary with different parameters and status of those systems, establishing different connections between the properties and the information-theoretic measures, so even allowing to perform direct comparisons between systems which, very usually, it would be a much more complex task.

Conclusiones

El objetivo principal de este trabajo consiste en establecer una relación directa entre diferentes medidas teórico-informacionales aplicadas a un conjunto variado de sistemas cuánticos, y medidas físico-químicas representativas de dichos sistemas. Concretamente se han estudiado sistemas atómicos, tanto neutros como ionizados, en régimen relativista y no relativista; sistemas moleculares; y el oscilador armónico relativista. Para el estudio se han empleado medidas individuales de la teoría de la información, además de medidas de complejidad y de divergencia. Todas ellas se han definido y discutido en profundidad en el Capítulo 1.

El Capítulo 2 está dedicado a la comparación entre la divergencia de Fisher (FD) y la divergencia de Jensen-Fisher (JFD), cuando ambas son aplicadas a densidades de sistemas atómicos neutros e ionizados en espacio de posiciones y de momentos. Al calcular FD en función de la carga atómica pudo comprobarse como su definición en términos de cocientes provoca que FD_r presente un comportamiento unimodal, ya que esta pronuncia las diferencias entre densidades. Sin embargo, la definición de JFD en términos de una suma produce un enmascaramiento de dichas diferencias, otorgándole una estructura bimodal. Dicha estructura viene provocada principalmente por las diferencias de carga atómica. Por otro lado, la aparición de numerosos extremos locales en las divergencias calculadas en espacio de momentos vienen gobernadas por las diferencias y semejanzas en la configuración electrónica de los sistemas comparados. Nuevamente, se encuentra que al sustituir el cociente en FD por una suma en JFD produce un enmascaramiento, lo que hace desaparecer algunos extremos en JFD en comparación con FD. Aunque la estructura global se conserva, solo algunos extremos correspondientes a sistemas con llenado anómalo de capas permanecen. En lo concerniente a la comparación entre sistemas neutros con sus iones simples mediante medidas de divergencia de tipo Fisher, ambas medidas FDy JFD muestran el mismo patrón, correspondiente al potencial de ionización de los sistemas neutros considerados. Todos los extremos se conservan para ambas medidas en las capas de tipo s.

En el Capítulo 3 se ha expuesto el análisis de la comparación realizada entre la divergencia de Jensen-Shannon y la divergencia de Kullback-Leibler aplicadas ambas al estudio de la cuantificación de efectos relativistas en sistemas atómicos para densidades relativistas en espacio de posiciones y momentos. En espacio de posiciones ambas medidas

mostraron que existía una correlación entre la carga nuclear del átomo considerado y una mayor relevancia de los efectos relativistas, lo cuál se manifestaba como un mayor contraste entre densidades relativistas y no relativista. En espacio de momentos se encontró que en aquellos sistemas con capas llena o semillena los efectos relativistas eran más relevantes. Se encontraron evidencias que mostraban que una posible explicación de esos extremos venía dada por el diferente comportamiento a largas distancias de las densidades de Hartree-Fock y Dirac-Fock.

En el Capítulo 4 se ha analizado la contribución y relevancia que tienen diferentes regiones de la densidad atómica a los efectos relativistas mediante el uso del índice de similitud cuántico generalizado. Se encontró que los efectos relativistas son altamente dependientes de los patrones de llenado de capas de los sistemas atómicos considerados; siendo aquellos con capa cerrada, capa semillena y llenado anómalo lo que presentan unos efectos relativistas más importantes. También se ha corroborado que las regiones externas son las más afectadas por los efectos relativistas. El índice de similitud cuántico generalizado se confirma como herramienta muy útil y efectiva en el estudio de efectos atómicos regionalmente dependientes, debido a su capacidad de controlar el peso que se le otorga a diferentes localizaciones de la densidad a través de la variación de su parámetro.

El Capítulo 5 se centra en el estudio de las densidades a dos cuerpos y la diferencia que presentan al ser comparadas con las densidades monoelectrónicas, para el cuál se han empleado diferentes medidas teórico-informacionales. La entropía de Shannon se aplicó con éxito a densidades electrónicas de pares, manifestando una dependencia en la estructura atómica de capas, de forma similar a la mostrada por las densidades monoelectrónicas. A pesar de mostrar de forma generalizada un valor superior para la densidad de pares, la entropía de Shannon no es capaz de detectar las diferencias críticas entre ambos paradigmas, ya que la medida muestra un comportamiento muy similar en ambos, en espacio de posiciones y momentos, para densidades a un cuerpo y a dos cuerpos. El desequilibrio muestra un comportamiento análogo a la entropía de Shannon, pero para espacios opuestos. En la complejidad LMC se pone de manifiesto la predominancia del factor correspondiente a Shannon por encima del factor del desequilibrio en espacio de posiciones, mientras que el desequilibrio es el responsable de la aparición de los extremos en el espacio de momentos, donde la entropía de Shannon hace simplemente de modulador. Tanto la entropía de Shannon como el desequilibrio actúan como cuantificadores de la interacción electrónica y de su importancia sobre la repulsión nuclear, proporcionando una clara imagen de su importancia relativa a lo largo de las diferentes especies atómicas. Las medidas de divergencia se utilizaron también con éxito como herramienta de comparación directa entre los dos tipos de densidades. La divergencia de Jensen-Shannon probó la conexión existente entre el número de electrones y la correlación electrónica. Mostrando además los sistemas con un electrón desapareado como aquellos en los que ambos tipos de densidades muestran las diferencias mas significativas,

mientras que los sistemas con capa llena son presentados como los más similares. Al usar la divergencia de Jensen-Shannon en el estudio de cationes y aniones se descubrió que, en espacio de posiciones las diferencias entre densidades disminuían al aumentar el número de electrones del sistema. Sin embargo, en espacio de momentos, la tendencia monótona se invertía a partir de un determinado valor de electrones (concretamente para $z = 17$). Los sistemas de tipo alcalino presentaban la diferencia más importante entre densidades, tanto para cationes como para aniones en ambos espacios. En los cálculos de índice de similitud cuántico se encontró que las diferencias entre ambos tipos de densidades no solo dependía de la configuración electrónica, si no que también ejercía un papel relevante el número de electrones; mostrándose que, en algunas regiones de la tabla periódica, la diferencia de configuración electrónica se hacía irrelevante, siendo el número de electrones el factor decisivo. En conjunto, se ha visto como las medidas de información han sido una herramienta de análisis muy eficaz, corroborándose que no hay ninguna que sea capaz de sustituir al resto, ya que cada una describe una serie de aspectos relevantes de la relación entre las densidades a un cuerpo/dos cuerpos.

El Capítulo 6 está dedicado al análisis de sistemas moleculares mediante medidas de divergencia con el objetivo de establecer una primera aproximación a este campo. Se ha probado la intrínseca complejidad de esta materia, mostrándose la gran dificultad que comprende el establecer una relación directa entre propiedades químicas y magnitudes informacionales debido a la enorme variedad que supone la naturaleza molecular de estos sistemas. No obstante, sí que se han podido conseguir algunos resultados preliminares al respecto. Para un conjunto restringido de moléculas se ha encontrado como el valor de la divergencia de Jensen-Shannon es independiente de la molécula de referencia considerada en la comparación con otra molécula de un grupo diferente, apareciendo una excepción a este caso en moléculas con un muy elevado número de electrones. Sin embargo, cuando se realizó una comparación entre una molécula del mismo grupo, el valor de JSD se probó dependiente del número de electrones. Esto representa una prueba de que la estructura electrónica correspondiente al tipo de molécula considerada tiene un efecto mas relevante en la densidad de la molécula que el mero número de electrones. Se alcanzó una conclusión similar al calcular la divergencia de Jensen-Fisher, la cuál mostraba una dependencia en el número de electrones cuando se comparaban moléculas dentro de la misma clasificación. Mientras que, al comparar moléculas de diferentes tipos se obtenía un comportamiento independiente del número de electrones de la molécula.

En el Capítulo 7, se estudió la densidad radial del oscilador armónico relativista mediante el cálculo de diferentes magnitudes informacionales con el objetivo de analizar la mayor o menor similitud entre los diferentes estados de dicho sistema. El desequilibrio, la entropía de Shannon y la información de Fisher cuantifican el pronunciamiento de los extremos y el incremento de la homogeneidad provocadas por el incremento en el momento angular total; la homogeneización y la aparición de nuevas oscilaciones producidas por el aumento del número cuántico principal; y la concentración en torno al origen a

la par que estrechamiento de las oscilaciones al aumentar los valores de la frecuencia. La complejidad LMC mostró líneas de isocomplejidad para mismos valores del número cuántico principal y del momento angular total independientemente de la variación de la frecuencia; y la predominancia del desequilibrio frente a la entropía de Shannon en el resto de casos. La complejidad Fisher-Shannon reveló el modo en que el incremento del gradiente es más relevante que el efecto de compresión de la densidad.

En conjunto, esta Tesis ha mostrado el modo en que diferentes medidas teórico-informacionales son capaces de cuantificar diferentes propiedades físicas, químicas y estructurales de los sistemas cuánticos a los que son aplicadas. Dichas medidas se han probado altamente efectivas en el análisis y escrutinio en el modo en que dichas propiedades se modifican al variar el estado y parámetros de tales sistemas, estableciendo diferentes conexiones entre las propiedades y las medidas teórico-informacionales, permitiendo incluso la comparación directa entre sistemas que, con otros medios, sería una tarea mucho más compleja.

Bibliography

[1] R. V. Hartley. *Transmision of information.* Bell Sys. Tech. J., **7** 335 (1928).

[2] C. E. Shannon. *A mathematical theory of communication.* Bell Syst. Tech. J., **27** 379 (1948).

[3] C. E. Shannon and W. Weaver. *The Mathematical Theory of Communication.* University of Illinois Press, Urbana (1949).

[4] J. Piqueira and L. Mortoza. *Brazilian exchange rate complexity: Financial crisis effects.* Communications in Nonlinear Science and Numerical Simulation, **17** 1690 (2012).

[5] J. Xuan, X. Luo, G. Zhang, J. Lu and Z. Xu. *Uncertainty analysis for the keyword system of web events.* IEEE Transactions on Systems Man and Cybernetics, **46** 829 (2016).

[6] H. Strobel, W. Muessel, D. Linnemann, T. Zibold, D. Hume, L. Pezze, A. Smerzi and M. Oberthaler. *Fisher information and entanglement of non-gaussian spin states.* Science, **345** 424 (2014).

[7] J. Lee, E. Renard, G. Bernard, P. Dupont and M. Verleysen. *Type 1 and 2 mixtures of kullback-leibler divergences as cost functions in dimensionality reduction based on similarity preservation.* Neurocomputing, **112** 92 (2013).

[8] P. Bernaola-Galván, I. Grosse, P. Carpena, J. Oliver, R. Román-Roldán and H. Stanley. *Finding borders between coding and noncoding dna regions by an entropic segmentation method.* Physical Review Letters, **85** 1342 (2000).

[9] P. Carpena, P. Bernaola-Galván, M. Hackenberg and A. Coronado. *Level statistics of words: Finding keywords in literary texts and symbolic sequences.* Physical Review E, **79** (2009).

[10] R. Bruna, J. Poza, C. Gomez, M. Garcia, A. Fernandez and R. Hornero. *Analysis of spontaneous meg activity in mild cognitive impairment and alzheimer's disease using spectral entropies and statistical complexity measures.* J. Neural Eng., **9** (2012).

[11] I. Grosse, P. Bernaola-Galván, P. Carpena, R. Román-Roldán, J. L. Oliver and H. E. Stanley. *Analysis of symbolic sequences using the Jensen-Shannon divergence.* Phys. Rev. E, **65** 041905 (2002).

[12] A. Borst and F. E. Theunissen. *Information theory and neural coding.* Nature Neurosci., **2** 947 (1999).

[13] A. Berger, V. D. Pietra and S. D. Pietra. *A maximum entropy approach to natural language processing.* Comp. Linguis., **22** 39 (1996).

[14] D. Bouwmeester, A. Ekert and A. Zeilinger. *The Physics of Quantum Information.* Springer, Berlin (2000).

[15] E. T. Jaynes. *Information theory and statistical mechanics.* Phys. Rev., **106** 620 (1957).

[16] E. T. Jaynes. *Information theory and statistical mechanics. II.* Phys. Rev., **108** 171 (1957).

[17] S. Sears and S. Gadre. *An information theoretix synthesis and analysis on compton profiles.* J. Chem. Phys., **75** 4626 (1981).

[18] J. C. Angulo. *Information entropy and uncertainty in D-dimensional many-body systems.* Phys. Rev. A, **50** 311 (1994).

[19] A. Tripathi, V. S. Jr., R. Sagar and R. Esquivel. *Electron correlation in momentum space for the neon-atom isoelectronic sequence from f- through ar8+.* Phys. Rev. A, **54** (1996).

[20] S. Liu. *On the realtionship between densities of Shannon entropy and Fisher information for atoms and molecules.* J. Chem. Phys., **126** 191107 (2007).

[21] K. C. Chatzisavvas, C. C. Moustakidis and C. P. Panos. *Information entropy, information distances, and complexity in atoms.* J. Chem. Phys., **123** 174111 (2005).

[22] J. C. Angulo and J. Antolín. *Atomic complexity measures in position and momentum spaces.* J. Chem. Phys., **128** 164109 (2008).

[23] A. Borgoo, P. Geerlings and K. D. Sen. *Electron density and Fisher information of Dirac-Fock atoms.* Phys. Lett. A, **372**(31) 5106 (2008).

[24] J. C. Angulo, J. Antolín and K. D. Sen. *Fisher-Shannon plane and statistical complexity of atoms.* Physics Letters A, **372** 670 (2008).

[25] R. Esquivel, M. Molina-Espiritu, J. Dehesa, J. Angulo and J. Antolin. *Concurrent phenomena at the transition region of selected elementary chemical reactions: An information-theoretical complexity analysis.* Int J Quantum Chem (2012).

[26] K. D. Sen, J. Antolín and J. C. Angulo. *Fisher-Shannon analysis of ionization processes and isoelectronic series.* Phys. Rev. A, **76** 032502 (2007).

[27] J. Antolín and J. C. Angulo. *Complexity analysis of ionization processes and isoelectronic series.* Int. J. Quant. Chem., **109** 586 (2009).

[28] N. Aquino, A. Flores-Riveros and J. Rivas-Silva. *Shannon and fisher entropies for a hydrogen atom under soft spherical confinement.* Physics Letters A, **377** 2062 (2013).

[29] S. Kullback. *Information Theory and Statistics.* Dover, New York (1959).

[30] R. A. Fisher. *Theory of statistical estimation.* Proc. Cambridge Phil. Soc., **22** 700 (1925). Reprinted in Collected Papers of R. A. Fisher, edited by J.H. Bennet (University of Adelaide Press, South Australia), 1972, pp. 15–40.

[31] P. Adriaans and J. van Benthem. *Philosophy of Information.* Elsevier, Amsterdam (2007).

[32] Y. Bar-Hillel and R. Carnap. *Semantic information.* British J. Philos. Sci., **3** 147 (1958).

[33] H. Atmanspachera and G. Weidenmann. *Information Dynamics.* Plenum, New York (1991).

[34] U. Birchler and M. Bütler. *Information Economics.* Routledge, London (2007).

[35] M. A. Nielsen and I. L. Chuang. *Quantum Computation and Quantum Information.* Cambridge University Press, Cambridge (2000).

[36] C. Arndt. *Information Measures.* Springer, Berlin (2001).

[37] E. T. Jaynes. *On the rationale of maximum entropy methods.* Proc. IEEE, **70** 939 (1982).

[38] B. R. Frieden. *Science from Fisher Information.* Cambridge University Press, Cambridge (2004).

[39] P. Hohenberg and W. Kohn. *Inhomogeneous electron gas.* The American Physical Society, **22** (1964).

[40] T. Cover and J. Thomas. *Elements of Information Theory.* Wiley-Interscience (1991).

[41] I. Bialynicki-Birula and J. Mycielski. *Uncertainty relations for information entropy in wave mechanics.* Commun. Math. Phys., **44** 129 (1975).

[42] Y. Zhang, S. Wang, P. Phillips, Z. Dong, G. Ji and J. Yang. *Detection of alzheimer's disease and mild cognitive impairment based on structural volumetric mr images using 3d-dwt and wta-ksvm trained by psotvac.* Biomedical Signal Processing and Control, **21** 58 (2015).

[43] P. Benharash, E.Buch, P. Frank, M. Share, R. Tung, K. Shivkumar and R. Mandapati. *Quantitative analysis of localized sources identified by focal impulse and rotor modulation mapping in atrial fibrillation.* Circulation-Arrhythmia and Electrophysiology, **8** 554 (2015).

[44] A.M.Eren, H. Morrison, P. Lescault, J. Reveillaud, J. Vineis and M. Sogin. *Minimum entropy decomposition: Unsupervised oligotyping for sensitive partitioning of high-throughput marker gene sequences.* ISME Journal, **9** 968 (2015).

[45] U. Sengul, M. Eren, S. Shiraz, V. Gezder and A. Sengul. *Fuzzy topsis method for ranking renewable energy supply systems in turkey.* Renewable Energy, **75** 617 (2015).

[46] L. P. inequalities from stable curvature conditions on metric spaces. *T. rajala.* Calculus of Variations and Partial Differential Equations, **44** 477 (2012).

[47] K. Zyczkowski. *Rényi extrapolation of Shannon entropy.* Open Syst. Inf. Dyn., **10** 297 (2003).

[48] C. Tsallis. *Possible generalization of Boltzmann-Gibbs statistics.* J. Stat. Phys., **52** 479 (1988).

[49] C. Tsallis. *Introduction to Nonextensive Statistical Mechanics. Approaching a Complex World.* Springer, Berlin (2009).

[50] J. B. M. Uffink. *Measures of Uncertainty and the Uncertainty Principle.* Ph.D. Thesis. University of Amsterdam (1990).

[51] A. Zygmund. *Trigonometric Series.* Cambridge University Press, Cambridge (1959).

[52] G. H. Hardy, J. E. Littlewood and G. Polya. *Inequalities.* Cambridge University Press, Cambridge (1934).

[53] G. U. Yule. *On some properties of the normal distribution, univariate and bivariate, based on the sum of squares of frequencies.* Biometrika, **30** 1 (1938).

[54] H. S. Sichel. *Fitting growth and frequency curves by the method of frequency moments.* J. Roy. Sta. Soc. Ser. A, **110** 337 (1947).

[55] S. Liu and R. G. Parr. *Expansions of the correlation-energy density functional $E_c[\rho]$ and its kinetic-energy component $T_c[\rho]$ in terms of homogeneous functionals.* Phys. Rev. A, **53** 2211 (1996).

[56] S. Liu and R. G. Parr. *Expansions of density functionals in terms of homogeneous functionals: Justification and nonlocal representation of the kinetic energy, exchange energy,and classical Coulomb repulsion energy for atoms.* Phys. Rev. A, **55** 1792 (1997).

[57] H. Maassen and J. B. M. Uffink. *Generalized entropic uncertainty relations.* Phys. Rev. Lett., **60** 1103 (1988).

[58] M. J. W. Hall. *Universal geometric approach to uncertainty, entropy and information.* Phys. Rev. A, **59** 2602 (1999).

[59] R. López-Ruiz, H. L. Mancini and X. Calbet. *A statistical measure of complexity.* Phys. Lett. A, **209** 321 (1995).

[60] I.V.Toranzo, D. Puertas-Centeno and J. Dehesa. *Entropic properties of d-dimensional rydberg systems.* Physica A, **462** 1197 (2016).

[61] A. I. Aptekarev, D. Tulyakov, I. Toranzo and J. Dehesa. *Renyi entropies of the highly-excited states of multidimensional harmonic oscillators by use of strong laguerre asymptotics.* European Physical Journal B, **89** (2016).

[62] D. Petz. *Quantum Information Theory and Quantum Statistics.* Springer, Berlin (2008).

[63] S. R. Gadre. *Reviews of Modern Quantum Chemistry: A Celebration in the Contributions of Robert G. Parr.* vol. 1. World Scientific, Singapore (2003).

[64] S. B. Sears, R. G. Parr and U. Dinur. *On the quantum-mechanical kinetic-energy as a measure of the information in a distribution.* Israel J. Chem., **19** 165 (1980).

[65] S. E. Massen and C. P. Panos. *A link of information entropy and kinetic energy for quantum many-body systems.* Phys. Lett. A, **280** 65 (2001).

[66] E. Romera and J. S. Dehesa. *Weiszacker energy of many-electron systems.* Phys. Rev. A, **59** 256 (1994).

[67] A. Nagy. *Fisher information in density functional theory.* J. Chem. Phys., **119** 9401 (2003).

[68] J. C. Angulo and J. S. Dehesa. *Tight rigorous bounds to atomic information entropies.* J. Chem. Phys., **97** 6485 (1992). Erratum: J. Chem. Phys. **98** 9223 (1993).

[69] A. Katz. *Principles of Statistical Mechanics.* Freeman, San Francisco (1967).

[70] B. R. Frieden and B. H. Soffer. *A critical comparison of the three information-based approaches to physics.* Found. Phys. Lett., **13** 89 (2000).

[71] T. Yamano. *A statistical complexity measure with nonextensive entropy and quasi-multiplicativity.* J. Math. Phys., **45** 1974 (2004).

[72] E. Romera and J. S. Dehesa. *The Fisher-Shannon information plane, an electron correlation tool.* J. Chem. Phys., **120** 8906 (2004).

[73] J. S. Dehesa, P. Sánchez-Moreno and R. J. Yáñez. *Cramér-Rao information plane of orthogonal hypergeometric polynomials.* J. Comput. Appl. Math., **186** 523 (2006).

[74] M. Taddei, B. Escher, L. Davidovich and R. de Matos. *Quantum speed limit for physical processes.* Phys. Rev. Lett., **110** (2013).

[75] C. Haberl and L. Parapatits. *The centro-affine hadwiger theorem.* Journal of the American Mathematical Society, **27**(3) 685 (2014).

[76] P. Hauke, M. Heyl, L. Tagliacozzo and P. Zoller. *Measuring multipartite entanglement through dynamic susceptibilities.* Nature Physics, **12**(8) 778 (2016).

[77] A. N. Kolmogorov. *Three approaches to the quantitative definition of information.* Probl. Inf. Transm., **1** 3 (1965).

[78] C. Anteneodo and A. R. Plastino. *Some features of the López-Ruiz-Mancini-Calbet (LMC) statistical measure of complexity.* Phys. Lett. A, **223** 348 (1996).

[79] R. G. Catalan, J. Garay and R. López-Ruiz. *Features of the extension of a statistical measure of complexity to continuous systems.* Phys. Rev. E, **66** 011102 (2002).

[80] R. López-Ruiz. *Shannon information, LMC complexity and Rényi entropies: a straightforward approach.* Biophys. Chem., **115** 215 (2005).

[81] T. Yamano. *A statistical measure of complexity with nonextensive entropy.* Physica A, **340** 131 (2004).

[82] S. López-Rosa, J. C. Angulo and J. Antolín. *Rigorous properties and uncertainty-like relationships on product-complexity measures: Applications to atomic systems.* Physica A, **388** 2081 (2009).

[83] A. Borgoo, F. De Proft, P. Geerlings and K. D. Sen. *Complexity of Dirac-Fock atom increases with atomic number.* Chemical Physics Letters, **444** 186 (2007).

[84] O. A. Rosso, M. T. Martin and A. Plastino. *Brain electrical activity analysis using wavelet-based informational tools (II): Tsallis non-extensivity and complexity measures.* Physica A, **320** 497 (2003).

[85] A. Dembo, T. Cover and J. Thomas. *Information theoretic inequalities.* IEEE Trans. Infom. Theory, **37** 1501 (1991).

[86] W. Yahya, K. Oyewumi and K. Sen. *Information and complexity measures for the ring-shaped modified kratzer potential.* Indian Journal of Chemistry A, **53** 1307 (2014).

[87] K. Pearson. *On the criterion that a given system of deviations from the probable in the case of a correlated system of variables is such that it can be reasonably supposed to have arised from random sampling.* Phils. Mag., **50** 157 (1900).

[88] S. Kullback and A. Leibler. *On information and sufficient.* Ann. Math. Stat., **22** 79 (1951).

[89] H. Jeffreys. *An invariant form for the prior probability in estimation problems.* Proc. R. Soc. London, Ser A, **186** 453 (1946).

[90] A. Bhattacharyya. *On some analaogue of the amount of information and their use in statistical estimation.* Sankhya, **8** 1 (1946).

[91] I. Csiszár. *Information-type measures of difference of probability distributions and indirect observation.* Stud. Sci. Math. Hung., **2** 299 (1967).

[92] J. H. Lin. *Divergence measures based on the Shannon entropy.* IEEE Trans. Inf. Theory, **37** 145 (1991).

[93] I. J. Taneja, P. L. Pardo, D. Morales and M. L. Menéndez. *On generalized information and divergence measures and their applications: a brief review.* Questiio, **13** 47 (1989).

[94] I. J. Taneja. *On Generalized Information Measures and Thermalir Applications.* Academic, New York (1989).

[95] J. Burbea and C. R. Rao. *On the convexity of some divergence measures based on entropy functions.* IEEE Trans. Inf. Theory, **28** 489 (1982).

[96] J. Antolín, J. C. Cuchí and J. C. Angulo. *Minimum-cross-entropy estimation of atomic charge densities from scattering factors.* J. Phys. B: At. Mol. Opt., **32** 577 (1999).

[97] M. Ho, R. Sagar, H. Schmider, D. Weaver, V. Smith and Jr. *Measures of distance for atomic charge and momentum densities and their relationship to physical properties.* J. Quantum Chem., **53** 627 (1995).

[98] A. Borgoo, M. Godefroid, P. Indelicato, F. D. Proft and P. Geerling. *Quantum similarity study of atomic density functions: Insights from information theory and the role of relativistic effects.* J. Chem. Phys., **126** 044102 (2007).

[99] A. Borgoo, P. Jaque, A. Toro-Labbé, C. Van Alsenoy and P. Geerlings. *Analyzing Kullback-Leibler information profiles: an indication of their chemical relevance.* Phys. Chem. Chem. Phys., **11** 476 (2009).

[100] M. Wang, Y. Gao, K. Lu and Y. Rui. *View-based discriminative probabilistic modeling for 3d object retrieval and recognition.* IEEE Transactions on Image Processing, **22** 1395 (2013).

[101] D. Yu, K. Yao, H. Su, G. Li and F. Seide. *Kl-divergence regularized deep neural network adaptation for improved large vocabulary speech reconition.* IEEE International Conference on Acoustics, Speech and Signal Procesing, 7893–7897 (2013).

[102] J. O'Reilly, U. Schuffelgen, S. Cuell, T. Behrens, R. Mars and M. Rushworth. *Dissociable effects of surprise and model update in parietal and anterior cingulate cortex.* Proceedings of the National Academy of Sciences of the United States of America, **110** E3660 (2013).

[103] J. Tian, S. Cui and P. Reinartz. *Building change detection based on satellite stereo imagery and digital surface models.* IEEE Transactions on Geoscience and Remote Sensing, **52** 406 (2014).

[104] A. K. C. Wong and M. You. *Entropy and distance of random graphs with application to structural pattern-recognition.* IEEE Trans. Pattern. Anal. Mach. Intell., **7** 599 (1985).

[105] C. R. Rao and T. Nayak. *Cross entropy, dissimilarity measures, and characterizations of quadratic entropy.* IEEE Trans. Inf. Theory, **31** 589 (1985).

[106] F. Österreicher and I. Vajda. Ann. Inst. Statist. Math, **55** 639 (2003).

[107] A. B. Hamza. *Nonextensive information-theoretic measure for image edge detection.* J. Electron. Imaging, **15** 013011 (2006).

[108] J. Lin and S. Wong. *A new directed divergence measures and its characterization.* Int. J. Gen. Syst., **17** 73 (1990).

[109] P. Lamberti and A. Majtey. *Non-logarithmic Jensen-Shannon divergence.* Physica A, **329** 81 (2003).

[110] L. Bai and E. Hancock. *Graph kernels from the jensen-shannon divergence.* Journal of Mathematical Imaging and Vision, **47** 60 (2013).

[111] K. Sasahara, Y. Hirata, M. Toyoda, M. Kitsuregawa and K. Aiahara. *Quantifying collective attention from tweet stream.* PLOS One (2013).

[112] C. Radhakrishnan, M. Parthasarathy, S. Jambulingam and T. Byrnes. *Distribution of quantum coherence in multipartite systems.* Physical Review Letters, **116** (2016).

[113] L. Wu, X. Hua, N. Yu, W. Ma and S. Li. *Flickr distance: A relationship measure for visual concepts.* IEEE Transactions on Pattern Analysis and Machine Intelligence, **34** 863 (2012).

[114] Q. Xu, Y. Liu, X. Li, Z. Yang, J. Wang, M. Sbert and R. Scopigno. *Browsing and exploration of video sequences: A new scheme for key frame extraction and 3d visualization using entropy based jensen divergence.* Information Sciences, **278** 736 (2014).

[115] J. Antolín, J. Angulo and S. Lopez-Rosa. *Fisher and jensen-shannon divergences: Quantitative comparisons among distributions. application to position and momentum atomic densities.* Journal of Chemical Physics, **130** (2009).

[116] R. Román-Roldán, P. Bernaola-Galván and J. Oliver. *Sequence compositional complexity of dna through an entropic segmentation method.* Phys. Rev. Lett., **80** 1344 (1998).

[117] P. Hammad. *Measure d'ordre α de l'information au sens de Fisher.* Revue de Statistique Appliquée, **26** 73 (1978).

[118] R. J. Yáñez, P. Sánchez-Moreno, A. Zarzo and J. S. Dehesa. *Fisher information of special functions and second-order differential equations.* J. Math. Phys., **49** 082104 (2008).

[119] R. Konig and G. Smith. *The entropy power inequality for quantum systems.* IEEE Transations on Information theory, **60** 1536 (2014).

[120] P. Sánchez-Moreno, A. Zarzo and J. Dehesa. *Jensen divergence based on fisher's information.* J. Phys. A, **45** 125305 (2012).

[121] S. López-Rosa. *Information Theoretical Measures of Atomic and Molecular Systems.* Ph.D. thesis, University of Granada (Spain) (2010).

[122] R. Carbó-Dorca, X. Girones and P. G. Mezey. *Fundamentals of Molecular Similarity.* Kluwer Academic, New York/Plenum, New York (2001).

[123] M. Solá, J. Mestres, J. M. Oliva, M. Durán and R. Carbó-Dorca. *The use of ab initio quantum molecular self-similarity measures to analyze electronic charge density distributions.* Int. J. Quant. Chem., **58** 361 (1996).

[124] I. Varga and J. Pipek. *Rényi entropies characterizing the shape and the extension of the phase space representation of quantum wave functions in disordered systems.* Phys. Rev. E, **68** 026202 (2003).

[125] J. Angulo and J. Antolín. *Atomic quantum similarity indices in position and momentum spaces.* Journal of Chemical Physics, **126** (2007).

[126] R. Carbo-Dorca. *Quantum polyhedra, definitions, statistics and the construction of a collective quantum similarity index.* Journal of Mathematical Chemistry, **53** 171 (2015).

[127] R. Carbo-Dorca and D. Barragan. *Communications on quantum similarity (4): collective distances computed by means of similarity matrices, as generators of intrinsic ordering among quantum multimolecular polyhedra.* Wiley Interdisciplinary Reviews - Computational Molecular Science, **5** 380 (2015).

[128] A. Morales-Bayuelo and J. Caballero. *New insights into steric and electronic effects in a series of phosphine ligands from the perspective of local quantum similarity using the fukui function.* Journal of Molecular Modeling, **21** (2015).

[129] P. Bouvrie, J. Antolín and J. Angulo. *Generalized quantum similarity index: Applications in atoms.* Chem. Phys. Lett., **506** 326 (2011).

[130] W. Li. *New stopping criteria for segmenting dna sequences.* Phys. Rev. Lett., **86** 5815 (2001).

[131] J.F.Gómez-Lopera, J. Martínez-Aroza, A. Robles-Pérez and R. Román-Roldán. *An analysis of edge detection by using the jensen-shannon divergence.* Journal of Mathematical Imaging and Vision, **13** 35 (2000).

[132] R. F. Nalewajski and R. Parr. *Information theory, atoms in molecules, and molecular similarity.* Proc. Natl. Acad. Sci. U.S.A., **97** 8879 (2000).

[133] D. Bielinska-Waz, P. Waz and T. Clark. *Similarity studies of DNA sequences using genetic methods.* Chem. Phys. Lett., **445** 68 (2007).

[134] V. V. Cross and T. A. Sudkamp. *Similarity and Compatibilit in Fuzzy Set Theory: Assessnebt abd Apoplications.* Springe-Verlag, Heidelberg (2002).

[135] P. W. Lamberti, A. P. Majtey, A. Borras, M. Casas and A. Plastino. *Metric character of the quantum jensen-shannon divergence.* Phys. Rev. A, **77** 052311 (2008).

[136] A. P. Majtey, A. Borrás, M. Casas, P. W. Lamberti and A. Plastino. *Jensen–Shannon divergence as a measure of the degree of entanglement.* Int. J. Quant. Inform., **6** 715 (2008).

[137] R. Carbó, L. Lleyda and M. Arnau. *How similar is a molecule to another? An electron density measure of similarity between two molecular structures.* Int. J. Quant. Chem., **17** 1185 (1980).

[138] A. Borgoo, M. Godefroid, K. D. Sen, F. De Proft and P.Geerlings. *Quantum similarity of atoms: a numerical hartree-fock and information theory approach.* Chem. Phys. Lett., **399** 186 (2004).

[139] M. Ho, R. P. Sagar, H. Schmider, D. F. Weaver and V. H. Smith. *Measures of distance for atomic charge and momentum densities and their relationship to physical-properties.* Int. J. Quant. Chem., **108** 5469 (1998).

[140] S. Janssens, A. Borgoo, C. V. Alsenoy and P. Geerlings. *Information theoretical study of chirality: Enantiomers with one and two asymmetric centra.* JPCA, **112** 10560 (2008).

[141] D. Robert and R. Carbó-Dorca. *General trends in atomic and nuclear quantum similarity measures.* Int. J. Quant. Chem., **77** 685 (2000).

[142] F. De Proft, P. Ayers, K. Sen and P. Geerlings. *On the importance of the "density per particle" (shape function) in the density functional theory.* J. Chem. Phys., **120** 9969 (2004).

[143] R. G. Parr and W. Yang. *Density-Functional Theory of Atoms and Molecules.* Oxford University Press, New York (1989).

[144] T. Koga, K. Kanayama, S. Watanabe and A. Thakkar. *Analytical hartree-fock wave functions subject to cusp and asymptotic constraints: He to xe, li+ to cs+, h- to i-.* Int. J. Quant. Chem., **71** 491 (1999).

[145] T. Koga, K. Kanayama, S. Watanabe, T. Imai and A. J. Thakkar. *Analytical Hartree-Fock wave functions for the atoms Cs to Lr.* Theor. Chem. Acc., **104** 411 (2000).

[146] R. Carbó-Dorca, L. Amat, E. Besalu, X. Girones and D. Robert. *Quantum mechanical origin of QSAR: theory and applications.* J. Mol. Struct., **504** 181 (2000).

[147] A. Martín, J. Angulo and J. Antolín. *Fisher-like atomic divergences: Mathematical grounds and physical applications.* Physica A, **392** 5552 (2013).

[148] J. Antolín, P. Bouvrie and J. Angulo. Phys. Rev. A, **84** 032504 (2011).

[149] P. Bouvrie, J. Angulo and J. Antolín. Chem. Phys. Lett., **539** 191 (2012).

[150] R. Benesch and V. H. Smith Jr. *Wave Mechanics: The First Fifty Years.* Butterworths, London (1973).

[151] S. Lopez-Rosa, J. Antolín, J. Angulo and R. Esquivel. *Divergence analysis of atomic ionization processes and isoelectronic series.* Physical Review A, **80** (2009).

[152] N. Cordero, N. March and J. Alonso. *Ionization potentials of neutral atoms and positive ions in the limit of large atomic number.* Phys. Rev. A, **75** 012505 (2007).

[153] H. Nakatsuji and H. Nakashima. *Analytically solving the relativistic dirac-coulomb equation for atoms and molecules.* Phys. Rev. Lett., **95** 050407 (205).

[154] S. Roy, R. Prasad, S. Datta and P. Chandra. *Electron correlation and relativistic effects in atomic structure calculations of th+, th2+ ions.* Chem. Phys. Lett., **25** 550 (2012).

[155] F. Jorge, A. C. Neto, G. Camiletti and S. Machado. *Contracted gaussian basis sets for douglas-kroll-hess calculations: Estimating scalar relativistic effects of some atomic and molecular properties.* J. Chem. Phys., **130** 064108 (2009).

[156] K. Sen. *Statistical Complexity. Applications in Electronic Structure.* Springer (2011).

[157] P. Kumar and I. J. Taneja. *Generalized relative j-divergence measure and properties.* Int. J. Contemp. Math. Sci., **1** 597 (2006).

[158] J. Angulo, J. Antolín, S. López-Rosa and R. Esquivel. *Jensen-shannon divergence in conjugate spaces: The entropy excess of atomic systems and sets with respect to their constituents.* Physica A, **389** 899 (2010).

[159] V. Burke and I. Grant. *Effect of relativity on atomic wave functions.* Proc. Phys. Soc., **90** 297 (1967).

[160] J. Katriel and K. D. Sen. *Relativistic effects on information measures for hydrogen-like atoms.* Journal of Computational and Applied Mathematics, **233** 1399 (2010). Proceedings of Special Functions, Information Theory, and Mathematical Physics, dedicated to Professor Jesus Sanchez Dehesa on the occasion of his 60th birthday.

[161] P. Maldonado, A. Sarsa, E. Buendía and F. Gálvez. *Relativistic quantum similarities in atoms in position and momentum spaces.* Phys. Lett. A, **375** 2544 (2011).

[162] P. Carpena and P. Bernaola-Galván. *Statistical characterization of the mobility edge of vibrational states in disordered materials.* Phys. Rev. B, **60** 201 (1999).

[163] A. P. Majtey, P. W. Lamberti and D. P. Prato. *Jensen-Shannon divergence as a measure of distinguishability between mixed quantum states.* Phys. Rev. A, **72** 052310 (2005).

[164] A. Martín, S. López-Rosa, J. Angulo and J. Antolín. *Jensen-shannon and kullback-leibler divergences as quantifiers of relativistic effects in neutral atoms.* Chem. Phys. Lett., **75** 642.

[165] J. Desclaux and P. Indelicato. *The relativistic atomic program mcdfgme v 2005.10* (2005).

[166] J. Desclaux. *A multiconfiguration relativistic dirac-fock program.* Comput. Phys. Commun, **9** 31 (1975).

[167] A. Borgoo, O. Scharf, G. Gaigalas and M. Godefroid. *Multiconfiguration electron density function for the atsp2k-package.* Comput. Phys. Commun, **181** 426 (2010).

[168] J. Antolín, J. Angulo, S. Mulas and S. Lopez-Rosa. *Relativistic global and local divergences in hydrogenic systems: A study in position and momentum spaces.* Phys. Rev. A: At., Mol., Opt. Phys., **90** (2014).

[169] P. Bouvrie, S. López-Rosa and J. Dehesa. *Quantifying dirac hydrogenic effects via complexity measures.* Phys. Rev. A, **86** 012507 (2012).

[170] P. Pyykkö. *Relativistic effects in chemistry: More common than you thought.* Annu. Rev. Phys. Chem., **63** 45 (2012).

[171] P. Pyykkö. *Relativistic effects in structural chemistry.* P. Chem. Rev., **88** 563 (1988).

[172] M. Iliaš, V. Kellö and M. Urban. *Relativistic effects in atomic and molecular properties.* Acta Phys. Slovaca, **60** 259 (2010).

[173] T. Sato, M. Asai, A. Borschevsky, T. Stora, N. Sato, Y. Kaneya, K. Tsukada, C. Düllmann, K. Eberhardt, E. Eliav, S. Ichikawa, U. Kaldor, J. Kratz, S. Miyashita, Y. Nagame, K. Ooe, A. Osa, D. Renisch, J. Runke, M. Schädel, P. Thörle-Pospiech, A. Toyoshima and N. Trautmann. *Measurement of the first ionization potential of lawrencium, element 103.* Nature, **520** 209 (2015).

[174] D. Lide. *CRC Handbook of Chemistry and Physics.* CRC Press (2005).

[175] P. Schwerdtfeger, L. Pasteka, A. Punnett and P. Bowman. *Relativistic and quantum electrodynamic effects in superheavy elements.* Nuclear Phys. A, **944** 551 (2015).

[176] J. Desclaux. *At. Data Nucl. Data Tables*, volume 12 (1973).

[177] J. Dehmer. *Phase-amplitudemethod in atomic physics .2. z-dependence of spin-orbit coupling.* Phys. Rev. A, **7** 4 (1973).

[178] W. Schwarzt, E. van Wezenbeek, E. Baerends and J. Snijders. *The origin of relativistic effects of atomic orbitals.* J. Phys. B: At. Mol. Opt., **22** 1515 (1989).

[179] V. A. Dzuba, M. S. Safronova and U. Safronova. *Atomic properties of superheavy elements no, lr, and rf.* Phys. Rev. A, **90** 012504 (2014).

[180] J. Desclaux and B. Fricke. *Relativistic predicttion of the ground-state of atomic lawrencium.* J. Phys., **41** 943 (1980).

[181] P. Neogrády, V. Kellö, M.Urban and A. Sadlej. *Ionization potentials and electron affinities of cu, ag, and au: Electron correlation and relativistic effects.* Int. J. Quant. Chem., **63** 557 (1997).

[182] J. S. Shiner, M. Davison and P. T. Landsberg. *Simple measure for complexity.* Phys. Rev. E, **59** 1459 (1999).

[183] J. Sañudo and R. López-Ruiz. *Alternative evaluation of statistical indicators in atoms: The non-relativistic and relativistic cases.* Phys. Lett. A, **37(3)**(30) 2549 (2009).

[184] P. Maldonado, A. Sarsa, E. Buendía and F. Gálvez. *Relativistic effects on complexity indexes in atoms in position and momentum spaces.* Phys. Lett. A, **374** 3847 (2010).

[185] R. Sagar, H. Laguna and N. Guevara. *Electron pair density information measures in atomic systems.* Int. J. Quant. Chem., **111** 3497 (2011).

[186] T. Yamano. *A generalization of the kullback-leibler divergence and its properties.* J. Math. Phys., **50** 043302 (2009).

[187] T. Yamano. *Phase space gradient of dissipated work and information: A role of relative fisher information.* J. Math. Phys., **54** 113301 (2013).

[188] A. Martín, J. Angulo, J. Antolín and S. Lopez-Rosa. *Generalized quantum similarity in atomic systems: A quantifier of relativistic effects.* Physica A, **467** 315 (2017).

[189] N. Guevara, R. Sagar and R. Esquivel. *Shannon-information entropy sum as a correlation measure in atomic systems.* Physical Review A, **67** (2003).

[190] J. Antolín and J. Angulo. *Quantum similarity indices for atomic ionization processes.* European Physical Journal D, **46** 21 (2008).

[191] K. Banyard and J. Moore. *Angular and radial correlation effects in momentum space for h-, he and li+.* Journal of Physics B, **10** 2781 (1977).

[192] N. Guevara, R. Sagar and R. Esquivel. *Local correlation measures in atomic systems.* Journal of Chemical Physics, **122** (2005).

[193] R. Sagar and N. Guevara. *Mutual information and correlation measures in atomic systems.* Journal of Chemical Physics, **123** (2005).

[194] R. Ponec and M. Strnad. *Similarity ideas in the theory of pericyclic reactivity.* Journal of Chemical Information and Computer Sciences, **32** 693 (1992).

[195] R. Sagar, H. Laguna and N. Guevara. *Statistical correlation between atomic electron pairs.* Chemical Physics Letters, **514** 352 (2011).

[196] H. Peng and Y. Ho. *Statistical correlations of the n-particle moshinsky model.* Entropy, **17** 1882 (2015).

[197] X. Fradera, M.Duran and J. Mestres. *Second-order quantum similarity measures from intracule and extracule densities.* Theoretical Chemistry Accounts, **99** 44 (1998).

[198] N. Guevara, R. Sagar and R. Esquivel. *Information uncertainty-type inequalities in atomic systems.* Journal of Chemical Physics, **119** 7030 (2003).

[199] R. Bader and M. Stephens. *Spatial localization of electronic pair and number distributon in molecules.* Journal of the American Chemical Society, **97** (1975).

[200] M. Kohout. *Bonding indicators from electron pair density functionals.* Faraday Discussions, **135** 43 (2007).

[201] E. Davidson. *N-representability of the electron pair density.* Chemical Physics Letters, **246** 209 (1995).

[202] A. Coleman, E. Yukalova and V. Yukalov. *Pairon distributions and the spectra of reduced hamiltonians.* International Journal of Quantum Chemistry, **54** 211 (1995).

[203] S. Samvelyan. *N-representability of diagonal elements of second-order reduced density matrices.* International Journal of Quantum Chemistry, **65** 127 (1997).

[204] M. Pistol. *N-representability of two-electron densities and density matrices and the application to the few-body problem.* Chemical Physics Letters, **400** 548 (2004).

[205] P. Ayers and E. Davidson. *Necessary conditions for the n-representability of pair distribution functions.* International Journal of Quantum Chemistry, **1006** 1487 (2006).

[206] P. Ziesche. *Attempts toward a pair density functional theory.* International Journal of Quantum Chemistry, **60** Attempts toward a pair density functional theory (1996).

[207] M.Levy and P. Ziesche. *The pair density functional of the kinetic energy and its simple scaling property.* Journal of Chemical Physics, **115** 9110 (2001).

[208] P. Ayers and M. Levy. *Generalized density-functional theory: Conquering the n-representability problem with exact functionals for the electron pair density and the second-order reduced density matrix.* Journal of Chemical Sciences, **117** 507 (2005).

[209] X. Fradera., M. Duran and J. Mestres. *The relevance of the laplacian of intracule and extracule density distributions for analyzing electron-electron interactions in molecules.* Journal of Chemical Physics (1997).

[210] T. K. Ghanty and S. K. Ghosh. *Correlation between hardness, polarizability, and size of atoms, molecules, and clusters.* J. Chem. Phys., **97** 4951 (1993).

[211] S. Hati and D. Datta. *Hardness and Electric Dipole Polarizability. Atoms and Clusters.* J. Phys. Chem., **98** 10451 (1994).

[212] R. G. Parr, R. F. Nalewajski and P. W. Ayers. *What is an atom in a molecule.* J. Phys. Chem. A, **109** 3957 (2005).

[213] C. Amovilli and N. H. March. *Quantum information: Jaynes and Shannon entropies in a two-electron entangled artificial atom.* Phys. Rev. A, **69**(5) 054302 (2004).

[214] R. S. Gadre and R. D. Bendale. *Rigorous relationships among quantum-mechanical kinetic energy and atomic information entropies: Upper and lower bounds.* Phys. Rev. A, **36** 1932 (1987).

[215] C. Dobson. *Chemical space and biology.* Nature, **432** 824 (2004).

[216] C. Lipinski and A. Hopkins. *Navigating chemical space for biology and medicine.* Nature, **432** 855 (2004).

[217] J. C. Angulo, J. Antolín and R. O. Esquivel. *Atomic and molecular complexities: Their physical and chemical interpretations.* In K. D. Sen, ed., *Statistical Complexities: Applications in electronic structures.* Springer, Berlin (2010).

[218] M. Ho, R. P. Sagar, J. M. Pérez-Jordá, V. H. Smith Jr and R. O. Esquivel. *A numerical study of molecular information entropies.* Chem. Phys. Lett., **219** 15 (1994).

[219] M. Ho, H. Schmider, D. F. Weaver, V. H. Smith, R. P. Sagar and R. O. Esquivel. *Shannon entropy of chemical changes: S(N)2 displacement reactions.* Int. J. Quant. Chem., **77** 376 (2000).

[220] M. Ho, V. H. Smith Jr., D. F. Weaver, C. Gatti, R. P. Sagar and R. O. Esquivel. *Molecular similarity based on information entropies and distances.* J. Chem. Phys., **108** 5469 (1998).

[221] S. López-Rosa, R. O. Esquivel, J. C. Angulo, J. Antolín, J. S. Dehesa and N. Flores-Gallegos. *Analysis of complexity measures and information planes of selected molecules in position and momentum spaces.* Phys. Chem. Chem. Phys., **6** (2010).

[222] R. O. Esquivel, N. Flores-Gallegos, C. Iuga, E. Carrera, J. C. Angulo and J. Antolín. *Phenomenological description of selected elementary chemical reactions mechanisms: An information-theoretic study.* Phys. Lett. A (2009).

[223] R. O. Esquivel, N. Flores-Gallegos, J. S. Dehesa, J. C. Angulo, J. Antolín, S. López-Rosa and K. D. Sen. *Phenomenological description of a three center insertion reaction: an information-theoretic study.* J. Phys. Chem. A, **114** 1906 (2010).

[224] R. O. Esquivel, N. Flores-Gallegos, C. Iuga, E. Carrera, J. C. Angulo and J. Antolín. *Phenomenological description of the transition state, and the bond/breaking and cond/forming processes of selected elementary chemical reactions:an information-theoretic study.* Theor. Chem. Acc., **124** 445 (2009).

[225] S. López-Rosa, R. O. Esquivel, J. C. Angulo, J. Antolín, J. S. Dehesa and N. Flores-Gallego. *Fisher information study in position and momentum spaces for elementary chemical reactions.* J. Chem. Theor. Comp., **6** 145 (2010).

[226] S. López-Rosa, R. O. Esquivel, J. C. Angulo, J. Antolín, J. S. Dehesa and N. Flores-Gallegos. *Fisher Information study in position and momentum spaces for elementary chemical reactions.* J. Chem. Theory Comput., **6** 145 (2010).

[227] Molina-Espíritu, M, Esquivel, RO, Dehesa and JS. *Information-Theoretical Complexity Analysis of Selected Elementary Chemical Reactions.* Springer (2013).

[228] R. O. Esquivel, S. López-Rosa and J. S. Dehesa. *Quantum entanglement as a measure of non dynamical correlation in helium isoelectronic series.* preprint (2014).

[229] R. O. Esquivel, A. L. Rodriguez, R. P. Sagar, M. Ho and V. H. S. Jr. *Physical interpretation of information entropy: Numerical evidence of the Collins conjecture.* Phys. Rev. A, **54** 259 (1996).

[230] J. Ramírez, C. Soriano, R. Esquivel, R. P. Sagar, M. Ho and V. S. Jr. *Jaynes information entropy of small molecules: Numerical evidence of the Collins conjecture.* Phys. Rev. A, **56** 4477 (1997).

[231] C. Soriano-Correa, C. Barrientos-Salcedo, A. Raya, C. Rubio-Póo and R. Esquivel. *The influence of electron donor and electron acceptor groups on the electronic structure of the anti-inflammatory tripeptide Cys-Asn-Ser.* Int. J. Quant. Chem., **110** 2398 (2010).

[232] R. Esquivel, S. Lopez-Rosa, M. Molina-Espíritu, J. Angulo and J. Dehesa. *Information-theoretic space from simple atomic and molecular systems to biological and pharmacological molecules.* Theoretical Chemistry Accounts, **135** (2016).

[233] S. Lopez-Rosa, M. Molina-Espíritu, R. Esquivel, C. Soriano-Correa and J. Dehesa. *Study of the chemical space of selected bacteriostatic sulfonamides from an information theory point of view.* Chemphyschem, **17** 4003 (2016).

[234] R. Carbó-Dorca and X. Girones. *Foundation of quantum similarity measures and their relationship to qspr: Density function structure, approximations, and application examples.* International Journal of Quantum Chemistry, **101** 8 (2005).

[235] R. Carbó-Dorca. *Quantum similarity, volume functions and generalized carb indices.* Journal of Mathematical Chemistry, **49** 2109 (2011).

[236] R. Carbó-Dorca and L. Mercado. *Commentaries on quantum similarity (1): Density gradient quantum similarity.* Journal of Computational Chemistry, **31** 2195 (2010).

[237] R. Carbó-Dorca. *Scaled euclidian distances: a general dissimilarity index with a suitably defined geometrical foundation.* Journal of Mathematical Chemistry, **50** 734 (2012).

[238] L. Amay, E. Besalu, R. Carbó-Dorca and R. Ponec. *Identification of active molecular sites using quantum-self-similarity measures.* Journal of Chemical Information and Computer Sciences, **41** 978 (2001).

[239] A. Saliner and X. Girones. *Topological quantum similarity measures: applications in qsar.* Journal of Molecular Structure, **727** 97 (2005).

[240] P. Bultinck and R. Carbó-Dorca. *Molecular quantum similarity using conceptual dft descriptors.* Journal of Chemical Sciences, **117** 425 (2005).

[241] R. Carbó-Dorca and B. Calabuig. *Quantum similarity meaasures, molecular cloud descriptions, and structure properties relationships.* Journal of Chemical Information and Computer Sciences, **32** 600 (1992).

[242] J. Janak. *Proof that e ni= in density-functional theory.* Physical Review B, **18** 7165 (1978).

[243] T. A. Koopmans. *ber die Zuordnung von Wellenfunktionen und Eigenwerten zu den Einzelnen Elektronen eines Atoms.* Physica, **1** 104 (1933).

[244] P. Geerlings, F. de Proft and W. Langenaeker. *Conceptual density functional theory.* Chem. Rev., **103** 1793 (2003).

[245] T. Koopmans. *Über die zuordnung von wellenfunktionen und eigenwerten zu den einzelnen elektronen eines atoms.* Physica, **1** 104 (1934).

[246] D. Tozer and F. De Proft. *Computation of the hardness and the problem of negative electron affinities in density functional theory.* Journal of Physical Chemistry A, **109** 8923 (2005).

[247] X. Girones, D. Robert and R. Carbó-Dorca. *Tgsa: A molecular superposition program based on topo-geometrical considerations.* Journal of Computational Chemistry, **22** 255 (2001).

[248] M. J. Frisch, G. W. Trucks, H. B. Schlegel, G. E. Scuseria, M. A. Robb, J. R. Cheeseman, J. A. Montgomery Jr., T. Vreven, K. N. Kudin, J. C. Burant, J. M. Millam, S. S. Iyengar, J. Tomasi, V. Barone, B. Mennucci, M. Cossi, G. Scalmani, N. Rega, G. A. Petersson, H. Nakatsuji, M. Hada, M. Ehara, K. Toyota, R. Fukuda, J. Hasegawa, M. Ishida, T. Nakajima, Y. Honda, O. Kitao, H. Nakai, M. Klene, X. Li, J. E. Knox, H. P. Hratchian, J. B. Cross, V. Bakken, C. Adamo, J. Jaramillo, R. Gomperts, R. E. Stratmann, O. Yazyev, A. J. Austin, R. Cammi, C. Pomelli, J. W. Ochterski, P. Y. Ayala, K. Morokuma, G. A. Voth, P. Salvador, J. J. Dannenberg, V. G. Zakrzewski, S. Dapprich, A. D. Daniels, M. C. Strain,

O. Farkas, D. K. Malick, A. Rabuck, K. Raghavachari, J. B. Foresman, J. V. Ortiz, Q. Cui, A. G. Baboul, S. Clifford, J. Cioslowski, B. B. Stefanov, G. Liu, A. Liashenko, P. Piskorz, I. Komaromi, R. L. Martin, D. J. Fox, T. Keith, M. A. Al-Laham, C. Y. Peng, A. Nanayakkara, M. Challacombe, P. M. W. Gill, B. Johnson, W. Chen, M. W. Wong, C. González and J. A. Pople. *Gaussian 03 Revision D.01* (2004).

[249] J. M. Pérez-Jordá and E. San-Fabián. *A simple, efficient and more reliable scheme for automatic numerical integration.* Comput. Phys. Commun, **77** 46 (1993).

[250] J. M. Pérez-Jordá, A. D. Becke and E. San-Fabián. *Automatic numerical integration techniques for polyatomic molecules.* J. Chem. Phys., **100** 6520 (1994).

[251] M. Kohout. *DGrid 4.6.*

[252] S. Schweber. *An introduction to relativistic quantum field theory.* Harper and Row (1964).

[253] J. Katriel and G. Adam. *A system with infinitely degenerate bound states.* American Journal of Physics (1969).

[254] M. Moshinsky and A. Szczepaniak. *The dirac oscillator.* Journal of Physics A, **22** L817 (1989).

[255] R. Martínez-Romero and A. Salas-Brito. *Conformal invariance in a dirac oscillator.* Journal of Mathematical Physics, **33** (1998).

[256] J. Benitez, R. P. Martínez-Romero, H. Núñez-Yépez and A. L. Salas-Brito. *Solution and hidden supersymmetry of a dirac oscillator.* Physical Review Letters, **64** 1643 (1990).

[257] V. Aguiar and I. Guedes. *Shannon entropy, fisher information and uncertainty relations for log-periodic oscillators.* Physica A, **423** 72 (2015).

[258] V. Aguiar and I.Guedes. *Joint entropy of quantum damped harmonic oscillators.* Physica A, **401** 156 (2014).

[259] V. Aguiar and I. Guedes. *Fisher information of quantum damped harmonic oscillators.* Physica Scripta (2015).

[260] R. P. Martínez-Romero, H. N. Núñez-Yépez and A. L. Salas-Brito. *Relativistic quantum mechanics of a dirac oscillator.* Arxiv (1999).

[261] M. Moreno and A. Zentella. *Covariance, cpt and the foldy-wouthuysen transtransform for the dirac oscillator.* Journal of Physics A, **22** L821 (1989).

[262] W. Greiner. *Theoretical Physics 3: Relativistic Quantum Mechanics.* Springer, Berlin (1991).

List of Figures

1.1 How to decompose a choice from three different possibilities 13

2.1 Fisher-like divergences JFD and FD between Boron ($Z = 5$) and all neutral atoms with nuclear charges $Z = 1 - 103$, in (a) position and (b) momentum spaces. Atomic units are used. 32
2.2 Jensen-Fisher divergences JFD of Argon and Calcium (nuclear charges $Z = 18, 20$ respectively) with respect to all neutral atoms with nuclear charges $Z = 1 - 103$, in (a) position and (b) momentum spaces. Atomic units are used. 35
2.3 Position-space divergence of each noble gas with respect to all neutral atoms with nuclear charges $Z = 1-103$, by using (a) the Fisher divergence FD_r, and (b) the Jensen-Fisher divergence JFD_r. Atomic units are used. 39
2.4 Momentum-space divergence of each noble gas with respect to all neutral atoms with nuclear charges $Z = 1-103$, by using (a) the Fisher divergence FD_p, and (b) the Jensen-Fisher divergence JFD_p. Atomic units are used. 41
2.5 Position- and momentum-space Jensen-Fisher divergences $JFD(NC)$ between each neutral atom (N) and its singly-charged cation (C) with nuclear charges $Z = 3 - 55$, and a qualitative fit in terms of the atomic ionization potential (AIP) of the neutral atom. Atomic units are used. . . 43

3.1 Quantum similarity index $QSI(Sch, Dir)$ between the Schrödinger (non-relativistic) and Dirac (relativistic) one-particle densities for ground-state neutral atoms with nuclear charge $Z = 1 - 103$. Atomic units (a.u.) are used. 51
3.2 Jensen-Shannon $JSD(Sch, Dir)$ and Kullback-Leibler $KL(Sch, Dir)$ divergences between the Schrödinger (non-relativistic) and Dirac (relativistic) one-particle densities for ground-state neutral atoms with nuclear charge $Z = 1 - 103$. Atomic units (a.u.) are used. 52
3.3 Schrödinger-Dirac quotients $D_S(r)/D_D(r)$ of radial densities $D(r) = r^2\rho(r)$ for contiguous atomic systems $Z = 50, 51, 52$. Atomic units (a.u.) are used. 54

4.1 Atomic ionization potential (AIP, in eV) of ground-state neutral atoms in Group 12: copper (Cu, nuclear charge $Z = 29$), silver (Ag, $Z = 47$) and gold (Au, $Z = 79$). Curves correspond to AIP values obtained from: non-relativistic ROS-HF (red filled squares), non-relativistic CCSD(T) (green crosses), relativistic CCSD(T)-DK (blue stars), and experiments (magenta empty squares). 58

4.2 (a) High-order ($1.0 \leq q \leq 2.0$) and (b) low-order ($0.4 \leq q \leq 1.0$) generalized quantum similarity index $QSI_q(Sch, Dir)$, between Schrödinger and Dirac densities for neutral atoms with nuclear charge $Z = 1 - 103$. Atomic units (a.u.) are used. 63
4.3 Generalized quantum similarity index $QSI_q(Sch, Dir)$ of order $q = 0.9$, and Jensen-Shannon divergence $JSD(Sch, Dir)$, between Schrödinger and Dirac densities for neutral atoms with nuclear charge $Z = 1-103$. Atomic units (a.u.) are used. 68
4.4 Quotient of Schrödinger and Dirac radial densities $D(r)$ for the trios of neutral atoms with nuclear charges (a) $Z = 6, 7, 8$, and (b) $Z = 50, 51, 52$. Atomic units (a.u.) are used. 70
4.5 Quotient of Schrödinger and Dirac radial densities $D(r)$ for the trio of neutral atoms with nuclear charges $Z = 29, 30, 31$. Atomic units (a.u.) are used. 71

5.1 Shannon entropy in position space of both monoelectronic and electron pair densities respectively, of neutral atoms with nuclear charge $Z = 2 - 103$ (a) in lineal scale, (b) in logarithmic scale. Atomic units are used (a.u.) 80
5.2 Shannon entropy in position space of the monoelectronic and electron pair density $S(\rho)$ and $S(\Gamma)$ respectively, for neutral atoms with $Z = 2 - 103$; (a) $S(\rho)$ and $S(\Gamma)$ vs. Z, (b) $2S(\rho)$ and $S(\Gamma)$ vs. Z. Atomic units (a.u.) are used. 84
5.3 Shannon entropy of the monoelectronic and electron pair densities for neutral atoms with $Z = 2 - 103$ in momentum space Atomic units (a.u.) are used. 85
5.4 Disequilibrium for monoelectronic and electron pair densities $D(\rho)$ and $D(\Gamma)$, respectively, in position space for atomic system with $Z = 2 - 103$. Atomic units (a.u.) are used. 85
5.5 Disequilibrium for monoelectronic and electron pair densities $D(\rho)$ and $D(\Gamma)$, respectively, in momentum space for atomic system with $Z = 2 - 103$. Atomic units (a.u.) are used. 86
5.6 LMC complexity (C_{LMC}) of the (a) Electron pair and (b) Monoelectronic density, in position and momentum space for system with nuclear charge $Z = 2 - 103$ on a logarithmic scale. 88
5.7 Information planes: (a) $D - L$ plane for monoelectronic and electron pair densities, (b) $D^2 - L^2$ plane for monoelectronic densities and $D - L$ for electron pair densities. Atomic units (a.u.) are used. 89
5.8 Jensen-Shannon divergence in position space, JSD_r, between the electron pair density and the product of monoelectronic densities, for atoms with nuclear charge $Z = 2 - 103$. Atomic units (a.u.) are used. 90
5.9 Jensen-Shannon divergence in momentum and position spaces, JSD_r and JSD_p, respectively, between electron pair densities and a product of monoelectronic densities, for neutral atoms with nuclear charge $Z = 2 - 103$. Atomic units (a.u.) are used. 91
5.10 Jensen-Shannon divergence calculated in momentum and position space between a neutral atom electron pair density and its corresponding simple (a) cation, (b) anion density for systems with an atomic charge $Z \in (2, 54)$. Atomic units (a.u.) are used. 92

5.11 Jensen-Shannon divergence calculated in momentum and position space between a (a) cation, (b) anion atom electron pair density and the correspondent monoelectronic density for systems with an atomic charge $Z \in (2, 54)$. Atomic units (a.u.) are used. 94
5.12 Quantum similarity index in position space, QSI between the electron pair density correspondent to Helium, Lithium, Beryllium and Neon, and the others atoms with nuclear charge $Z = 2 - 103$. Atomic units (a.u.) are used. 95
5.13 Quantum similarity index in momentum space, QSI between the electron pair density correspondent to Helium and Lithium, and the others atoms with nuclear charge $Z = 2 - 103$. Atomic units (a.u.) are used. 96
5.14 Quantum similarity index in momentum space, QSI_r between the electron pair density correspondent to Helium and Neon, and the others atoms with nuclear charge $Z = 2 - 103$. Atomic units (a.u.) are used. 96
5.15 Quantum similarity index in momentum space, QSI_r between the electron pair density correspondent to Lithium and Beryllium, and the others atoms with nuclear charge $Z = 2 - 103$. Atomic units (a.u.) are used. . . 97

6.1 Jensen-Fisher divergence calculated between the molecular densities of (a) H_2 and (b) NaH, and the whole list of complex molecules. 106
6.2 Jensen-Fisher divergence between the densities of a molecule and the rest of molecules of the hydrides group 108
6.3 Jensen-Shannon divergence calculated between molecules in the H-group (H_2,HF, HCl, HBr, HI) molecules and the rest of the molecules. 109
6.4 Jensen-Shannon divergence calculated between molecules in the Na-group (NaH,NaF, $NaCl$, $NaBr$, NaI) and the rest of molecules. 110
6.5 Jensen-Fisher divergence calculated between molecules in the H-group (H_2,HF, HCl, HBr, HI) and the rest of molecules. 111
6.6 Jensen-Fisher divergence calculated between molecules in Na-group (NaH,NaF, $NaCl$, $NaBr$, NaI) and the rest of molecules. 113
6.7 Jensen-Shannon divergence (red) calculated between the molecular densities of H_2 and the rest of molecules of both groups and the difference of the hardness of the compared molecules (green) 114
6.8 Jensen-Shannon divergence (red) calculated between the molecular densities of HI and the rest of molecules of both groups and the difference of the hardness of the compared molecules (green) 114

7.1 Comparison of the large ($F_{n,l}(r)$) and small ($G_{n,l}(r)$) components of the harmonic oscillator Dirac density. Atomic units (a.u.) are used. 121
7.2 Radial density of the relativistic harmonic oscillator for fixed values $n = 5$, $w = 1$ and two different values of j, $j = 1/2$ (red) and $j = 9/2$ (blue). Atomic units (a.u.) are used. 122
7.3 Radial density of the relativistic harmonic oscillator for a fixed value of $j = 1/2$, $w = 1$ and two different values of n, $n = 2$ (red) and $n = 5$ (blue). Atomic units (a.u.) are used. 123
7.4 Radial density of the relativistic harmonic oscillator for a fixed value of $n = 3$, $j = 1/2$ and two different values of w, $w = 1$ (red) and $w = 5$ (blue). Atomic units (a.u.) are used. 124

7.5 Disequilibrium of the radial density of the relativistic harmonic oscillator, for fixed values of $n = 5$ and $w = 1$, and $j \in \left[\frac{1}{2}, \frac{9}{2}\right]$. Atomic units (a.u.) are used. 124
7.6 Disequilibrium of the radial density of the relativistic harmonic oscillator, for each of the values of $j = \frac{1}{2}, \frac{3}{2}$ and $\frac{5}{2}$, with $w = 1$ and $n \in [3, 10]$. Atomic units (a.u.) are used. 125
7.7 Disequilibrium of the radial density of the relativistic harmonic oscillator, for a fixed value of $j = \frac{1}{2}, \frac{3}{2}$ and $\frac{5}{2}$, and $n = 3$, with frequency $w \in [1, 5]$. Atomic units (a.u.) are used. 126
7.8 Shannon entropy for the radial density of the relativistic harmonic oscillator, for a fixed value of $n = 5$, $w = 1$ and $j \in \left[\frac{1}{2}, \frac{9}{2}\right]$. Atomic units (a.u.) are used. 126
7.9 Shannon entropy of the radial density of the relativistic harmonic oscillator, for each of the values $j = \frac{1}{2}, \frac{3}{2}$ and $\frac{5}{2}$, with $w = 1$ and $n \in [3, 10]$. Atomic units (a.u.) are used. 127
7.10 Shannon entropy of the radial density of the relativistic harmonic oscillator, for each of the values of $j = \frac{1}{2}, \frac{3}{2}$ and $\frac{5}{2}$, and $n = 3$, with $w \in [1, 5]$. Atomic units (a.u.) are used. 127
7.11 Fisher information of the radial density of the relativistic harmonic oscillator, for a fixed value of $n = 5$, $w = 1$ and $j \in \left[\frac{1}{2}, \frac{9}{2}\right]$. Atomic units (a.u.) are used. 128
7.12 Fisher information of the radial density of the relativistic harmonic oscillator, for a fixed value of $j = \frac{1}{2}, \frac{3}{2}$ and $\frac{5}{2}$, $w = 1$ and $n \in [3, 10]$. Atomic units (a.u.) are used. 129
7.13 Fisher information of the radial density of the relativistic harmonic oscillator, for each of the values $j = \frac{1}{2}, \frac{3}{2}$ and $\frac{5}{2}$, with $n = 3$, and frequency $w \in [1, 5]$. Atomic units (a.u.) are used. 129
7.14 LMC complexity of the radial density of the relativistic harmonic oscillator, for $n = 5$, $w = 1$ and $j \in \left[\frac{1}{2}, \frac{9}{2}\right]$. Atomic units (a.u.) are used. . . . 130
7.15 LMC complexity of the radial density of the relativistic harmonic oscillator, for each of the values $j = \frac{1}{2}, \frac{3}{2}$ and $\frac{5}{2}$, with $w = 1$ and $n \in [3, 10]$. Atomic units (a.u.) are used. 131
7.16 (a) LMC complexity measure, and (b) information plane subtended by the exponential entropy (L) and the disequilibrium (D) of the radial density of the relativistic harmonic oscillator, for each of the values $j = 1/2,3/2$ and $5/2$, $n = 3$, and frequency $w \in (1, 5)$. Atomic units (a.u.) are used. 132
7.17 Fisher-Shannon complexity of the radial density of the relativistic harmonic oscillator, for a fixed value of $n = 5$ and $w = 1$, and $j \in \left[\frac{1}{2}, \frac{9}{2}\right]$. Atomic units (a.u.) are used. 133
7.18 Fisher-Shannon complexity of the radial density of the relativistic harmonic oscillator, for each of the values $j = \frac{1}{2}, \frac{3}{2}$ and $\frac{5}{2}$, with $n \in [3, 10]$. Atomic units (a.u.) are used. 133
7.19 Fisher-Shannon complexity calculated for the radial density of the relativistic harmonic oscillator, for each of values $j = \frac{1}{2}, \frac{3}{2}$ and $\frac{5}{2}$, $n = 3$, with $w \in [1, 5]$. Atomic units (a.u.) are used. 134

List of Tables

3.1 Classification scheme of most local extrema of JSD (up) and KL (down) between Schrödinger-Dirac densities for atoms with nuclear charges within the range $Z = 1-103$. 'Anomalous' or outermost orbitals are given within parentheses. 53

4.1 $QSI_q(Sch, Dir)$ local minima ($0.2 \leq q \leq 2.0$), classified into three categories, for ground-state neutral atoms with nuclear charge $Z = 1 - 103$. For systems with anomalous shell filling, the anomaly is specified within parentheses. Systems that are also local maxima of JSD are shown in bold (and in red, online) 65

5.1 Local extrema of Shanon entropies, $S(\rho)$ and $S(\Gamma)$ in position space for neutral atoms with nuclear charge $Z = 2 - 103$. 82
5.2 Valence subshell of systems corresponding to the local extrema of Shannon entropy in position space. 83

6.1 List of molecules considered in the first approach to the information-theoretical molecular analysis. Labeled from 1 to 101. 107